Reactivity of Niobium and Tantalum Imido and Bis(imido) Complexes

By

Benjamin Michael Kriegel

A dissertation submitted in partial satisfaction of the requirements for the degree of

Doctor of Philisophy

in

Chemistry

in the

Graduate Division

of the

University of California, Berkeley

Committee in charge:

Professor John Arnold, Chair

Professor Robert G. Bergman

Professor T. Don Tilley

Professor Jeffrey A. Reimer

Fall 2016

Abstract

Reactivity of Niobium and Tantalum Imido and Bis(imido) Complexes

By

Benjamin Michael Kriegel

Doctor of Philosophy in Chemistry

University of California, Berkeley

Professor John Arnold, Chair

Chapter 1. Previous collaborative work between the Arnold and Bergman groups on niobium and tantalum systems supported by *N,N'*-diaryl-β-diketiminate (BDI, aryl = 2,6-$^{i}Pr_2$-C_6H_3) and *tert*-butylimido ligands is summarized. Routes to prepare high-valent niobium and tantalum halide and alkyl starting materials are described, and the reactions of these complexes with small molecule substrates are discussed. Reactions to access low-valent niobium systems are described, and several examples are provided in which low-valent niobium systems promote unusual stoichiometric and catalytic transformations. In addition, the chemistry of high-valent BDI niobium bis(imido) systems is discussed.

Chapter 2. The nitrene transfer reactivity of a series of BDI niobium bis(imido) complexes is reported. A novel metathesis process results in nitrene fragment exchange between alkylimido groups in Nb(V) bis(imido) complexes and arylisocyanide substrates. Calculations and experimental evidence indicate that these reactions likely proceed through cycloaddition and cycloreversion steps involving Nb(V) η^2-carbodiimide intermediates, and occurs at a single metal center without elimination of carbodiimide. In contrast, reaction with unhindered alkylisocyanides results in extrusion of dialkylcarbodiimide, a process that was rendered catalytic in the presence of excess azide. This represents a rare example of oxidative nitrene transfer promoted by an early transition metal complex, in which reactivity across an imido group and two-electron metal-based redox chemistry are used in tandem to effect catalytic turnover.

Chapter 3. BDI niobium bis(imido) complexes are shown to react with a variety of substrates across their Nb-N π-bonds by cycloaddition and 1,2-addition. Niobium bis(imido) intermediates generated by treatment of a Nb(III) precursor with azide substrates react further with azide substrates via [3+2] cycloaddition to give niobium tetrazene complexes. These compounds exist in equilibrium with the corresponding bis(imido) complexes, and are competent catalyst precursors for oxidative nitrene transfer to generate carbodiimides. Isolated bis(imido) complexes are also shown to engage in stoichiometric 1,2-addition reactions with dihydrogen, silanes, boranes, thiols, and terminal alkynes. These bis(imido) compounds also exhibit [2+2] cycloaddition and cycloreversion reactivity with carbon dioxide and carbon disulfide. Through these studies, the first example of an isolated early transition metal (group 3 to 5) complex bearing both a terminal imido

and a terminal oxo ligand is accessed. Likely as a consequence of π-loading effects, this compound is reactive toward 1,2-addition of silane substrates across its oxo group.

Chapter 4. The cyclometallated tantalum(V) hydride complex {ArNC(Me)CHC(Me)N[2-($CHMeCH_2$)-6-^{i}Pr-C_6H_3]}Ta(N^{t}Bu)H was prepared from hydrogenolysis of (BDI)TaN^{t}BuMe_2 (BDI = *N*,*N*′-diaryl-β-diketiminate, aryl = 2,6-$^{i}Pr_2$-C_6H_3). Based on mechanistic studies, formation of the hydride complex likely proceeds through a dihydride intermediate generated from successive σ-bond metathesis steps. Low-valent Ta(III) dicarbonyl derivatives are accessed by either introducing CO atmosphere to the DMAP adduct at room temperature, or by directly adding CO at low temperature. Instead of promoting reductive elimination, 2,6-dimethylphenylisocyanide reacts with the tantalum hydride complex via migratory insertion to give a product containing a unique metallaimidazole ring. This complex can be reversibly oxidized by one electron either electrochemically or chemically to give a tantalum radical cation species. DFT calculations, as well as X-ray crystallographic and EPR spectroscopic data are consistent with the electron being removed from an orbital primarily composed of Ta-C π-bonding character, but also delocalized over the tantalaimidazole ring.

Chapter 5. The synthesis and reactivity of niobium and tantalum complexes bearing *tert*-butylimido and *N*,*N*′-di-2,4,6-trimethylphenyl-β-diketiminate (BDI^{Ar}) or *N*,*N*′-di2,6-dichlorophenyl-β-diketiminate (BDI^{Cl}) ligands is reported. Reaction of dimethyl complex (BDI^{Ar})Nb(N^{t}Bu)Me_2 with dihydrogen leads to generation of bis-μ-hydrido Nb(IV)-Nb(IV) complex {(BDI^{Ar})Nb(N^{t}Bu)(μ-H)}$_2$. One-electron oxidation of this complex results in release of dihydrogen to generate the imido-bridged mixed-valent Nb(III)-Nb(IV) dimer [{(BDI^{Ar})Nb(μ-N^{t}Bu)}$_2$][$B(C_6F_5)_4$]. EPR spectroscopic measurements and DFT calculations are consistent with a symmetric structure containing a Nb-Nb single bond in which the unpaired electron is delocalized over both niobium centers.

Reactivity of Niobium and Tantalum Imido and Bis(imido) Complexes

Table of Contents

Acknowledgments

In similar fashion to probably just about anyone who has ever written a thesis (except, I suppose, for some devout religious folk who might start with an imaginary bearded fellow), I will start by thanking my principal advisor, John Arnold, for everything he has done for me over the past five years. My first interaction with John was literally life changing—back in January 2011, mere weeks after submitting my grad school apps, I got a phone call from John in which he informed me I had been accepted to UC Berkeley. Obviously, I decided to accept Berkeley's offer and ultimately join John's research group. I have not once regretted either decision. John has been an amazingly supportive advisor. He has given me an enormous amount of freedom to explore whatever research questions I've been excited about and has provided me with the intellectual tools (as well as more tangible tools like Schlenk lines, gloveboxes, chemicals, and of course a generous stipend) to tackle those questions. John has also been a great advisor to interact with on a personal level. He is always open to discuss things (research related or not), and sometimes even argue, which I have sincerely appreciated in him. For those of you who know me, you may have noticed that arguing is one of my favorite ways of interacting with peopl (up there with complaining); the ability to have a friendly, productive argument is something I truly value.

In addition to John, I have had the amazing fortune of being co-advised by the legendary Bob Bergman. My advising meetings with John and Bob have always been full of useful insights. Countless times, Bob has suggested a new idea or an interpretation of results that neither John nor myself would ever have thought of. Bob's physical organic chemistry class was among the best classes I have ever taken, and was a large influence on my decision to join the early metal imido project. Teaching both through lecture and research advising has always clearly been an important priority for Bob; few other professors are willing to devote as much time and effort as he is in order to make sure a student truly understands a concept.

My next acknowledgment goes to Thomas Gianetti, my mentor and friend for my first three years of grad school. Having come in to graduate school with almost no background in air-sensitive organometallic chemistry, Thomas's guidance played a vital role in getting me started. He taught me everything I know about handling air-sensitive compounds, as well as much of what I know about NMR spectroscopy, X-ray crystallography and DFT calculations, all of which has of course been pivotal to my research. Thomas has also been a great person to bounce ideas off of and discuss results. I remember many incidences during my first couple years at Berkeley in which we would start excitedly discussing a new research idea at a bar, restaurant, or group trip, much to the chagrin of some of our co-workers.

I should mention here that my Ph.D. hasn't exactly been smooth sailing. My second year—qual time—was especially rough. It has always meant a lot to me that John, Bob and Thomas all supported me and encouraged me after the first time didn't go so well. Our practice sessions helped me build confidence to get me through to where I am now, and I am extremely grateful for that.

During my third year at Berkeley I began to transition into more of a mentorship role. One of my most valuable experiences at Berkeley was mentoring Lauren Grant, one of the most hard-working and motivated people I have ever met. During her two-year tenure in the Arnold group,

Lauren carried out some of the important synthetic work in this thesis, among other projects. I am thrilled that Lauren decided to continue pursuing organometallic chemistry as a graduate student at U Penn, and I anticipate she will be very successful in all her future endeavors. At first, Lauren and I didn't exactly see eye-to-eye on everything, but working with her was a very valuable experience for me, as I learned how to mentor and collaborate with someone with a work style and personality different from my own. Since our early days of constant bickering, Lauren and I have grown to be good friends.

I have also had the pleasure of mentoring Lara Naested, a Masters student from EPFL in Switzerland for six months during my fourth year at Berkeley. Her work also contributed to the results presented in this thesis. Lara is one of the most cheerful and friendly people I have ever met, and we also became fast friends outside of lab. I really enjoyed the evenings we spent playing board games together!

Some of the synthetic work presented in this thesis was carried out collaboratively with Michael Nechayev, a previous Berkeley undergrad who worked with Thomas and is now a Ph.D. student at Princeton, and with Andreas Obenhuber, a previous postdoc who is now working in Germany. I am very grateful for their contributions.

Two other co-workers and friends who have also profoundly impacted my life as a Ph.D. student are Jessica Ziegler and Trevor Lohrey. Both are current Ph.D. students in the group working on projects related to mine, and have not only been spectacular confidants in our joint research meetings with John and Bob, but have also been extremely fun and friendly people to have shared office space with for the last few years.

I also need to thank all of my other lab mates over the years, especially Ashleigh Ward, Leah Rubin, Michael Boreen, Bernard Parker, Alison Altman, Stephan Hohloch and Nick Settineri, for helping to make the Arnold group a great place to work and for offering a lot of useful advice and insights. The group has changed quite a bit over the years, but it has always been a fun, accepting bunch of people.

I am also glad to have made some amazing friends in other research groups at UC Berkeley, several of whom have made significant intellectual contributions to my work in the form of advice and discussions. Andy Nguyen has not only been one of my best friends, but also a source of endless ideas and knowledge throughout my entire Ph.D. Willie Wolf, Stephen von Kugelgen, Kurt Van Allsburg and James Dombrowski have also been especially helpful and supportive.

It is important to point out that my Ph.D. project built upon a larger body of collaborative work that has been going on in the Arnold and Bergman groups for close to a decade. Many of the ideas that played a significant role in my research originated from the work of Neil Tomson (Asst. Prof. at U. Penn.) and Pete La Pierre (Asst. Prof. at Georgia Tech), previous Arnold/Bergman group members who worked on early transition metal chemistry before I started my Ph.D. I hope that equally talented students will join the Arnold group in the coming years to continue carrying out work on early transition metal imido chemistry.

I wouldn't have been able to complete any of this work without the help of collaborators at various institutions. Specifically, I would like to thank Greg Nocton, Kolluru Lakshmi and Ruchira Chatterjee for assistance with EPR spectroscopic data acquisition and simulation and Nikolas Kaltsoyannis for assistance with DFT calculations.

I also owe a special thanks to the facilities staff members at UC Berkeley for their assistance with data acquisition and analysis: Yinka Olatunji-Ojo and Kathy Durkin (DFT), Chris Canlas and Hasan Celik (NMR), Elena Kreimer (EA) and Antonio Dipasquale (XRD). Administrative staff members, in particular Ivette Quintanilla, Rain Simar, Lynn Keithlin and Aileen Harris have also played an important role in ensuring that I get paid every month and that I've done all the proper paperwork to graduate. I'd also like to thank Jim Breen in the glass shop as well as all of the folks in the wood shop, machine shop and electrical shop for all of the repairs and modifications they have made for me and my group over the years.

During the second year of my Ph.D., I had the unique opportunity to work with the Mashima group at Osaka University in Osaka, Japan for three months. This was an extraordinary experience and I'd like to thank both John for allowing me to take this opportunity as well as everyone in the Mashima research group for putting up with me for those three months. I am especially thankful to Teruhiko Saito, the Ph.D. student who served as both my friend and my research mentor during my time in Osaka, and later came to Berkeley to work in the Arnold group for two months, as well as my advisors in Japan, Prof. Hayato Tsurugi and Prof. Kazushi Mashima.

I thank Don Tilley for reading my thesis and acting as my qualifying exam committee chair, and for some useful insights on my research over the years. I also thank Jeff Reimer for reading my thesis as my outside committee member and Dick Anderson, Matt Francis and Ron Gronsky for serving on my qualifying exam committee.

I would never have wound up as a Ph.D. student at UC Berkeley without the excellent education I received as an undergraduate student at New College of Florida. When I started my undergraduate education, I had very little idea what I wanted to do with my life. My decision to study chemistry was largely influenced by my introductory organic chemistry classes with Prof. Paul Scudder. From Prof. Scudder's classes, I gained a deep love for physical organic chemistry and NMR spectroscopy which I have been able to put to good use during my Ph.D. Upon finishing my second year of college, I realized that if I wanted to pursue chemistry, I should get involved in research. Hence, I spent the summer after my second year doing rotational spectroscopy research with Prof. Steve Shipman, a young assistant professor at New College. While I obviously didn't end up pursuing physical chemistry much further, this opportunity helped me get started in the world of research and set me up for future opportunities. Steve has been an amazing friend and resource ever since.

During the summer after my third year of undergrad, I had the opportunity to carry out research in the Parkin group at Columbia University through the NSF REU program. This opportunity was very important to my future, as it was my first entry into molecular inorganic chemistry and X-Ray crystallography. I'd like to thank the entire Parkin group of Summer 2010, in particular Ged Parkin (who taught me that the covalent model is superior to the ionic model 99% of the time) and

Ahmed Al-Harbi, Wes Sattler and Aaron Sattler for all of their time spent teaching and training me. During my last year at New College, I carried out my undergraduate thesis research under Prof. Suzanne Sherman, in which I was able to develop my budding interest in molecular inorganic chemistry, which I then carried forward into my Ph.D. studies.

My time at New College also led me to some of my best friends, especially Tricia, Katie, Colin, Emily and Kat, who have always been there for me when things have gotten tough. I enjoy spending time with them more than pretty much anyone else in the world, and am always looking forward to the next time we get to hang out.

Of course, I wouldn't be anywhere without my family. My Dad, Mom, Grandma Barbara, Aunt Kim, Uncle Seth and cousins Noah, Talia and Megan have offered me tremendous support throughout my life and the course of my Ph.D., picking me up when I've been down and giving me great places to go for the holidays. It meant so much to me that almost all of them were able to make it to my graduation ceremony! I'd also like to pay my respects to my other three grandparents Joan, Bob and Jack who are unfortunately no longer alive, but all had such a huge influence on getting me to where I am.

Finally, I would like to acknowledge Microsoft Word for at least having AutoSave to get me through the countless times it crashed while writing this thesis.

Chapter 1

Overview of Previous Work on Niobium and Tantalum Complexes Supported by β-Diketiminate and Imido Ligands

Preparation of Niobium and Tantalum BDI Complexes

Beginning in the mid-1990s, β-diketiminate ligands with sterically encumbering N-aryl substituents began to see use in organometallic and coordination chemistry.[1–3] By the mid-2000s, β-diketiminate ligands had become well established for supporting reactive low-coordinate complexes of early transition metals, base metals, and main group metals, but had not yet been explored in the chemistry of niobium and tantalum.[4] Tomson, Arnold, and Bergman hypothesized that BDI ligands would provide a good support for low-valent, low coordinate niobium and tantalum complexes, as well as high-valent complexes containing reactive functionalities like terminal imido, oxo, alkylidene and nitrido groups. While attempts to metallate BDI ligands with bulky aryl substituents using MCl_5 (M = Nb, Ta) were largely unsuccessful, the lithium salts BDILi·Et_2O or BDILi·THF readily and cleanly reacted with the terminal imido species M(N^{t}Bu)Cl_3Py_2 via salt metathesis to yield six-coordinate imido compounds **1.1** and **1.2** (Scheme 1.1).[5,6] The analogous base free, square-based pyramidal niobium complex **1.3** was prepared via pyridine abstraction from **1.1** using strong Lewis acids. Both **1.3** and the related arylimido analog **1.4** were also accessed using Nb(NR)$(Cl)_3$(DME) (R = Ar, ^{t}Bu) as a metal source (Scheme 1.1). Complexes **1.1 – 1.3** were found to be valuable starting materials for exploring the chemistry of a wide range of niobium and tantalum complexes in both low-and high-valent states.

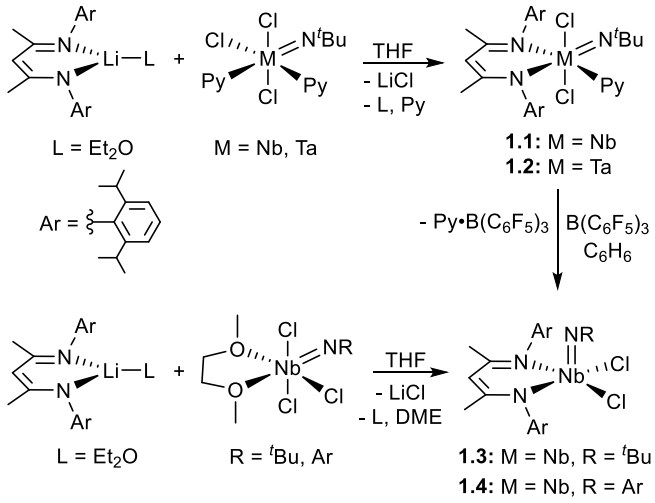

Scheme 1.1 Preparation of niobium and tantalum BDI imido dichloride complexes.

High-valent Niobium and Tantalum Chemistry

Reaction of the dichlorides **1.1** and **1.2** with methyl Grignard yielded the trigonal bipyramidal Nb(V) and Ta(V) dimethyl derivatives **1.5** and **1.6** (Scheme 1.2).[5–7] Notably, pyridine is lost in this transformation and no subsequent evidence for coordination of σ-donating ligands to **1.5** or **1.6** has been observed.

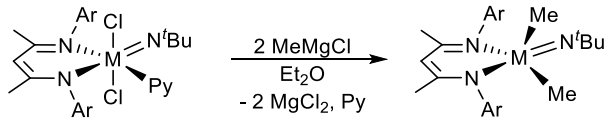

1.1: M = Nb
1.2: M = Ta

1.5: M = Nb
1.6: M = Ta

Scheme 1.2 Synthesis of Nb and Ta dimethyl complexes.

The BDI supported niobium dimethyl complex **1.5** reacted readily with a variety of substrates, including π-acids,[7] Lewis acids,[6] and dihydrogen.[8–11] Reaction between **1.5** and CO resulted in conversion to a mixture of the green dicarbonyl complex **1.7** and orange enediolate complex **1.8** in ratios that depended on solvent coordinating ability and CO pressure (Scheme 1.3).[7] While **1.7** was found to be the major product in THF, **1.8** was favored in non-coordinating solvents such as pentane. This was explained by observing that coordination of THF would disfavor coordination of a second equivalent of CO necessary to access **1.8** prior to reaction of a single equivalent of CO with both methyl groups to release acetone and generate **1.7**. When lower pressures of CO were introduced to **1.5**, compound **1.9**, which is generated from net reaction of **1.5** with only a single equivalent of CO was also observed as a product.

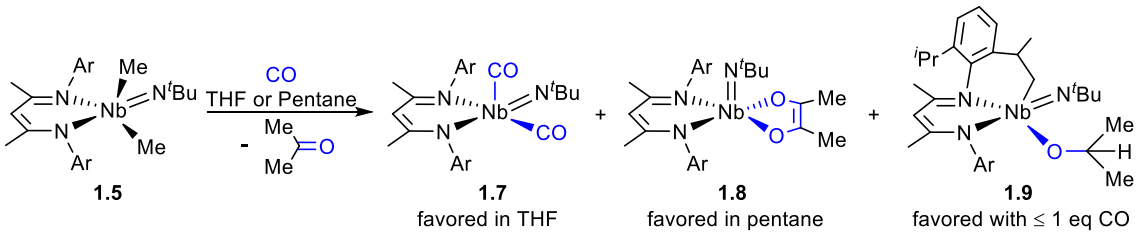

1.5

1.7
favored in THF

1.8
favored in pentane

1.9
favored with ≤ 1 eq CO

Scheme 1.3 Reactivity of **1.5** toward carbon monoxide.

Reaction of niobium and tantalum dimethyl compounds **1.5** and **1.6** with trityl cation resulted in abstraction of a methyl group to generate cationic complexes **1.10** and **1.11** (Scheme 1.4).[6] In common with related high-valent group 4 imido cations in the literature,[12–15] the niobium derivative catalyzed the conversion of ethylene to high-density polyethylene at room temperature. Interestingly, the tantalum derivative was unreactive under the same conditions.

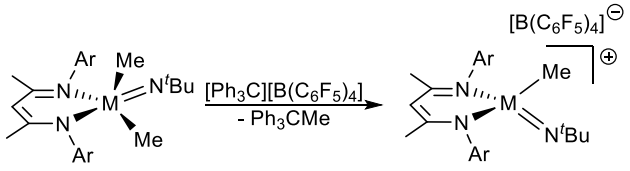

1.5: M = Nb
1.6: M = Ta

1.10: M = Nb
1.11: M = Ta

Scheme 1.4 Methyl abstraction to form cationic complexes.

Low-valent Niobium Chemistry

Low-valent early transition metal complexes are often very reactive and have been shown to be useful in C-C bond forming reductive coupling reactions.[16–19] With this in mind, the two-electron reduction chemistry of niobium dichloride complex **1.1** has been explored in detail (Scheme 1.5).[8] Compound **1.1** reacted with 2 equivalents potassium graphite at low temperature to give a blue suspension, which changed color to yellow upon warming to room temperature. The blue color was attributed to the reactive Nb(III) intermediate **1.12**, while the yellow product was isolated and characterized as the monoazadiene Nb(V) bis(imido) complex **1.13**, resulting from reductive cleavage of the BDI ligand. Reductive C-N bond cleavage is precedented in low-valent group 4 and 5 BDI complexes, and is often promoted in the presence of σ-donating ligands like THF or pyridine.[20–24] The Nb(III) intermediate could be trapped by introduction of π-accepting ligands such as CO and isocyanides to solutions of **1.12** to give compounds **1.14** and **1.15**. Curiously, reaction with KC_8 carried out in the presence of dimethylphosphinoethane (dmpe) resulted only in conversion to the Nb(IV) species **1.16**, even in the presence of excess KC_8 indicating that dmpe coordination drastically decreased the reduction potential of **1.16**. The chelating ability of dmpe seemed to play an important role here, as the same reaction in the presence of monodentate phosphines gave only **1.13**.

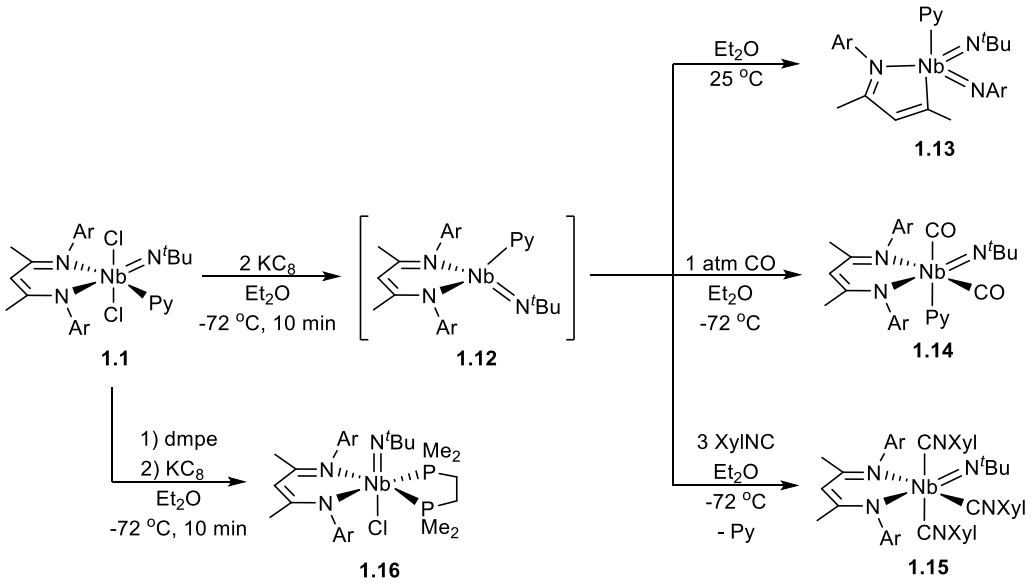

Scheme 1.5 Generation of low-valent Nb complexes using KC_8.

The 5-coordinate dicarbonyl complex **1.7** represented an attractive source of potentially reactive Nb(III). While **1.7** could be isolated in moderate yields following the procedure shown in Scheme 1.3, a preferred method for its preparation involved a two-step, one-pot procedure in which the η^2-imine complex **1.17** was first produced by insertion of isocyanide, followed by displacement of the imine with CO (Scheme 1.6).[7,8] As an example of the reactivity of **1.7**, an oxo group could be transferred from the oxidant Ph_2SO with displacement of CO to generate bis-μ-oxo Nb(V) dimer **1.18**.[8]

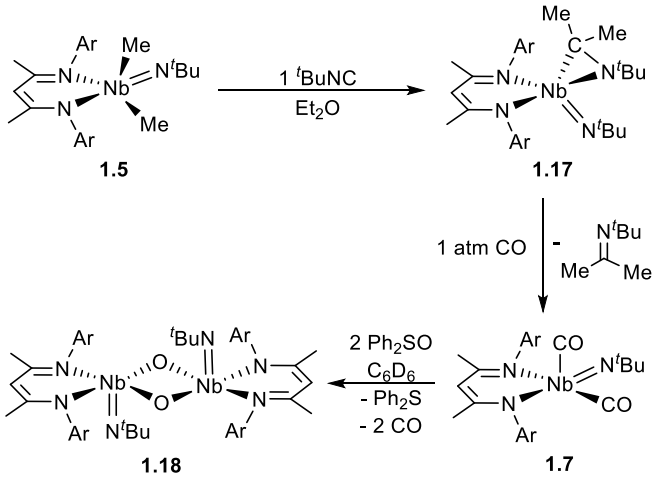

Scheme 1.6 Mild route to access Nb(III) dicarbonyl.

With the ability to access Nb(III) under relatively mild conditions and the knowledge that the BDI ligand was also capable of stabilizing Nb(V) chemistry, the BDI Nb(III) system was investigated for use in catalytic applications. For example, the Nb(III) dicarbonyl complex **1.7** proved functional as a catalyst for the selective semihydrogenation of internal alkynes to Z-alkenes.[25,26] This reaction was shown to proceed by a new mechanism, as outlined in Scheme 1.7.

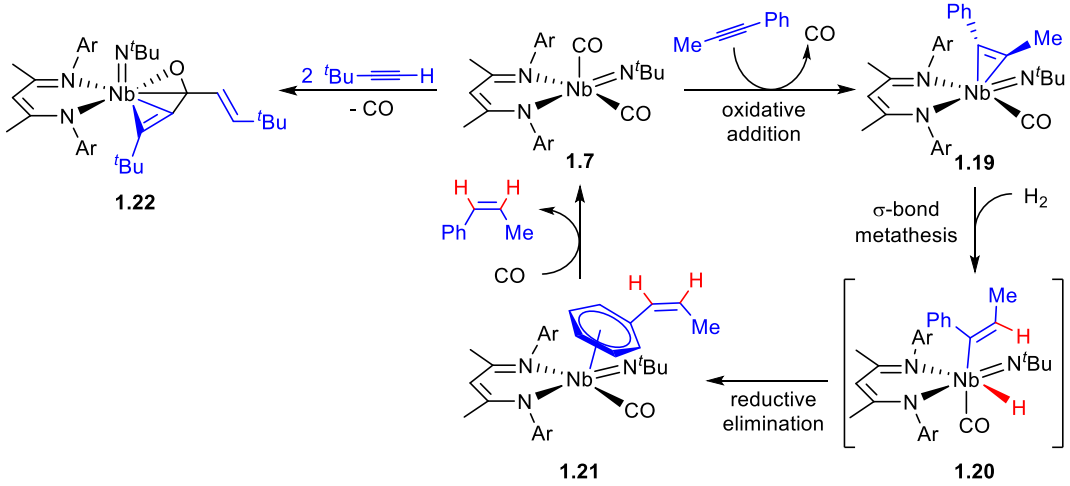

Scheme 1.7 Hydrogenation catalysis using Nb(III)/(V) couple.

Alkyne displaced CO to form the isolable Nb(V) η^2-alkyne complex **1.19**,[8] which then underwent σ-bond metathesis with H_2 to generate vinyl hydride intermediate **1.20**. Reductive elimination to give **1.21** followed by displacement of coordinated arene by CO regenerated the starting dicarbonyl. Although **1.20** could not be directly observed, intermediate **1.21** was seen using ^{1}H NMR spectroscopy.[25] Notably, the Nb center cycled between high and low-valent oxidation states within the catalytic cycle. While reductive elimination and oxidative addition processes are commonplace in late transition metal catalysis, it is uncommon for two-electron redox chemistry to be supported in early transition metal systems within catalytic cycles. This

catalytic reactivity was limited to internal alkynes; **1.7** instead underwent stoichiometric reaction with *tert*-butylacetylene to give **1.22** rather than releasing hydrogenated product.[27]

While dicarbonyl complex **1.7** exhibited novel catalytic reactivity, the reactivity of **1.7** in general was quite limited compared to many of the highly reactive Nb(III) compounds reported in the literature[18,28–35] due to the stabilizing effect of strong π-acids on d^2 metal centers. Hence, alternative routes to access isolable, yet highly reactive Nb(III) sources were targeted. Hydrogenolysis of the dimethyl precursor **1.5** proved to be a very effective method for generating the transient Nb(III) intermediate **1.23**, which went on to a variety of products depending on solvent (Scheme 1.8).[8–11]

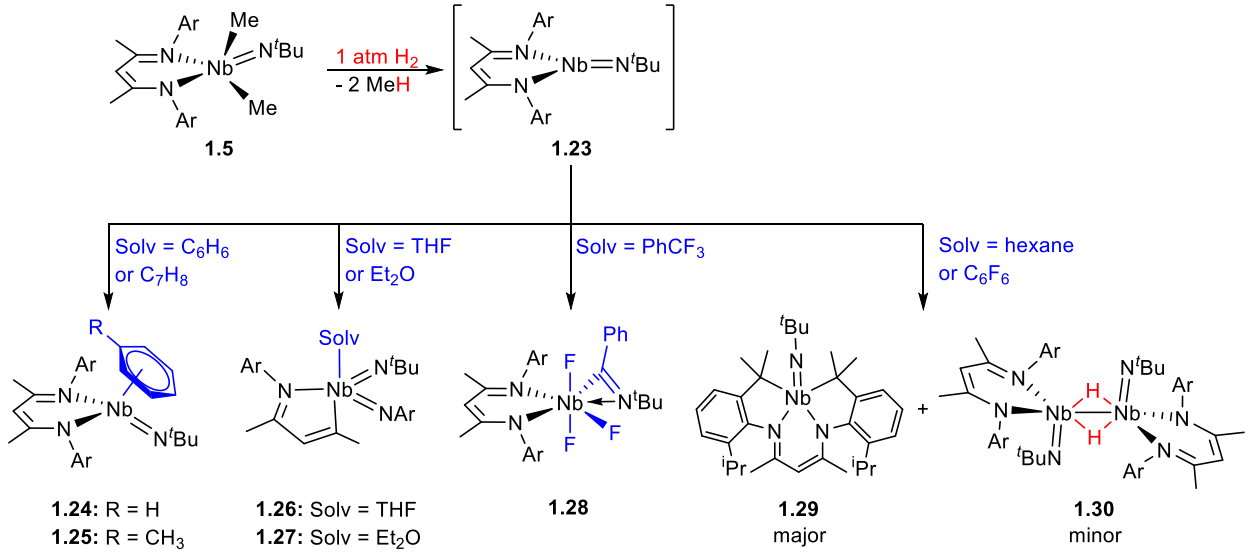

Scheme 1.8 Solvent-dependent reactivity of **1.5** with dihydrogen.

The most synthetically useful products were the dark red η^6-arene complexes **1.24** and **1.25** prepared from hydrogenolysis in benzene or toluene respectively;[9] the reactivity of these compounds will be discussed in more detail below. Not unexpectedly based on related reactions of the dichloride precursor **1.1** with KC_8 (Scheme 1.5), reaction of **1.5** with dihydrogen in either THF or Et_2O led to isolation of products **1.26** and **1.27** resulting from reductive C-N cleavage of the BDI ligand.[8,11] The highly reactive nature of the Nb(III) species generated by hydrogenolysis was showcased by the reaction of **1.5** with H_2 in α-trifluorotoluene to give **1.28**, which resulted from activation of all three typically inert benzylic C-F bonds.[10] In non-coordinating solvents such as hexane, C-H activation of the BDI ligand by a Nb(III) center resulted in conversion to **1.29**. Additionally, relatively small amounts of the purple diamagnetic Nb(IV)-Nb(IV) bis-μ-hydrido dimer **1.30** were isolated from reactions conducted in non-coordinating solvents and also observed as a trace impurity from reactions in benzene or Et_2O.[10]

Compound **1.24** reacted with a variety of reagents such as CO, XylNC, N_2O, and THF to give previously characterized products **1.7**, **1.15**, **1.18**, and **1.26** respectively. Upon standing at room temperature in hexane, **1.24** and **1.25** converted to the inverted sandwich complexes **1.31** and **1.32**

in a process that was shown to be first order in Nb(III) starting material and dissociative in arene (Scheme 1.9).[9] The spectroscopic and crystallographic data for both **1.24** and **1.31** were consistent with Nb(III) metal centers coordinated by neutral arene ligands. This was also consistent with the arene ligand being displaced to generate a transient 3-coordinate Nb(III) intermediate in the transformation from **1.24** to **1.31**. In contrast to **1.24**, which was shown to be very reactive, compound **1.31** showed an almost complete lack of reactivity toward most reagents.

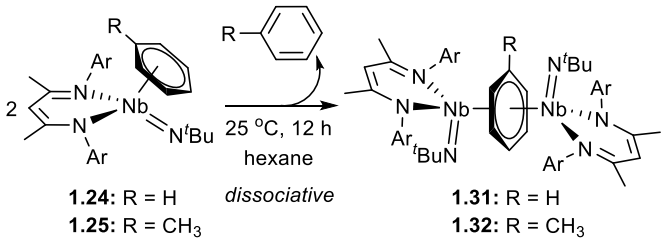

Scheme 1.9 Dimerization of η^6-arene complexes of Nb(III).

Furthermore, the niobium η^6-benzene complex **1.24** was shown to activate the C-F bond of fluorobenzene in order to generate phenyl fluoride complex **1.35** (Scheme 1.10).[36] The η^6-fluorobenzene adduct compound **1.33** could be observed as an intermediate that built up during conversion to **1.35** by ^{1}H NMR and ^{19}F NMR spectroscopy. Catalytic turnover for this C-F activation process was accomplished through addition of a sacrificial silane reductant. DFT calculations indicated that the reaction likely proceeded through bimetallic intermediate **1.34**. This catalytic process was also extended to a series of polyfluorinated arene substrates; however, in contrast to most other hydrodefluorination catalysts in the literature, mono and difluorinated arenes were activated preferentially over more heavily fluorinated arenes. In a separate study, it was also shown that isocyanides could insert into the Nb-C bond of **1.35**,[37] a step toward using this C-F activation chemistry for defluorofunctionalization of C-F bonds, although only stoichiometric reactivity to give **1.37** and **1.38** was observed upon addition of phenylsilane to **1.36**.

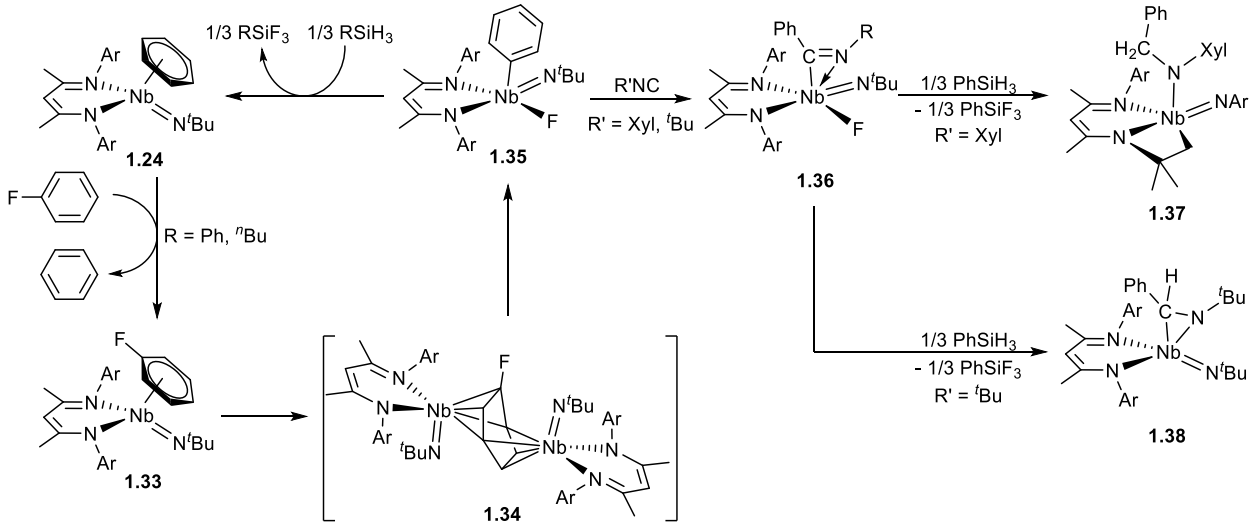

Scheme 1.10 Catalytic hydrodefluorination of fluoroarenes mediated by Nb(III).

One-electron oxidation of inverted sandwich complex **1.31** led to isolation of **1.39**, an unusual Nb(IV)-Nb(III) mixed-valence compound that exhibited a rare asymmetric μ-η^2:η^4-benzene binding mode (Scheme 1.11).[38] Spectroscopic and crystallographic data were again consistent with a neutral bridging benzene molecule, and unlike **1.31**, the dimeric structure of **1.39** readily broke up to generate monomeric Nb(III) and Nb(IV)$^+$ fragments **1.24** and **1.40** which engaged in reactivity with a variety of substrates including THF to re-form **1.31** and give Nb(IV) cation **1.41**, DCE to give Nb(V)-Nb(V) dimer **1.42**, and ^{t}BuN$_3$ to give Nb(V) complexes **1.43** and **1.44**.

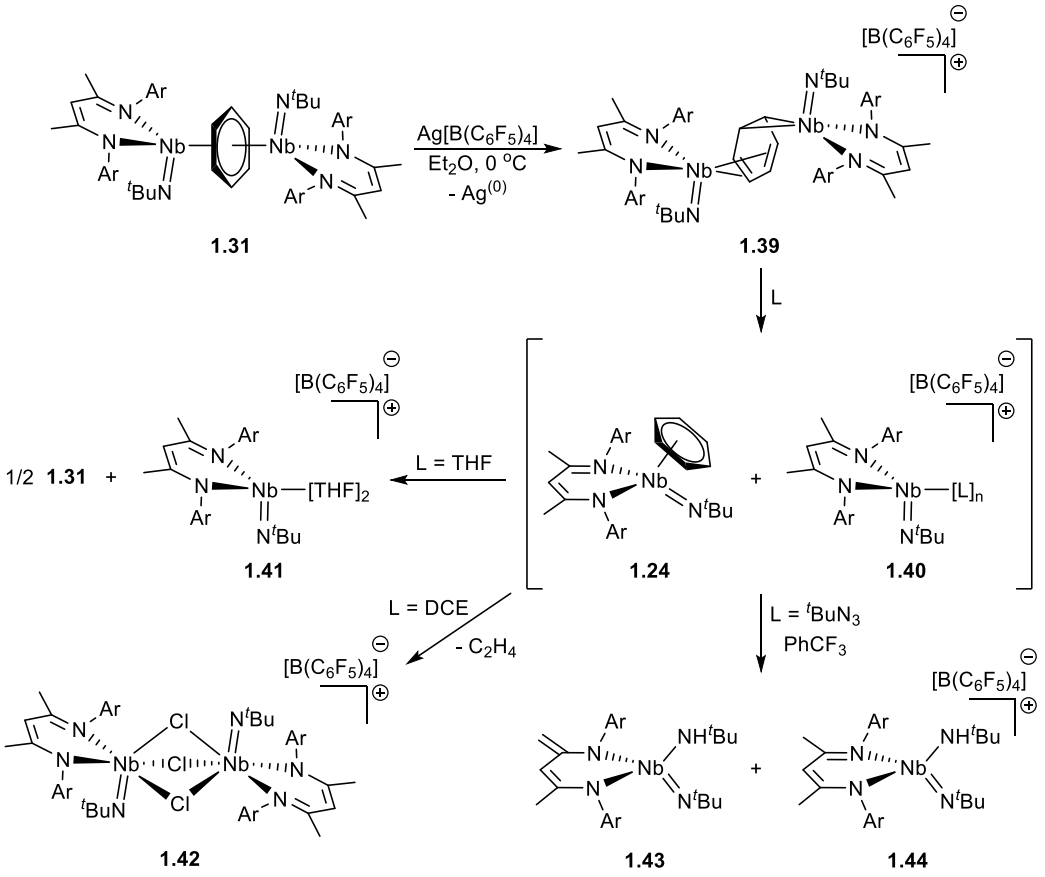

Scheme 1.11 One electron oxidation of the Nb(III) dimer **1.31** and reactivity of the mixed-valent product.

Chemistry of Niobium Bis(imido) Complexes

While imido groups in early transition metal compounds are often reactive toward cycloaddition and 1,2-addition processes,[39–54] for both high- and low-valent niobium and tantalum complexes of the (BDI)M(N^{t}Bu) scaffold, the imido group behaved entirely as a supporting ligand in almost all cases (a notable exception is compound **1.28**). It was hypothesized that introduction of a second imido group would serve to increase reactivity across the imido groups by creating a "π-loading" effect,[5,55–59] increasing the polarization of the imido bonds by electronically saturating the niobium d_π orbitals. 5-coordinate bis(imido) complexes **1.45** and **1.46** could be accessed either from reduction of **1.1** and trapping with azide[8] or from reaction of **1.1** with LiNH^{t}Bu,[5] as shown in Scheme 1.12. In

order to access the more reactive 4-coordinate bis(imido) species **1.47**, pyridine was removed using $B(C_6F_5)_3$. Under these conditions, **1.47** could be accessed in situ, but degraded to **1.43** faster than it could be isolated from the byproduct $Py{\cdot}B(C_6F_5)_3$. Conversion to **1.43** likely occurred by an intermolecular process, in this case catalyzed by $Py{\cdot}B(C_6F_5)_3$. Although conversion to **1.43** in the presence of $Py{\cdot}B(C_6F_5)_3$ occurred faster than reactions of **1.47** with most other substrates, **1.47** did react with *tert*-butyl isocyanate across an imido group to generate **1.48**, which subsequently degraded rapidly to mixtures of products.[5]

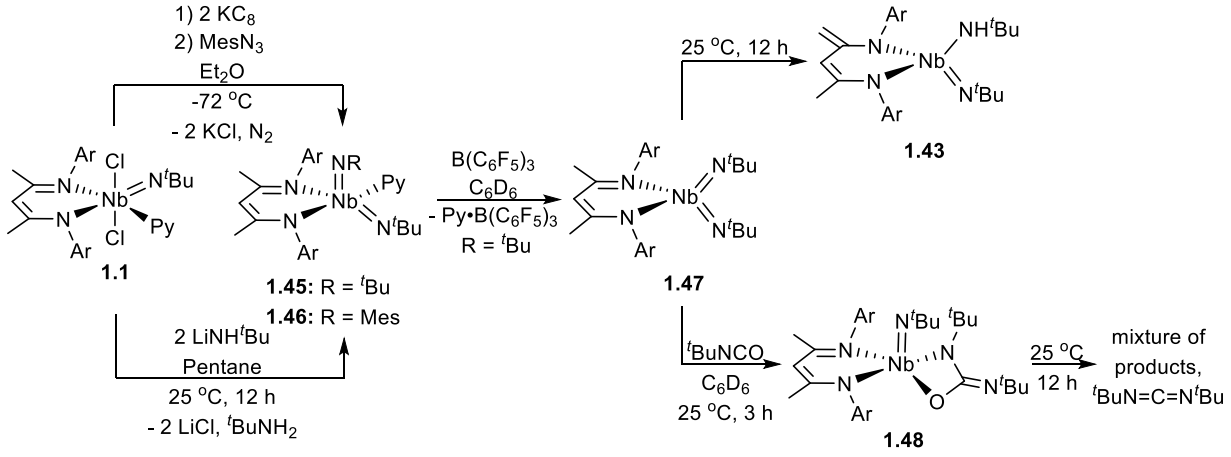

Scheme 1.12 Synthesis of Nb bis(imido) complexes from **1.1** and cycloaddition reactivity with *tert*-butylisocyanate.

BDI-supported niobium bis(imido) compounds could also be accessed via the routes shown in Scheme 1.13.[11] In a process likely similar to that undergone by related titanium and vanadium alkylidene and alkylidyne complexes,[60–62] intact BDI ligands were re-formed from **1.26** or **1.27** to give either mixtures of **1.47** and **1.49** in the presence of $^tBuN_3$ or mixtures of **1.50** and **1.51** in the presence of ArN_3. Under these conditions, each of these compounds could be isolated and fully characterized; compound **1.47** only very slowly underwent thermal conversion to **1.43** at room temperature over several days. Formation of compound **1.49** resulted from C-H activation of the ^{t}Bu BDI N-substituent across a reactive imido group.

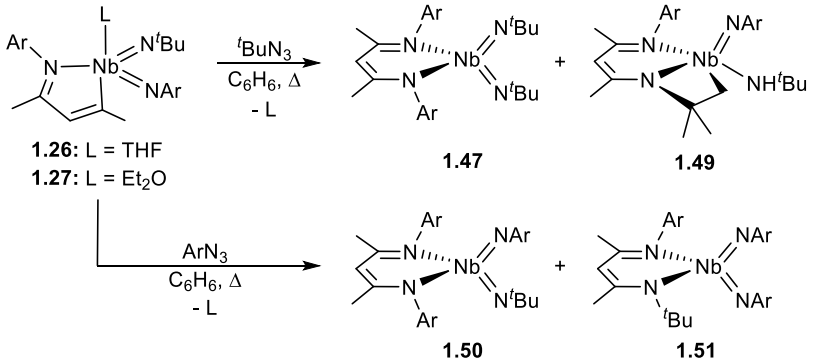

Scheme 1.13 Synthesis of bis(imido) compounds by re-forming BDI framework.

The results summarized here have clearly demonstrated that the BDI imido ligand scaffold is excellent for accessing niobium complexes in a range of oxidation states bearing a variety of reactive moieties. Moreover, not only can both Nb(III) and Nb(V) complexes be generated under mild conditions, but the Nb(III)/Nb(V) redox couple can be utilized in conjunction with σ-bond metathesis reactivity in order to access unique catalytic reactions that proceed by unusual pathways, such as hydrogenation[25] and hydrodefluorination.[36]

Based on these findings, it seemed prudent to delve further into the chemistry of this system, focusing in particular on several different facets. First, although reactions across multiply bonded ligands is a relatively common and often extremely useful mode of reactivity in early transition metal complexes, reactions across imido groups were virtually unexplored in this system due to the inert nature of the imido moiety. While initial studies demonstrated that introducing π-loading through incorporation of a second imido group was an effective way to attain reactivity with a single substrate,[5] the reactivity of complexes containing *reactive* terminal imido or terminal oxo groups had not been thoroughly investigated. Moreover, since both Nb(III) and Nb(V) systems could be readily accessed in this system, it seemed plausible that the Nb(III)/(V) redox couple could be used in conjunction with imido based reactivity to effect new types of catalytic transformations. Second, while low, mid, and high valent niobium complexes containing a variety of different functionalities had been reported, only a handful of high valent complexes of tantalum had been reported in a single publication.[6] Hence, the chemistry of tantalum complexes supported by the BDI imido ligand scaffold warranted further attention. Third, the complexes described thus far are all supported by BDI ligands bearing 2,6-diisopropylphenyl (Dipp) substituents. While BDI ligands bearing Dipp substituents have been among the most successful ligands for stabilizing low-coordinate metal complexes in the literature, perturbing the electronic and steric environment around the niobium or tantalum center by modifying the aryl substituent provided a way to better understand and potentially access new chemistry with this system.

Notes and References

(1) Feldman, J.; Mclain, S. J.; Parthasarathy, A.; Marshall, W. J.; Calabrese, J. C.; Arthur, S. D.; The, S.; Arndc, R.; Me, M. C. *Organometallics* **1997**, *16*, 1514.
(2) Budzelaar, P. H. M.; van Oort, A. B.; Orpen, A. G. *Eur. J. Inorg. Chem.* **1998**, 1485.
(3) Gibson, V. C.; Newton, C.; Redshaw, C.; Solan, G. A.; White, A. J. P.; Williams, D. J.; Maddox, P. J. *Chem. Commun.* **1998**, No. 16, 1651.
(4) Bourget-Merle, L.; Lappert, M. F.; Severn, J. R. *Chem. Rev.* **2002**, *102* (9), 3031.
(5) Tomson, N. C.; Arnold, J.; Bergman, R. G. *Organometallics* **2010**, *29*, 2926.
(6) Tomson, N. C.; Arnold, J.; Bergman, R. G. *Dalton Trans.* **2011**, *40* (30), 7718.
(7) Tomson, N. C.; Yan, A.; Arnold, J.; Bergman, R. G. *J. Am. Chem. Soc.* **2008**, *130*, 11262.
(8) Tomson, N. C.; Arnold, J.; Bergman, R. G. *Organometallics* **2010**, *29*, 5010.
(9) Gianetti, T. L.; Nocton, G.; Minasian, S. G.; Tomson, N. C.; Kilcoyne, A. L. D.; Kozimor, S. A.; Shuh, D. K.; Tyliszczak, T.; Bergman, R. G.; Arnold, J. *J. Am. Chem. Soc.* **2013**, *135* (8), 3224.
(10) Gianetti, T. L.; Bergman, R. G.; Arnold, J. *J. Am. Chem. Soc.* **2013**, *135* (22), 8145.
(11) Obenhuber, A. H.; Gianetti, T. L.; Berrebi, X.; Bergman, R. G.; Arnold, J. *J. Am. Chem. Soc.* **2014**, *136* (8), 2994.
(12) Bolton, P. D.; Mountford, P. *Adv. Synth. Catal.* **2005**, *347* (2–3), 355.

(13) Adams, N.; Arts, H. J.; Bolton, P. D.; Cowell, D.; Dubberley, S. R.; Friederichs, N.; Grant, C. M.; Kranenburg, M.; Sealey, A. J.; Wang, B.; Wilson, P. J.; Cowley, A. R.; Mountford, P.; Schröder, M. *Chem. Commun.* **2004**, No. 4, 434.
(14) Bigmore, H. R.; Dubberley, S. R.; Kranenburg, M.; Lawrence, S. C.; Sealey, A. J.; Selby, J. D.; Zuideveld, M. A.; Cowley, A. R.; Mountford, P. *Chem. Commun.* **2006**, No. 4, 436.
(15) Hayday, G. J.; Wang, C.; Rees, N. H.; Mountford, P. *Dalton Trans.* **2008**, No. 25, 3301.
(16) Sato, F.; Urabe, H.; Okamoto, S. *Chem. Rev.* **2000**, *100* (8), 2835.
(17) McLain, S. J.; Wood, C. D.; Schrock, R. R. *J. Am. Chem. Soc.* **1979**, *101* (16), 4558.
(18) Roskamp, E. J.; Pedersen, S. F. *J. Am. Chem. Soc.* **1987**, *109* (21), 6551.
(19) Bruck, A.; Copenhaver, A. S.; Wigley, D. E. *J. Am. Chem. Soc.* **1987**, *109*, 6525.
(20) Chang, K.-C.; Lu, C.-F.; Wang, P.-Y.; Lu, D.-Y.; Chen, H.-Z.; Kuo, T.-S.; Tsai, Y.-C. *Dalton Trans.* **2011**, *40* (10), 2324.
(21) Basuli, F.; Kilgore, U. J.; Brown, D.; Huffman, J. C.; Mindiola, D. J. *Organometallics* **2004**, *23* (26), 6166.
(22) Basuli, F.; Huffman, J. C.; Mindiola, D. J. *Inorganica Chim. Acta* **2007**, *360* (1), 246.
(23) Hamaki, H.; Takeda, N.; Tokitoh, N. *Organometallics* **2006**, *25* (10), 2457.
(24) Bai, G.; Wei, P.; Stephan, D. W. *Organometallics* **2006**, *25* (10), 2649.
(25) Gianetti, T. L.; Tomson, N. C.; Arnold, J.; Bergman, R. G. *J. Am. Chem. Soc.* **2011**, *133*, 14904.
(26) Gianetti, T. L.; La Pierre, H. S.; Arnold, J. *Eur. J. Inorg. Chem.* **2013**, *2013* (22–23), 3771.
(27) Gianetti, T. L.; Bergman, R. G.; Arnold, J. *Polyhedron* **2014**, *84*, 19.
(28) Steffey, B. D.; Chesnut, R. W.; Kerschner, J. L.; Pellechia, P. J.; Fanwick, P. E.; Rothwell, I. P. *J. Am. Chem. Soc.* **1989**, *111* (1), 378.
(29) Yu, J. S.; Fanwick, P. E.; Rothwell, I. P. *J. Am. Chem. Soc.* **1990**, *112* (22), 8171.
(30) Rothwell, I. P. *Chem. Commun.* **1997**, No. 15, 1331.
(31) Fryzuk, M. D.; Kozak, C. M.; Bowdridge, M. R.; Patrick, B. O.; Rettig, S. J. *J. Am. Chem. Soc.* **2002**, *124* (28), 8389.
(32) Figueroa, J. S.; Cummins, C. C. *J. Am. Chem. Soc.* **2003**, *125* (14), 4020.
(33) Figueroa, J. S.; Cummins, C. C. *Dalton Trans.* **2006**, No. 18, 2161.
(34) Kilgore, U. J.; Yang, X.; Tomaszewski, J.; Huffman, J. C.; Mindiola, D. J. *Inorg. Chem.* **2006**, *45* (26), 10712.
(35) Searles, K.; Carroll, P. J.; Chen, C.-H.; Pink, M.; Mindiola, D. J. *Chem. Commun.* **2015**, *51* (17), 3526.
(36) Gianetti, T. L.; Bergman, R. G.; Arnold, J. *Chem. Sci.* **2014**, *5* (6), 2517.
(37) Nechayev, M.; Gianetti, T. L.; Bergman, R. G.; Arnold, J. *Dalton Trans.* **2015**, *44* (45), 19494.
(38) Gianetti, T. L.; Nocton, G.; Minasian, S. G.; Kaltsoyannis, N.; Kilcoyne, A. L. D.; Kozimor, S. A.; Shuh, D. K.; Tyliszczak, T.; Bergman, R. G.; Arnold, J. *Chem. Sci.* **2015**, *6* (2), 993.
(39) Duncan, A. P.; Bergman, R. G. *Chem. Rec.* **2002**, *2* (6), 431.
(40) Hazari, N.; Mountford, P. *Acc. Chem. Res.* **2005**, *38* (11), 839.
(41) Cummins, C. C.; Baxter, S. M.; Wolczanski, P. T. *J. Am. Chem. Soc.* **1988**, *110*, 8731.
(42) Schaller, C. P.; Wolczanski, P. T. *Inorg. Chem.* **1993**, *32*, 131.
(43) Walsh, P. J.; Hollander, F. J.; Bergman, R. G. *J. Am. Chem. Soc.* **1988**, *110*, 8729.
(44) Walsh, P. J.; Baranger, A. M.; Bergman, R. G. *J. Am. Chem. Soc.* **1992**, *114*, 1708.

(45) Walsh, P. J.; Hollander, F. J.; Bergman, R. G. *Organometallics* **1993**, *12* (9), 3705.
(46) Meyer, K. E.; Walsh, P. J.; Bergman, R. G. *J. Am. Chem. Soc.* **1995**, *117* (3), 974.
(47) Anderson, L. L.; Arnold, J.; Bergman, R. G. *Org. Lett.* **2004**, *6*, 2519.
(48) Blake, A. J.; Collier, P. E.; Gade, L. H.; McPartlin, M.; Mountford, P.; Schubart, M.; Scowen, I. J. *Chem. Commun.* **1997**, No. 16, 1555.
(49) Dunn, S. C.; Hazari, N.; Cowley, A. R.; Green, J. C.; Mountford, P. *Organometallics* **2006**, *25* (7), 1755.
(50) Li, Y.; Shi, Y.; Odom, A. L. *J. Am. Chem. Soc.* **2004**, *126* (6), 1794.
(51) Basuli, F.; Aneetha, H.; Huffman, J. C.; Mindiola, D. J. *J. Am. Chem. Soc.* **2005**, *127* (51), 17992.
(52) Chu, J.; Lu, E.; Liu, Z.; Chen, Y.; Leng, X.; Song, H. *Angew. Chem. Int. Ed. Engl.* **2011**, *50* (33), 7677.
(53) Blake, R. E.; Antonelli, D. M.; Henling, L. M.; Schaefer, W. P.; Hardcastle, K. I.; Bercaw, J. E. *Organometallics* **1998**, *17* (4), 718.
(54) Gilbert, Z. W.; Hue, R. J.; Tonks, I. A. *Nat. Chem.* **2016**, *8* (1), 63.
(55) La Pierre, H. S.; Arnold, J.; Toste, F. D. *Angew. Chemie Int. Ed.* **2011**, *50*, 3900.
(56) La Pierre, H. S.; Arnold, J.; Bergman, R. G.; Toste, F. D. *Inorg. Chem.* **2012**, *51*, 13334.
(57) De With, J.; Horton, A. D.; Orpen, A. G. *Organometallics* **1993**, *12* (5), 1493.
(58) Cundari, T. R. *Organometallics* **1994**, *13* (8), 2987.
(59) O'Reilly, M. E.; Ghiviriga, I.; Abboud, K. A.; Veige, A. S. *J. Am. Chem. Soc.* **2012**, *134* (27), 11185.
(60) Basuli, F.; Tomaszewski, J.; Huffman, J. C.; Mindiola, D. J. *J. Am. Chem. Soc.* **2003**, *125* (34), 10170.
(61) Basuli, F.; Bailey, B. C.; Tomaszewski, J.; Huffman, J. C.; Mindiola, D. J. *J. Am. Chem. Soc.* **2003**, *125* (20), 6052.
(62) Basuli, F.; Bailey, B. C.; Brown, D.; Tomaszewski, J.; Huffman, J. C.; Baik, M.-H.; Mindiola, D. J. *J. Am. Chem. Soc.* **2004**, *126* (34), 10506.

Chapter 2

Nitrene Metathesis and Catalytic Nitrene Transfer Promoted by Niobium Bis(imido) Complexes

Introduction

Since the initial discovery of C-H activations and cycloadditions across terminal zirconium imido π-bonds in 1988,[1] a number of nitrene transfer processes involving reactions across metal-nitrogen multiple bonds, especially those in high-valent group IV complexes have been explored.[2,3] Many of these systems have been shown to undergo cycloadditions with a variety of unsaturated substrates.[2-4] This reactivity has been developed into useful redox-neutral catalytic nitrene transfer processes including hydroaminations[2,5] and carboaminations[6] as well as imine[7] and azide[8] metatheses. In contrast to group IV systems, relatively few studies have focused on reactions across imido groups in group III[9] and group V systems.[10-12] While group IV imido systems have been well developed as catalysts for redox-neutral transformations, limited examples of *stoichiometric* oxidative nitrene transfers[13] and only two examples of *catalytic* oxidative nitrene transfer using group IV catalysts have been reported.[14]

In our efforts to design group V systems that are reactive across metal-nitrogen multiple bonds, we have been investigating niobium and tantalum imido complexes supported by β-diketiminate (BDI) ligands.[15] We have found that the BDI imido ligand system is able to support niobium in both low and high valent states, in two cases, even within catalytic cycles. While we found that the imido group behaves purely as an ancillary ligand for a variety of low and high-valent mono(imido) derivatives, we hypothesized that introduction of a *second* imido moiety could enhance the reactivity of the imido groups. This 'π-loading' effect results from interactions of multiple ligand-based p orbitals with the same metal-based d orbital, which causes a net decrease in bonding character of the HOMO.[12,15b,16] We recently reported a synthetic route to a series of four-coordinate niobium bis(imido) complexes,[11] and we aimed to take advantage of both reactivity across imido groups as well as two-electron redox reactivity in these systems in order to carry out catalytic oxidative nitrene transfer chemistry. Herein we report the novel stoichiometric and catalytic reactivity of these niobium bis(imido) complexes with alkyl and aryl isonitriles.

Results and Discussion

Niobium bis(imido) complexes **2.2 – 2.4** were prepared by reaction of the Nb(III) precursor **1** with azides RN_3 (R = 2,6-Dipp, ^{t}Bu, TMS) (Scheme 2.1). While the synthesis of compounds **2.2** and **2.4** has been previously described, the route described here offered access to these compounds in higher yield and purity. Moreover, the N-TMS derivative, compound **2.3**, was prepared for the first time using this route.

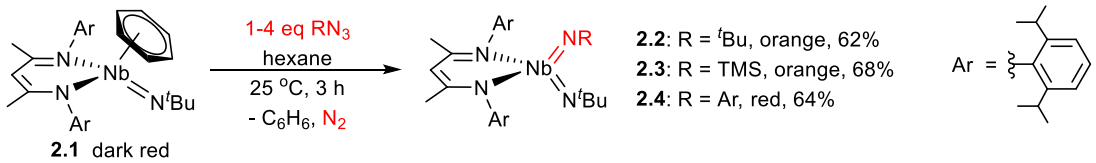

Scheme 2.1 Synthesis of niobium bis(imido) compounds from a Nb(III) precursor.

Compound **2.3** was characterized by ^{1}H NMR spectroscopy and single crystal X-ray diffraction; like compound **2.4**, it exhibited C_s symmetry in solution and nearly perfect C_s symmetry in the solid state (Figure 1). Notably, the Nb-N(3)-C(30) angle is 155.9(1)˚, making this

the most bent terminal imido group reported for a niobium complex apart from limited examples in which the imido group is a part of a larger chelate system that constrains its geometry. In contrast, the Nb-N(4)-Si angle is nearly linear at 171.32(8)˚; the reason the TMS imido moiety is much more linear than the ^{t}Bu imido moiety may be a π component to the bonding between the nitrogen and the silicon center, but since the silicon center is nearly perfectly tetrahedral, the discrepancy in the bond angles is more likely simply caused by crystal packing effects. The average Nb-N-C angles for compounds **2.2** and **2.4** are also less linear than for most other terminal niobium imido compounds in the literature. The Nb-N(3) and Nb-N(4) distances observed in **2.3** of 1.794(1) Å and 1.819(1) Å, respectively, are relatively long for terminal imido groups, and similar to those of compounds **2.2, 2.4**, as well as other terminal niobium(V) bis(imido) compounds. This lengthening of the Nb-N bonds and bending of the imido groups is consistent with a π-loading effect in which the imido groups are activated toward reactivity.

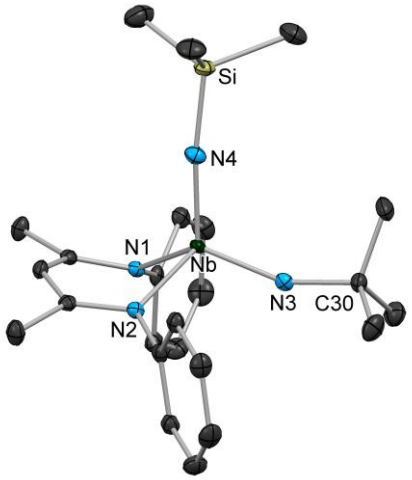

Figure 2.1 Molecular structure of **2.3** determined by X-ray diffraction. H atoms and aryl ^{i}Pr groups have been omitted for clarity; thermal ellipsoids are displayed at the 50% probability level. Selected bond lengths (Å): Nb-N(1): 2.122(1), Nb-N(2): 2.121(1), Nb-N(3): 1.794(1), Nb-N(4): 1.819(1). Selected bond angles (˚): N(1)-Nb-N(2): 92.19(5), N(1)-Nb-N(3): 115.21(5), N(1)-Nb-N(4): 113.34(5), N(2)-Nb-N(3): 107.83(5), N(2)-Nb-N(4): 112.92(5), N(3)-Nb-N(4): 113.40(6), Nb-N(3)-C(30): 155.9(1), Nb-N(4)-Si: 171.32(8).

Addition of 2,6-dimethylphenylisocyanide (XylNC) to a solution of **2.2** resulted in slight lightening of the color of the orange solution; ^{1}H NMR spectroscopic and crystallographic analysis of the yellow crystals (Figure 2.2, left) obtained from this reaction were consistent with isocyanide adduct **2.2·XylNC**. Upon heating to 60 °C for 2.5 h, a yellow solution of **2.2·XylNC** in toluene underwent a color change to give an orange solution from which bright orange crystals were isolated. NMR spectroscopic and crystallographic data indicated clean conversion to **2.5a**, in which the nitrene fragments from one *tert*-butylimido group and the coordinated isonitrile were exchanged to generate a complex containing a thermodynamically-favored aryl(imido) ligand with coordinated ^{t}BuNC (Scheme 2.2). The X-ray crystal structure of **2.5a** (Figure 2.2, middle) showed a geometry intermediate between trigonal bipyramidal and square pyramidal ($\tau = 0.41$);[17] a similar geometry was observed for **2.2·XylNC** ($\tau = 0.47$). Notably, clean conversion of **2.2·XylNC** to **2.5a**

was also observed by heating solid **2.2·XylNC** to 80 °C for 12 h. While reactions of early transition metal imido complexes with isocyanides across imido groups have been documented in the literature, these reactions typically lead to either coupling of multiple equivalents of isocyanide after addition,[4c,4e] formation of η^2-carbodiimide complexes,[4a] or production of carbodiimide.[13b,14a] To our knowledge, the conversion of **2.2** to **2.5** is the first example in which the nitrene fragments are simply exchanged to generate a new imido group and a new isocyanide. Hence, this represents a new method for both incorporation of imido moieties into metal complexes and integration of various substituents into isonitriles.

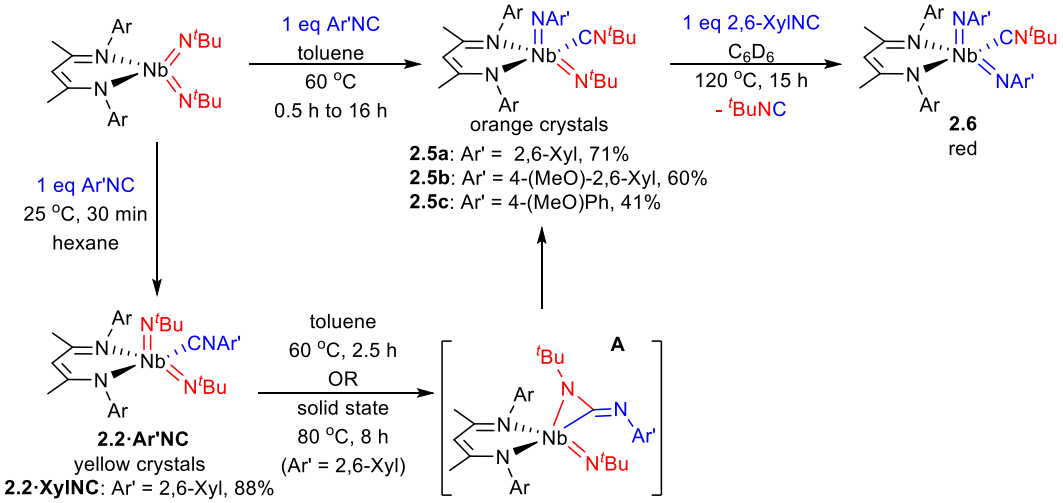

Scheme 2.2 Nitrene metathesis of arylisocyanide substrates with niobium imido groups.

Although it still contained a basic *tert*-butylimido group, **2.5a** was much less reactive toward nitrene metathesis than **2.2**; addition of a second equivalent of XylNC to **2.5a** resulted in establishment of an equilibrium between ^{t}BuNC and XylNC adducts, but heating to 120 °C for 15 h was required to exchange the remaining *tert*-butylimido group, generating one equivalent of free ^{t}BuNC and a new niobium compound identified as BDINb(NXyl)$_2$CN^{t}Bu (**2.6**) by ^{1}H and ^{13}C NMR spectroscopy.

Compound **2.2** reacted with 4-methoxy substituted arylisocyanides to give compounds **2.5b** and **2.5c** as shown in Scheme 2. Formation of **2.5b** proceeded much more slowly than formation of **2.5a**; addition of 4-methoxy-2,6-dimethylphenylisocyanide (MeOXylNC**)** to a solution of **2** again resulted in immediate formation of adduct **2.2·MeOXylNC**, but heating to 60 °C for 16 h was required to observe 95% conversion to **2.5b** by ^{1}H NMR spectroscopy. In contrast, **2.2·XylNC** underwent 95% conversion to **5a** after heating to 60 °C for 2 h**.** This observation can be rationalized by the fact that the donating 4-methoxy substituent increases electron density at the isocyanide carbon, making it a less electrophilic target for nucleophilic attack by an imido moiety. Conversely, formation of **2.5c** proceeded significantly faster than formation of either **2.5a** or **2.5b** (>95% conversion within 0.5 h at 60 °C), indicating both that a) the rate-determining transition state is relatively sterically encumbered compared to the starting isocyanide adduct and b) reducing the steric profile of the isocyanide by eliminating the *o*-methyl substituents has a more pronounced effect on the reaction rate than adding a donating *p*-methoxy substituent.

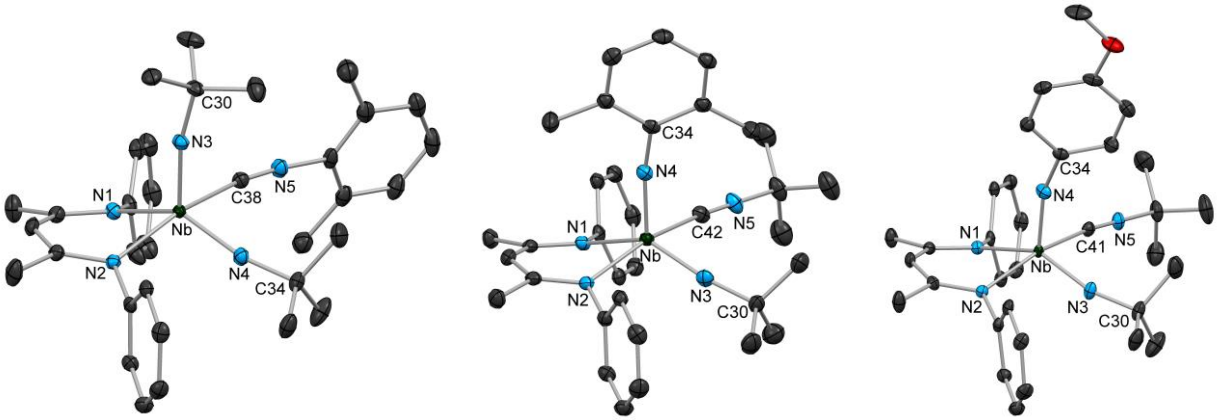

Figure 2.2 Molecular structures of **2.2·XylNC** (left), **2.5a** (middle), and **2.5c** (right) determined by X-ray diffraction. H atoms and aryl ^{i}Pr groups have been omitted for clarity; thermal ellipsoids are displayed at the 50% probability level. For **2.2·XylNC** (left), selected bond lengths (Å): Nb-N(1): 2.276(1), Nb-N(2): 2.207(1), Nb-N(3): 1.810(1), Nb-N(4): 1.814(1), Nb-C(38): 2.271(2); selected bond angles (˚): N(2)-Nb-C(38): 161.16(5), N(1)-Nb-N(4): 133.12(6), Nb-N(3)-C(30): 167.6(1), Nb-N(4)-C(34): 168.2(1), Nb-C(38)-N(5): 167.3(1). For **2.5a** (middle), selected bond lengths (Å): Nb-N(1): 2.265(2), Nb-N(2): 2.198(2), Nb-N(3): 1.812(2), Nb-N(4): 1.826(2), Nb-C(42): 2.274(2); selected bond angles (˚): N(2)-Nb-C(42): 160.53(7), N(3)-Nb-N(4): 136.14(7), Nb-N(3)-C(30): 170.3(2), Nb-N(4)-C(34): 167.3(2), Nb-C(42)-N(5): 170.2(2). For **2.5c** (right), selected bond lengths (Å): Nb-N(1): 2.282(1), Nb-N(2): 2.199(1), Nb-N(3): 1.802(1), Nb-N(4): 1.820(1), Nb-C(41): 2.289(2); selected bond angles (˚): N(2)-Nb-C(41): 159.46(6), N(1)-Nb-N(3): 137.94(6), Nb-N(3)-C(30): 165.4(1), Nb-N(4)-C(34): 160.9(1), Nb-C(41)-N(5): 171.1(2).

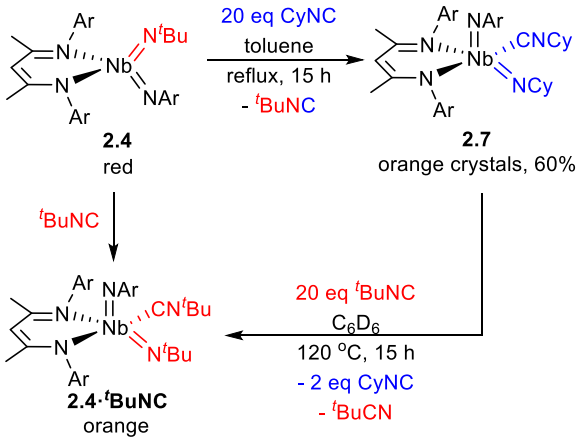

Scheme 2.3 Reversible nitrene metathesis reactivity with alkylisocyanide substrates.

While no evidence of nitrene metathesis was observed from reactions of alkyl-substituted isocyanides with **2.2** (see below), the mixed aryl/alkyl bis(imido) complex **2.4** reacted with alkylisocyanides to generate ^{t}BuNC and exchange the alkyl substituent into the imido position. The reaction with cyclohexylisocyanide (CyNC) was particularly clean, and compound **2.7** was isolated after heating a solution of **2.4** in refluxing toluene in the presence of excess CyNC for 15

h (Scheme 2.3). Heating isolated **2.7** to 120 °C in the presence of excess ^{t}BuNC resulted in conversion to **2.4·^{t}BuNC** identified by ^{1}H NMR and prepared independently from coordination of ^{t}BuNC to **2.4**. Interestingly, during the course of this reaction, a significant amount of ^{t}BuNC was isomerized to unreactive ^{t}BuCN, hampering conversion of **2.7** to **2.4·^{t}BuNC**. This isomerization did not occur in the absence of the niobium complex, indicating it was likely metal-catalyzed; limited examples of this metal-catalyzed process exist in the literature.[16]

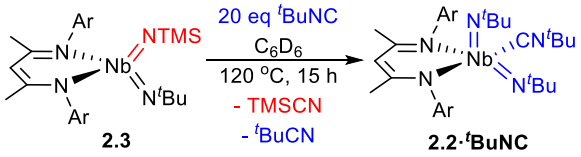

Scheme 2.4 Nitrene metathesis converting **2.3** to **2.2·^{t}BuNC**.

While reactions with **2.3** were not explored in as much detail due to a lack of selectivity between reactions across TMS and ^{t}Bu imido groups leading to mixtures of products, **2.3** did react with a large excess of ^{t}BuNC on heating to 120 °C for 15 h to give **2.2·^{t}BuNC** (Scheme 2.4). In this case, isomerization of ^{t}BuNC to ^{t}BuCN was also observed, halting the reaction to give **2.2·^{t}BuNC** after ~ 60% conversion.

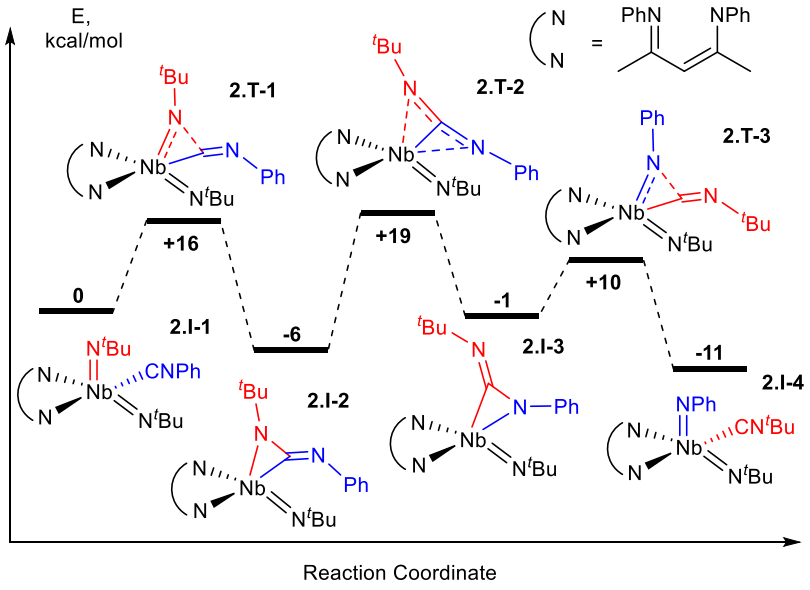

Figure 2.3 DFT calculated energy profile for nitrene metathesis.

DFT calculations provided support for the proposed mechanistic pathway shown in Figure 2.3. Coordinated isocyanide first adds across an imido moiety in **2.I-1** to give η^2-carbodiimide intermediate **2.I-2**, as has precedent in the literature.[4a,13b,14a] The lowest energy pathway found for the following step involves passing through the nearly linear η^3-carbodiimide-like transition state **2.T-2** to give **2.I-3**, which then proceeds to give the thermodynamically favored product **2.I-4** by the reverse of the first step. While the highest energy transition state **2.T-2** is 25 kcal/mol higher in energy than intermediate **2.I-2**, it is not unreasonable that this process could proceed readily at

60 °C. In fact, neither intermediates **2.I-2** nor **2.I-3** are observed experimentally when the reaction is followed by ^{1}H NMR spectroscopy, indicating they are likely higher in energy than the calculated values relative to **2.I-1**. Diisopropylphenyl substituents were modeled as phenyl substituents in the calculations, so this discrepancy is not surprising, as **2.I-2** and **2.I-3** are much more prone to steric clashing with BDI aryl groups than **2.I-1** since the imido and isocyanide substituents of **2.I-1** are nearly 180° from the metal center. Calculated reaction pathways for analogs incorporating 4-MeOPh and 2,6-Xyl isocyanide substituents are shown in Figure 2.8 in the experimental section (see below), and are consistent with the experimentally observed influence of electron donating ability and steric bulk of the isocyanide aryl substituent on reaction rate (see above).

Reaction of **2.2** with primary alkylisocyanides AkNC (Ak = ^{n}Bu, Bn) resulted in color changes to red-brown solutions. In both cases, conversion to a single major niobium-containing product was observed by ^{1}H NMR spectroscopy, within 12 h for Ak = ^{n}Bu or within 20 min for Ak = Bn. In contrast to reactions with arylisocyanides, both reactions proceeded at room temperature without any generation of ^{t}BuNC; instead, in each case, generation of one equivalent of the organic product AkN=C=N^{t}Bu (Ak = ^{n}Bu, Bn) was observed.

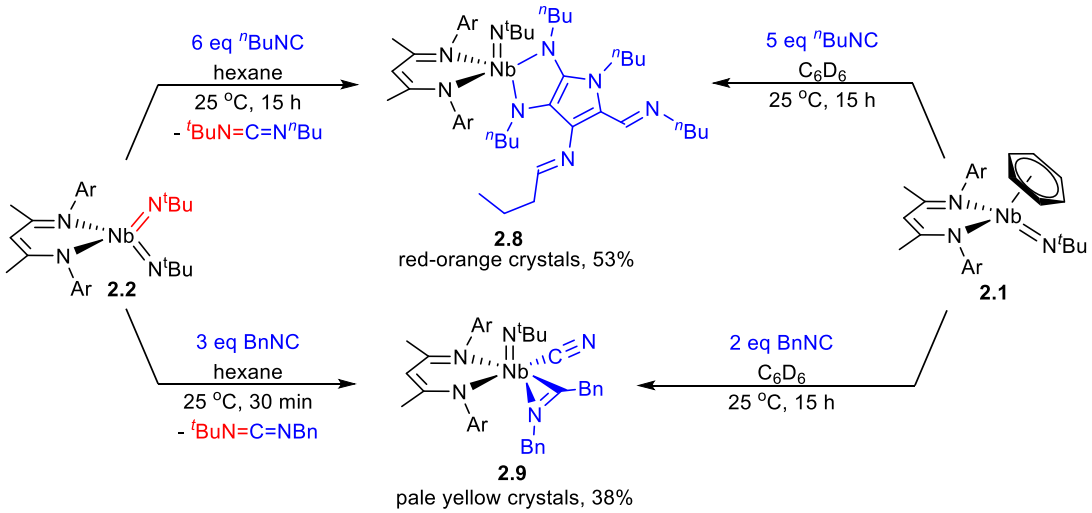

Scheme 2.5 Release of carbodiimides and formation of **2.8** and **2.9** upon reaction of **2.2** with alkylisocyanides (left) and production of **2.8** and **2.9** from Nb(III) precursor **2.1** (right).

Remarkably, compound **2.2** reacted with *six* equivalents of ^{n}BuNC to release one equivalent of ^{n}BuN=C=N^{t}Bu and give compound **2.8** as red-orange microcrystalline material in 53% yield (Scheme 2.5, top). The reaction to give **2.8** involved the formation of four new C-C bonds and a C-N bond to generate a heavily substituted κ^2-N,N-pyrrolediamido ligand. The solid-state structure (Figure 2.4, left) showed a distorted square pyramidal geometry ($\tau = 0.1$) with the imido moiety in the apical position. While related couplings of isocyanides by reduced metal centers have been observed,[19] to our knowledge this is the first example of formation of a pyrrole-diamido transition metal complex. A related reaction occurred between **2.2** and three equivalents benzylisocyanide (BnNC) to give **2.9**, which precipitated from the reaction mixture within minutes as pale yellow needles (Scheme 2.5, bottom). Compound **2.9** has also been characterized crystallographically

(Figure 2.4, right). In order to give **2.9**, a benzyl group transferred from one equivalent of isocyanide to another to give a C-bound terminal cyanide ligand and an η^2-iminoacyl ligand.

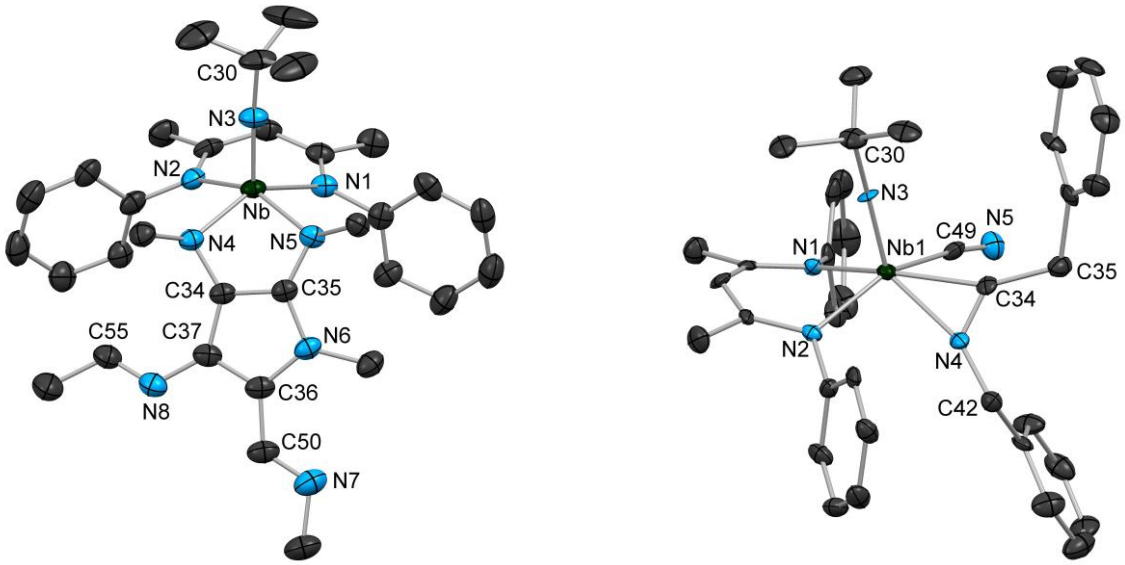

Figure 2.4 Molecular structures of **2.8** (left) and **2.9** (right) determined by X-ray diffraction. H atoms, aryl ^{i}Pr groups, a molecule of toluene that co-crystallized with **2.9** and a second crystallographically inequivalent molecule of **2.9** have been omitted and ^{n}alkyl groups in **2.8** have been truncated for clarity; thermal ellipsoids are displayed at the 50% probability level. For **2.8** (left), selected bond lengths (Å): Nb-N(1): 2.266(3), Nb-N(2): 2.281(3), Nb-N(3): 1.760(3), Nb-N(4): 2.037(3), Nb-N(5): 2.063(3), N(4)-C(34): 1.399(4), N(5)-C(35): 1.369(4), C(34)-C(35): 1.403(5), C(35)-N(6): 1.391(5), N(6)-C(36): 1.398(5), C(36)-C(37): 1.392(5), C(34)-C(37): 1.431(5), C(36)-C(50): 1.446(5), C(50)-N(7): 1.270(5), C(37)-N(8): 1.397(5), N(8)-C(55): 1.261(5); selected bond angles (˚): N(2)-Nb-N(5): 151.5(1), N(1)-Nb-N(4): 145.5(1), N(4)-Nb-N(5): 83.3(1), N(3)-Nb-N(4): 108.7(1), N(3)-Nb-N(5): 103.9(1), Nb-N(4)-C(34): 98.0(2), Nb-N(5)-C(35): 98.5(2), C(37)-N(8)-C(55): 120.0(3), C(36)-C(50)-N(7): 125.4(4). For **2.9** (right), selected bond lengths (Å): Nb(1)-N(1): 2.212(6), Nb(1)-N(2): 2.179(6), Nb(1)-N(3): 1.768(6), Nb(1)-N(4): 2.174(6), Nb(1)-C(34): 2.105(7), Nb(1)-C(49): 2.282(8), N(4)-C(34): 1.263(9), C(49)-N(5): 1.145(8); selected bond angles (˚): N(2)-Nb(1)-C(49): 150.3(3), N(1)-Nb(1)-C(34): 148.1(2), Nb(1)-N(3)-C(30): 171.6(6), Nb(1)-C(49)-N(5): 171.9(7), Nb(1)-N(4)-C(42): 162.6(5), Nb(1)-C(34)-C(35): 155.5(6), N(4)-C(34)-C(35): 128.4(7), C(34)-N(4)-C(42): 127.4(7).

A proposed mechanism for the formation of both **2.8** and **2.9** is outlined in Scheme 2.6. **2.2·AkNC** and η^2-carbodiimide intermediate **2.B** likely exist in equilibrium, although only **2.2·AkNC** is observed in solution. Intermediate **2.B** can release carbodiimide to generate a Nb(III) intermediate that is trapped by additional isocyanide to give Nb(III) isocyanide adduct **2.C**. Two isocyanide ligands then undergo reductive coupling to give η^2-N,C-1,2-diiminoethylene complex **2.D**.[19] This complex readily undergoes insertion of another equivalent of isocyanide into the Nb-C bond to give **2.E**, followed by insertion of yet another equivalent of isocyanide to give **2.F**. At some point during the reaction, a 1,5-sigmatropic hydride shift occurs; although it is depicted after net reaction with 5 equiv. of isocyanide in order to generate **2.G**, this could also occur after either

the previous or following steps in the mechanism. Insertion of a final equivalent of isocyanide results in formation of the six-membered metallacyclic intermediate **2.H**, which then reductively eliminates in order to form a five-membered organic heterocycle which binds in a κ^2-N,N fashion to the resulting Nb(III) center in order to give **2.I**. A two-electron transfer from the niobium center to the ligand results in aromatization of the ligand to give the κ^2-N,N-pyrrolediamidoniobium(V) product **2.8**. Starting from intermediate **2.C**, formation of **2.9** results from transfer of a benzyl group from one isocyanide equivalent to another to give a C-bound terminal cyanide ligand and an η^2-iminoacyl ligand, which presumably occurs faster for Ak = Bn than reductive C-C coupling.

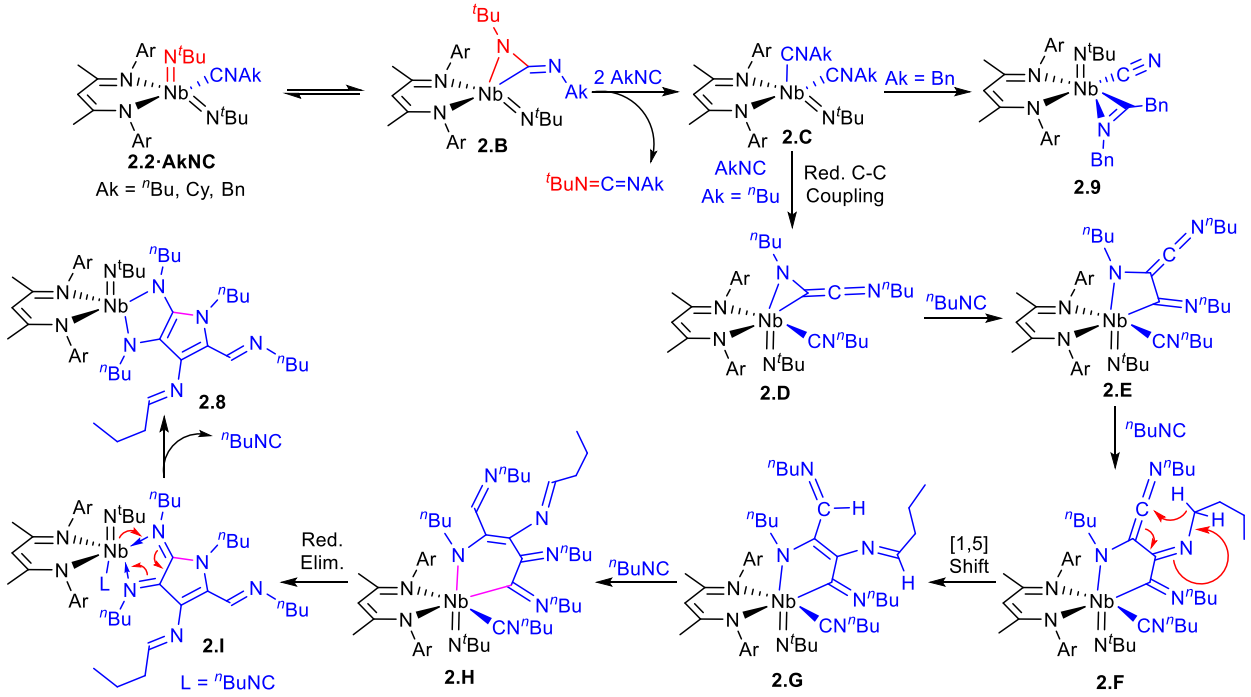

Scheme 2.6 Proposed mechanism for formation of compounds **2.8** and **2.9**.

Several pieces of experimental evidence support that these reactions proceed through Nb(III) intermediates. First, the same products **2.8** and **2.9** were observed from the reactions of Nb(III) complex **2.1** with either five equivalents ^{n}BuNC or two equivalents BnNC (Scheme 2.5, right). Second, addition of one equivalent BnNC to **2.2** to give **2.2·BnNC** followed by addition of three equivalents 2,6-XylNC resulted in immediate color change to green-blue and a ^{1}H NMR spectrum consistent with formation of the reported Nb(III) complex **2.10** and release of carbodiimide (Scheme 2.7).[12c]

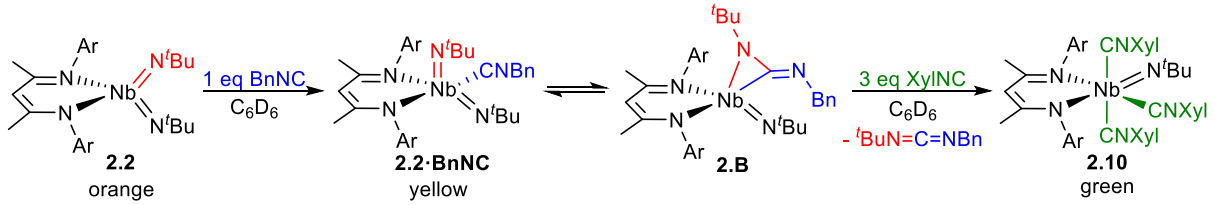

Scheme 2.7 Trapping of a Nb(III) intermediate with 2,6-XylNC.

Based on these results, it seemed plausible that the Nb(III) intermediate generated in these reactions could be trapped by an azide to regenerate the 4-coordinate bis(imido) starting material, thus rendering the formation of carbodiimide catalytic. In fact, within seconds at room temperature, addition of excess $^{t}BuN_3$ to a solution of **2.2·BnNC** resulted in color change from yellow-orange to orange consistent with conversion to the 4-coordinate bis(imido) complex **2.2**. Conversion to **2.2** and production of BnN=C=N^{t}Bu was confirmed by ^{1}H NMR spectroscopy and GC-MS. Similarly, generation of **2.2** and the corresponding carbodiimide was observed after adding excess $^{t}BuN_3$ to **2.2·^{n}BuNC** or **2.2·CyNC**, although reaction with **2.2·^{n}BuNC** only proceeded within 12 h at room temperature and reaction with **2.2·CyNC** required heating at 60 °C for 15 h to go to completion. No formation of carbodiimide was observed with ^{t}BuNC even at temperatures up to 120 °C. Catalytic reactions were carried out in J. Young valve NMR tubes using mixtures of C_6D_6 and $^{t}BuN_3$ as solvent and following the conversion to carbodiimide by ^{1}H NMR spectroscopy; higher turnover numbers were observed when the catalytic reactions were carried out in the presence of a large excess (~ 200 equivalents) of $^{t}BuN_3$. Up to 17 turnovers (6% cat. loading) were observed for Ak = Cy (20 h at 80 °C) before complete catalyst degradation, while lower turnover numbers (5-8 turnovers) were observed for Ak = Bn and Ak = ^{n}Bu.

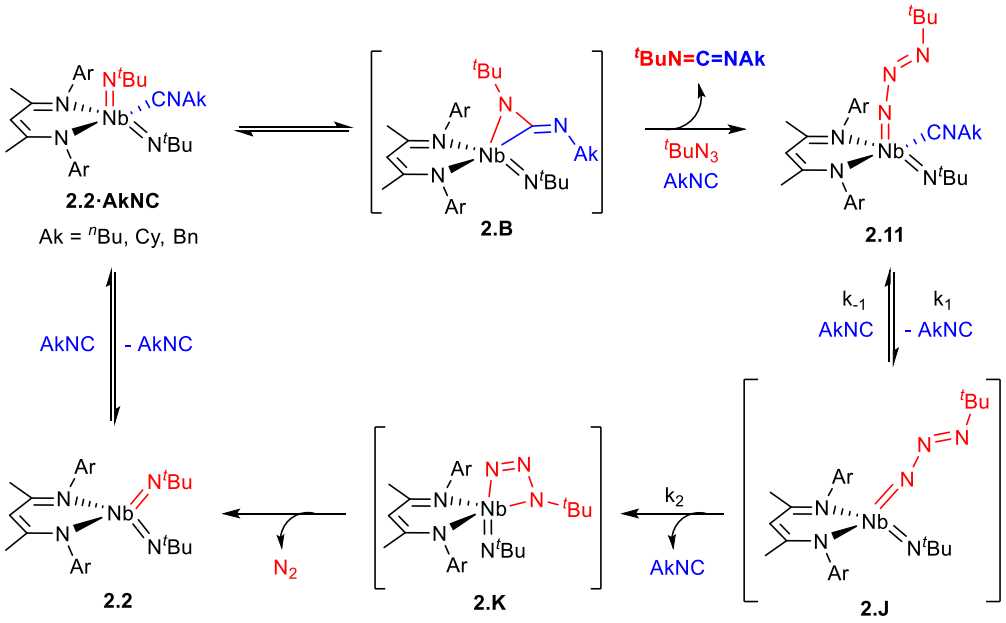

Scheme 2.8 Proposed mechanism for catalytic nitrene transfer to give asymmetric dialkylcarbodiimides.

The catalytic reactions likely proceeded via the mechanism outlined in Scheme 2.8. Notably, buildup of an intermediate was observed by ^{1}H NMR spectroscopy under the catalytic conditions. The intermediate was especially prominent for Ak = ^{n}Bu; in fact, upon leaving a solution containing **2.2·^{n}BuNC**, four additional equivalents ^{n}BuNC, and 17 equivalents $^{t}BuN_3$ at room temperature for 16 h, complete conversion of **2.2·^{n}BuNC** to this new species was observed (Scheme 2.9). The product of this reaction was isolated in 61% yield and identified by X-Ray crystallography and NMR spectroscopy as the terminal *tert*-butylazidoniobium complex **2.11**. A

representation of the crystal structure is shown in Figure 2.5. The Nb-N(5) distance is 1.849(2) Å and the Nb-N(5)-N(6) angle is 153.6(2)˚, consistent with a Nb-N interaction that is intermediate between a double and triple bond. Moreover, the N(5)-N(6) distance is 1.324(3) Å, intermediate between a typical N-N single bond and N-N double bond, while the N(6)-N(7) distance is 1.261(3) Å, in agreement with a N-N double bond, thus consistent with the azide ligand engaging the niobium center as a dianionic X_2L ligand.

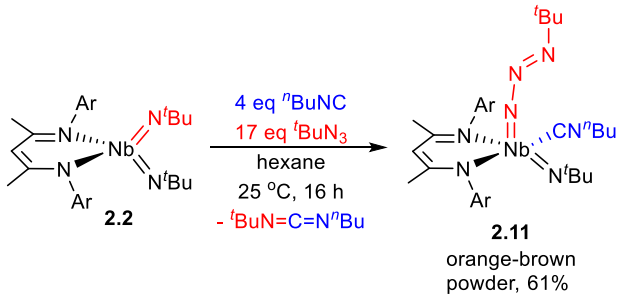

Scheme 2.9 Preparation of a terminal alkylazidoniobium complex.

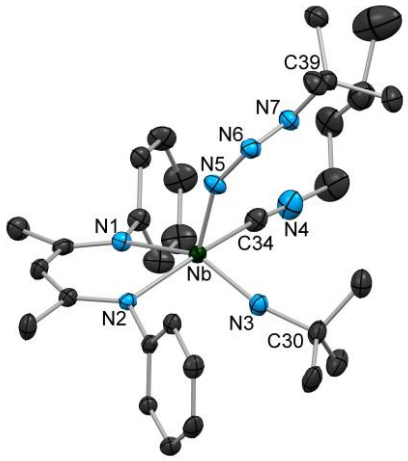

Figure 2.5 Molecular structure of **2.11** determined by X-ray diffraction. H atoms and aryl ^{i}Pr groups have been omitted for clarity; thermal ellipsoids are displayed at the 50% probability level. Selected bond lengths (Å): Nb-N(1): 2.262(2), Nb-N(2): 2.205(2), Nb-N(3): 1.788(2), Nb-N(5): 1.849(2), Nb-C(34): 2.260(3), N(5)-N(6): 1.324(3), N(6)-N(7): 1.261(3). Selected bond angles (˚): N(2)-Nb-C(34): 163.28(8), N(1)-Nb-N(3): 138.03(8), Nb-N(3)-C(30): 165.9(2), Nb-C(48)-N(5): 173.9(2), Nb-N(4)-C(42): 176.8(3), Nb-N(5)-N(6): 153.6(2), N(5)-N(6)-N(7): 115.5(2), N(6)-N(7)-C(39): 113.3(2).

Compound **2.11** represents the first characterized example of a terminal organoazido niobium complex, but sparse examples of other terminal organoazidometal species exist in the literature.[20] In one notable example,[20c] detailed mechanistic studies have shown that a related phenylazidotantalum complex is an intermediate species in nitrene transfer from an azide to a low-valent tantalum center, and that nitrene transfer to generate an imido group and release N_2 goes through a 4-centered intermediate analogous to **2.K** (Scheme 2.8). Similarly, isolated **2.11** slowly

converts to **2.2·^{n}BuNC** and N_2 in solution and is also a competent catalyst for carbodiimide formation. In order to probe the mechanism, the kinetics of conversion from **2.11** to **2.2·^{n}BuNC** were followed by ^{1}H NMR spectroscopy. The reaction followed clean first order kinetics in **2.11** (Figure 2.6, left), and an Eyring analysis was carried out using kinetic data collected over a temperature range from 40 ˚C to 50 ˚C (Figure 2.6, right). From the Eyring analysis, the enthalpy and entropy of activation were found to be +30(1) kcal/mol and +21(3) cal/(K·mol), respectively. The large positive entropy of activation was indicative of dissociation of isocyanide from **2.11** being an important step in the reaction rate, but not necessarily the rate-determining step. In the presence of excess ^{n}BuNC, the reaction proceeded much more slowly, indicating that isocyanide reversibly dissociates from **2.11**, establishing an equilibrium with intermediate **2.J** (Scheme 2.8). In contrast, if dissociation of isocyanide was irreversible and rate-determining, the reaction rate would be unaffected by addition of excess isocyanide.

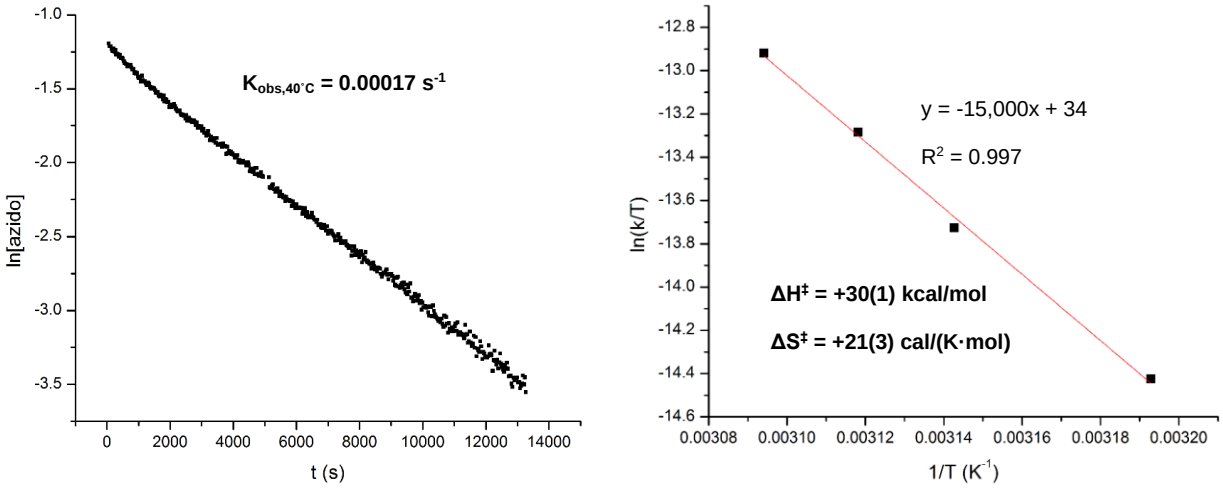

Figure 2.6 Left: plot of ln[**2.11**] versus time at 40 ˚C showing first order dependence on [**2.11**]. Right: Eyring plot for the conversion of **2.11** to **2.2·^{n}BuNC** and activation parameters derived from the Eyring plot.

Applying the steady state approximation (asserting that d[**2.J**]/dt = 0), the following rate equation can be derived:

$$d[\mathbf{2.2\cdot^{n}BuNC}]/dt = k_1k_2[\mathbf{2.11}]/(k_2 + k_{-1}[^n\text{BuNC}]) \qquad \text{Eq 1}$$

where $K = k_1/k_{-1}$ is the equilibrium constant for **2.11** and **2.J** + ^{n}BuNC and k_2 is the rate constant for a subsequent rate-determining irreversible step which likely proceeds through intermediate **2.K**, although further experiments are needed in order to confirm.

While a handful of mid and late transition metal catalysts for catalytic carbodiimide formation have been reported,[21] this represents only the second example mediated by an early metal complex.[14a] In the previous example, the Zr center remained in its more stable Zr(IV) oxidation state throughout the cycle, while 2-electron redox changes were mediated by a redox-active ligand. In the present case, the energy difference between high valent Nb(V) and low valent Nb(III) is small enough that reductive elimination of η^2-carbodiimide occurs readily in the presence of either

an alkylazide or excess isocyanide. As demonstrated here and in our previous work,[15e,15f] a niobium center with a suitable ligand environment can both give access to the unique reactivity observed for early transition metal complexes and allow cycling between Nb(III) and Nb(V) in catalytic processes.

Summary and Conclusions

To summarize, we have discovered a novel nitrene exchange process in which a substituent is exchanged between an alkylimido group in a Nb(V) bis(imido) complex and an arylisocyanide. The reaction likely proceeds through cycloaddition and cycloreversion involving Nb(V) η^2-carbodiimide intermediates, and occurs at a single metal center without elimination of carbodiimide. In contrast, reaction with unhindered alkylisocyanides resulted in extrusion of dialkylcarbodiimide, a process that was rendered catalytic in the presence of excess azide. This represented a rare example of oxidative nitrene transfer promoted by an early transition metal complex, in which reactivity across an imido group and two-electron metal-based redox chemistry are used in tandem to effect catalytic turnover. Further exploration of the scope and mechanism of stoichiometric and catalytic nitrene transfer processes is ongoing.

Experimental

General Considerations: Unless otherwise noted, all reactions were performed using standard Schlenk line techniques or in an MBraun inert atmosphere glove box under an atmosphere of nitrogen (<1 ppm O_2/H_2O). Glassware and Celite were stored in an oven at ca. 140˚ C. Molecular sieves (4 Å) were activated by heating to 300 °C overnight under vacuum prior to storage in a glovebox. Hexane, n-pentane, diethyl ether, dichloromethane, benzene, toluene, pyridine, and THF were purified by passage through columns of activated alumina and degassed by sparging with nitrogen. HMDSO was vacuum distilled from sodium/benzophenone, degassed by sparging with nitrogen, and stored over molecular sieves. ^{t}BuNH$_2$ was distilled from CaH_2. Deuterated solvents were vacuum-transferred from sodium/benzophenone, degassed with three freeze-pump-thaw cycles, and stored over molecular sieves. Azides were degassed with three freeze-pump-thaw cycles and filtered through activated alumina. Isocyanides were degassed with three freeze-pump-thaw cycles and stored over molecular sieves. NMR spectra were recorded on Bruker AV-600, AVB-400, AVQ-400, AV-500, and DRX-500 spectrometers. ^{1}H and ^{13}C{^{1}H} chemical shifts are given relative to residual solvent peaks. Proton and carbon NMR assignments were routinely confirmed by ^{1}H-^{1}H (COSY and NOESY) and ^{1}H-^{13}C (HSQC and HMBC) experiments. FT-IR samples were prepared as Nujol mulls and were taken between KBr disks using a Nicolet iS10 FT-IR spectrometer. Melting points were determined using an OptiMelt automated melting point system. ^{t}BuN$_3$,[22] DIPPN$_3$,[23] MeOXylNH$_2$ (MeOXyl = 4-MeO-2,6-Me$_2$C$_6$H$_2$),[24] MeOXylNC,[25] HBDI,[26] Li(BDI)•OEt$_2$,[27] Nb(N^{t}Bu)Cl$_3$Py$_2$,[28] (BDI)Nb(N^{t}Bu)Me$_2$,[15b] and (BDI)Nb(N^{t}Bu)(η^6-C$_6$H$_6$) (**2.1**)[15d] (BDI = ArNC(Me)CHC(Me)NAr, Ar = 2,6-diisopropylphenyl) were prepared using the literature procedures. All other reagents were acquired from commercial sources and used as received. Elemental analyses were determined either at the College of Chemistry, University of California, Berkeley or at the School of Human Sciences, Science Center, London Metropolitan University. X-ray structural determinations were performed at CHEXRAY, University of California, Berkeley on a SMART APEX II QUAZAR Diffractometer.

(BDI)Nb(N^{t}Bu)$_2$ (2.2): An alternative procedure for synthesizing **2.2** has been reported previously;[11] the following presents a preferred synthetic method. Compound **2.1** (2.6 g, 4.0 mmol) was added to a 20 mL vial. In a separate vial, *tert*-butylazide (1.6 mL, 1.4 g, 14 mmol) was dissolved in 12 mL hexane. The *tert*-butylazide solution was added to **2.1** in one portion, and the mixture was stirred until all of **2.1** had dissolved. Upon addition of the azide solution, visible effervescence of dinitrogen was observed, but subsided within 5 min. The vial was left uncapped for ca. 15 min and then was capped and left at 25 °C for an additional 3 h, resulting in a color change from dark red to lighter red-brown. The mixture was filtered through a pad of Celite to give a red-brown solution. The volatile materials were removed under vacuum and the red-brown residue was washed with 7 mL HMDSO to give an orange powder and a red-brown supernatant. The supernatant was removed by pipette and compound **2.2** was isolated as an orange powder and residual solvent was removed under vacuum (1.6 g, 62%). Spectroscopic data were consistent with previously recorded data for **2.2**.[11]

(BDI)Nb(N^{t}Bu)(NTMS) (2.3): Compound **2.1** (1.0 g, 1.5 mmol) was added to a 100 mL flask and dissolved in 10 mL benzene to give a dark red solution. Azidotrimethylsilane (0.8 mL) was added in one portion by pipette. The solution was stirred at 60 ˚C for 1.5 h, resulting in a color change from dark red to lighter red. The volatile materials were removed under vacuum, leaving a red-orange residue. The residue was extracted with hexanes and concentrated. The solution was stored at -40 ˚C overnight, yielding orange-yellow crystals of **2.3**. The crystals were isolated and residual solvent was removed under vacuum (0.69 g, 68%, 2 crops). **^{1}H NMR (600 MHz, C$_6$D$_6$, 293 K):** δ 7.13-7.06 (m, 6H, Ar), 5.27 (s, 1H, *H*C(C(Me)NAr)$_2$), 3.47 (sep, 2H, C*H*Me$_2$), 3.20 (sep, 2H, C*H*Me$_2$), 1.60 (s, 6H, HC(C(*Me*)NAr)$_2$), 1.46 (d, 6H, CH*Me*$_2$), 1.38 (d, 6H, CH*Me*$_2$), 1.27 (d, 6H, CH*Me*$_2$), 1.16 (s, 9H, ^{t}Bu), 1.09 (d, 6H, CH*Me*$_2$), 0.42 (s, 9H, Si*Me*$_3$). **^{13}C{^{1}H} NMR (600 MHz, C$_6$D$_6$, 293 K):** δ 170.9 (HC(*C*(Me)NAr)$_2$), 144.1 (Ar), 142.6 (Ar), 141.7 (Ar), 127.2 (Ar), 124.4 (Ar), 124.1 (Ar), 100.1 (H*C*(C(Me)NAr)$_2$), 65.1 (C$_\alpha$, ^{t}Bu), 33.3 (C$_\beta$, ^{t}Bu), 28.6 (*C*HMe$_2$), 27.8 (*C*HMe$_2$), 26.4 (CH*Me*$_2$), 25.0 (CH*Me*$_2$), 24.7 (HC(C(*Me*)NAr)$_2$), 24.4 (CH*Me*$_2$), 24.0 (CH*Me*$_2$), 4.4 (Si*Me*$_3$). Anal calcd (%) for $Nb_1Si_1N_4C_{36}H_{59}$: C, 64.64; H, 8.89; N, 8.38. Found: C, 64.61; H, 8.98; N, 8.44. MP: dec. 171–191 °C.

(BDI)Nb(N^{t}Bu)(NAr) (2.4): An alternative procedure for synthesizing **2.4** has been reported previously; the following presents a preferred synthetic method.[11] Compound **2.1** (2.6 g, 4.0 mmol) was added to a 20 mL vial. In a separate vial, 2,6-diisopropylphenylazide (1.1 g, 5.4 mmol) was dissolved in 15 mL hexane. The 2,6-diisopropylphenylazide solution was added to **2.1** in one portion, and the mixture was stirred until all of **2.1** had dissolved. Upon addition of the azide solution, visible effervescence of dinitrogen was observed, but subsided within 5 min. The vial was left uncapped for ca. 15 min and then was filtered through a pad of Celite. The vial was capped and left at 25 °C for an additional 3 h, resulting in a color change from dark red to a lighter shade of dark red and precipitation of red crystals. The crystals were isolated and residual solvent was removed under vacuum. The supernatant was concentrated and stored at -40 ˚C overnight, yielding an additional crop of red crystals (1.9 g, 64%, 2 crops). Spectroscopic data were consistent with previously recorded data for **2.4**.[11]

(BDI)Nb(N^{t}Bu)(NXyl)(CN^{t}Bu) (2.5a): Compound **2.2** (210 mg, 0.32 mmol) was added to a 50 mL flask and dissolved in 5 mL toluene to give an orange solution. 2,6-dimethylphenylisocyanide (42 mg, 0.32 mmol) was dissolved in 5 mL toluene in a 20 mL vial, and then added to the solution of **2.2** by pipette. Upon addition of isocyanide, the solution changed color from orange to yellow-orange. The solution was heated at 60 °C for 2.5 h, resulting in a gradual color change from yellow-orange to orange-red. The volatile materials were removed under vacuum, leaving an orange-red residue. The residue was triturated once with hexanes, and then extracted with hexanes and concentrated. The solution was stored at -40 ˚C overnight, yielding bright orange crystals of **2.5a**. The crystals were isolated and residual solvent was removed under vacuum (180 mg, 71%, 2 crops). **^{1}H NMR (600 MHz, C$_6$D$_6$, 293 K):** δ 7.20 (m, 2H, Xyl), 7.19-7.13 (m, 3H, Ar), 6.99-6.93 (m, 3H, Ar), 6.86 (t, 1H, Xyl), 5.17 (s, 1H, *H*C(C(Me)NAr)$_2$), 3.81 (sep, 1H, C*H*Me$_2$), 3.69 (sep, 1H, C*H*Me$_2$), 3.47 (sep, 1H, C*H*Me$_2$), 3.46 (sep, 1H, C*H*Me$_2$), 2.78 (s, 3H, Xyl C*H*$_3$), 2.73 (s, 3H, Xyl C*H*$_3$), 1.72 (s, 3H, HC(C(*Me*)NAr)$_2$), 1.61 (s, 3H, HC(C(*Me*)NAr)$_2$), 1.58 (d, 3H, CH*Me*$_2$), 1.36 (d, 3H, CH*Me*$_2$), 1.30 (d, 3H, CH*Me*$_2$), 1.28 (d, 3H, CH*Me*$_2$), 1.23 (d, 3H, CH*Me*$_2$), 1.22 (d, 3H, CH*Me*$_2$), 1.19 (d, 3H, CH*Me*$_2$), 1.05 (s, 9H, NbN^{t}Bu), 1.04 (d, 3H, CH*Me*$_2$), 0.75 (s, 9H, C≡N^{t}Bu). **^{13}C{^{1}H} NMR (600 MHz, C$_6$D$_6$, 293 K):** δ 166.8 (HC(*C*(Me)NAr)$_2$), 166.3 (HC(*C*(Me)NAr)$_2$), 156.9 (Ar), 152.3 (Ar), 151.8 (Ar), 143.4 (Ar), 143.0 (Ar), 141.9 (Ar), 141.7 (Ar), 133.6 (Ar), 127.3 (Ar), 126.7 (Ar), 125.6 (Ar), 125.2 (Ar), 124.9 (Ar), 124.0 (Ar), 123.2 (Ar), 120.9 (Ar), 100.4 (H*C*(C(Me)NAr)$_2$), 65.3 (C$_\alpha$, NbN^{t}Bu), 56.4 (C$_\alpha$, C≡N^{t}Bu), 32.6 (C$_\beta$, NbN^{t}Bu), 29.2 (C$_\beta$, C≡N^{t}Bu), 28.9 (*C*HMe$_2$), 28.8 (*C*HMe$_2$), 28.0 (*C*HMe$_2$), 27.8 (*C*HMe$_2$), 25.1 (HC(C(*Me*)NAr)$_2$), 25.0 (CH*Me*$_2$), 24.9 (CH*Me*$_2$), 24.7 (CH*Me*$_2$), 24.7 (HC(C(*Me*)NAr)$_2$), 24.5 (CH*Me*$_2$), 24.5 (CH*Me*$_2$), 24.2 (CH*Me*$_2$), 23.7 (CH*Me*$_2$), 23.1 (CH*Me*$_2$), 21.2 (Xyl *C*H$_3$), 20.0 (Xyl *C*H$_3$). FT-IR (KBr, Nujol, cm^{-1}): 2190 (s, C≡N stretch). Anal calcd (%) for $Nb_1N_5C_{46}H_{68}$: C, 70.47; H, 8.74; N, 8.93. Found: C, 70.56; H, 8.70; N, 8.83. MP: dec. 180–207 °C.

(BDI)Nb(N^{t}Bu)(N(4-MeO-2,6-Me$_2$C$_6$H$_2$))(CN^{t}Bu) (2.5b): Compound **2.2** (250 mg, 0.38 mmol) was added to a 50 mL flask and dissolved in 5 mL benzene to give an orange solution. 4-methoxy-2,6-dimethylphenylisocyanide (64 mg, 0.40 mmol) was dissolved in 2 mL toluene in a 4 mL vial, and then added to the solution of **2.2** by pipette. Upon addition of isocyanide, the solution changed color from orange to yellow-orange. The solution was heated at 60 °C for 16 h, resulting in a gradual color change from yellow-orange to orange-red. The volatile materials were removed under vacuum, leaving an orange-red residue. The residue was extracted with hexanes and concentrated. The solution was stored at -40 ˚C overnight, yielding **2.5b** as a bright orange microcrystalline powder. The powder was isolated and residual solvent was removed under vacuum (165 mg, 55%, 2 crops). **^{1}H NMR (600 MHz, C$_6$D$_6$, 293 K):** δ 7.21-7.14 (m, 3H, Ar), 7.01-6.94 (m, 3H, Ar), 6.84 (d, 1H, Xyl), 6.83 (d, 1H, Xyl), 5.18 (s, 1H, *H*C(C(Me)NAr)$_2$), 3.82 (sep, 1H, C*H*Me$_2$), 3.71 (sep, 1H, C*H*Me$_2$), 3.48 (sep, 1H, C*H*Me$_2$), 3.46 (s, 3H, *Me*OXyl), 3.45 (sep, 1H, C*H*Me$_2$), 2.78 (s, 3H, Xyl C*H*$_3$), 2.73 (s, 3H, Xyl C*H*$_3$), 1.73 (s, 3H, HC(C(*Me*)NAr)$_2$), 1.63 (s, 3H, HC(C(*Me*)NAr)$_2$), 1.59 (d, 3H, CH*Me*$_2$), 1.37 (d, 3H, CH*Me*$_2$), 1.35 (d, 3H, CH*Me*$_2$), 1.28 (d, 3H, CH*Me*$_2$), 1.25 (d, 3H, CH*Me*$_2$), 1.24 (d, 3H, CH*Me*$_2$), 1.20 (d, 3H, CH*Me*$_2$), 1.07 (d, 3H, CH*Me*$_2$), 1.06 (s, 9H, NbN^{t}Bu), 0.76 (s, 9H, C≡N^{t}Bu). **^{13}C{^{1}H} NMR (600 MHz, C$_6$D$_6$, 293 K):** δ 166.6 (HC(*C*(Me)NAr)$_2$), 166.1 (HC(*C*(Me)NAr)$_2$), 154.2 (Ar), 152.3 (Ar), 151.9 (Ar), 151.9 (Ar), 143.4 (Ar), 143.0 (Ar), 141.9 (Ar), 141.6 (Ar), 135.0 (Ar), 125.5 (Ar), 125.5 (Ar), 125.1 (Ar), 124.9 (Ar), 124.0 (Ar), 123.2 (Ar), 112.9 (Xyl), 112.1 (Xyl), 100.3 (H*C*(C(Me)NAr)$_2$),

65.0 (C_α, NbN^{t}Bu), 56.4 (C_α, C≡N^{t}Bu), 54.9 (*Me*OXyl), 32.7 (C_β, NbN^{t}Bu), 29.3 (C_β, C≡N^{t}Bu), 28.9 (*C*HMe$_2$), 28.8 (*C*HMe$_2$), 28.1 (*C*HMe$_2$), 27.8 (*C*HMe$_2$), 25.1 (HC(C(*Me*)NAr)$_2$), 25.0 (CH*Me*$_2$), 24.9 (CH*Me*$_2$), 24.8 (CH*Me*$_2$), 24.7 (CH*Me*$_2$), 24.6 (CH*Me*$_2$), 24.6 (HC(C(*Me*)NAr)$_2$), 24.5 (CH*Me*$_2$), 24.2 (CH*Me*$_2$), 23.8 (CH*Me*$_2$), 21.5 (Xyl *C*H$_3$), 20.2 (Xyl *C*H$_3$). FT-IR (KBr, Nujol, cm^{-1}): 2187 (s, C≡N stretch). Anal calcd (%) for $Nb_1N_5C_{47}H_{70}$: C, 69.35; H, 8.67; N, 8.60. Found: C, 68.96; H, 8.40; N, 8.52. MP: dec. 177–211 °C.

(BDI)Nb(N^{t}Bu)(N(4-MeOC$_6$H$_4$))(CN^{t}Bu) (2.5c): Compound **2.2** (240 mg, 0.37 mmol) was added to a 50 mL flask and dissolved in 5 mL benzene to give an orange solution. 4-methoxyphenylisocyanide (53 mg, 0.40 mmol) was dissolved in 2 mL benzene in a 4 mL vial, and then added to the solution of **2.2** by pipette. Upon addition of isocyanide, the solution changed color from orange to red-brown. The solution was heated at 60 °C for 0.5 h, resulting in a color change from red-brown to red-orange. The volatile materials were removed under vacuum, leaving a red-orange residue. The residue was extracted with hexanes and concentrated. The solution was stored at -40 ˚C overnight, yielding **2.5b** as an orange microcrystalline powder. The powder was isolated and residual solvent was removed under vacuum (118 mg, 41%, 2 crops). **^{1}H NMR (400 MHz, C$_6$D$_6$, 293 K):** δ 7.21-7.16 (m, 3H, Ar), 7.10 (d, 2H, MeO*Ph*), 7.03-6.95 (m, 3H, Ar), 6.82 (d, 1H, MeO*Ph*), 5.18 (s, 1H, *H*C(C(Me)NAr)$_2$), 3.99 (sep, 1H, C*H*Me$_2$), 3.66 (sep, 1H, C*H*Me$_2$), 3.54 (sep, 1H, C*H*Me$_2$), 3.48 (sep, 1H, C*H*Me$_2$), 3.35 (s, 3H, *Me*OPh), 2.73 (s, 3H, Xyl), 1.77 (s, 3H, HC(C(*Me*)NAr)$_2$), 1.67 (s, 3H, HC(C(*Me*)NAr)$_2$), 1.61 (d, 3H, CH*Me*$_2$), 1.40 (d, 3H, CH*Me*$_2$), 1.37 (d, 3H, CH*Me*$_2$), 1.35 (d, 3H, CH*Me*$_2$), 1.30 (d, 3H, CH*Me*$_2$), 1.25 (d, 3H, CH*Me*$_2$), 1.21 (d, 3H, CH*Me*$_2$), 1.19 (d, 3H, CH*Me*$_2$), 1.10 (s, 9H, NbN^{t}Bu), 0.79 (s, 9H, C≡N^{t}Bu). **^{13}C{^{1}H} NMR (500 MHz, C$_6$D$_6$, 293 K):** δ 166.0 (HC(*C*(Me)NAr)$_2$), 165.8 (HC(*C*(Me)NAr)$_2$), 154.3 (Ar), 154.1 (Ar), 151.4 (Ar), 151.3 (Ar), 142.8 (Ar), 142.5 (Ar), 141.5 (Ar), 141.3 (Ar), 127.3 (Ar), 125.1 (Ar), 125.0 (Ar), 124.5 (Ar), 124.4 (Ar), 123.7 (Ar), 123.4 (Ar), 122.8 (Ar), 99.4 (H*C*(C(Me)NAr)$_2$), 65.4 (C_α, NbN^{t}Bu), 55.9 (C_α, C≡N^{t}Bu), 54.5 (*Me*OPh), 32.7 (C_β, NbN^{t}Bu), 29.1 (C_β, C≡N^{t}Bu), 28.5 (*C*HMe$_2$), 28.4 (*C*HMe$_2$), 27.7 (*C*HMe$_2$), 27.6 (*C*HMe$_2$), 25.1 (CH*Me*$_2$), 24.9 (CH*Me*$_2$), 24.8 (HC(C(*Me*)NAr)$_2$), 24.6 (CH*Me*$_2$), 24.6 (CH*Me*$_2$), 24.6 (CH*Me*$_2$), 24.4 (HC(C(*Me*)NAr)$_2$), 24.2 (CH*Me*$_2$), 24.0 (CH*Me*$_2$), 23.2 (CH*Me*$_2$). FT-IR (KBr, Nujol, cm^{-1}): 2187 (s, C≡N stretch). Anal calcd (%) for $Nb_1O_1N_5C_{45}H_{66}$: C, 68.77; H, 8.46; N, 8.91. Found: C, 68.02; H, 8.28; N, 8.47. MP: dec. 191–208 °C.

(BDI)Nb(NXyl)$_2$(CN^{t}Bu) (2.6): Compound **2.5a** (10 mg, 13 μmol) was dissolved in 0.25 mL C_6D_6 in a 4 mL vial. In a separate vial, XylNC (1.7 mg, 13 μmol) was dissolved in 0.25 mL C_6D_6 and added to the solution of **2.5a** in one portion, resulting in a slight color change from orange to orange-yellow. The solution was transferred to an LPV NMR tube and heated at 120 °C for 15 h, resulting in a color change from orange-yellow to red. Compound **2.6** was characterized in solution by ^{1}H NMR spectroscopy. **^{1}H NMR (400 MHz, C$_6$D$_6$, 293 K):** δ 7.15-6.89 (m, 10H, Ar/Xyl), 6.78 (t, 1H, Xyl), 6.64 (t, 1H, Xyl), 5.08 (s, 1H, *H*C(C(Me)NAr)$_2$), 4.00 (sep, 1H, C*H*Me$_2$), 3.78 (sep, 1H, C*H*Me$_2$), 3.61 (sep, 1H, C*H*Me$_2$), 3.58 (sep, 1H, C*H*Me$_2$), 2.75 (s, 3H, Xyl C*H*$_3$), 2.48 (s, 3H, Xyl C*H*$_3$), 2.13 (br s, 3H, Xyl C*H*$_3$), 2.06 (s, 3H, Xyl C*H*$_3$), 1.71 (s, 3H, HC(C(*Me*)NAr)$_2$), 1.68 (s, 3H, HC(C(*Me*)NAr)$_2$), 1.42 (d, 3H, CH*Me*$_2$), 1.29 (d, 3H, CH*Me*$_2$), 1.29 (d, 3H, CH*Me*$_2$), 1.19 (d, 3H, CH*Me*$_2$), 1.16 (d, 3H, CH*Me*$_2$), 1.14 (d, 3H, CH*Me*$_2$), 1.03 (d, 3H, CH*Me*$_2$), 0.95 (d, 3H, CH*Me*$_2$), 0.58 (s, 9H, ^{t}Bu). **^{13}C{^{1}H} NMR (600 MHz, C$_6$D$_6$, 293 K):** δ 167.0 (HC(*C*(Me)NAr)$_2$),

166.7 (HC(*C*(Me)NAr)$_2$), 156.6 (Ar), 156.5 (Ar), 152.4 (Ar), 150.5 (Ar), 148.9 (Ar), 143.7 (Ar), 142.7 (Ar), 142.3 (Ar), 141.8 (Ar), 136.2 (Ar), 134.9 (Ar), 134.6 (Ar), 128.4 (Ar), 128.0 (Ar), 127.8 (Ar), 127.1 (Ar), 126.0 (Ar), 125.6 (Ar), 125.0 (Ar), 124.5 (Ar), 124.1 (Ar), 123.6 (Ar), 123.2 (Ar), 122.0 (Ar), 121.2 (Ar), 99.3 (H*C*(C(Me)NAr)$_2$), 56.5 (C$_\alpha$, ^{t}Bu), 30.5 (*C*HMe$_2$), 30.4 (C$_\beta$, ^{t}Bu), 30.3 (*C*HMe$_2$), 27.9 (*C*HMe$_2$), 27.9 (*C*HMe$_2$), 25.5 (HC(C(*Me*)NAr)$_2$), 25.2 (CH*Me*$_2$), 25.2 (HC(C(*Me*)NAr)$_2$), 24.9 (CH*Me*$_2$), 24.8 (CH*Me*$_2$), 24.7 (CH*Me*$_2$), 24.6 (CH*Me*$_2$), 24.3 (CH*Me*$_2$), 23.8 (CH*Me*$_2$), 23.1 (CH*Me*$_2$), 19.5 (Xyl *C*H$_3$), 19.3 (Xyl *C*H$_3$), 19.2 (Xyl *C*H$_3$), 18.7 (Xyl CH$_3$).

(BDI)Nb(NCy)(NAr)(CNCy) (2.7): Compound **2.4** (200 mg, 0.26 mmol) was added to a 50 mL flask and dissolved in 10 mL toluene to give a red solution. Cyclohexylisocyanide (580 mg, 5.3 mmol) was dissolved in 2 mL toluene and added to the solution of **2.4**, resulting in an immediate color change from red to orange. The orange solution was heated to reflux and stirred for 15 h, resulting in a color change to red-brown. The volatile materials were removed by heating to 80 °C under vacuum, leaving a red-brown oil. The oil was triturated with hexane, then extracted with HMDSO and concentrated. The solution was stored at -40 °C for 3 days, yielding **2.7** as an orange-red microcrystalline powder. The powder was isolated and residual solvent was removed under vacuum (140 mg, 60%). **^{1}H NMR (600 MHz, C$_6$D$_6$, 293 K):** δ 7.25 (d, 1H, Ar), 7.25 (d, 1H, Ar), 7.17-7.13 (m, 3H, Ar), 7.05 (t, 1H, Ar), 7.03-7.00 (m, 2H, Ar), 6.96 (t, 1H, Ar), 5.18 (s, 1H, *H*C(C(Me)NAr)$_2$), 5.03 (sep, 1H, C*H*Me$_2$), 4.48 (sep, 1H, C*H*Me$_2$), 3.65 (m, 2H, C*H*Me$_2$/Cy C*H*), 3.55 (sep, 1H, C*H*Me$_2$), 3.51 (sep, 1H, C*H*Me$_2$), 3.44 (sep, 1H, C*H*Me$_2$), 2.93 (m, 1H, Cy C*H*), 1.78 (m, Cy C*H*$_2$), 1.76 (s, 3H, HC(C(*Me*)NAr)$_2$), 1.68 (s, 3H, HC(C(*Me*)NAr)$_2$), 1.65 (m, Cy C*H*$_2$), 1.58 (d, 3H, CH*Me*$_2$), 1.56 (d, 3H, CH*Me*$_2$), 1.49 (m, Cy C*H*$_2$), 1.44 (d, 3H, CH*Me*$_2$), 1.43 (d, 3H, CH*Me*$_2$), 1.42 (d, 3H, CH*Me*$_2$), 1.39 (m, Cy C*H*$_2$), 1.33 (m, Cy C*H*$_2$), 1.29 (d, 3H, CH*Me*$_2$), 1.26 (d, 3H, CH*Me*$_2$), 1.25 (d, 3H, CH*Me*$_2$), 1.22 (d, 3H, CH*Me*$_2$), 1.19 (m, Cy C*H*$_2$), 1.18 (d, 3H, CH*Me*$_2$), 1.16 (d, 3H, CH*Me*$_2$), 1.13 (d, 3H, CH*Me*$_2$), 1.10 (m, Cy C*H*$_2$), 1.06 (m, Cy C*H*$_2$), 0.96 (m, Cy C*H*$_2$), 0.83 (m, Cy C*H*$_2$), 0.73 (m, Cy C*H*$_2$). **^{13}C{^{1}H} NMR (600 MHz, C$_6$D$_6$, 293 K):** δ 166.6 (HC(*C*(CH$_2$)NAr)), 166.0 (HC(*C*(CH$_2$)NAr)), 152.6 (Ar), 151.0 (Ar), 145.3 (Ar), 143.8 (Ar), 142.8 (Ar), 142.3 (Ar), 141.5 (Ar), 139.0 (Ar), 125.5 (Ar), 125.2 (Ar), 125.0 (Ar), 124.9 (Ar), 124.7 (Ar), 123.5 (Ar), 123.5 (Ar), 122.3 (Ar), 122.0 (Ar), 122.0 (Ar), 99.5 (H*C*(C(Me)NAr)$_2$), 71.1 (Cy *C*H), 64.8 (C$_\alpha$, ^{t}Bu), 53.7 (Cy *C*H), 37.5 (Cy *C*H$_2$), 36.0 (Cy *C*H$_2$), 31.8 (Cy *C*H$_2$), 31.7 (Cy *C*H$_2$), 29.1 (*C*HMe$_2$), 28.7 (*C*HMe$_2$), 27.9 (*C*HMe$_2$), 27.8 (*C*HMe$_2$), 26.8 (*C*HMe$_2$), 26.7 (*C*HMe$_2$), 26.0 (Cy *C*H$_2$), 25.8 (CH*Me*$_2$), 25.8 (Cy *C*H$_2$), 25.3 (CH*Me*$_2$), 25.1 (Cy *C*H$_2$), 25.0 (CH*Me*$_2$), 25.0 (HC(C(*Me*)NAr)$_2$), 24.9 (HC(C(*Me*)NAr)$_2$), 24.9 (Cy *C*H$_2$), 24.7 (CH*Me*$_2$), 24.7 (CH*Me*$_2$), 24.6 (CH*Me*$_2$), 24.5 (CH*Me*$_2$), 24.0 (CH*Me*$_2$), 23.3 (Cy *C*H$_2$), 23.0 (CH*Me*$_2$). FT-IR (KBr, Nujol, cm^{-1}): 2196 (s, C≡N stretch). Anal calcd (%) for Nb$_1$N$_5$C$_{54}$H$_{80}$: C, 72.70; H, 9.04; N, 7.85. Found: C, 70.01; H, 8.57; N, 7.91. MP: dec. 164–195 °C.

(BDI)Nb(N^{t}Bu)-η^2-(N^2,N^3,1-tributyl-4-(((*E*)-butylidene)amino)-5-((*E*)-(butylimino)methyl)-1*H*-pyrrole-2,3-diamide) (2.8): Compound **2.2** (225 mg, 0.34 mmol) was added to a 20 mL vial and dissolved in 5 mL hexane to give an orange solution. In a separate vial, ^{n}BuNC (.358 mL, 286 mg, 3.4 mmol) was added to the solution of **2.2** in one portion by micropipette, resulting in a color change to dark red-brown within 5 minutes. The solution was left at room temperature for 15 h. The volatile materials were removed under vacuum, leaving a red-brown oil. The oil was triturated

with hexane, then extracted with HMDSO and concentrated. The solution was stored at -40 °C overnight, yielding **2.8** as a red-orange microcrystalline powder. The powder was isolated and residual solvent was removed under vacuum (183 mg, 53%). **^{1}H NMR (400 MHz, C_6D_6, 293 K):** δ 8.90 (s, 1H, *H*C=N^{n}Bu), 7.33 (t, 2H, Ar), 7.21-7.03 (m, 4H, Ar), 6.53 (dd, ^{3}J = 5.5 Hz, ^{3}J = 3.5 Hz, 1H, (^{n}Pr)*H*C=N), 4.94 (s, 1H, *H*C(C(Me)NAr)$_2$), 4.58-4.37 (m, 3H, C*H*Me$_2$/C*H*Me$_2$/NC*H*$_2$), 3.96-3.79 (m, 2H, NC*H*$_2$/NC*H*$_2$), 3.56 (dt, ^{2}J = 12.0 Hz, ^{3}J = 6.4 Hz, NC*H*$_2$), 3.40 (dt, ^{2}J = 12.0 Hz, ^{3}J = 6.4 Hz, NC*H*$_2$), 3.30 (m, 1H, NC*H*$_2$), 3.18 (m, 1H, NC*H*$_2$), 2.63 (td, ^{2}J = 3.6 Hz, ^{3}H = 12.3 Hz, 1H, NC*H*$_2$), 2.42 (m, 3H, C*H*Me$_2$/C*H*Me$_2$/NCH$_2$C*H*$_2$), 2.30 (m, 2H, (CH$_3$CH$_2$C*H*$_2$)HC=N), 1.74-0.70 (m, 71H, ^{t}Bu (9H)/2x HC(C(*Me*)NAr)$_2$ (6H)/12x CH*Me*$_2$ (24H)/17x C*H*$_2$ (17H)/5x CH$_2$C*H*$_3$ (15H). **^{13}C{^{1}H} NMR (500 MHz, C_6D_6, 293 K):** δ 167.3 (HC(*C*(CH$_2$)NAr)), 167.2 (HC(*C*(CH$_2$)NAr)), 163.1 ((^{n}Pr)H*C*=N), 153.1 (Ar), 152.5 (Ar), 151.5 (H*C*=N^{n}Bu), 142.5 (Ar), 141.9 (Ar), 141.6 (Ar), 140.9 (Ar), 132.7 (Pyrrole), 129.4 (Pyrrole), 127.4 (Pyrrole), 125.5 (Ar), 125.4 (Ar), 124.8 (Ar), 124.6 (Ar), 124.2 (Ar), 124.0 (Ar), 106.0 (Pyrrole), 99.7 (*H*C(C(Me)NAr)$_2$), 69.4 (C$_\alpha$, ^{t}Bu), 62.6 (N*C*H$_2$), 56.6 (N*C*H$_2$), 56.5 (N*C*H$_2$), 47.3 (N*C*H$_2$), 39.4 ((CH$_3$CH$_2$*C*H$_2$)HC=N)), 34.5 (NCH$_2$*C*H$_2$CH$_2$CH$_3$), 34.0 (NCH$_2$*C*H$_2$CH$_2$CH$_3$), 33.4 (C$_\beta$, ^{t}Bu), 32.7 (NCH$_2$*C*H$_2$CH$_2$CH$_3$), 31.9 (NCH$_2$*C*H$_2$CH$_2$CH$_3$), 29.1 (*C*HMe$_2$), 28.7 (*C*HMe$_2$), 28.6 (*C*HMe$_2$), 28.1 (*C*HMe$_2$), 27.3 (HC(C(*Me*)NAr)$_2$), 26.8 (HC(C(*Me*)NAr)$_2$), 25.7 (CH*Me*$_2$), 25.7 (CH*Me*$_2$), 25.5 (CH*Me*$_2$), 25.1 (CH*Me*$_2$), 25.0 (CH*Me*$_2$), 24.9 (CH*Me*$_2$), 24.7 (CH*Me*$_2$), 24.3 (CH*Me*$_2$), 21.0 (NCH$_2$CH$_2$*C*H$_2$CH$_3$), 21.0 (NCH$_2$CH$_2$*C*H$_2$CH$_3$), 20.9 (NCH$_2$CH$_2$*C*H$_2$CH$_3$), 20.8 (NCH$_2$CH$_2$*C*H$_2$CH$_3$), 20.0 ((CH$_3$*C*H$_2$CH$_2$)HC=N)), 14.4 ((*C*H$_3$CH$_2$CH$_2$)HC=N)), 14.4 (NCH$_2$CH$_2$CH$_2$*C*H$_3$), 14.4 (NCH$_2$CH$_2$CH$_2$*C*H$_3$), 14.2 (NCH$_2$CH$_2$CH$_2$*C*H$_3$), 14.2 (NCH$_2$CH$_2$CH$_2$*C*H$_3$). FT-IR (KBr, Nujol, cm^{-1}): 1615 (s, C=N stretch). Anal calcd (%) for $Nb_1N_8C_{58}H_{95}$: C, 69.85; H, 9.60; N, 11.24. Found: C, 69.76; H, 9.71; N, 11.14. MP: dec. 141–151 °C.

(BDI)Nb(N^{t}Bu)-η^2-(BnNCBn)(CN) (2.9): Compound **2.2** (225 mg, 0.34 mmol) was added to a 20 mL vial and dissolved in 5 mL hexane to give an orange solution. In a separate vial, BnNC (121 mg, 1.0 mmol) was dissolved in 1 mL hexane and added to the solution of **2.2** in one portion, resulting in a color change to dark red-brown within 5 minutes. The solution was left at room temperature for 1 h, during which time pale yellow needles of **2.9** precipitated from solution. The crystals were isolated and washed three times with hexane, and residual solvent was removed under vacuum (108 mg, 38%). X-ray quality crystals were grown from slow cooling of a toluene solution. **^{1}H NMR (400 MHz, C_6D_6, 293 K):** δ 7.61 (d, 2H, Bn), 7.41 (d, 1H, Bn), 7.34 (t, 1H, Bn), 7.19 (t, 2H, Bn), 7.17-7.13 (m, 3H, Ar), 7.10 (d, 1H, Ar), 7.04 (t, 2H, Bn), 6.96 (d, 1H, Ar), 6.91 (t, 1H, Ar), 6.72 (d, 2H, Bn), 5.25 (s, 1H, *H*C(C(Me)NAr)$_2$), 4.85 (d, 1H, Bn C*H*$_2$), 4.27 (d, 1H, Bn C*H*$_2$), 4.00 (d, 1H, Bn C*H*$_2$), 3.99 (sep, 1H, C*H*Me$_2$), 3.42 (sep, 1H, C*H*Me$_2$), 2.75 (d, 1H, Bn C*H*$_2$), 2.70 (sep, 1H, C*H*Me$_2$), 2.69 (sep, 1H, C*H*Me$_2$), 1.89 (d, 3H, CH*Me*$_2$), 1.71 (s, 6H, HC(C(*Me*)NAr)$_2$), 1.61 (s, 6H, HC(C(*Me*)NAr)$_2$), 1.40 (d, 3H, CH*Me*$_2$), 1.18 (d, 6H, CH*Me*$_2$), 1.07 (d, 3H, CH*Me*$_2$), 0.96 (s, 9H, ^{t}Bu), 0.93 (d, 3H, CH*Me*$_2$), 0.82 (d, 3H, CH*Me*$_2$), 0.42 (d, 3H, CH*Me*$_2$). **^{13}C{^{1}H} NMR (600 MHz, C_6D_6, 293 K):** δ 169.6 (HC(*C*(Me)NAr)$_2$), 168.0 (HC(*C*(Me)NAr)$_2$), 152.0 (Bn), 150.7 (Ar), 142.6 (Ar), 143.6 (Ar), 142.7 (Ar), 141.8 (Ar), 141.1 (Ar), 136.6 (Bn), 136.4 (Ar), 131.0 (Bn), 128.8 (Ar), 128.8 (Ar), 128.4 (Ar), 127.3 (Ar), 127.1 (Ar), 126.8 (Bn), 126.6 (Bn), 126.3 (Ar), 125.2 (Bn), 125.2 (Ar), 125.1 (Ar), 123.6 (Bn), 103.5 (H*C*(C(Me)NAr)$_2$), 71.9 (C$_\alpha$, ^{t}Bu), 49.5 (Bn *C*H$_2$), 41.3 (Bn *C*H$_2$), 32.4 (C$_\beta$, ^{t}Bu), 28.9 (*C*HMe$_2$),

28.8 (*C*HMe$_2$), 28.0 (*C*HMe$_2$), 26.9 (*C*HMe$_2$), 26.7 (HC(C(*Me*)NAr)$_2$), 25.9 (CH*Me*$_2$), 25.5 (HC(C(*Me*)NAr)$_2$), 25.4 (CH*Me*$_2$), 25.2 (CH*Me*$_2$), 24.9 (CH*Me*$_2$), 24.8 (CH*Me*$_2$), 24.7 (CH*Me*$_2$), 23.4 (*C*HMe$_2$). FT-IR (KBr, Nujol, cm^{-1}): 2114 (w, C≡N stretch), 1638 (s, C=N stretch). Anal calcd (%) for $Nb_1N_5C_{49}H_{64}$: C, 72.13; H, 7.91; N, 8.58. Found: C, 72.36; H, 7.99; N, 8.38. MP: dec. 172–178 °C.

(BDI)Nb(N^{t}Bu)(N$_3{}^t$Bu)(CN^{n}Bu) (2.11): Compound **2.2** (250 mg, 0.38 mmol) was added to a 20 mL vial and dissolved in 4 mL hexane to give an orange solution. The solution of **2.2** was transferred to another 20 mL vial containing ^{t}BuN$_3$ (645 mg, 6.5 mmol). In a separate 4 mL vial, ^{n}BuNC (127 mg, 1.5 mmol) was dissolved in 2 mL hexane and added to the solution of **2.2** and azide in one portion. The solution was left at room temperature for 16 h, resulting in a slow color change to brown. The volatile materials were removed under vacuum, leaving a brown residue. The residue was extracted with HMDSO and concentrated. The solution was stored at -40 ˚C overnight, yielding **2.11** as an orange-brown microcrystalline powder. The powder was isolated and residual solvent was removed under vacuum (178 mg, 61%). **^{1}H NMR (600 MHz, C$_6$D$_6$, 293 K):** δ 7.29 (d, 1H, Ar), 7.22 (t, 1H, Ar), 7.15 (d, 1H, Ar), 7.08 (d, 1H, Ar), 7.03 (d, 1H, Ar), 6.96 (t, 1H, Ar), 5.08 (s, 1H, *H*C(C(Me)NAr)$_2$), 4.21 (sep, 1H, C*H*Me$_2$), 3.41 (sep, 1H, C*H*Me$_2$), 3.37 (sep, 1H, C*H*Me$_2$), 3.32 (sep, 1H, C*H*Me$_2$), 2.53-2.40 (m, 2H, NC*H*$_2$CH$_2$CH$_2$CH$_3$), 1.82 (d, 3H, CH*Me*$_2$), 1.72 (s, 3H, HC(C(*Me*)NAr)$_2$), 1.63 (s, 3H, HC(C(*Me*)NAr)$_2$), 1.57 (d, 3H, CH*Me*$_2$), 1.45 (d, 3H, CH*Me*$_2$), 1.38 (s, 9H, ^{t}Bu), 1.38 (d, 3H, CH*Me*$_2$), 1.26 (d, 3H, CH*Me*$_2$), 1.22 (d, 3H, CH*Me*$_2$), 1.17 (d, 3H, CH*Me*$_2$), 1.09-0.97 (m, 4H, NCH$_2$C*H*$_2$C*H*$_2$CH$_3$), 0.95 (s, 9H, ^{t}Bu), 0.67 (t, 3H, NCH$_2$CH$_2$CH$_2$C*H*$_3$). **^{13}C{^{1}H} NMR (600 MHz, C$_6$D$_6$, 293 K):** δ 166.6 (HC(*C*(Me)NAr)$_2$), 165.9 (HC(*C*(Me)NAr)$_2$), 151.5 (Ar), 151.0 (Ar), 143.8 (Ar), 143.0 (Ar), 141.9 (Ar), 141.5 (Ar), 125.7 (Ar), 125.5 (Ar), 125.0 (Ar), 124.5 (Ar), 124.0 (Ar), 123.0 (Ar), 99.7 (H*C*(C(Me)NAr)$_2$), 59.4 (C$_\alpha$, ^{t}Bu), 42.3 (NCH$_2$CH$_2$CH$_2$CH$_3$), 32.7 (C$_\beta$, ^{t}Bu), 29.9 (NCH$_2$*C*H$_2$CH$_2$CH$_3$), 29.1 (C$_\beta$, ^{t}Bu), 29.0 (*C*HMe$_2$), 28.9 (*C*HMe$_2$), 28.1 (*C*HMe$_2$), 28.0 (*C*HMe$_2$), 26.4 (CH*Me*$_2$), 25.7 (CH*Me*$_2$), 25.1 (CH*Me*$_2$), 25.0 (CH*Me*$_2$), 25.0 (CH*Me*$_2$), 25.0 (HC(C(*Me*)NAr)$_2$), 24.8 (CH*Me*$_2$), 24.7 (HC(C(*Me*)NAr)$_2$), 24.5 (CH*Me*$_2$), 23.6 (CH*Me*$_2$), 19.6 (NCH$_2$CH$_2$*C*H$_2$CH$_3$), 13.1 (NCH$_2$CH$_2$CH$_2$*C*H$_3$). FT-IR (KBr, Nujol, cm^{-1}): 2210 (s, C≡N stretch), 2115 (s, N$_3$ stretch). Anal calcd (%) for $Nb_1N_7C_{42}H_{68}$: C, 66.03; H, 8.97; N, 12.83. Found: C, 63.86; H, 8.86; N, 8.79 (Compound **2.11** was found to be thermally unstable, which is likely responsible for low % C and N observed in combustion analysis). MP: dec. 95-108 °C.

(BDI)Nb(N^{t}Bu)$_2$(CNXyl) (2.2·XylNC): Compound **2.2** (170 mg, 0.27 mmol) was added to a 20 mL vial and dissolved in 3 mL hexane to give an orange solution. 2,6-dimethylphenylisocyanide (35 mg, 0.27 mmol) was dissolved in 3 mL hexanes in a separate 20 mL vial, and then added to the solution of **2.2** by pipette. Upon addition of isocyanide, the solution changed color from orange to yellow-orange. Within 5 min, yellow crystals of **2.5a** began to form on the walls of the vial. The solution was stored at -40 ˚C overnight, yielding yellow crystals of **2.5a**. The crystals were isolated and residual solvent was removed under vacuum (183 mg, 88%). **^{1}H NMR (500 MHz, C$_6$D$_6$, 293 K):** δ 7.20 (m, 2H, Xyl), 7.19-7.13 (m, 3H, Ar), 7.07-6.98 (m, 3H, Ar), 6.62 (t, 1H, Xyl), 6.53 (d, 2H, Xyl), 5.10 (s, 1H, *H*C(C(Me)NAr)$_2$), 3.93 (br m, 4H, C*H*Me$_2$), 1.95 (s, 6H, Xyl), 1.72 (s, 3H, HC(C(*Me*)NAr)$_2$), 1.65 (br d, 3H, CH*Me*$_2$), 1.58 (s, 3H, HC(C(*Me*)NAr)$_2$), 1.43-1.26 (br m, 36H, CH*Me*$_2$/ ^{t}Bu). ^{1}H NMR (500 MHz, C$_7$D$_8$, 213 K): 7.24 (br m, 2H, Ar), 7.17 (br t, 1H, Ar), 7.01 (br

d, 1H, Ar), 6.95 (br m, 1H, Ar), 6.85 (br d, 1H, Ar), 4.96 (s, 1H, *H*C(C(Me)NAr)$_2$), 4.41 (br sep, 1H, C*H*Me$_2$), 4.28 (br sep, 1H, C*H*Me$_2$), 3.61 (br sep, 1H, C*H*Me$_2$), 3.41 (br sep, 1H, C*H*Me$_2$), 1.84 (br d, 3H, CH*Me*$_2$), 1.72 (s, 6H, Xyl C*H*$_3$), 1.66 (s, 3H, HC(C(*Me*)NAr)$_2$), 1.55 (br d, 3H, CH*Me*$_2$), 1.50-1.46 (m, 9H, CH*Me*$_2$/HC(C(*Me*)NAr)$_2$) 1.33-1.13 (m, 18H, CH*Me*$_2$/^{t}Bu), 1.01 (^{t}Bu). **^{13}C{^{1}H} NMR (600 MHz, C$_6$D$_6$, 293 K):** δ 166.5 (HC(*C*(Me)NAr)$_2$), 166.3 (HC(*C*(Me)NAr)$_2$), 152.6 (Ar), 151.8 (Ar), 143.0 (Ar), 142.3 (Ar), 134.6 (Ar), 129.2 (Ar), 125.7 (Ar), 125.4 (Ar), 124.4 (Ar), 99.7 (H*C*(C(Me)NAr)$_2$), 64.5 (C$_\alpha$, ^{t}Bu), 33.8 (C$_\beta$, ^{t}Bu), 28.2 (*C*HMe$_2$), 26.0 (CH*Me*$_2$), 25.8 (HC(C(*Me*)NAr)$_2$), 25.3 (HC(C(*Me*)NAr)$_2$), 25.2 (CH*Me*$_2$), 25.1 (CH*Me*$_2$), 24.7 (CH*Me*$_2$), 19.2 (Xyl *C*H$_3$). FT-IR (KBr, Nujol, cm^{-1}): 2148 (s, C≡N stretch). Anal calcd (%) for $Nb_1N_5C_{46}H_{68}$: C, 70.47; H, 8.74; N, 8.93. Found: C, 70.20; H, 8.66; N, 8.95. MP: dec. 112–132 °C.

(BDI)Nb(N^{t}Bu)$_2$(CN^{t}Bu) (2.2·^{t}BuNC): Compound **2.2** (170 mg, 0.27 mmol) was dissolved in 5 mL hexanes to give an orange solution. *Tert*-butylisocyanide (30 μL, 22 mg, 0.27 mmol) was added in one portion by micropipette. Upon addition of isocyanide, the solution changed color from orange to yellow-orange. The solution was left at room temperature for 30 min, and then the volatile materials were removed under vacuum, leaving an orange residue. The residue was extracted with HMDSO and concentrated. The solution was stored at -40 ˚C overnight, yielding yellow crystals of **2.9**. The crystals were isolated and residual solvent was removed under vacuum (132 mg, 80%). **^{1}H NMR (500 MHz, C$_6$D$_6$, 293 K):** δ 7.25-7.20 (m, 3H, Ar), 7.07-7.01 (m, 3H, Ar), 5.05 (s, 1H, *H*C(C(Me)NAr)$_2$), 3.92 (sep, 2H, C*H*Me$_2$), 3.69 (sep, 2H, C*H*Me$_2$), 1.68 (s, 3H, HC(C(*Me*)NAr)$_2$), 1.62 (s, 3H, HC(C(*Me*)NAr)$_2$), 1.61 (d, 6H, CH*Me*$_2$), 1.37 (d, 6H, CH*Me*$_2$), 1.34 (d, 6H, CH*Me*$_2$), 1.32 (s, 18H, NbN^{t}Bu), 1.28 (d, 6H, CH*Me*$_2$), 0.75 (s, 9H, C≡N^{t}Bu). **^{13}C{^{1}H} NMR (600 MHz, C$_6$D$_6$, 293 K):** δ 166.6 (HC(*C*(Me)NAr)$_2$), 165.8 (HC(*C*(Me)NAr)$_2$), 153.6 (Ar), 152.2 (Ar), 142.8 (Ar), 142.2 (Ar), 125.2 (Ar), 125.2 (Ar), 124.3 (Ar), 124.0 (Ar), 99.7 (H*C*(C(Me)NAr)$_2$), 64.2 (C$_\alpha$, NbN^{t}Bu), 56.1 (C$_\alpha$, C≡N^{t}Bu), 34.1 (C$_\beta$, NbN^{t}Bu), 29.3 (C$_\beta$, C≡N^{t}Bu), 28.2 (*C*HMe$_2$), 28.0 (*C*HMe$_2$), 25.8 (HC(C(*Me*)NAr)$_2$), 25.7 (CH*Me*$_2$), 25.6 (CH*Me*$_2$), 25.5 (HC(C(*Me*)NAr)$_2$), 25.0 (CH*Me*$_2$), 24.8 (CH*Me*$_2$). FT-IR (KBr, Nujol, cm^{-1}): 2190 (s, C≡N stretch). Anal calcd (%) for $Nb_1N_5C_{42}H_{68}$: C, 68.55; H, 9.31; N, 9.52. Found: C, 68.49; H, 9.26; N, 9.63. MP: dec. 170–186 °C.

(BDI)Nb(N^{t}Bu)$_2$(CN(4-MeO-2,6-Me$_2$C$_6$H$_2$)) (2·MeOXylNC): Compound **2.2** (10 mg, 15 μmol) was dissolved in 0.25 mL C$_6$D$_6$ in a 4 mL vial. In a separate 4 mL vial, 4-methoxy-2,6-dimethylphenylisocyanide (2.4 mg, 15 μmol) was dissolved in 0.25 mL C$_6$D$_6$ and added to the solution of **2.2** in one portion, resulting in a slight color change from orange to orange-yellow. The product **2.2·MeOXylNC** was characterized in solution by ^{1}H NMR spectroscopy. **^{1}H NMR (600 MHz, C$_6$D$_6$, 293 K):** δ 7.27-7.21 (m, 3H, Ar), 7.09 (d, 2H, Ar), 7.04 (d, 1H, Ar), 6.20 (s, 2H, Xyl), 5.11 (s, 1H, *H*C(C(Me)NAr)$_2$), 3.96 (br s, 4H, C*H*Me$_2$), 3.05 (s, 3H, *Me*OXyl), 1.94 (s, 6H, Xyl C*H*$_3$), 1.73 (s, 3H, HC(C(*Me*)NAr)$_2$), 1.67 (br d, 6H, CH*Me*$_2$), 1.60 (s, 3H, HC(C(*Me*)NAr)$_2$), 1.47-1.26 (br m, 36H, ^{t}Bu/CH*Me*$_2$).

(BDI)Nb(N^{t}Bu)$_2$(CN^{n}Bu) (2.2·^{n}BuNC): Compound **2.2** (10 mg, 15 μmol) was dissolved in 0.5 mL C$_6$D$_6$ in a 4 mL vial. ^{n}BuNC (1.3 mg, 1.6 μL, 15 μmol) was added to the solution of **2.2** in one portion by microsyringe, resulting in a slight color change from orange to orange-yellow. The product **2.2·^{n}BuNC** was characterized in solution by ^{1}H NMR spectroscopy. **^{1}H NMR (400 MHz,**

C_6D_6, 293 K): δ 7.26-7.22 (m, 3H, Ar), 7.09 (d, 2H, Ar), 7.00 (t, 1H, Ar), 5.05 (s, 1H, *H*C(C(Me)NAr)$_2$), 3.94 (sep, 2H, C*H*Me$_2$), 3.72 (sep, 2H, C*H*Me$_2$), 2.37 (t, 2H, NC*H*$_2$CH$_2$CH$_2$CH$_3$), 1.70 (s, 3H, HC(C(*Me*)NAr)$_2$), 1.65 (s, 3H, HC(C(*Me*)NAr)$_2$), 1.61 (d, 6H, CH*Me*$_2$), 1.37 (d, 6H, CH*Me*$_2$), 1.35 (d, 6H, CH*Me*$_2$), 1.33 (s, 18H, ^{t}Bu), 1.29 (d, 6H, CH*Me*$_2$), 0.84 (m, 4H, NCH$_2$C*H*$_2$C*H*$_2$CH$_3$), 0.57 (t, 3H, NCH$_2$CH$_2$CH$_2$C*H*$_3$).

(BDI)Nb(N^{t}Bu)$_2$(CNCy) (2.2·CyNC): Compound **2.2** (10 mg, 15 μmol) was dissolved in 0.25 mL C_6D_6 in a 4 mL vial. In a separate 4 mL vial, CyNC (1.7 mg, 15 μmol) was dissolved in 0.25 mL C_6D_6 and added to the solution of **2.2** in one portion, resulting in a slight color change from orange to orange-yellow. The product **2.2·CyNC** was characterized in solution by ^{1}H NMR spectroscopy. **^{1}H NMR (600 MHz, C_6D_6, 293 K):** δ 7.27-7.21 (m, 3H, Ar), 7.08 (d, 2H, Ar), 7.02 (t, 1H, Ar), 5.06 (s, 1H, *H*C(C(Me)NAr)$_2$), 3.95 (sep, 2H, C*H*Me$_2$), 3.74 (sep, 2H, C*H*Me$_2$), 2.83 (tt, 1H, Cy C*H*), 1.70 (s, 3H, HC(C(*Me*)NAr)$_2$), 1.65 (s, 3H, HC(C(*Me*)NAr)$_2$), 1.63 (d, 6H, CH*Me*$_2$), 1.40 (d, 6H, CH*Me*$_2$), 1.36 (s, 18H, ^{t}Bu), 1.35 (d, 6H, CH*Me*$_2$), 1.29 (d, 6H, CH*Me*$_2$), 1.38-1.14 (m, 5H, Cy C*H*$_2$), 1.09-0.98 (m, 2H, Cy C*H*$_2$), 0.83-0.64 (m, 3H, Cy C*H*$_2$).

(BDI)Nb(N^{t}Bu)$_2$(CNBn) (2.2·BnNC): Compound **2.2** (10 mg, 15 μmol) was dissolved in 0.25 mL C_6D_6 in a 4 mL vial. In a separate 4 mL vial, BnNC (1.8 mg, 15 μmol) was dissolved in 0.25 mL C_6D_6 and added to the solution of **2.2** in one portion, resulting in a slight color change from orange to orange-yellow. The product **2.2·BnNC** was characterized in solution by ^{1}H NMR spectroscopy. **^{1}H NMR (400 MHz, C_6D_6, 293 K):** δ 7.25-7.19 (m, 3H, Ar), 7.08 (d, 2H, Ar), 7.03-6.93 (m, 4H, Ar/Bn), 6.72 (d, 2H, Bn), 5.05 (s, 1H, *H*C(C(Me)NAr)$_2$), 3.92 (sep, 2H, C*H*Me$_2$), 3.71 (sep, 2H, C*H*Me$_2$), 3.54 (s, 2H, Bn C*H*$_2$), 1.69 (s, 3H, HC(C(*Me*)NAr)$_2$), 1.66 (s, 3H, HC(C(*Me*)NAr)$_2$), 1.59 (d, 6H, CH*Me*$_2$), 1.34 (d, 6H, CH*Me*$_2$), 1.32 (d, 6H, CH*Me*$_2$), 1.28 (d, 6H, CH*Me*$_2$), 1.27 (s, 18H, ^{t}Bu).

(BDI)Nb(N^{t}Bu)(NTMS)(CN^{t}Bu) (2.3·^{t}BuNC): Compound **2.3** (10 mg, 15 μmol) was dissolved in 0.5 mL C_6D_6 in a 4 mL vial. ^{t}BuNC (6.2 mg, 8.5 μL, 75 μmol) was added to the solution of **2.3** in one portion by micropipette, resulting in a color change from orange-yellow to yellow. The product **2.3·^{t}BuNC** was characterized in solution by ^{1}H NMR spectroscopy. **^{1}H NMR (400 MHz, C_6D_6, 293 K):** δ 7.26-7.16 (m, 3H, Ar), 7.06-6.99 (m, 3H, Ar), 5.03 (s, 1H, *H*C(C(Me)NAr)$_2$), 4.05 (sep, 1H, C*H*Me$_2$), 3.64 (sep, 1H, C*H*Me$_2$), 3.60 (sep, 1H, C*H*Me$_2$), 3.52 (sep, 1H, C*H*Me$_2$), 1.71 (d, 3H, CH*Me*$_2$), 1.65 (s, 3H, HC(C(*Me*)NAr)$_2$), 1.60 (s, 3H, HC(C(*Me*)NAr)$_2$), 1.58 (d, 3H, CH*Me*$_2$), 1.43 (d, 3H, CH*Me*$_2$), 1.38 (d, 3H, CH*Me*$_2$), 1.34 (d, 3H, CH*Me*$_2$), 1.29 (d, 3H, CH*Me*$_2$), 1.26 (d, 3H, CH*Me*$_2$), 1.18 (d, 3H, CH*Me*$_2$), 1.17 (s, 9H, NbN^{t}Bu), 0.77 (s, 9H, C≡N^{t}Bu), 0.34 (s, 9H, TMS).

(BDI)Nb(N^{t}Bu)(NAr)(CN^{t}Bu) (2.4·^{t}BuNC): Compound **2.4** (10 mg, 13 μmol) was dissolved in 0.5 mL C_6D_6 in a 4 mL vial. ^{t}BuNC (22 mg, 30 μL, 260 μmol) was added to the solution of **2.3** in one portion by microsyringe, resulting in a color change from red to orange. The product **2.4·^{t}BuNC** was characterized in solution by ^{1}H NMR spectroscopy. **^{1}H NMR (600 MHz, C_6D_6, 293 K):** δ 7.21-7.08 (m, 5H, Ar), 7.03-6.96 (m, 4H, Ar), 5.21 (s, 1H, *H*C(C(Me)NAr)$_2$), 4.92 (sep, 1H, C*H*Me$_2$), 4.45 (sep, 1H, C*H*Me$_2$), 3.54 (sep, 1H, C*H*Me$_2$), 3.49-3.37 (m, 3H, C*H*Me$_2$), 1.72 (s, 3H, HC(C(*Me*)NAr)$_2$), 1.62 (s, 3H, HC(C(*Me*)NAr)$_2$), 1.52 (d, 3H, CH*Me*$_2$), 1.43 (d, 3H, CH*Me*$_2$), 1.36 (d, 3H, CH*Me*$_2$), 1.34 (d, 3H, CH*Me*$_2$), 1.33 (d, 3H, CH*Me*$_2$), 1.22 (d, 6H, CH*Me*$_2$),

1.19 (d, 3H, CH*Me*$_2$), 1.17 (d, 3H, CH*Me*$_2$), 1.15 (d, 3H, CH*Me*$_2$), 1.12 (d, 3H, CH*Me*$_2$), 1.07 (d, 3H, CH*Me*$_2$), 0.97 (s, 9H, NbN^{t}Bu), 0.83 (s, 9H, C≡N^{t}Bu).

(BDI)Nb(N^{t}Bu)(NAr)(CN^{n}Bu) (2.4·^{n}BuNC): Compound **2.4** (10 mg, 13 μmol) was dissolved in 0.5 mL C_6D_6 in a 4 mL vial. ^{n}BuNC (1.1 mg, 1.4 μL, 13 μmol) was added to the solution of **2.4** in one portion by microsyringe, resulting in a color change from red to orange. The product **2.4·^{n}BuNC** was characterized in solution by ^{1}H NMR spectroscopy. **^{1}H NMR (600 MHz, C_6D_6, 293 K):** δ 7.24 (dd, 1H, Ar), 7.22 (dd, 1H, Ar), 7.19-7.12 (m, 3H, Ar), 7.06-6.99 (m, 3H, Ar), 6.93 (t, 1H, Ar), 5.21 (s, 1H, *H*C(C(Me)NAr)$_2$), 5.03 (sep, 1H, C*H*Me$_2$), 4.48 (sep, 1H, C*H*Me$_2$), 3.56-3.42 (m, 4H, C*H*Me$_2$), 2.49 (m, 2H, NC*H*$_2$CH$_2$CH$_2$CH$_3$), 1.78 (s, 3H, HC(C(*Me*)NAr)$_2$), 1.70 (s, 3H, HC(C(*Me*)NAr)$_2$), 1.55 (d, 3H, CH*Me*$_2$), 1.49 (d, 3H, CH*Me*$_2$), 1.41 (d, 3H, CH*Me*$_2$), 1.40 (d, 3H, CH*Me*$_2$), 1.39 (d, 3H, CH*Me*$_2$), 1.25 (d, 6H, CH*Me*$_2$), 1.24 (d, 3H, CH*Me*$_2$), 1.18 (d, 3H, CH*Me*$_2$), 1.17 (d, 3H, CH*Me*$_2$), 1.16 (d, 3H, CH*Me*$_2$), 1.09 (d, 3H, CH*Me*$_2$), 1.01 (s, 9H, ^{t}Bu), 1.01-0.79 (m, 4H, NCH$_2$C*H*$_2$C*H*$_2$CH$_3$), 0.61 (t, 3H, NCH$_2$CH$_2$CH$_2$C*H*$_3$).

(BDI)Nb(N^{t}Bu)(NAr)(CNCy) (2.4·CyNC): Compound **2.4** (10 mg, 13 μmol) was dissolved in 0.25 mL C_6D_6 in a 4 mL vial. In a separate 4 mL vial, CyNC (1.4 mg, 13 μmol) was dissolved in 0.25 mL C_6D_6 and added to the solution of **2.4** in one portion, resulting in a color change from red to orange. The product **2.4·CyNC** was characterized in solution by ^{1}H NMR spectroscopy. **^{1}H NMR (400 MHz, C_6D_6, 293 K):** δ 7.24 (t, 2H, Ar), 7.19-7.12 (m, 3H, Ar), 7.07-6.92 (m, 4H, Ar), 5.04 (s, 1H, *H*C(C(Me)NAr)$_2$), 4.50 (sep, 1H, C*H*Me$_2$), 3.62-3.41 (m, 4H, C*H*Me$_2$), 2.92 (tt, 1H, Cy C*H*), 1.77 (s, 3H, HC(C(*Me*)NAr)$_2$), 1.69 (s, 3H, HC(C(*Me*)NAr)$_2$), 1.56 (d, 3H, CH*Me*$_2$), 1.51 (d, 3H, CH*Me*$_2$), 1.42 (d, 3H, CH*Me*$_2$), 1.41 (d, 3H, CH*Me*$_2$), 1.39 (d, 3H, CH*Me*$_2$), 1.25 (d, 6H, CH*Me*$_2$), 1.24 (d, 3H, CH*Me*$_2$), 1.22 (d, 3H, CH*Me*$_2$), 1.19 (d, 3H, CH*Me*$_2$), 1.17 (d, 3H, CH*Me*$_2$), 1.12 (d, 3H, CH*Me*$_2$), 1.05 (s, 9H, ^{t}Bu), 1.31-1.01 (m, 5H, Cy C*H*$_2$), 0.98-0.60 (m, 5H, Cy C*H*$_2$).

(BDI)Nb(N^{t}Bu)(NAr)(CNBn) (2.4·BnNC): Compound **2.4** (10 mg, 13 μmol) was dissolved in 0.25 mL C_6D_6 in a 4 mL vial. In a separate 4 mL vial, BnNC (1.8 mg, 13μL) was dissolved in 0.25 mL C_6D_6 and added to the solution of **2.4** in one portion, resulting in a color change from red to orange. The product **2.4·BnNC** was characterized in solution by ^{1}H NMR spectroscopy. **^{1}H NMR (600 MHz, C_6D_6, 293 K):** δ 7.23 (d, 1H, Ar), 7.21 (d, 1H, Ar), 7.17-7.11 (m, 3H, Ar), 7.07-6.95 (m, 6H, Ar/Bn), 6.84 (t, 1H, Bn), 6.78 (d, 2H, Bn), 5.21 (s, 1H, *H*C(C(Me)NAr)$_2$), 4.99 (sep, 1H, C*H*Me$_2$), 4.47 (sep, 1H, C*H*Me$_2$), 3.66 (d, 1H, Bn C*H*$_2$), 3.61 (d, 1H, Bn C*H*$_2$), 3.55-3.41 (m, 4H, C*H*Me$_2$), 1.77 (s, 3H, HC(C(*Me*)NAr)$_2$), 1.71 (s, 3H, HC(C(*Me*)NAr)$_2$), 1.53 (d, 3H, CH*Me*$_2$), 1.45 (d, 3H, CH*Me*$_2$), 1.41 (d, 3H, CH*Me*$_2$), 1.39 (d, 3H, CH*Me*$_2$), 1.37 (d, 3H, CH*Me*$_2$), 1.25 (d, 3H, CH*Me*$_2$), 1.24 (d, 3H, CH*Me*$_2$), 1.21 (d, 3H, CH*Me*$_2$), 1.18 (d, 3H, CH*Me*$_2$), 1.16 (d, 3H, CH*Me*$_2$), 1.08 (d, 3H, CH*Me*$_2$), 1.07 (d, 3H, CH*Me*$_2$), 0.89 (s, 9H, ^{t}Bu).

^{1}H NMR Kinetic Studies: Reaction kinetics for the transformation from **2.11** to **2.2·^{n}BuNC** were followed by ^{1}H NMR spectroscopy in J. Young NMR tubes with 0.02 M **2.11** and 0.02 M 1,3,5-trimethoxybenzene as an internal standard in C_6D_6 over a range of temperatures from 40 ˚C to 50˚C. Concentrations of **2.11** and **2.2·^{n}BuNC** were determined by integrating their isopropyl methine resonances at 4.21 ppm and 3.94 ppm, respectively, relative to the internal standard signal at 6.23 ppm. Rate constants were calculated by plotting ln[**2.11**] or ln[**2.2·^{n}BuNC**] versus time at

each temperature. Rate constants determined based on disappearance of starting material and appearance of products were identical, and mass balance was conserved in each experiment.

Catalytic production of carbodiimides

N-*tert*-butyl-N'-*n*-butylcarbodiimide: Compound **2.2** (10 mg, 15 μmol, 1 equiv.) and 1,3,5-$(MeO)_3Ph$ (2.6 mg, 15 μmol, 1 equiv.) were dissolved in a mixture of $^tBuN_3$ (0.36 mL, 300 mg, 3.1 mmol, 200 eq) and 0.3 mL C_6D_6 in a 4 mL vial and transferred to a J. Young NMR tube. ^{n}BuNC (16 μL, 150 μmol, 10 equiv.) was added in one portion and the NMR tube was sealed. The solution was then heated at 60 °C for 20 h, resulting in a gradual color change from orange to orange-brown and catalytic production of carbodiimide, which was identified by ^{1}H NMR spectroscopy (85% NMR yield) and GC-MS. **^{1}H NMR (600 MHz, C_6D_6, 293 K):** δ 3.01 (t, 2H, $NCH_2CH_2CH_2CH_3$), 1.39 (m, 2H, $NCH_2CH_2CH_2CH_3$), 1.26 (m, 2H, $NCH_2CH_2CH_2CH_3$), 1.15 (s, 9H, ^{t}Bu), 0.79 (t, 3H, $NCH_2CH_2CH_2CH_3$). MS: m/z calcd for $C_9H_{18}N_2$: 154 found: 139 (molecular ion minus methyl group; MS is a close match to that of N,N'-di-*tert*-butylcarbodiimide). Spectroscopic data are in agreement with previous reports.[29]

N-*tert*-butyl-N'-cyclohexylcarbodiimide: Compound **2.2** (10 mg, 15 μmol, 1 equiv.) and 1,3,5-$(MeO)_3Ph$ (2.6 mg, 15 μmol, 1 equiv.) were dissolved in a mixture of $^tBuN_3$ (0.36 mL, 300 mg, 3.1 mmol, 200 eq) and 0.3 mL C_6D_6 in a 4 mL vial and transferred to a J. Young NMR tube. CyNC (32 μL, 260 μmol, 17 equiv.) was added in one portion and the NMR tube was sealed. The solution was then heated at 80 °C for 20 h, resulting in a gradual color change from orange to orange-brown and catalytic production of carbodiimide, which was identified by ^{1}H NMR spectroscopy (quantitative NMR yield) and GC-MS. **^{1}H NMR (600 MHz, C_6D_6/^{t}BuN$_3$, 293 K):** δ 3.04 (tt, 1H, Cy C*H*), 1.78 (m, 2H, Cy CH_2), 1.58 (m, 2H, Cy CH_2), 1.44-1.11 (m, 6H, Cy CH_2), 1.16 (s, 9H, ^{t}Bu). MS: m/z calcd for $C_{11}H_{20}N_2$: 180 found: 180. Spectroscopic data are in agreement with previous reports.[30]

N-*tert*-butyl-N'-benzylcarbodiimide: Compound **2.2** (10 mg, 15 μmol, 1 equiv.), $^tBuN_3$ (30 mg, 36 μL, 310 μmol, 20 equiv.), and 1,3,5-$(MeO)_3Ph$ (2.6 mg, 15 μmol, 1 equiv.) were dissolved in 0.5 mL C_6D_6 in a 4 mL vial and transferred to a J. Young NMR tube. Benzyl isocyanide was added in small increments (0.9 μL, 8 μmol, 0.5 equiv. each) and left at room temperature over a period of 6 h, resulting in a gradual color change from orange to brown and catalytic production of carbodiimide, which was identified by ^{1}H NMR spectroscopy and GC-MS. **^{1}H NMR (500 MHz, C_6D_6/^{t}BuN$_3$, 293 K):** δ 7.15 (d, 2H, Ar), 7.12 (t, 2H, Ar), 7.04 (t, 1H, Ar), 4.08 (s, 2H, CH_2), 1.04 (s, 9H, ^{t}Bu). MS: m/z calcd for $C_{12}H_{16}N_2$: 188, found: 188. Spectroscopic data are in agreement with previous reports.[31]

X-Ray Crystallographic Studies: Single crystals of **2.2·XylNC, 2.3, 2.5a, 5c, 2.7, 2.8, 2.9** and **2.11** were coated in Paratone-N oil, mounted on a Kaptan loop, transferred to a Bruker APEX CCD area detector,[32] centered in the beam, and cooled by a nitrogen flow low-temperature apparatus that had been previously calibrated by a thermocouple placed at the same position as the crystal. Preliminary orientation matrices and cell constants were determined by collection of 36 10 s frames, followed by spot integration and least-squares refinement. An arbitrary hemisphere of data was collected, and the raw data were integrated using SAINT.[33] Cell dimensions reported were

calculated from all reflections with $I > 10$ (Table 1). The data were corrected for Lorentz and polarization effects, but no correction for crystal decay was applied. An empirical absorption correction based on comparison of redundant and equivalent reflections was applied using SADABS.[34] Structures were solved by direct methods with the aid of successive difference Fourier maps and were refined against all data using the SHELXTL 5.0 software package.[35] Thermal parameters for all non-hydrogen atoms were refined anisotropically. ORTEP diagrams were created using the ORTEP-3 software package[36] and Mercury.[37]

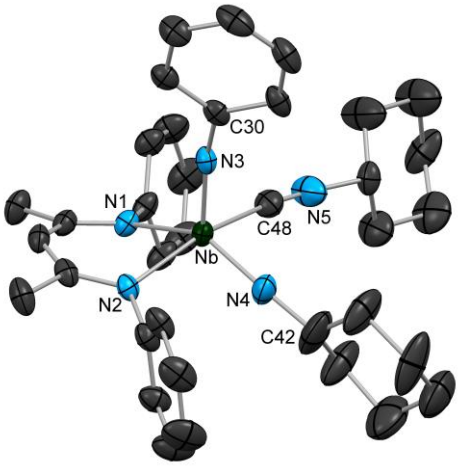

Figure 2.7 Molecular structure of **2.7** determined by X-ray diffraction. H atoms and aryl ^{i}Pr groups have been omitted for clarity; thermal ellipsoids are displayed at the 50% probability level. Selected bond lengths (Å): Nb-N(1): 2.261(2), Nb-N(2): 2.191(3), Nb-N(3): 1.826(3), Nb-N(4): 1.798(3), Nb-C(48): 2.268(4). Selected bond angles (˚): N(2)-Nb-C(48): 158.4(1), N(1)-Nb-N(4): 136.9(1), Nb-N(3)-C(30): 167.2(2), Nb-N(4)-C(42): 176.8(3), Nb-C(48)-N(5): 171.0(3).

Table 2.1 Crystallographic data for compounds **2.2·XylNC**, **2.3**, **2.5a**, and **2.5c**.

Compound	**2.2·XylNC**	**2.3**	**2.5a · 0.6 C_6H_{14}**	**2.5c**
Empirical formula	$C_{46}H_{68}N_5Nb$	$C_{36}H_{59}N_4NbSi$	$C_{49.75}H_{76.75}N_5Nb$	$C_{45}H_{66}N_5NbO$
Formula weight (amu)	783.96	668.87	837.82	785.93
Wavelength (Å)	0.71073	0.71073	0.71073	0.71073
Space group	$P2_1/n$	P-1	$P2_1/n$	$P2_1/n$
a (Å)	12.2648(5)	11.0636(5)	11.1908(4)	18.891(1)
b (Å)	20.8147(9)	13.0724(6)	17.8757(7)	11.1216(6)
c (Å)	17.2712(7)	13.4439(6)	24.6374(9)	21.154(1)
α (°)	90	92.209(2)	90	90
β (°)	100.263(2)	102.071(2)	90.4053(8)	100.794(2)
γ (°)	90	96.205(2)	90	90
V (Å^3)	4338.6(3)	1886.5(2)	4928.4(3)	4367.6(4)
Z	4	2	4	4
ρ_{calcd} (g/cm^3)	1.200	1.178	1.129	1.195
μ (mm^{-1})	0.313	0.378	0.280	0.313
F_{000} (e$^-$)	1680	716	1805	1680
Crystal size (mm^3)	.14 x .12 x .08	.12 x .10 x .10	.10 x .10 x .06	.10 x .10 x .08
Theta min / max (˚)	1.547 / 25.369	1.552 / 25.414	1.407 / 25.354	1.327 / 25.378
Reflections collected	88948	51010	54203	74082
R_{int}	0.0273	0.0269	0.0424	0.0359
T_{max} / T_{min}	0.7452 / 0.7182	0.7452 / 0.7003	0.7452 / 0.6696	0.7452 / 0.7001
Data / restr. / param.	7954 / 0 / 487	6934 / 0 / 395	9031 / 0 / 544	7978 / 0 / 486
GoF	1.021	1.076	1.094	1.068
R_1 / wR_2 (I>2σ(I))	0.0258 / 0.0594	0.0211 / 0.0525	0.0357 / 0.0730	0.0257 / 0.0622
R_1 / wR_2 (all data)	0.0300 / 0.0623	0.0229 / 0.0535	0.0454 / 0.0768	0.0299 / 0.0644
Res. peak / hole (e$^-$/Å^3)	0.563 / -0.426	0.330 / -0.304	0.429 / -0.382	0.382 / -0.327

Table 2.2 Crystallographic data for compounds **2.7**, **2.8**, **2.9**, and **2.11**

Compound	**2.7**	**2.8**	**2.9·C_7H_8**	**2.11**
Empirical formula	$C_{54}H_{80}N_5Nb$	$C_{58}H_{95}N_8Nb$	$C_{56}H_{72}N_5Nb$	$C_{42}H_{68}N_7Nb$
Formula weight (amu)	892.14	997.32	908.09	763.94
Wavelength (Å)	0.71073	0.71073	0.71073	0.71073
Space group	$P2_1/c$	$P2_1/n$	$P2_1/c$	$P2_1/n$
a (Å)	19.790(2)	13.0963(5)	32.287(2)	13.1917(7)
b (Å)	15.626(1)	20.4362(7)	3.8363(8)	16.3220(8)
c (Å)	17.021(1)	21.6295(7)	24.043(1)	19.952(1)
α (°)	90	90	90	90
β (°)	103.833(4)	101.979(2)	110.578(3)	95.670(2)
γ (°)	90	90	90	90
V (Å^3)	5111.0(7)	5662.8(3)	10055(1)	4274.9(4)
Z	4	4	8	4
ρ_{calcd} (g/cm^3)	1.159	1.170	1.200	1.187
μ (mm^{-1})	0.274	0.255	0.280	0.317
F_{000} (e$^-$)	1920	2160	3872	1640
Crystal size (mm^3)	.06 x .04 x .04	.07 x .06 x .05	.18 x .08 x .06	.10 x .07 x .05
Theta min / max (˚)	1.680 / 25.425	1.385 / 25.405	1.347 / 25.461	1.615 / 25.383
Reflections collected	63130	54452	61211	69669
R_{int}	0.0868	0.0619	0.0730	0.0679
T_{max} / T_{min}	0.7452 / 0.7083	0.7452 / 0.6831	0.7452 / 0.7021	0.7452 / 0.6512
Data / restr. / param.	9390 / 12 / 487	10382 / 0 / 622	61211 / 30 / 1134	7831 / 0 / 487
GoF	1.019	1.046	1.024	1.050
R_1 / wR_2 (I>2σ(I))	0.0481 / 0.1011	0.0571 / 0.1047	0.0590 / 0.1430	0.0390 / 0.0963
R_1 / wR_2 (all data)	0.0844 / 0.1189	0.0823 / 0.1572	0.0741 / 0.1515	0.0504 / 0.1024
Res. peak / hole (e$^-$/Å^3)	0.888 / -0.440	1.907 / -0.577	1.361 / -0.766	1.461 / -0.640

DFT Calculations: All structures and energies were calculated using the Gaussian09 suite of programs.[38] Self-consistent field computations were performed with tight convergence criteria on ultrafine grids, while geometry optimizations were converged to tight geometric convergence criteria for all compounds. Frequencies were calculated analytically at 298.15 K and 1 atm. Structures were considered true minima if they did not exhibit imaginary vibration modes and were considered as transition states when only one imaginary vibration mode was found. Intrinsic Reaction Coordinates (IRC) calculations were performed to ensure the transition state geometries connected the reactants and the products. Optimized geometries were compared using the sum of

their electronic and zero-point energies. In order to reduce the computational time, the system was structurally simplified by replacing 2,6-diisopropylphenyl groups by phenyl groups. The B3LYP hybrid functional was used throughout this computational study.[39] For geometry optimizations and frequency calculations, the light atoms (H, C, N and F) were treated with the 6-31G(d,p) basis,[40] while the niobium atom was treated with a Stuttgart/Dresden ECP pseudopotential (SDD).[41]

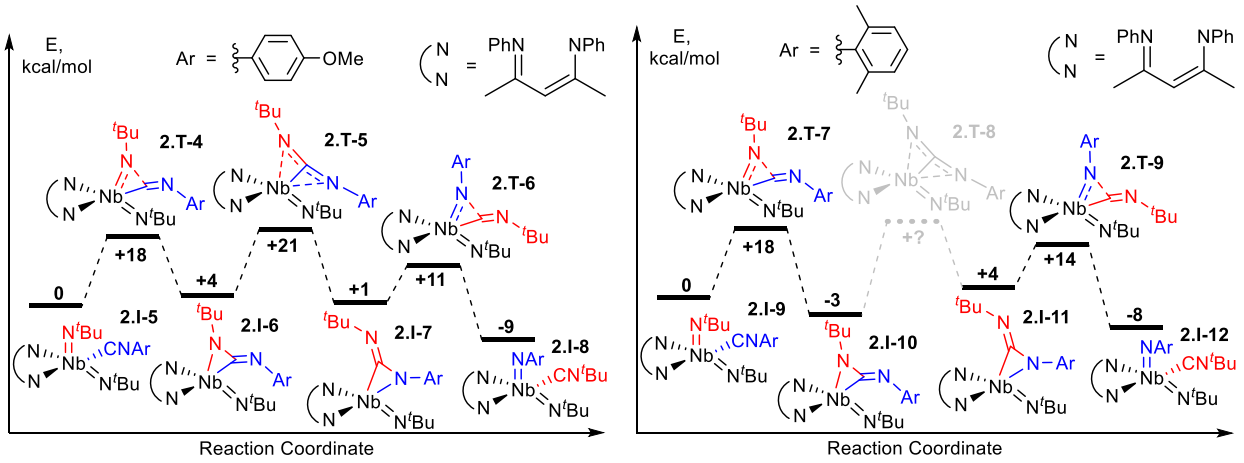

Figure 2.8 DFT calculated energy profile for nitrene metathesis with Ar = *p*-MeOPh (left) and Ar = 2,6-Xyl (right). Transition state **2.T-8** could not be found.

Notes and References

(1) (a) Cummins, C. C.; Baxter, S. M.; Wolczanski, P. T. *J. Am. Chem. Soc.* **1988**, *110*, 8731. (b) Walsh, P. J.; Hollander, F. J.; Bergman, R. G. *J. Am. Chem. Soc.* **1988**, *110*, 8729.

(2) Duncan, A. P.; Bergman, R. G. *Chem. Rec.* **2002**, *2*, 431.

(3) Hazari, N.; Mountford, P. *Acc. Chem. Res.* **2005**, *38*, 839.

(4) (a) Walsh, P. J.; Hollander, F. J.; Bergman, R. G. *Organometallics* **1993**, *12*, 3705. (b) Lee, S. Y.; Bergman, R. G. *Tetrahedron* **1995**, *51*, 4255. (c) Bashall, A.; Collier, P. E.; Gade, L. H.; McPartlin, M.; Mountford, P.; Pugh, S. M.; Radojevic, S.; Schubart, M.; Scowen, I. J.; Trösch, D. J. M. *Organometallics* **2000**, *19*, 4784. (d) Guiducci, A. E.; Cowley, A. R.; Skinner, M. E. G.; Mountford, P. *J. Chem. Soc. Dalt. Trans.* **2001**, 1392. (e) Blake, A. J.; Collier, P. E.; Gade, L. H.; McPartlin, M.; Mountford, P.; Schubart, M.; Scowen, I. J. *Chem. Commun.* **1997**, 1555. (f) Li, Y.; Shi, Y.; Odom, A. L. *J. Am. Chem. Soc.* **2004**, *126*, 1794.

(5) (a) Walsh, P. J.; Baranger, A. M.; Bergman, R. G. *J. Am. Chem. Soc.* **1992**, *114*, 1708. (b) Odom, A. L.; McDaniel, T. J. *Acc. Chem. Res.* **2015**, *48*, 2822.

(6) (a) Basuli, F.; Aneetha, H.; Huffman, J. C.; Mindiola, D. J. *J. Am. Chem. Soc.* **2005**, *127*, 17992. (b) Ruck, R. T.; Zuckerman, R. L.; Krska, S. W.; Bergman, R. G. *Angew. Chem. Int. Ed. Engl.* **2004**, *43*, 5372.

(7) Zuckerman, R. L.; Krska, S. W.; Bergman, R. G. *J. Am. Chem. Soc.* **2000**, *122*, 751.

(8) Meyer, K. E.; Walsh, P. J.; Bergman, R. G. *J. Am. Chem. Soc.* **1995**, *117*, 974.

(9) (a) Chu, J.; Lu, E.; Liu, Z.; Chen, Y.; Leng, X.; Song, H. *Angew. Chem. Int. Ed. Engl.* **2011**, *50*, 7677. (b) Scott, J.; Basuli, F.; Fout, A. R.; Huffman, J. C.; Mindiola, D. J. *Angew. Chem.*

Int. Ed. Engl. **2008**, *47*, 8502. (c) Chu, T.; Piers, W. E.; Dutton, J. L.; Parvez, M. *Organometallics* **2012**, *32*, 1159.

(10) (a) Anderson, L. L.; Arnold, J.; Bergman, R. G. *Org. Lett.* **2004**, *6*, 2519. (b) Blake, R. E; Antonelli, D. M.; Henling, L. M.; Schaefer, W. P.; Hardcastle, K. I.; Bercaw, J. E. *Organometallics* **1998**, *17*, 718. (c) Schaller, C. P.; Wolczanski, P. T. *Inorg. Chem.* **1993**, *32*, 131.

(11) Obenhuber, A. H.; Gianetti, T. L.; Berrebi, X.; Bergman, R. G.; Arnold, J. *J. Am. Chem. Soc.* **2014**, *136*, 2994.

(12) (a) Obenhuber, A. H.; Gianetti, T. L.; Bergman, R. G.; Arnold, J. *Chem. Commun.* **2014**. (b) La Pierre, H. S.; Arnold, J.; Toste, F. D. *Angew. Chemie Int. Ed.* **2011**, *50*, 3900. (c) De With, J.; Horton, A. D.; Orpen, A. G. *Organometallics* **1993**, *12*, 1493.

(13) (a) Hanna, T. E.; Keresztes, I.; Lobkovsky, E.; Bernskoetter, W. H.; Chirik, P. J. *Organometallics* **2004**, *23*, 3448. (b) Dunn, S. C.; Hazari, N.; Cowley, A. R.; Green, J. C.; Mountford, P. *Organometallics* **2006**, *25*, 1755.

(14) (a) Nguyen, A. I.; Zarkesh, R. A.; Lacy, D. C.; Thorson, M. K.; Heyduk, A. F. *Chem. Sci.* **2011**, *2*, 166. (b) Gilbert, Z. W.; Hue, R. J.; Tonks, I. A. *Nat. Chem.* **2016**, *8*, 63.

(15) (a) Tomson, N. C.; Yan, A.; Arnold, J.; Bergman, R. G. *J. Am. Chem. Soc.* **2008**, *130*, 11262. (b) Tomson, N. C.; Arnold, J.; Bergman, R. G. *Organometallics* **2010**, *29*, 2926. (c) Tomson, N. C.; Arnold, J.; Bergman, R. G. *Organometallics* **2010**, *29*, 5010. (d) Gianetti, T. L.; Nocton, G.; Minasian, S. G.; Tomson, N. C.; Kilcoyne, A. L. D.; Kozimor, S. A.; Shuh, D. K.; Tyliszczak, T.; Bergman, R. G.; Arnold, J. *J. Am. Chem. Soc.* **2013**, *135*, 3224. (e) Gianetti, T. L.; Tomson, N. C.; Arnold, J.; Bergman, R. G. *J. Am. Chem. Soc.* **2011**, *133*, 14904. (f) Gianetti, T. L.; Bergman, R. G.; Arnold, J. *Chem. Sci.* **2014**, *5*, 2517. (g) Kriegel, B. M.; Bergman, R. G.; Arnold, J. *Dalton Trans.* **2014**, *43*, 10046.

(16) (a) Cundari, T. R. *Organometallics* **1994**, *13*, 2987. (b) O'Reilly, M. E.; Ghiviriga, I.; Abboud, K. A.; Veige, A. S. *J. Am. Chem. Soc.* **2012**, *134*, 11185.

(17) Addison, A. W.; Rao, T. N.; Reedijk, J.; van Rijn, J.; Verschoor, G. C. *J. Chem. Soc. Dalton Trans.* **1984**, 1349.

(18) (a) Jones, W. D.; Kosar, W. P. *Organometallics* **1986**, *5*, 1823. (b) Millich, F. *Chem. Rev.* **1972**, *72*, 101.

(19) Boyarskiy, V. P.; Bokach, N. A.; Luzyanin, K. V.; Kukushkin, V. Y. *Chem. Rev.* **2015**, *115*, 2698.

(20) (a) Fickes, M. G.; Davis, W. M.; Cummins, C. C. *J. Am. Chem. Soc.* **1995**, *117*, 6384. (b) Proulx, G.; Bergman, R. G. *J. Am. Chem. Soc.* **1995**, *117*, 6382. (c) Proulx, G.; Bergman, R. G. *Organometallics* **1996**, *15*, 684.

(21) (a) Wiese, S.; Aguila, M. J. B.; Kogut, E.; Warren, T. H. *Organometallics* **2013**, *32*, 2300. (b) Laskowski, C. A.; Hillhouse, G. L. *Organometallics* **2009**, *28*, 6114. (c) Saegusa, T.; Ito, Y.; Shimizu, T. *J. Org. Chem.* **1970**, *35*, 3995. (d) Cowley, R. E.; Golder, M. R.; Eckert, N. A.; Al-Afyouni, M. H.; Holland, P. L. *Organometallics* **2013**, *32*, 5289. (e) Zhang, Z.; Li, Z.; Fu, B.; Zhang, Z. *Chem. Commun.* **2015**, *51*, 16312. (f) Yousif, M.; Tjapkes, D. J.; Lord, R. L.; Groysman, S. *Organometallics* **2015**, *34*, 5119.

(22) Bottaro, J. C.; Penwell, P. E.; Schmitt, R. J. *Synth. Commun.* 1997, *27*, 1465.

(23) Barral, K.; Moorhouse, A. D.; Moses, J. E. *Org. Lett.* **2007**, *9*, 1809.

(24) Micksch, M.; Tenne, M.; Strassner, T. *European J. Org. Chem.* **2013**, *2013*, 6137.
(25) Nanjo, T.; Tsukano, C.; Takemoto, Y. *Org. Lett.* **2012**, *14*, 4270.
(26) Feldman, J.; Mclain, S. J.; Parthasarathy, A.; Marshall, W. J.; Calabrese, J. C.; Arthur, S. D. *Organometallics*, **1997**, *95*, 1514.
(27) Budzelaar, P. H. M.; van Oort, A. B.; Orpen, A. G. *Eur. J. Inorg. Chem.* **1998**, 1485.
(28) Sundermeyer, J.; Putterlik, J.; Foth, M.; Field, J.; Ramesar, N. *Chem. Ber.* **1994**, *127*, 1201.
(29) Pri-Bar, I.; Schwartz, J. *Chem. Commun.* **1997**, 347.
(30) Keaton, R. J.; Jayaratne, K. C.; Henningsen, D. A.; Koterwas, L. A.; Sita, L. R. *J. Am. Chem. Soc.* **2001**, *123*, 6197.
(31) Volonterio, A.; Ramirez de Arellano, C.; Zanda, M. *J. Org. Chem.* **2005**, *70*, 2161.
(32) SMART: Area-Detector Software Package; Bruker Analytical X-ray Systems, Inc.: Madison, WI, 2001-2003.
(33) SAINT: SAX Area-Detector Integration Program; Bruker Analytical X-ray Systems Inc.: Madison, WI, 2003.
(34) SADABS: Bruker-Nonius Area Detector Scaling and Absorption; Bruker Analytical X-ray Systems, Inc.: Madison, WI, 2003.
(35) Sheldrick, G. M. *Acta Crystallogr. Sect. A* **2008**, *64*, 112.
(36) Farrugia, L. J. *Journal of Applied Crystallography*, **1997**, *30*, 565.
(37) Macrae, C. F.; Bruno, I. J.; Chisholm, J. A.; Edgington, P. R.; McCabe, P.; Pidcock, E.; Rodriguez-Monge, L.; Taylor, R.; van de Streek, J.; Wood, P. A. *J. Appl. Crystallogr.* **2008**, *41*, 466.
(38) Frisch, M.; Trucks, G.; Schlegel, H.; Scuseria, G.; Robb, M.; Cheeseman, J.; Scalmani, G.; Barone, V.; Mennucci, B.; Petersson, G.; Nakatsuji, H.; Caricato, M.; Li, X.; Hratchian, H.; Izmaylov, A.; Bloino, J.; Zheng, G.; Sonnenberg, J.; Hada, M.; Ehara, M.; Toyota, K.; Fukuda, R.; Hasegawa, J.; Ishida, M.; Nakajima, T.; Honda, Y.; Kitao, O.; Nakai, H.; Vreven, T.; Montgomery, J.; Peralta, J.; Ogliaro, F.; Bearpark, M.; Heyd, J.; Brothers, E.; Kudin, K.; Staroverov, V.; Kobayashi, R.; Normand, J.; Raghavachari, K.; Rendell, A.; Burant, J.; Iyengar, S.; Tomasi, J.; Cossi, M.; Rega, N.; Millam, J.; Klene, M.; Knox, J.; Cross, J.; Bakken, V.; Adamo, C.; Jaramillo, J.; Gomperts, R.; Stratmann, R.; Yazyev, O.; Austin, A.; Cammi, R.; Pomelli, C.; Ochterski, J.; Martin, R.; Morokuma, K.; Zakrzewski, V.; Voth, G.; Salvador, P.; Dannenberg, J.; Dapprich, S.; Daniels, A.; Farkas; Foresman, J.; Ortiz, J.; Cioslowski, J.; Fox, D. *Gaussian 09, Revis. D.01, Gaussian, Inc., Wallingford CT* **2009**.
(39) Lee, C.; Yang, W.; Parr, R. G. *Phys. Rev. B* **1988**, *37*, 785.
(40) Hariharan, P. C.; Pople, J. A. *Mol. Phys.* **2006**, *27*, 209.
(41) Fuentealba, P.; Preuss, H.; Stoll, H.; Von Szentpály, L. *Chem. Phys. Lett.* **1982**, *89*, 418.

Chapter 3

Cycloaddition and 1,2-Addition Reactions of Niobium Bis(imido) Complexes

Introduction

Addition of substrates across metal-ligand multiple bonds is an important reaction pathway in catalytic and stoichiometric reactions, especially in high-valent early- and mid-transition metal complexes.[1–4] The ability of group IV terminal imido complexes to engage in C-H activations of methane and other hydrocarbons as well as cycloadditions of unsaturated substrates was first realized in the late 1980s.[5,6] Since then, further work in investigating reactions across terminal imido groups in high-valent early transition metal complexes has led to the development of a number of catalytic processes involving nitrene transfers,[7,8] including imine and azide metatheses,[9–12] hydroaminations of alkenes and alkynes,[13–18] carboaminations to give α,β-unsaturated imines,[19–21] and oxidative nitrene transfers to form carbodiimides and pyrroles.[22,23]

In contrast to well-known nitrene transfer chemistry involving metal imido complexes, catalytic reactions that cleave a bond in the substrate *without* nitrene transfer are rare. This type of strategy has been used in reactive group 4 alkylidyne complexes to stoichiometrically dehydrogenate linear alkanes into terminal olefins.[24,25] While the reactivity observed in these systems is impressive, reaction across the multiple bond is extremely thermodynamically downhill, precluding any catalytic turnover by regeneration of the reactive alkylidyne moiety. Recently, the bis(imido)vanadium cation **3.I** was shown to function as a catalyst for the selective semi-hydrogenation of internal alkynes to Z-alkenes.[26,27] This study constituted a new mechanism for alkyne hydrogenation involving 1,2-addition of dihydrogen across a V=N bond to give **3.II**, followed by insertion to give **3.III** and finally α-elimination to release the product (Scheme 3.1). In contrast to most transition metal catalyzed hydrogenations, the metal center remains in a single oxidation state throughout the catalytic cycle. We have since become interested in developing group 5 systems that can carry out more complex functionalizations of unsaturated substrates, such as hydroboration and hydrosilation by an analogous mechanistic pathway.

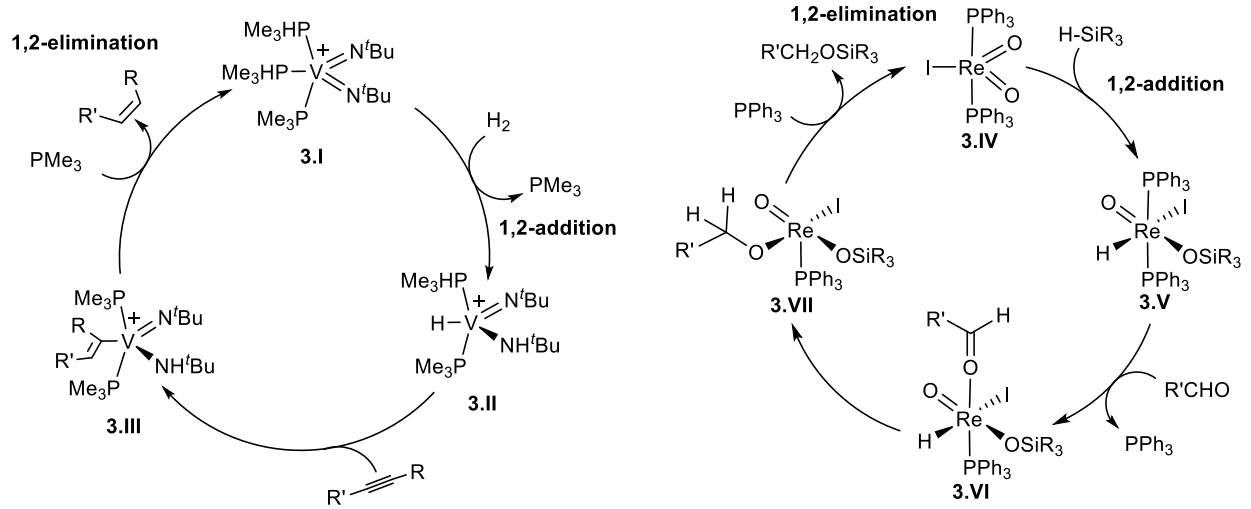

Scheme 3.1 Mechanisms for hydrogenation of alkynes catalyzed by a vanadium (V) bis(imido) complex (left) and hydrosilation of aldehydes by a rhenium (V) bis(oxo) complex (right).

In related work, rhenium (V) and molybdenum (VI) dioxo complexes have been shown to catalyze hydrogenations, hydrosilations, hydroborations and hydrophosphonylations of ketones, aldehydes, and imines.[28–32] While the mechanisms for these reactions are not clear in all cases,[33–35] studies in the rhenium system $ReIO_2(PPh_3)$ (**3.IV**) have implicated the 1,2-addition pathway shown in Scheme 3.1, in which the rhenium center does not change oxidation state throughout the catalytic cycle.[31] High-valent group 3,[36,37] group 4,[38–41] and actinide[42,43] imido complexes have also been shown to activate dihydrogen, silanes and/or boranes across imido bonds, but in all of these cases, only stoichiometric reactivity could be observed. Although the reaction chemistry of related group 4 terminal chalcogenide complexes has been much less explored,[44–50] a handful of titanium and zirconium oxo and sulfido complexes were shown to react with dihydrogen and silanes.[51–53] In contrast, while many examples of group 5 terminal imido and terminal oxo complexes have been reported, only a few have been shown to exhibit 1,2-addition reactivity.[26,27,54,55] We hoped to take advantage of π-loading[26,56–59] in niobium bis(imido) complexes and niobium oxo-imido complexes in order to carry out related hydrofunctionalizations using 1,2-addition and elimination reactions across imido groups.

In the previous chapter and in recent publications, we described the synthesis and nitrene transfer reactivity of niobium bis(imido) complexes.[60,61] In contrast to related mono(imido) niobium systems supported by BDI ligands,[62–69] π-loading effects in these compounds were shown to engender reactivity across their Nb-N π-bonds.[56,60] Here we describe their [3+2] and [2+2] cycloaddition and 1,2-addition reactivity with a variety of small molecule substrates including azides, carbon dioxide, dihydrogen, silanes and boranes. Moreover, we describe the utility of these bis(imido) complexes in accessing isolobal niobium terminal oxo-imido complexes.

Results and Discussion

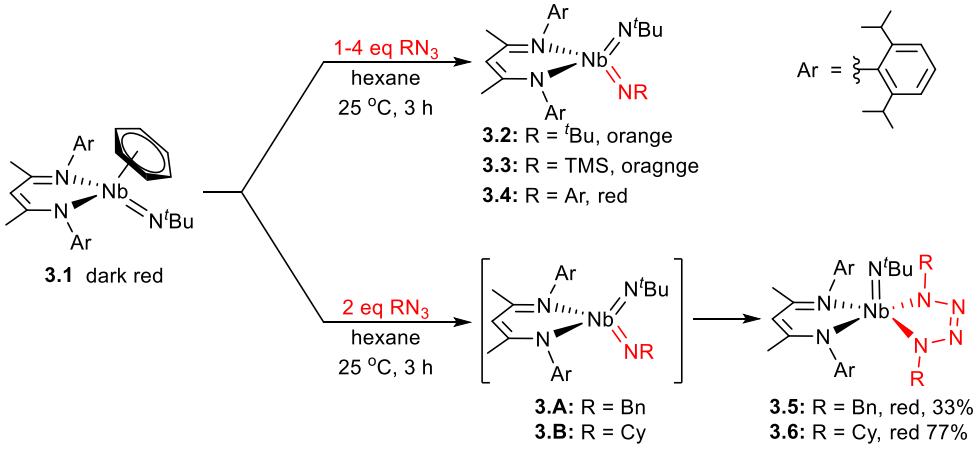

Scheme 3.2 Formation of tetrazene complexes from cycloaddition to bis(imido) intermediates.

As discussed in the previous chapter, bis(imido) complexes **3.2** – **3.4** were produced from reaction of azides with **2.1**; in contrast, reaction with the less hindered alkyl azides RN_3 (R = Bn, Cy) instead gave conversion to niobatetrazene complexes **3.5** and **3.6**, which were isolated as red needles from a saturated diethyl ether solution in 33% yield (R = Bn) or as red plates from a saturated hexane solution in 77% yield (R = Cy) (Scheme 3.2). Formation of these compounds

resulted from initial nitrene transfer to form bis(imido) intermediates **3.A** and **3.B**, followed by [3+2] cycloaddition of a second equivalent of azide. Related group 4 and group 5 tetrazene complexes have been accessed from [3+2] cycloadditions of azides across imido groups.[7,12,57,70] The ^{1}H NMR spectrum of **3.5** is consistent with C_s symmetry in solution, consisting of one singlet integrating for four protons for the benzylic protons, as well as two septets corresponding to two inequivalent isopropyl methine protons, each integrating for two protons. Compound **3.6** displays a similar ^{1}H NMR spectrum, also consistent with C_s solution symmetry.

Compounds **3.5** and **3.6** were also characterized in the solid state by X-ray crystallography; ORTEP diagrams along with relevant metrical parameters are shown in Figure 3.1. The benzyl derivative **3.5** is a distorted square-based pyramid ($\tau = 0.13$)[71] with one of the BDI nitrogen atoms occupying the apical position; hence, curiously, **3.5** displays C_1 symmetry in the solid state, in contrast to its C_s solution symmetry. In contrast, while **3.6** is also a distorted square-based pyramid ($\tau = 0.02$), the imido instead occupies the apical position, resulting in a solid-state structure with only slight distortions from C_s symmetry. Thus, the solution structure and solid-state structure of **3.6** are likely similar.

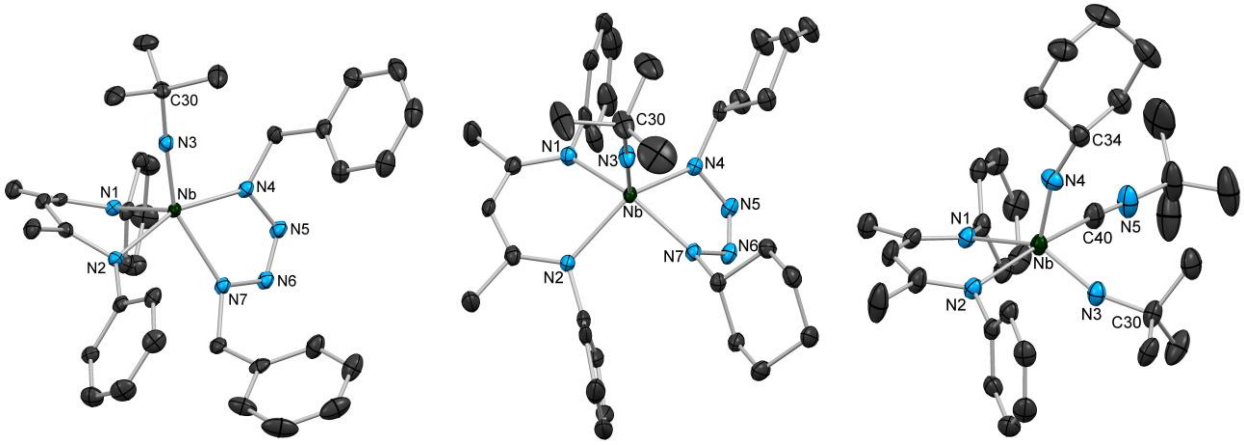

Figure 3.1 Molecular structures of **3.5** (left), **3.6** (middle) and **3.8a** (right) determined by X-ray diffraction. H atoms and aryl ^{i}Pr groups have been omitted for clarity; thermal ellipsoids are displayed at the 50% probability level. For **3.5** (left), selected bond lengths (Å): Nb-N(1) 2.117(2), Nb-N(2) 2.179(2), Nb-N(3) 1.785(2), Nb-N(4) 2.039(2), Nb-N(7) 2.173(2), N(4)-N(5) 1.391(3), N(5)-N(6) 1.272(3), N(6)-N(7) 1.365(3); selected bond angles (˚), N(2)-Nb-N(4) 160.04(7), N(3)-Nb-N(7) 152.52(8), N(1)-Nb-N(3) 103.07(8), Nb-N(3)-C(30) 175.4(2). For **3.6** (middle), selected bond lengths (Å): Nb-N(1) 2.231(2), Nb-N(2) 2.224(2), Nb-N(3) 1.756(2), Nb-N(4) 2.056(2), Nb-N(7) 2.042(2), N(4)-N(5) 1.373(3), N(5)-N(6) 1.288(3), N(6)-N(7) 1.381(3); selected bond angles (˚), N(1)-Nb-N(7) 143.95(9), N(2)-Nb-N(4) 143.07(9), N(1)-Nb-N(3) 107.0(1), Nb-N(3)-C(30) 179.0(2). For **3.8** (right), selected bond lengths (Å): Nb-N(1) 2.299(2), Nb-N(2) 2.207(2), Nb-N(3) 1.812(2), Nb-N(4) 1.800(2), Nb-C(40) 2.271(3); selected bond angles (˚): N(1)-Nb-N(3) 135.93(9), N(2)-Nb-C(40) 161.9(1), N(1)-Nb-N(4) 112.97(9), Nb-N(3)-C(30) 159.8(2), Nb-N(4)-C(34) 162.5(2).

In addition to **3.5**, a second compound could be observed by ^{1}H NMR spectroscopy as a minor reaction product (~10% relative to **3.5**). Based on the ^{1}H NMR spectrum, which showed two

separate singlets each integrating for two protons corresponding to the benzylic protons, this compound could be formulated as the C_1-symmetric structural isomer of **3.5** observed in the solid-state structure.

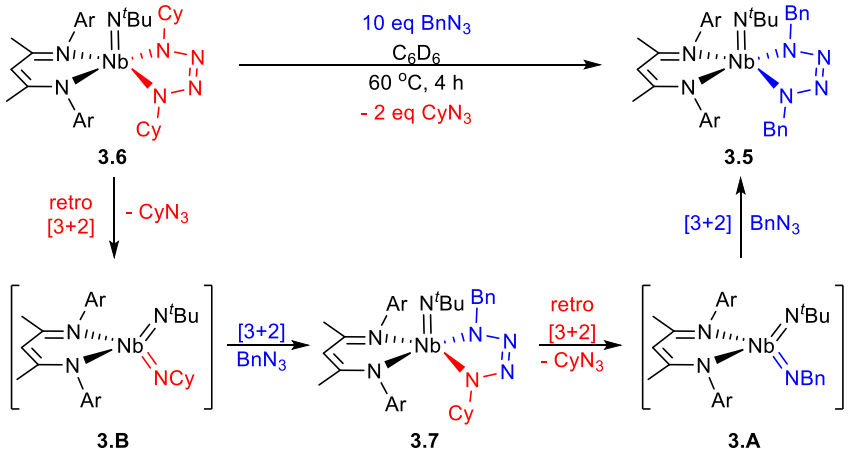

Scheme 3.3 Azide metathesis chemistry demonstrates reversibility of [3+2] cycloaddition.

Zirconium imido compounds have been shown to undergo [3+2] cycloaddition reactions with azides reversibly in order to promote catalytic azide metathesis; hence, we investigated the ability of **3.5** and **3.6** to engage in azide metathesis. Upon heating **3.6** with excess BnN_3, conversion to **3.5** coupled with loss of cyclohexyl azide was observed by ^{1}H NMR spectroscopy. This reaction likely proceeded through a series of reversible [3+2] cycloaddition and cycloreversion steps, as outlined in Scheme 3.3. Compound **3.7** was observed as an intermediate that built up during the reaction, but disappeared after its completion. Under similar conditions, **3.5** reacted more slowly with excess cyclohexylazide, and could not be fully converted to **3.6**, indicating **3.5** is thermodynamically favored over **3.6**, likely due primarily to steric considerations.

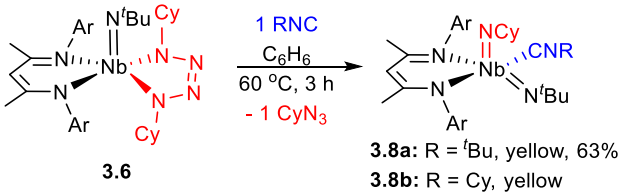

Scheme 3.4 Reactivity of **3.6** with isocyanides to generate bis(imido) complexes active for catalytic nitrene transfer.

Since four-coordinate bis(imido) compounds analogous to **3.2 – 3.4** were generated as reactive intermediates, it seemed plausible that **3.6** could be used as a source of *in-situ* generated **3.B** in order to carry out catalytic nitrene transfer chemistry, as discussed in Chapter 2. In fact, mild heating of a solution of **3.6** with *tert*-butylisocyanide resulted in release of cyclohexylazide and formation of niobium bis(imido) complex **3.8a** (Scheme 3.4) which was isolated as yellow crystals in 63% yield and characterized by ^{1}H and ^{13}C NMR spectroscopy and X-ray crystallography (Figure 3.1, right). The analogous cyclohexylisocyanide adduct, **3.8b**, was also prepared from reaction of **3.6** with cyclohexylisocyanide. Initial results have shown that **3.6**, **3.8a** and **3.8b** are

all active for catalytic nitrene transfer to generate dialkylcarbodiimides from azides and isocyanides. Interestingly, the cyclohexyl imido group was transferred selectively over the *tert*-butyl imido group to form only CyN=C=NCy (DCC) from CyN_3 and CyNC or $^tBuN{=}C{=}NCy$ from CyN_3 and ^tBuNC.

Having established that BDI niobum bis(imido) complexes readily engage in nitrene transfer and cycloaddition reactivity across their imido groups, we set out to explore their 1,2-addition reactivity toward substrates with element-hydrogen bonds. A solution of **3.2** in C_6D_6 lightened in color upon addition of 1 atm H_2; ^1H NMR spectroscopy indicated partial conversion to the niobium amido-hydride complex **3.9**, the result of 1,2-addition of H_2 across one of the imido groups (Scheme 3.5). Compound **3.9** displayed characteristic Nb-H (broad) and N-H (sharp) singlets at 9.1 and 7.8 ppm, respectively, and showed C_s symmetry in solution. The ratio of **3.9** to **3.2** in solution varied based on H_2 pressure introduced to the NMR tube, indicating that an equilibrium was established between the complexes ($K_{eq} \approx 8.0$ at 20 ˚C). The reaction could be driven almost completely to the right by addition of ca. 3.8 atm H_2 to an NMR tube containing **3.2**.

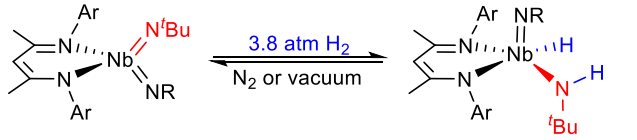

3.2: R = ^{t}Bu, orange
3.4: R = Ar, red

3.9: R = ^{t}Bu, yellow, 46%
3.10: R = Ar, orange

Scheme 3.5 Reversible 1,2-addition of dihydrogen across a *tert*-butylimido group.

Although removing H_2 either by exposing solutions of **3.9** to nitrogen atmosphere or placing it under vacuum resulted in conversion back to **3.2**, X-ray quality crystals of **3.9** could be grown by adding a dihydrogen atmosphere to a nearly concentrated solution of **3.2** in hexamethyldisiloxane (HMDSO) and slowly cooling. In contrast to its solution behavior, crystals of **3.9** appeared relatively stable to nitrogen atmosphere at -40 °C for weeks and to vacuum for at least 30 min. Dissolution of the crystals in C_6D_6 under nitrogen resulted in rapid effervescence of H_2(g);^1H NMR spectroscopy showed that the compound was converted mostly back to **3.2** within minutes.

The solid-state structure of **3.9** (Figure 3.2) showed a distorted square-based pyramidal geometry ($\tau = 0.02$), with the imido moiety occupying the apical position. The niobium hydride was located in the difference map and refined isotropically, while all other hydrogens including the amido protons were initially placed based on geometry. Disorder in the crystal structure between the imido and amido groups made the determination of amido Nb-N-C angles (Nb-N(3)-C(3) = 176.8(5)° and Nb-N(4)-C(34) = 127.5(4)°), somewhat tenuous, but were consistent with a structure containing both a linear *imido* and a bent *amido*. The Nb-H stretch, observed at 1652 cm^{-1}, is consistent with known niobium terminal hydrides.[72–74]

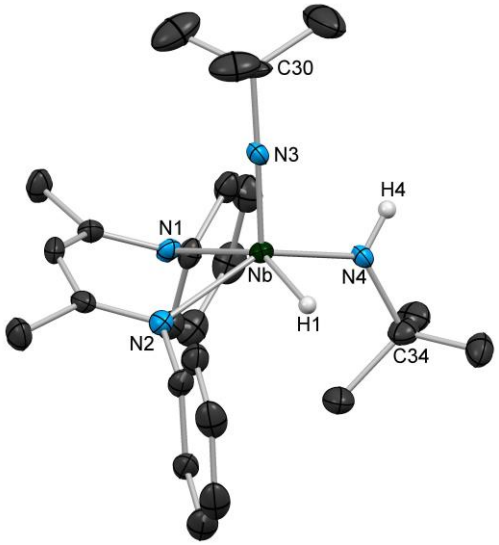

Figure 3.2 Molecular structure of **3.9** determined by X-ray diffraction. Selected H atoms and aryl ^{i}Pr groups have been omitted for clarity; thermal ellipsoids are displayed at the 50% probability level. Selected bond lengths (Å): Nb-N(1) 2.211(4), Nb-N(2) 2.266(4), Nb-N(3) 1.738(6), Nb-N(4) 1.955(7), Nb-H(1) 1.76(6); selected bond angles (˚): N(1)-Nb-H(1) 148(2), N(2)-Nb-N(4) 147.4(2), N(1)-Nb-N(3) 103.5(2), Nb-N(3)-C(30) 176.8(5), Nb-N(4)-C(34) 127.5(4).

Similarly, **3.4** reacted reversibly with dihydrogen, across the *tert*-butylimido moiety specifically, establishing an equilibrium between **3.4** and **3.10** ($K_{eq} \approx 2.5$ at 20 ˚C). In contrast, **3.3** reacted with little selectivity between the TMS and ^{t}Bu imido groups to give a mixture of starting material and the two possible 1,2-addition products. While no EXSY correlation was observed for mixtures of **3.2** and **3.9** at room temperature under 1 atm H_2, a strong EXSY correlation was observed at higher temperatures (≥65 °C) between the backbone methine signals for **3.2** and **3.9**, indicating that the process that interconverts **3.2** and **3.9** occurs on the NMR timescale at these temperatures. We are currently undertaking efforts to determine the exchange kinetics for this process.

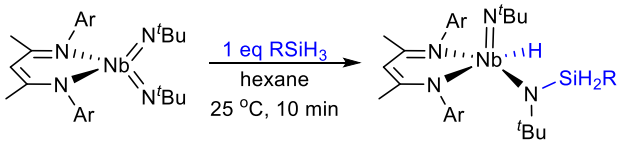

3.2

3.11: R = Ph, pale yellow, 85%
3.12: R = ^{n}Bu, pale yellow, 75%

Scheme 3.6 Reactions of silanes across an imido group of **3.2**.

Phenylsilane and ^{n}butylsilane each readily underwent 1,2-addition across an imido moiety to give silylamido-imido-hydrido niobium complexes **3.11** and **3.12**, respectively (Scheme 3.6). Both derivatives could be isolated via crystallization from either hexane or HMDSO as pale yellow crystals in 75-85% yields. These compounds each displayed ^{1}H NMR spectra containing mostly very broad peaks, indicating that the compounds experienced fluxionality in solution at room temperature. The ^{1}H NMR spectra of **3.11** and **3.12** showed very broad Nb-H shifts centered at

9.10 ppm and 8.65 ppm, respectively, as well as broad doublets at 6.07 and 5.58 ppm for **3.11** and very broad singlets at 5.34 ppm and 5.01 ppm for **3.12**, each corresponding to the silyl hydrogens. The spectrum of **3.11** sharpened significantly at -20 °C and clearly exhibited C_1 symmetry so that two sharp doublets with ^2J = 9.1 Hz were observed for the diastereotopic Si-H protons and four septets were observed for the isopropyl methine protons. Similar ^2J values have been observed in related tantalum phenylsilylamide complexes.[55] The FT-IR spectra of **3.11** and **3.12** both displayed broad absorptions at 1667 cm^{-1} attributable to the Nb-H stretches.

Compound **3.11** was also characterized by X-ray diffraction; a thermal ellipsoid plot of its solid-state structure is shown in Figure 3.3. In the solid state, **3.11** has a nearly ideal square based pyramidal structure ($\tau = 0.00$), analogous to that of **3.9**, with the imido moiety in the apical position.

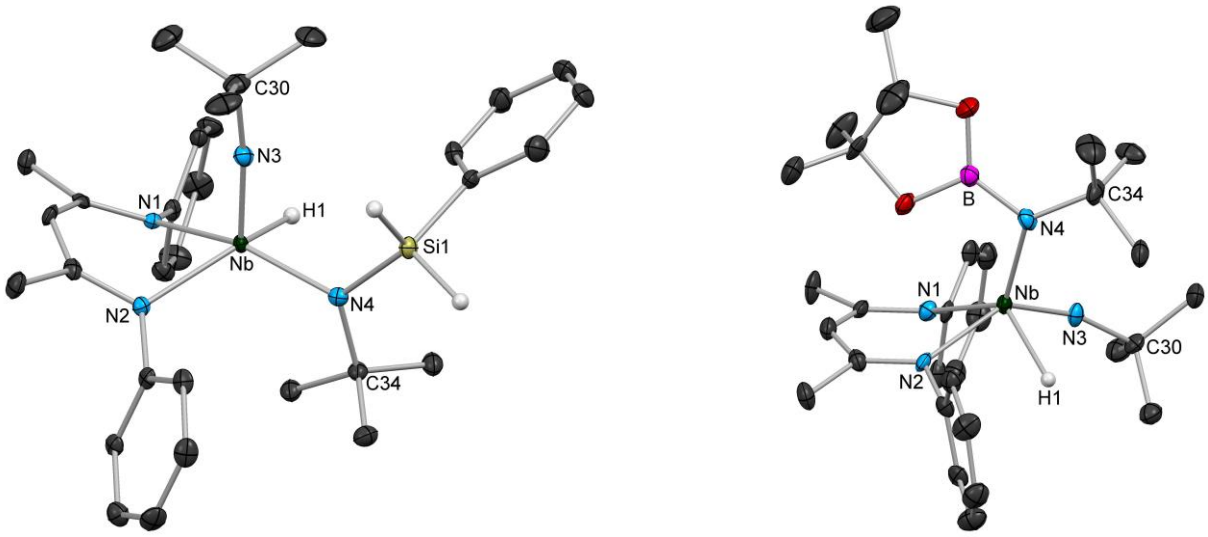

Figure 3.3 Molecular structures of **3.11** (left) and **3.13** (right) determined by X-ray diffraction. Selected H atoms, aryl ^{i}Pr groups and a molecule of HMDSO that co-crystallized with **3.11** have been omitted for clarity; thermal ellipsoids are displayed at the 50% probability level. For **3.11**, selected bond lengths (Å): Nb-N(1) 2.262(3), Nb-N(2) 2.228(3), Nb-N(3) 1.750(3), Nb-N(4) 2.017(3), Nb-H(1) 1.75(3); selected bond angles (˚): N(2)-Nb-H(1) 149(1), N(1)-Nb-N(4) 149.2(1), N(1)-Nb-N(3) 103.1(1), Nb-N(3)-C(30) 173.5(2), Nb-N(4)-C(34) 116.4(2), Nb-N(4)-Si(1) 121.3(1). For **3.13**, selected bond lengths (Å): Nb-N(1) 2.168(6), Nb-N(2) 2.292(7), Nb-N(3) 1.783(6), Nb-N(4) 2.068(6), Nb-H(1) 1.97(7); selected bond angles (˚): N(1)-Nb-H(1) 128(2), N(2)-Nb-N(3) 143.6(3), N(1)-Nb-N(4) 126.5(2), N(3)-Nb-N(4) 104.8(3), Nb-N(3)-C(30) 163.1(5), Nb-N(4)-C(34) 129.2(5), Nb-N(4)-B 110.0(5).

Treatment of **3.2** with pinacolborane gave the borylamido-imido-hydrido niobium complex **3.13** as a yellow microcrystalline powder in 39% isolated yield (Scheme 3.7). In contrast to what was observed for **3.11** and **3.12**, the ^{1}H NMR spectrum of **3.13** displayed sharp resonances at room temperature aside from the broad Nb-H resonance centered at 10.01 ppm and contained four distinct isopropyl methine resonances consistent with C_1 solution symmetry. The compound was characterized by X-ray crystallography; in contrast to **3.9** and **3.11**, the solid-state structure of **3.13**

(Figure 3.3, right) showed a distorted square-based pyramidal geometry with the borylamido group in the apical position ($\tau = 0.28$).

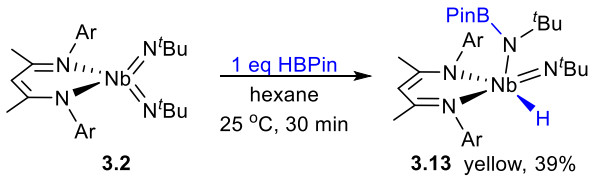

3.2 **3.13** yellow, 39%

Scheme 3.7 Reaction of pinacolborane across an imido group of **3.2**.

Addition of 1 atm CO_2 to either **3.12** or **3.13** in hexane resulted in immediate formation of corresponding formate complexes **3.14** and **3.15**, which were isolated as yellow crystals in 48% yield and 35% yield, respectively. (Scheme 3.8) The ^{1}H NMR spectra indicated disappearance of the broad Nb-H signal, and appearance of a sharp singlet corresponding to the formate C-H at 7.86 ppm for **3.14** or 8.60 ppm for **3.15**. The rest of the spectra were also sharp at room temperature, and consistent with C_1 solution symmetry.

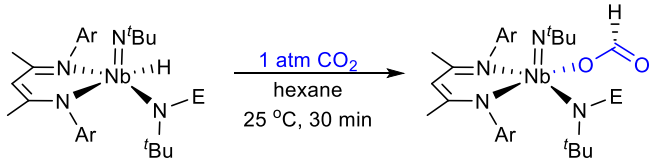

3.12: E = Si^{n}BuH$_2$
3.13: E = BPin

yellow crystals
3.14: E = Si^{n}BuH$_2$, 48%
3.15: E = BPin, 35%

Scheme 3.8 Insertion of carbon dioxide into niobium hydride functionalities of **3.12** and **3.13**.

The solid-state structures of both **3.14** and **3.15** revealed nearly ideal trigonal bipyramidal geometries (for **3.14**, $\tau = 0.02$ and for **3.15**, $\tau = 0.03$) analogous to the geometries of **3.9** and **3.11**, but notably quite different from the geometry of **3.13** (Figure 3.4). The reason for the unusual molecular geometry observed for **3.13** remains unclear, but likely does not result from steric effects based on the fact that **3.15** contains a slightly more sterically demanding ligand set than **3.13**, and yet is essentially isostructural with **3.9**, **3.11** and **3.12**. It is possible that there is a very small energy difference between the two geometries, and the geometry observed in the solid-state is therefore dictated by crystal packing effects. The Nb-O(1)-C(42) bond angle for the formate ligand of **3.14** is nearly linear (167.2(2)°), indicating there is some π-donation from both lone pairs of the oxygen to the niobium center. In contrast, the Nb-O(3)-C(44) angle of **3.15** is bent (127.8(4)˚) and the Nb-O bond distance is 0.027 Å longer than the analogous Nb-O bond in **3.14**, indicating only one lone pair donates to the metal center. Again, however, these bond angles and distances no doubt cause very small changes in the overall energies of these complexes, and the differences are most likely caused by crystal packing effects rather than any inherent differences between the electronic structures of the two compounds.

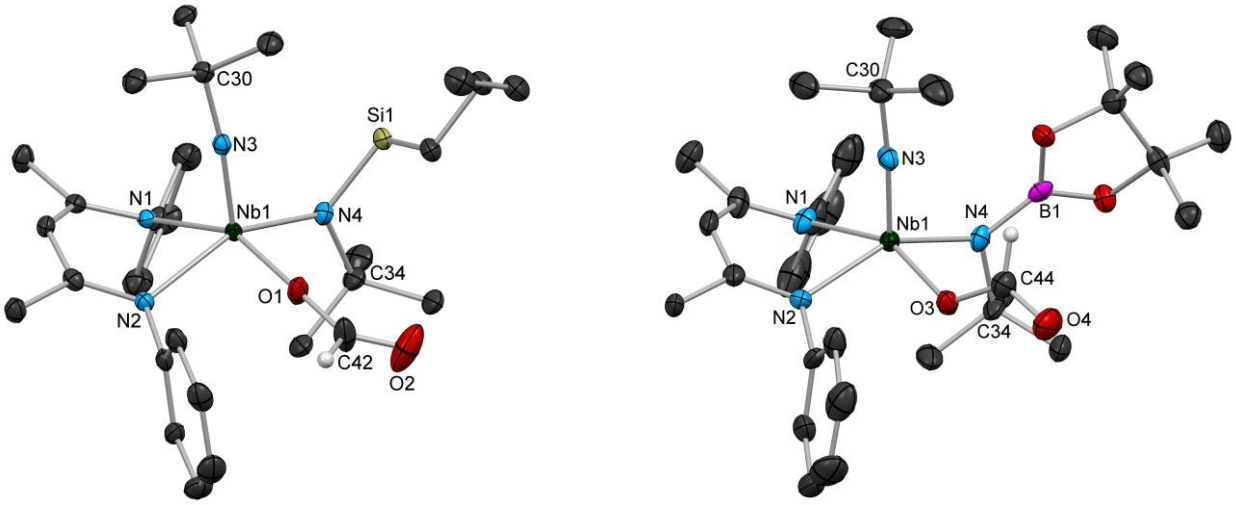

Figure 3.4 Molecular structures of **3.14** (left) and **3.15** (right) determined by X-ray diffraction. Selected H atoms, aryl ^{i}Pr groups and a second crystallographically inequivalent molecule of **3.15** have been omitted for clarity; thermal ellipsoids are displayed at the 50% probability level. For **3.14**, selected bond lengths (Å): Nb-N(1) 2.189(2), Nb-N(2) 2.282(2), Nb-N(3) 1.757(2), Nb-N(4) 2.016(2), Nb-O(1) 2.041(2); selected bond angles (˚): N(1)-Nb-O 154.55(8), N(2)-Nb-N(4) 155.78(8), N(1)-Nb-N(3) 98.00(9), Nb-N(3)-C(30) 173.6(2), Nb-N(4)-C(34) 118.1(2), Nb-N(4)-Si(1) 117.7(1), Nb-O(1)-C(42) 167.2(2). For **3.15**, selected bond lengths (Å): Nb-N(1) 2.192(4), Nb-N(2) 2.276(4), Nb-N(3) 1.746(4), Nb-N(4) 2.035(5), Nb-O(3) 2.068(4); selected bond angles (˚): N(1)-Nb-O(3) 154.8(2), N(2)-Nb-N(4) 152.7(2), N(1)-Nb-N(3) 98.6(2), Nb-N(3)-C(30) 175.0(4), Nb-N(4)-C(34) 113.7(3), Nb-N(4)-B(1) 127.6(4), Nb-O(3)-C(44) 127.8(4).

While **3.2** was found to be unreactive toward alkanes, alkenes and internal alkynes, it reacted with *tert*-butylacetylene upon mild heating in toluene to give the niobium amido-acetylide complex **3.16** as pale yellow crystals in 56% yield (Scheme 3.9). Terminal alkynes are relatively acidic, and C-H activations of terminal alkynes by group 4 and group 5 imido complexes are precedented.[38,40] The ^{1}H NMR spectrum of **3.16** contained two sets of broad peaks at room temperature (1.9:1 ratio), likely corresponding to two diastereoisomers. An EXSY correlation was observed between the resonances of the two isomers at room temperature, indicating that the observed fluxionality was likely caused by a process that interconverted the two diastereoisomers. The spectrum sharpened into two distinct sets of sharp signals, each consistent with C_1 symmetric compounds, at -20 ˚C. A 1.4:1 ratio of the two isomers was observed at -20 ˚C. At higher temperatures (60 – 80 ˚C), the two sets of peaks began to coalesce into a single set of very broad resonances, consistent with averaging between the two diastereoisomers on the NMR timescale.

In contrast, only a single isomer was observed in the solid-state structure of **3.16** (Figure 3.5, left). Like most of the other 1,2-addition products discussed so far, **3.16** has a distorted square-based pyramidal geometry with the imido group in the apical position. It is not clear which isomer observed in the NMR spectrum the crystal structure corresponds to, nor is it clear what the structure of the second diastereoisomer is, although distorted square-based pyramidal geometries in which one of the ligands other than the imido group occupies the apical position are likely.

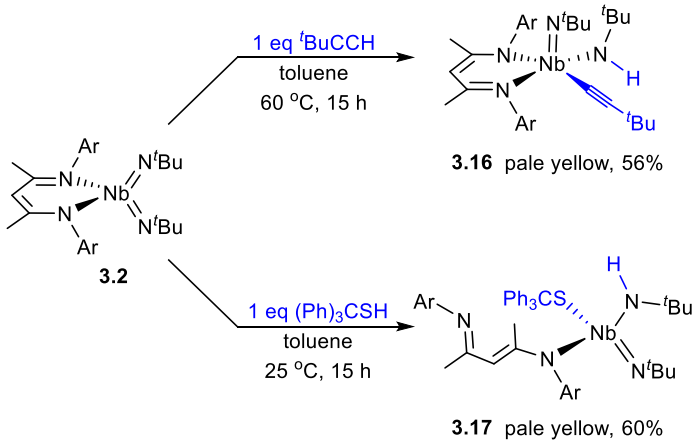

Scheme 3.9 Reactions of protic substrates across an imido group of **3.2**.

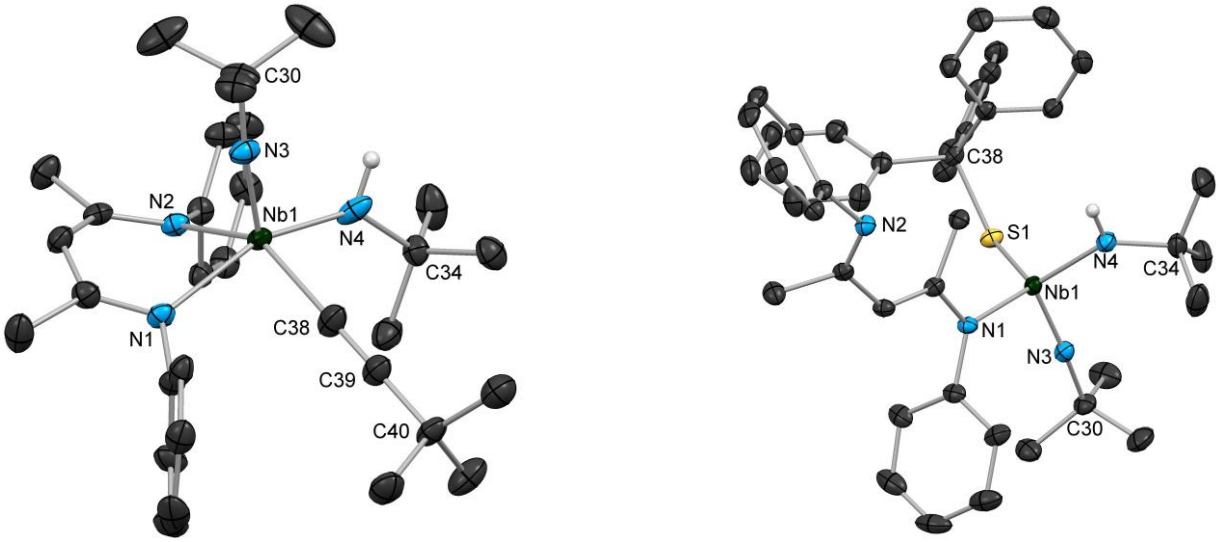

Figure 3.5 Molecular structures of **3.16** (left) and **3.17** (right) determined by X-ray diffraction. Selected H atoms and aryl ^{i}Pr groups have been omitted for clarity; thermal ellipsoids are displayed at the 50% probability level. For **3.16**, selected bond lengths (Å): Nb-N(1) 2.291(2), Nb-N(2) 2.204(2), Nb-N(3) 1.783(2), Nb-N(4) 1.959(3), Nb-C(38) 2.199(3), C(38)-C(39) 1.210(4); selected bond angles (˚): N(2)-Nb-C(38) 146.7(1), N(1)-Nb-N(4) 159.2(1), N(1)-Nb-N(3) 99.3(1), Nb-N(3)-C(30) 172.0(2), Nb-N(4)-C(34) 137.6(2), Nb-C(38)-C(39) 168.3(3), C(38)-C(39)-C(40) 179.1(3). For **3.17**, selected bond lengths (Å): Nb-N(1) 2.065(2), Nb-N(3) 1.748(2), Nb-N(4) 1.972(2), Nb-S(1) 2.414(1); selected bond angles (˚): N(1)-Nb-S(1) 117.21(5), N(1)-Nb-N(3) 103.71(7), N(1)-Nb-N(4) 115.28(7), N(3)-Nb-N(4) 106.72(8), N(3)-Nb-S(1) 92.92(6), N(4)-Nb-S(1) 116.60(5), Nb-N(3)-C(30) 172.3(2), Nb-N(4)-C(34) 139.5(2), Nb-S(1)-C(38) 121.63(6).

Compound **3.2** reacted with triphenylmethanethiol to give **3.17** as pale yellow crystals in 60% yield (Scheme 3.9). Notably, both 1H NMR spectroscopy and X-ray crystallography were consistent with a structure in which the BDI ligand was bound in a κ^1 fashion to the niobium center, presumably to accommodate the sterically demanding triphenylmethanethiolato ligand. The unusual κ^1 binding of the BDI ligand was apparent from the ^{1}H NMR spectrum based on the large

difference in chemical shift between the two BDI backbone methyl units, which appeared at 1.31 and 2.51 ppm respectively.[75] Compound **3.17** is four-coordinate with a distorted tetrahedral geometry (τ_4' = 0.89).[76] The Nb-N(1) distance is 2.065(2) Å, which is 0.1 to 0.2 Å shorter the distances observed in structures with κ^2-BDI ligands, consistent with the localized picture of the bonding in the BDI ligand depicted in Scheme 3.9, in which the Nb-N(1) interaction is best characterized as a covalent single bond. There may also be a small π-component to the bonding between the niobium center and either or both the BDI ligand and the thiolate ligand, which may serve to help stabilize the electron-deficient 4-coordinate niobium center (14 e^- without considering these interactions). In fact, the Nb-S(1) distance (2.414(1) Å, which is among the shortest of niobium thiolate bonds in the literature) is consistent with considerable Nb-S multiple bond character. The thiolate ligand is bent (Nb-S(1)-C(38) = 121.63(6)), consistent with other niobium thiolates, indicating that at most one of the sulfur p-orbitals interacts with the metal center.

With the intention of accessing reactive terminal oxo-imido and sulfido-imido niobium complexes isolobal to **3.2 – 3.4**, we began investigating the [2+2] cycloaddition reactivity of **3.2 – 3.4** toward carbon dioxide and carbon disulfide. For group 4, such reactions are known to lead to either isolable carbamate or dithiocarbamate complexes, products resulting from further reaction of carbon dioxide with carbamate intermediates, or extrusion of isocyanate or isothiocyanate to ultimately give stable bis-μ-oxo or bis-μ-sulfido dimers.[77–83] In contrast, there has only been one report of group 4 *terminal* oxo and sulfido complexes accessed via this route.[84] Reaction of **3.2** with carbon disulfide in benzene resulted in precipitation of bis-μ-sulfido complex **3.18** as large red crystals (Scheme 3.10). Formation of compound **3.18** resulted from [2+2] cycloaddition of carbon disulfide to give **3.C** followed by [2+2] cycloreversion to release *tert*-butylisothiocyanate (detected by ^{1}H NMR spectroscopy) and generate a terminal niobium sulfido complex, which readily dimerized. We reported the analogous niobium bis-μ-oxo complex, which formed from reaction of Nb(III) precursors with oxygen atom transfer reagents.[64,67] Like the bis-μ-oxo complex, **3.18** was sparingly soluble in most organic solvents; none the less it could be characterized by ^{1}H NMR spectroscopy by monitoring its appearance prior to precipitation. Characterization by ^{1}H NMR spectroscopy and X-ray crystallography (Figure 3.6, left) were consistent with C_{2h} symmetry in both solution and in the solid-state. The Nb-S distances in the dimer were consistent with those of related niobium complexes bearing bridging sulfide ligands.[85,86]

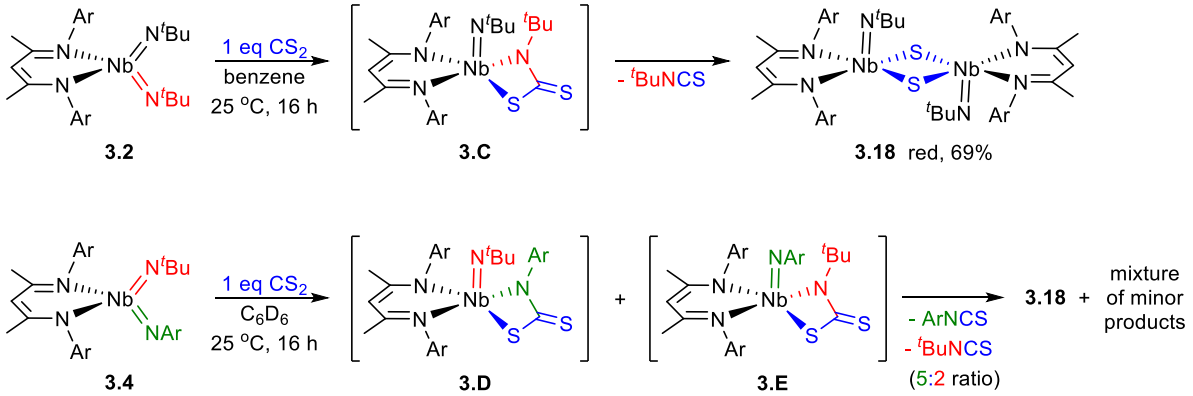

Scheme 3.10 Reaction of CS_2 across an imido group to give bis-μ-sulfido complex **3.18**.

Surprisingly, rather than reacting with CS_2 at the more basic *tert*-butylimido group, **3.4** reacted preferentially at the arylimido group to once again produce **3.18**, which precipitated, as well as a 5:2 mixture of arylisothiocyanate and *tert*-butylisothiocyanate. A complex mixture of other niobium-containing compounds was observed in solution, originating from a putative terminal sulfido intermediate resulting from release of *tert*-butylisothiocyanate from **3.E**. The relatively sterically encumbering nature of the remaining arylimido group disfavors dimerization of the resulting terminal sulfido complex. Hence, the highly reactive terminal sulfido intermediate instead either reacts reversibly with *tert*-butylisothiocyanate to regenerate **3.4** or degrades to a mixture of products.

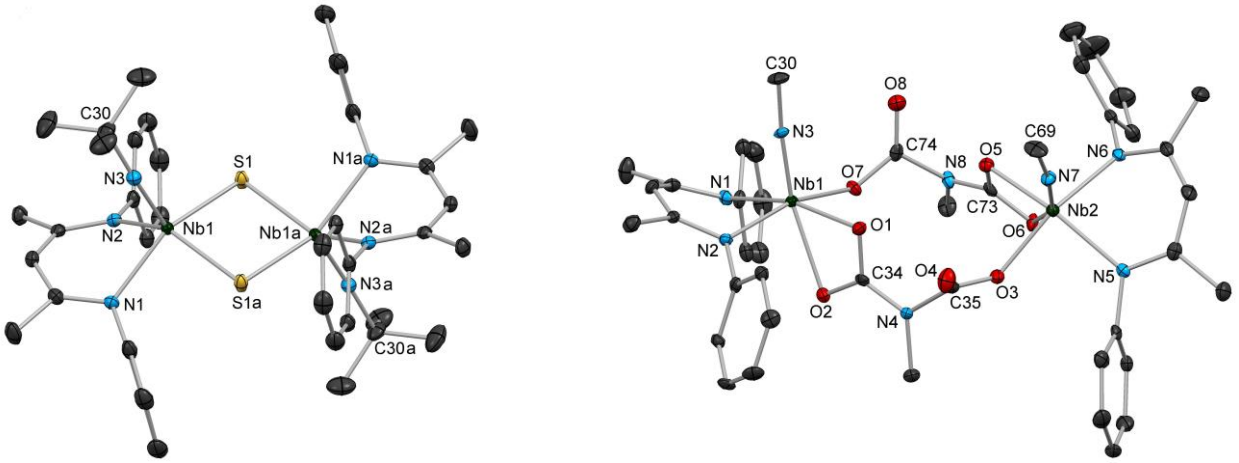

Figure 3.6 Molecular structures of **3.18** (left) and **3.19** (right) determined by X-ray diffraction. H atoms and aryl ^{i}Pr groups have been omitted and selected ^{t}Bu groups have been truncated to the α-carbon for clarity; thermal ellipsoids are displayed at the 50% probability level. For **3.18**, selected bond lengths (Å): Nb-N(1) 2.238(2), Nb-N(2) 2.204(1), Nb-N(3) 1.760(1), Nb-S(1) 2.385(1), Nb-S(1a) 2.419(1); selected bond angles (˚): N(1)-Nb-S(1) 155.12(4), N(2)-Nb-S(1a) 145.30(4), N(1)-Nb-N(3) 97.73(6), Nb-N(3)-C(30) 173.0(1). For **3.19**, selected bond lengths (Å): Nb(1)-N(1) 2.193(3), Nb(1)-N(2) 2.183(2), Nb(1)-N(3) 1.749(3), Nb(1)-O(1) 2.104(2), Nb(1)-O(2) 2.322(2), Nb(1)-O(7) 2.049(2); selected bond angles (˚): N(1)-Nb(1)-O(1) 163.0(1), N(2)-Nb(1)-O(7) 163.5(1), N(3)-Nb(1)-O(2) 157.4(1), Nb(1)-N(3)-C(30) 172.1(2), Nb(1)-O(1)-C(34) 95.7(2), Nb(1)-O(7)-C(74) 131.6(2).

Rather than accessing a terminal oxo complex, either as an intermediate or a product, introduction of carbon dioxide to a solution of **3.2** resulted in conversion to iminodicarboxylate-bridged dinuclear complex **3.19**, which was isolated as yellow-orange crystals (Scheme 3.11). Monomeric, chelating iminodicarboxylate complexes resulting from related reactions of titanium and scandium imido complexes with carbon dioxide have been reported.[78,80,81,87] When exposed to a single equivalent of carbon dioxide, **3.2** reacted to give a mixture of **3.19** and starting material, indicating that insertion of a second equivalent into the Nb-N bond of intermediate **3.F** occurred faster than [2+2] cycloreversion to release *tert*-butylisocyanate. Compound **3.19** exhibited C_{2h} symmetry in solution, containing a single BDI backbone methyl signal, a single ^{t}Bu signal, two isopropyl methine and four isopropyl methyl signals; some of these signals were broad in C_6D_6, indicating fluxionality in solution, but the signals were significantly sharper in $CDCl_3$. However,

3.19 did not exhibit any symmetry in the solid-state (Figure 3.6, right), containing two crystallographically distinct halves of the molecule.

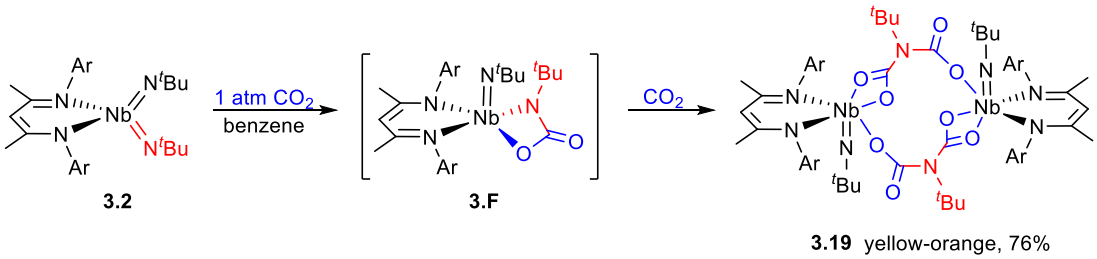

Scheme 3.11 Reaction of **3.2** with two equivalents of CO_2 to give diniobium complex **3.19**.

In contrast, reaction of niobium arylimido species **3.4** with carbon dioxide resulted in fast, relatively clean conversion to the carbamate complex **3.20** (Scheme 3.12). While **3.20** continued to react further with carbon dioxide in aromatic solvents (see below), when the reaction was instead carried out in hexane, it could be readily isolated as a red powder that precipitated within seconds of introducing CO_2. Analytically pure red crystals of **3.20** were obtained by recrystallization of the powder from diethyl ether. While the ^{1}H NMR spectrum of **3.20** displayed broad resonances at room temperature, the resonances sharpened into a spectrum consistent with C_1 solution symmetry at -40 ˚C. The X-ray crystal structure of **3.20** showed a distorted square-based pyramidal geometry ($\tau = 0.20$) with the arylimido group in the apical position (Figure 3.7, left).

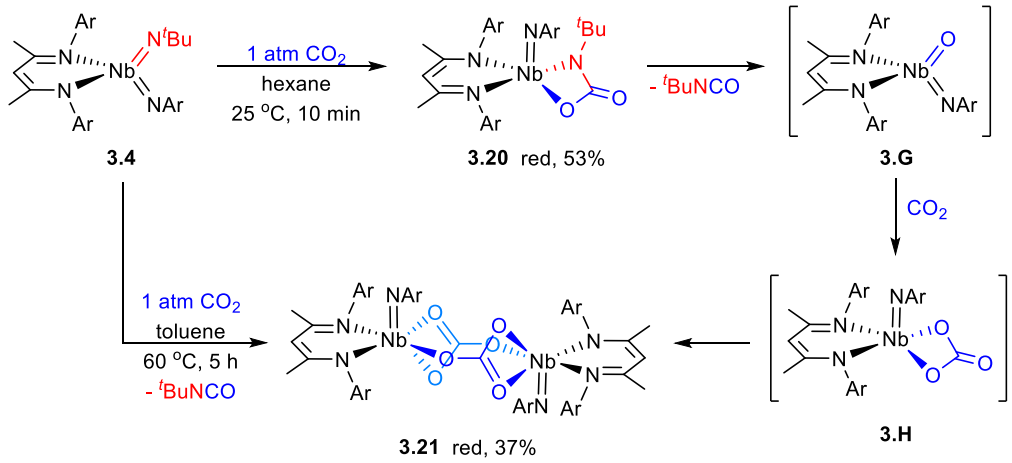

Scheme 3.12 Reactions of **3.4** with CO_2 to give carbamate complex **3.20** and bis-μ-carbonate complex **3.21**.

Leaving solutions of **3.4** under carbon dioxide atmosphere for extended periods resulted in partial conversion from **3.20** to a second major product resulting from further reaction with carbon dioxide. Heating a solution of either **3.4** or **3.20** under CO_2 resulted in conversion to **3.21**, which was isolated as red crystalline material in moderate yield (Scheme 3.12). Release of *tert*-butylisocyanate was observed by ^{1}H NMR spectroscopy. Unlike the related iminodicarboxylate-bridged dimer **3.19**, compound **3.21** exhibited sharp signals in the ^{1}H NMR spectrum consistent with C_1 symmetry in solution. The solution symmetry was also reflected in the solid-state structure

(Figure 3.7, right). Formation of **3.21** indicated that the putative 4-coordinate terminal oxo-arylimido intermediate **3.G** was generated during the course of the reaction. This intermediate reacted with carbon dioxide via [2+2] cycloaddition in order to give a niobium carbonate complex, which readily dimerized to give **3.21**.

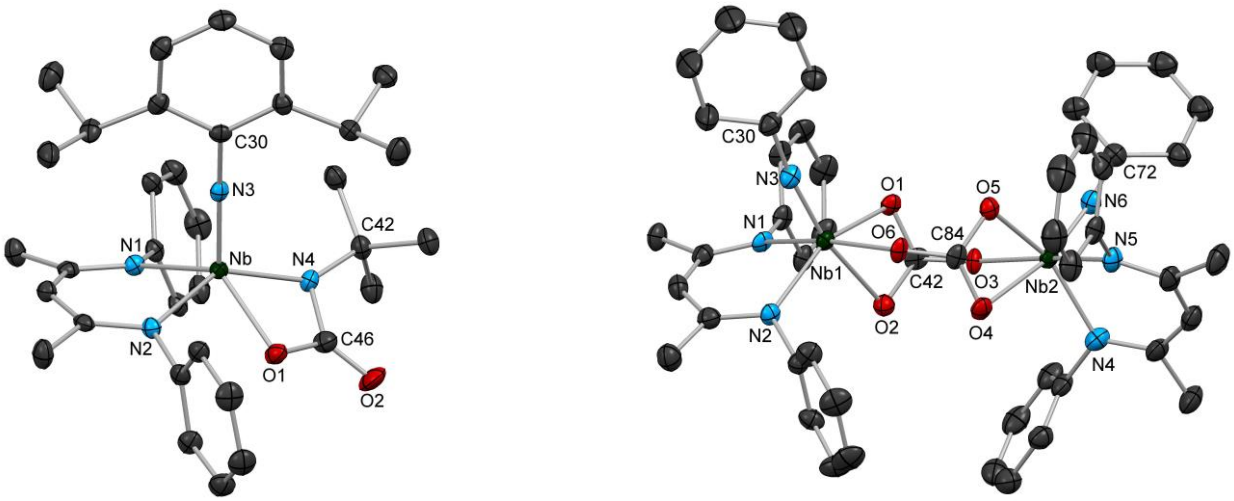

Figure 3.7 Molecular structures of **3.20** (left) and **3.21** (right) determined by X-ray diffraction. H atoms, selected aryl ^{i}Pr groups, a molecule of diethyl ether that co-crystallized with **3.20** and two molecules of HMDSO that co-crystallized with **3.21** have been omitted for clarity; thermal ellipsoids are displayed at the 50% probability level. For **3.20**, selected bond lengths (Å): Nb-N(1) 2.097(3), Nb-N(2) 2.211(3), Nb-N(3) 1.789(3), Nb-N(4) 2.071(3), Nb-O(1) 2.070(3), C(46)-N(4) 1.391(5), C(46)-O(1) 1.345(5), C(46)-O(2) 1.205(5); selected bond angles (˚): N(1)-Nb-O(1) 128.0(1), N(2)-Nb-N(4) 140.0(1), N(1)-Nb-N(3) 104.9(1), Nb-N(3)-C(30) 174.2(3), Nb-N(4)-C(42) 146.2(3). For **3.21**, selected bond lengths (Å): Nb(1)-N(1) 2.199(3), Nb(1)-N(2) 2.125(3), Nb(1)-N(3) 1.787(3), Nb(1)-O(1) 2.085(2), Nb(1)-O(2) 2.290(2), Nb(1)-O(6) 2.072(2); selected bond angles (˚): N(1)-Nb(1)-O(6) 165.7(1), N(2)-Nb(1)-O(1) 151.4(1), N(3)-Nb(1)-O(2) 166.9(1), Nb(1)-N(3)-C(30) 173.0(3), Nb(1)-O(1)-C(42) 93.6 (2), Nb(1)-O(6)-C(84) 126.0(2).

The reactivity of early transition metal terminal oxo complexes often manifests itself in dimerization, to form inert bis-μ-oxo complexes.[64,78] Thus, the following observations indicated that in the present system, the combination of a BDI ligand and an arylimido group provided enough steric encumbrance to prevent dimer formation: i) reaction of **3.4** with CS_2 gave **3.18** as the major product and did not produce the analogous arylimido-supported bis-μ-sulfido complex (see above, Scheme 3.10) and ii) oxo-imido intermediate **3.G** reacted with carbon dioxide to form **3.21** without generating any bis-μ-oxo complex (see above, Scheme 3.12). Spurred by these observations, we set out to trap terminal oxo-arylimido intermediate **3.G** and further study its reactivity.

Heating a solution of **3.20** with 20 equivalents of pyridine resulted in release of an equivalent of *tert*-butylisocyanate and relatively clean conversion to a new compound, which was characterized by ^{1}H NMR spectroscopy as the 5-coordinate pyridine adduct of **3.G**, compound **3.22** (Scheme 3.13). Compound **3.22** was isolated as orange-yellow crystals in 22% yield by

crystallization from toluene. While **3.22** exhibited broad ^{1}H NMR signals at room temperature, the signals sharpened in the presence of excess pyridine, indicating the fluxional process responsible for the broad signals involved reversible decoordination of pyridine. The low yield of **3.22** was attributed to thermal decomposition; **3.22** was only stable in solution at low temperature or in the presence of excess pyridine.

Thermal decomposition of **3.22** proceeded quite cleanly to give the highly dissymmetryic bis-μ-oxo dimer **3.23**, which was isolated as yellow crystals (Scheme 3.13). Based on the observation that thermal reaction of **3.22** proceeded much more rapidly without any excess pyridine in solution, the transformation was likely initiated by decoordination of pyridine to generate reactive 4-coordinate intermediate **3.G**, which presumably dimerized by reaction with an equivalent of **3.22**. The solid-state structure of **3.23** (Figure 3.8, left) revealed that in order to accommodate the demanding steric environment around the two niobium centers in a bis-μ-oxo dimer, one of the BDI ligands coordinated with an unusual κ^1 binding mode. This provided further confirmation that the κ^2-BDI and arylimido ligands provided sufficient steric support in order to prohibit formation of bis-μ-oxo complexes.

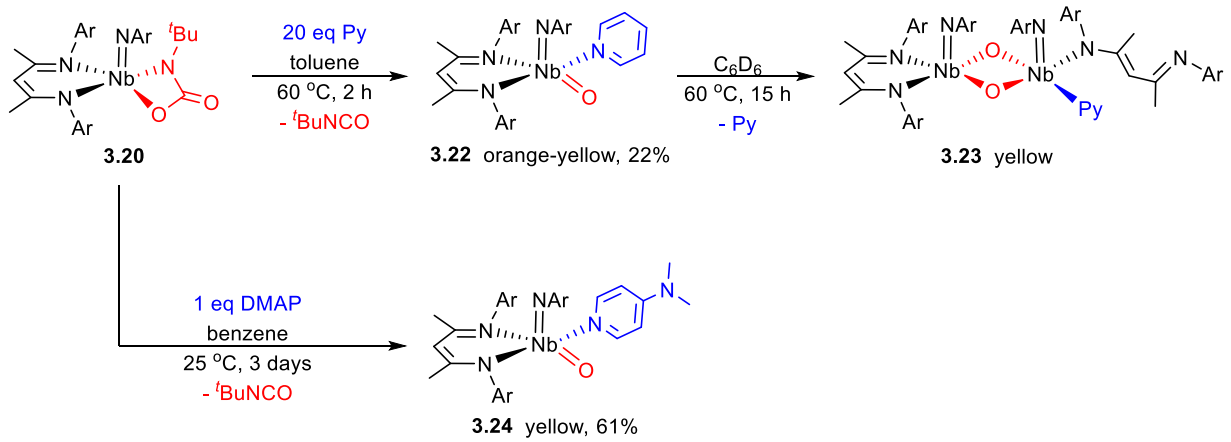

Scheme 3.13 Reactions of **3.20** with DMAP and Py to give isolable terminal oxo-imido complexes.

In order to access a more thermally stable analog of **3.22**, we investigated the reactivity of **3.20** toward more strongly coordinating ligands. Addition of 4-dimethylaminopyridine (DMAP) to **3.20** resulted in a slow color change from red to yellow and precipitation of a yellow powder. Upon workup, the yellow powder was isolated in 61% yield and characterized by NMR spectroscopy and X-ray crystallography as the five-coordinate terminal oxo-arylimido niobium complex **3.24** (Scheme 3.13). To the best of our knowledge, **3.24** represented the first structurally characterized example of an early transition metal (group 3 to 5) complex bearing *both* a terminal imido and a terminal oxo group (although many examples of related group 6, 7 and 8 complexes have been reported).[29,88–92] In contrast to the ^{1}H NMR spectrum of **3.22**, that of **3.24** exhibited sharp signals at room temperature, consistent with the more strongly coordinating DMAP ligand, along with a singlet at 5.35 ppm corresponding to the BDI backbone methine proton and six separate septets corresponding to the isopropyl methine protons, all of which indicated C_1 symmetry in solution.

The X-ray crystal structure of **3.24** (Figure 3.8, right) showed a distorted square-based pyramidal geometry with the imido group in the apical position and the oxo group in an equatorial position *trans* to a BDI nitrogen ($\tau = 0.18$). The Nb-O distance was 1.750(1) Å, within the typical range for terminal niobium oxo complexes (1.7–1.8 Å), while the imido bond distance was 1.816(1) Å, among the longest distances reported for terminal niobium imido bonds and similar to the distances observed in related bis(imido) complexes (see above). The Nb-N(3)-C(30) bond angle was 156.1(1), similarly among the most bent bond angles observed in niobium terminal imido complexes. Thus, in the solid-state structure, the π-loading in this system manifested itself primarily in the metrical parameters of the imido group; however, this was not an indication that the imido group was more reactive than the oxo group. In fact, although the reactivity of **3.24** has not yet been fully investigated, thus far, we have found that **3.24** reacts with substrates exclusively across the niobium oxo group.

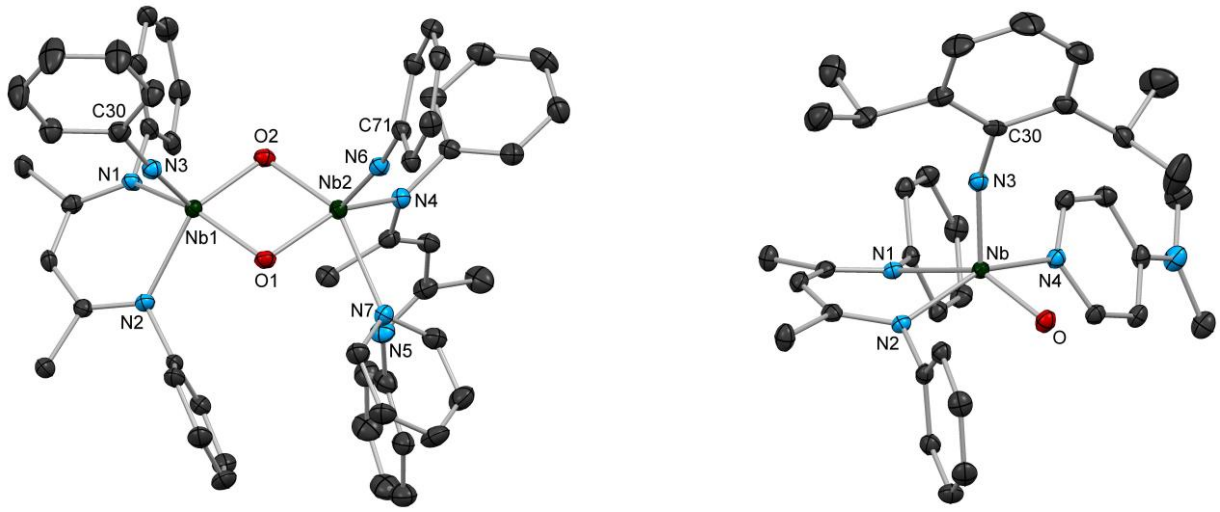

Figure 3.8 Molecular structures of **3.23** (left) and **3.24** (right) determined by X-ray diffraction. H atoms, selected aryl ^{i}Pr groups and two molecules of diethyl ether that co-crystallized with **3.24** have been omitted for clarity; thermal ellipsoids are displayed at the 50% probability level. For **3.23**, selected bond lengths (Å): Nb(1)-N(1) 2.221(2), Nb(1)-N(2) 2.217(2), Nb(1)-N(3) 1.800(3), Nb(1)-O(1) 1.938(2), Nb(1)-O(2) 1.949(2), Nb(2)-N(4) 2.100(3), Nb(2)-N(6) 1.777(3), Nb(2)-N(7) 2.413(2), Nb(2)-O(1) 1.980(2), Nb(2)-O(2) 1.969(2); selected bond angles (˚): N(1)-Nb(1)-O(1) 146.8(1), N(2)-Nb(1)-O(2) 141.4(1), N(3)-Nb(1)-N(1) 101.1(1), Nb(1)-N(3)-C(30) 173.2(2), Nb(1)-O(1)-Nb(2) 100.5(1), N(4)-Nb(2)-O(1) 145.3(1), N(7)-Nb(2)-O(2) 148.0(1), N(6)-Nb(2)-N(4) 101.7(1), Nb(2)-N(6)-C(71) 170.3(2). For **3.24**, selected bond lengths (Å): Nb-N(1) 2.299(1), Nb-N(2) 2.186(1), Nb-N(3) 1.816(1), Nb-N(4) 2.263(1), Nb-O 1.750(1); selected bond angles (˚): N(1)-Nb-O 143.72(5), N(2)-Nb-N(4) 154.70(5), N(1)-Nb-N(3) 103.89(6), Nb-N(3)-C(30) 156.1(1).

Group 4 early transition metal oxo complexes are known to engage in 1,2-additions and [2+2] cycloadditions across their very polarized oxo groups.[44–53] In contrast, while many niobium terminal oxo compounds have been reported, nearly all contain relatively inert Nb=O bonds and to our knowledge, none have been shown to undergo 1,2-addition reactions to generate niobium oxyhydrides.[93] Despite this, compound **3.24** reacted selectively and relatively cleanly across the

oxo group with silane reagents to generate the yellow siloxide compounds **3.25a – 3.25c** as well as free DMAP. While the reactivity of bis(imido) complexes **3.2 – 3.4** was limited to primary silanes, **3.24** reacted with the secondary and tertiary silanes diphenylsilane and dimethylphenylsilane within seconds at room temperature. All three products exhibited C_1 solution symmetry and exhibited broad singlets in the NMR between 11.0 and 11.3 ppm corresponding to the Nb-H units. In solution, **3.25a** and **3.25b** completely degraded to mixtures of products within 12 h at room temperature. While **3.25c** was somewhat more thermally stable, isolation of **3.25a – 3.25c** was also complicated by the generation of DMAP, which was difficult to separate from the hydride products. Hence, attempts to crystallize **3.25a – 3.25c** have not yet been successful. While addition across the oxo group rather than the imido group could not be confirmed crystallographically, the large geminal coupling constant for the Si-H protons observed for **3.25a** (^2J = 16 Hz) contrasted with the relatively small coupling constant observed for **3.11** (see above, ^2J = 9.1 Hz), indicating differing electronic environments for the diastereotopic silyl groups.[94] In contrast, **3.24** failed to react with alkynes or alkenes and instead underwent thermal decomposition upon heating (see below).

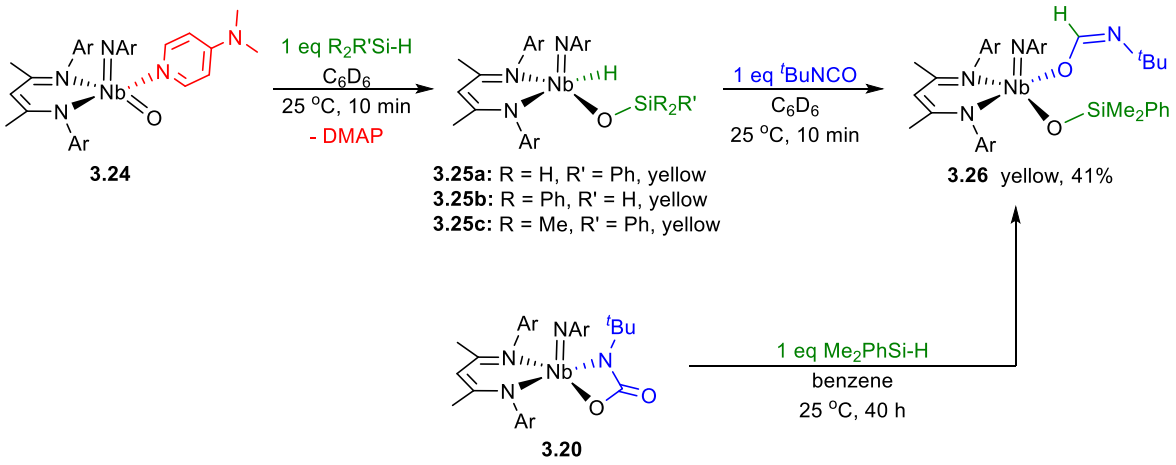

Scheme 3.14 Reactions of silane substrates across a niobium oxo bond of **3.24**.

Compound **3.25c** reacted with *tert*-butylisocyanate via insertion into the Nb-H bond to give the niobium κ^1-imidate **3.26** (Scheme 3.14). Compound **3.26** was also generated readily from reaction of carbamate complex **3.20** with dimethylphenylsilane (thus avoiding any generation of free DMAP) and isolated as yellow X-ray quality crystals in 41% yield. The solid-state structure of **3.26** (Figure 3.9, left) confirmed that silane added across the oxo group. Like the structures of the related compounds **3.11**, **3.14** and **3.15** described above, the geometry of **3.26** was a nearly ideal square-based pyramid (τ = 0.03).

While the strong Nb-O and Si-O bonds in **3.26** rendered the compound quite thermally stable and no catalytic hydrosilation of isocyanates could be observed, the reactivity of **3.25c** with isocyanate notably contrasted with that of silylamido niobium hydride complex **3.11** (see above), which did not undergo any reaction with isocyanates under similar conditions. Presumably, this was because the hydride ligands in **3.25a – 3.25c** were more sterically accessible to approach by substrates than in **3.11**. The reactive nature of the hydride ligand also likely manifested itself in

the thermal sensitivity of these compounds. We hope to expand upon this chemistry in order to use reactivity across oxo groups in catalytic hydrosilations and other hydrofunctionalizations of unsaturated substrates.

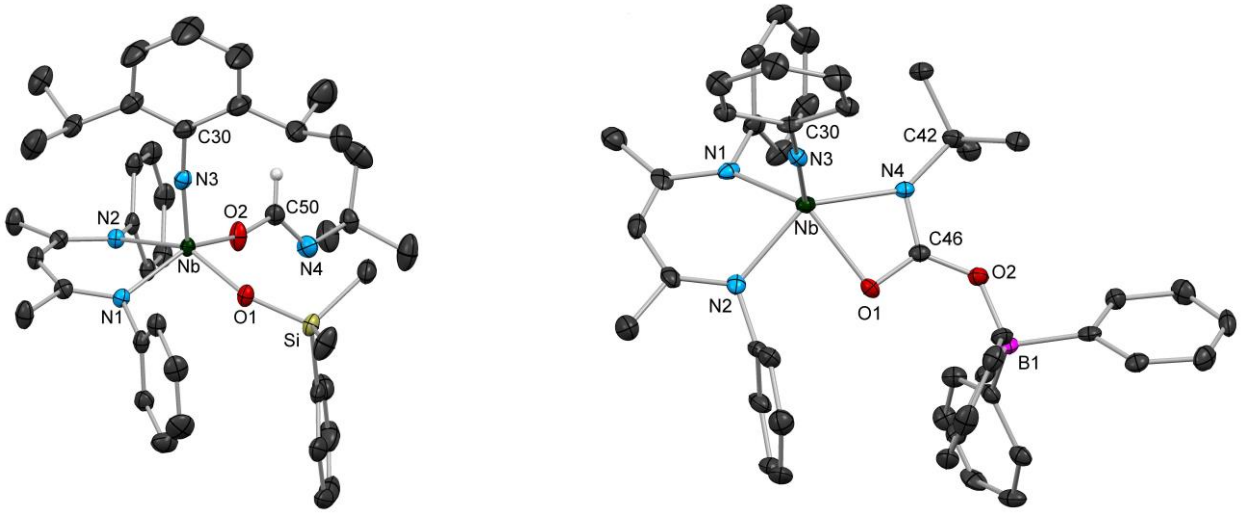

Figure 3.9 Molecular structures of **3.26** (left) and **3.28** (right) determined by X-ray diffraction. H atoms, selected aryl ^{i}Pr groups, a molecule of diethyl ether that co-crystallized with **3.28** and a second crystallographically inequivalent molecule of **3.28** have been omitted for clarity; thermal ellipsoids are displayed at the 50% probability level. For **3.26**, selected bond lengths (Å): Nb-N(1) 2.191(2), Nb-N(2) 2.218(2), Nb-N(3) 1.772(2), Nb-O(1) 1.925(2), Nb-O(2) 1.937(2); selected bond angles (˚): N(1)-Nb-O(2) 150.1(1), N(2)-Nb-O(1) 148.5(1), N(1)-Nb-N(3) 100.0(1), Nb-N(3)-C(30) 172.9(2), Nb-O(1)-Si 154.2(1), Nb-O(2)-C(50) 164.4(2). For **3.28**, selected bond lengths (Å): Nb-N(1) 2.076(4), Nb-N(2) 2.193(4), Nb-N(3) 1.758(4), Nb-N(4) 2.126(4), Nb-O(1) 2.134(4), C(46)-N(4) 1.325(6), C(46)-O(1) 1.302(6), C(46)-O(2) 1.293(6); selected bond angles (˚): N(1)-Nb-O(1) 134.8(1), N(2)-Nb-N(4) 140.5(2), N(1)-Nb-N(3) 103.7(2), Nb-N(3)-C(30) 174.0(4), Nb-N(4)-C(42) 144.2(3).

Having isolated the first examples of early transition metal terminal oxo-imido complexes, we next targeted isolable four-coordinate analogs. While the formation of unreactive dimeric products with κ^1-BDI ligands akin to **3.23** remained possible, it also seemed plausible that such species might only form in the presence of a labile σ-donating ligand like pyridine, which served to replace the pendant BDI nitrogen in the coordination sphere of the niobium center in **3.23** (see above). Attempts to remove the coordinating DMAP ligand from **3.24** to generate a four-coordinate complex resulted in degradation to mixtures of products. Next, we hypothesized that heating **3.20** might result in [2+2] cycloreversion to release *tert*-butylisocyanate and generate a four-coordinate terminal oxo complex. However, unproductive isomerization to the protonated κ^2-[O_2]-bound carbamate complex **3.27** was instead observed upon heating compound **3.20**. Finally, we aimed to trap a 4-coordinate terminal oxo-imido complex generated from **3.28** by capping either the oxo or imido moiety with a triarylborane. This approach has been used to trap complexes containing reactive basic functionalities in related systems.[95–98] In this case, however, the unbound oxygen of

the carbamate functionality simply engaged in a Lewis base-acid interaction with the triarylborane to generate **3.28**, which was isolated as purple crystals in 45% yield. The X-ray crystal structure of **3.28** (Figure 3.9, right) is quite similar to that of **3.20**, although coordination of the borane resulted in a ~0.9 Å lengthening of the C(46)-O(2) distance and consequential shortening of the C(46)-N(4) and C(46)-O(1) distances and lengthening of the Nb-N(4) and Nb-O(1) distances. Rather than leading to release of isocyanate and formation of a borane-capped oxo complex, prolonged heating of **3.28** led to mixtures of unidentified products. Future efforts will target alternative routes to reactive four-coordinate terminal oxo-imido, sulfido-imido and related complexes.

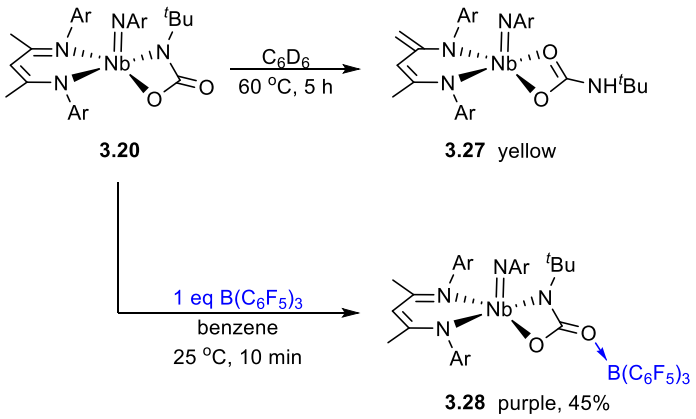

Scheme 3.15 Thermal degradation and formation of a Lewis acid adduct of **3.20**.

Summary and Conclusions

Niobium bis(imido) complexes were demonstrated to react with a variety of substrates across their Nb-N π-bonds. Under the oxidizing conditions utilized to generate niobium bis(imido) complexes **3.2 – 3.4**, the niobium bis(imido) intermediates **3.A** and **3.B** reacted further with azide substrates via [3+2] cycloaddition to give niobium tetrazene complexes **3.5** and **3.6**. These compounds were found to exist in equilibrium with the corresponding bis(imido) complexes, which could be trapped via addition of σ-donating isocyanide ligands, allowing for the use of these complexes in catalytic oxidative nitrene transfer chemistry. Compounds **3.2 – 3.4** were also shown to engage in stoichiometric 1,2-addition reactivity with dihydrogen, silanes, and boranes to generate niobium hydride complexes **3.9 – 3.13**, as well as substrates containing relatively acidic S-H or C-H bonds to generate products **3.16** and **3.17**. Work aimed at both expanding the scope of 1,2-addition reactions across imido groups in these systems as well as developing these stoichiometric processes into catalytic cycles for hydrofunctionalization reactions is ongoing.

Compounds **3.2** and **3.4** also exhibited [2+2] cycloaddition and cycloreversion reactivity with carbon dioxide and carbon disulfide. While reactions with **3.2** generated unreactive dimeric species, the reaction between **3.4** and carbon dioxide generated the monomeric niobium carbamate complex **3.20**. Under appropriate conditions, this compound was shown to behave as a source of the reactive 4-coordinate, monomeric niobium oxo-imido complex **3.G**, which could be trapped as the pyridine and DMAP adducts **3.22** and **3.24**. These represented the first isolated examples of early transition metal complexes containing both a terminal imido and a terminal oxo group. Likely as a

consequence of π-loading effects, compound **3.24** was reactive toward 1,2-addition of silane substrates across its oxo group. While related reactions across oxo groups have been observed in d^0 group 4 and group 6 complexes and d^2 group 7 complexes, this represented a new reaction pathway in group 5 chemistry, and the scope of stoichiometric and catalytic reactions this reactivity can be applied to remains to be explored. In addition to pursuing the reactivity of **3.24**, we are continuing to target 4-coordinate terminal oxo-imido complexes, as well as other isolobal π-loaded niobium complexes with reactive multiply-bonded ligands, such as terminal sulfides, selenides, phosphinidenes, and alkylidenes.

Experimental

General Considerations: Unless otherwise noted, all reactions were performed using standard Schlenk line techniques or in an MBraun inert atmosphere glove box under an atmosphere of nitrogen (<1 ppm O_2/H_2O). Glassware and Celite were stored in an oven at ca. 140˚ C. Molecular sieves (4 Å) were activated by heating to 300 °C overnight under vacuum prior to storage in a glovebox. Hexane, n-pentane, diethyl ether, dichloromethane, benzene, toluene, pyridine, and THF were purified by passage through columns of activated alumina and degassed by sparging with nitrogen. HMDSO was vacuum distilled from sodium/benzophenone, degassed by sparging with nitrogen, and stored over molecular sieves. ^{t}BuNH$_2$ was distilled from CaH_2. Deuterated solvents were vacuum-transferred from sodium/benzophenone, degassed with three freeze-pump-thaw cycles, and stored over molecular sieves. Azides were degassed with three freeze-pump-thaw cycles and filtered through activated alumina. Isocyanides were degassed with three freeze-pump-thaw cycles and stored over molecular sieves. NMR spectra were recorded on Bruker AV-600, AVB-400, AVQ-400, AV-500, and DRX-500 spectrometers. ^{1}H and ^{13}C{^{1}H} chemical shifts are given relative to residual solvent peaks. Proton and carbon NMR assignments were routinely confirmed by ^{1}H-^{1}H (COSY and NOESY) and ^{1}H-^{13}C (HSQC and HMBC) experiments. FT-IR samples were prepared as Nujol mulls and were taken between KBr disks using a Nicolet iS10 FT-IR spectrometer. Melting points were determined using an OptiMelt automated melting point system. ^{t}BuN$_3$,[99] DIPPN$_3$,[100] BnN$_3$,[101] CyN$_3$,[102] HBDI,[103] Li(BDI)•OEt$_2$,[104] Nb(N^{t}Bu)Cl$_3$Py$_2$,[105] (BDI)Nb(N^{t}Bu)Me$_2$,[56] (BDI)Nb(N^{t}Bu)(η^6-C$_6$H$_6$) (**3.1**),[67] (BDI)Nb(N^{t}Bu)$_2$ (**3.2**),[60] (BDI)Nb(N^{t}Bu)(NTMS) (**3.3**)[60] and (BDI)Nb(N^{t}Bu)(NAr) (**3.4**)[60] (BDI = ArNC(Me)CHC(Me)NAr, Ar = 2,6-diisopropylphenyl) were prepared using the literature procedures. All other reagents were acquired from commercial sources and used as received. Elemental analyses were determined either at the College of Chemistry, University of California, Berkeley or at the School of Human Sciences, Science Center, London Metropolitan University. X-ray structural determinations were performed at CHEXRAY, University of California, Berkeley on SMART APEX I and SMART APEX II QUAZAR diffractometers.

(BDI)Nb(NtBu)(BnNNNNBn) (3.5): Compound **3.1** (500 mg, 0.76 mmol) was dissolved in 5 mL benzene in a 20 mL vial. In a separate vial, benzylazide (200 mg, 1.5 mmol) was dissolved in 5 mL hexane. The benzylazide solution was added to the solution of **3.1**. The resulting solution was stirred at 60 °C for 3 h under N_2 atmosphere, resulting in a gradual lightening of the color from dark red to red. The volatile materials were removed under vacuum, leaving a dark red oily residue. The residue was extracted with hexane; upon dissolution of the residue in hexane, red crystalline

material immediately began forming. The crystalline material was isolated and residual solvent was removed under vacuum. The supernatant was concentrated and stored at -40 ˚C overnight, yielding an additional crop of red crystals. Yield: 220 mg, 35% over two crops. A 10:1 ratio of **3.5a** to **3.5b** was observed by ^{1}H NMR spectroscopy at 293 K. **^{1}H NMR (400 MHz, C_6D_6, 293 K):** Compound **3.5a**: δ 7.22–6.97 (m, 16H, Ar/Bn), 5.17 (s, 1H, *H*C(C(Me)NAr)$_2$), 4.22 (s, 4H, C*H*$_2$Ph), 3.70 (sep, 2H, C*H*Me$_2$), 2.67 (sep, 2H, C*H*Me$_2$), 1.62 (s, 6H, HC(C(*Me*)NAr)$_2$), 1.51 (d, 6H, CH*Me*$_2$), 1.31 (d, 6H, CH*Me*$_2$), 1.29 (s, 9H, ^{t}Bu), 1.25 (d, 6H, CH*Me*$_2$), 0.99 (d, 6H, CH*Me*$_2$). Compound **3.5b**: δ 7.50 (d, 2H, Ar or Bn), 7.31–6.94 (m, 14H, Ar/Bn), 6.05 (s, 2H, C*H*$_2$Ph), 5.08 (s, 2H, C*H*$_2$Ph), 3.28 (sep, 2H, C*H*Me$_2$), 2.88 (sep, 2H, C*H*Me$_2$), 1.60 (s, 6H, HC(C(*Me*)NAr)$_2$), 0.64 (s, 9H, ^{t}Bu). **^{13}C{^{1}H} NMR (600 MHz, C_6D_6, 293 K)** Compound **3.5a**: δ 169.7 (HC(*C*(Me)NAr)$_2$), 149.3 (Ar or Bn), 143.1 (Ar or Bn), 142.3 (Ar or Bn), 142.1 (Ar or Bn), 128.1 (Ar or Bn), 127.9 (Ar or Bn), 127.0 (Ar or Bn), 126.3 (Ar or Bn), 124.9 (Ar or Bn), 124.1 (Ar or Bn), 102.0 (H*C*(C(Me)NAr)$_2$), 71.7 (C$_\alpha$, ^{t}Bu), 58.7 (*C*H$_2$Ph), 33.4 (C$_\beta$, ^{t}Bu), 29.7 (*C*HMe$_2$), 28.0 (*C*HMe$_2$), 26.7 (HC(C(*Me*)NAr)$_2$), 26.3 (CH*Me*$_2$), 25.6 (CH*Me*$_2$), 24.9 (CH*Me*$_2$), 24.3 (CH*Me*$_2$). Anal. calcd (%) for $Nb_1N_7C_{47}H_{64}$: C, 68.85; H, 7.87; N, 11.96. Found: C, 68.73; H, 7.94; N, 11.77. MP: 137–142 ˚C.

(BDI)Nb(N^{t}Bu)(CyNNNNCy) (3.6): Compound **3.1** (300 mg, 0.45 mmol) was added to a 20 mL vial. In a separate vial, cyclohexylazide (120 mg, 0.96 mmol) was dissolved in 5 mL hexane. The cyclohexylazide solution was added to **2.1**, and the mixture was stirred until all of **2.1** had dissolved. Upon addition of the azide solution, visible effervescence of dinitrogen was observed, but subsided within 5 min. The vial was capped and left at room temperature for an additional 3 h, resulting in a gradual lightening of the color from dark red to red and precipitation of red crystalline material. The vial was stored at -40 ˚C overnight, resulting in further precipitation of crystalline material. The crystals were isolated and residual solvent was removed under vacuum. Yield: 280 mg, 77%. **^{1}H NMR (500 MHz, C_6D_6, 293 K):** δ 7.18–7.10 (m, 6H, Ar), 5.06 (s, 1H, *H*C(C(Me)NAr)$_2$), 3.77 (sep, 2H, C*H*Me$_2$), 3.14 (m, 2H, Cy C*H*), 2.62 (sep, 2H, C*H*Me$_2$), 1.71-1.60 (m, 8H, Cy C*H*$_2$), 1.56–1.36 (m, 3H, Cy C*H*$_2$), 1.52 (d, 6H, CH*Me*$_2$), 1.48 (s, 6H, HC(C(*Me*)NAr)$_2$), 1.46 (s, 9H, ^{t}Bu), 1.40 (d, 6H, CH*Me*$_2$), 1.33-0.94 (m, 9H, Cy C*H*$_2$), 1.27 (d, 6H, CH*Me*$_2$), 1.01 (d, 6H, CH*Me*$_2$). **^{13}C{^{1}H} NMR (600 MHz, C_6D_6, 293 K):** δ 169.5 (HC(*C*(Me)NAr)$_2$), 150.9 (Ar), 143.0 (Ar), 141.0 (Ar), 126.5 (Ar), 125.3 (Ar), 124.0 (Ar), 101.3 (H*C*(C(Me)NAr)$_2$), 71.3 (C$_\alpha$, ^{t}Bu), 64.9 (*C*H, Cy), 33.8 (C$_\beta$, ^{t}Bu), 33.6 (*C*H$_2$, Cy), 29.3 (*C*HMe$_2$), 28.3 (*C*HMe$_2$), 27.2 (*C*H$_2$, Cy), 26.8 (HC(C(*Me*)NAr)$_2$), 26.4 (*C*H$_2$, Cy), 25.4 (CH*Me*$_2$), 25.3 (CH*Me*$_2$), 25.3 (CH*Me*$_2$), 24.6 (CH*Me*$_2$). Anal. calcd (%) for $Nb_1N_7C_{45}H_{72}$: C, 67.22; H, 9.03; N, 12.19. Found: C, 67.01; H, 9.17; N, 12.08. MP: 146–150 ˚C.

(BDI)Nb(N^{t}Bu)(BnNNNNCy) (3.7): Compound **3.7** was observed as an intermediate by ^{1}H NMR spectroscopy upon either heating **3.5** with 10 equiv. cyclohexylazide at 60 ˚C in C_6D_6 for 4 h or allowing **3.6** react with 10 equiv. benzylazide at room temperature for 16 h. **^{1}H NMR (600 MHz, C_6D_6, 293 K):** δ 7.32–6.92 (m, 11H, Ar), 5.13 (s, 1H, *H*C(C(Me)NAr)$_2$), 4.06 (s, 2H, Bn C*H*$_2$), 3.70 (sep, 2H, C*H*Me$_2$), 3.34 (m, 1H, Cy C*H*), 2.66 (sep, 2H, C*H*Me$_2$), 1.69–0.98 (m, 10H, Cy C*H*$_2$), 1.56 (s, 6H, HC(C(*Me*)NAr)$_2$), 1.43 (d, 6H, CH*Me*$_2$), 1.36 (d, 6H, CH*Me*$_2$), 1.25 (d, 6H, CH*Me*$_2$), 0.99 (d, 6H, CH*Me*$_2$).

(BDI)Nb(N^{t}Bu)(NCy)(CN^{t}Bu) (3.8a): Compound **3.6** (300 mg, 0.37 mmol) was added to a 50 mL flask and dissolved in 5 mL benzene to give a red solution. *Tert*-butylisocyanide (84 μL, 62 mg, 0.75 mmol) was added by microsyringe. The solution was heated at 60 °C for 3 h, resulting in a color change from red to orange. The volatile materials were removed under vacuum, leaving an orange residue. The residue was extracted with HMDSO and the resulting solution was concentrated. The solution was stored at -40 ˚C overnight, yielding yellow crystals of **3.8a**. The crystals were isolated and residual solvent was removed under vacuum Yield: 180 mg, 63% over three crops. **^{1}H NMR (600 MHz, C$_6$D$_6$, 293 K):** δ 7.26–7.16 (m, 3H, Ar), 7.06–6.98 (m, 3H, Ar), 5.04 (s, 1H, *H*C(C(Me)NAr)$_2$), 4.48 (m, 1H, Cy C*H*), 4.12 (sep, 1H, C*H*Me$_2$), 3.76 (sep, 1H, C*H*Me$_2$), 3.56 (sep, 1H, C*H*Me$_2$), 3.51 (sep, 1H, C*H*Me$_2$), 2.44 (br d, 1H, Cy), 2.07 (br d, 1H, Cy), 1.85–1.15 (m, 8H, Cy), 1.74 (d, 3H, CH*Me*$_2$), 1.71 (s, 3H, HC(C(*Me*)NAr)$_2$), 1.65 (s, 3H, HC(C(*Me*)NAr)$_2$), 1.61 (d, 3H, CH*Me*$_2$), 1.46 (d, 3H, CH*Me*$_2$), 1.40 (d, 3H, CH*Me*$_2$), 1.37 (d, 3H, CH*Me*$_2$), 1.35 (d, 3H, CH*Me*$_2$), 1.29 (d, 3H, CH*Me*$_2$), 1.21 (d, 3H, CH*Me*$_2$), 1.09 (s, 9H, NbN^{t}Bu), 0.78 (s, 9H, C≡N^{t}Bu). **^{13}C{^{1}H} NMR (600 MHz, C$_6$D$_6$, 293 K):** δ 166.1 (HC(*C*(Me)NAr)$_2$), 165.7 (HC(*C*(Me)NAr)$_2$), 152.5 (Ar), 152.0 (Ar), 143.0 (Ar), 142.3 (Ar), 142.2 (Ar), 142.2 (Ar), 125.3 (Ar), 125.1 (Ar), 124.4 (Ar), 124.4 (Ar), 124.3 (Ar), 123.4 (Ar), 99.3 (H*C*(C(Me)NAr)$_2$), 71.3 (*C*H, Cy), 64.7 (C$_\alpha$, NbN^{t}Bu), 56.0 (C$_\alpha$, C≡N^{t}Bu), 38.6 (Cy), 38.4 (Cy), 33.2 (C$_\beta$, NbN^{t}Bu), 29.4 (C$_\beta$, C≡N^{t}Bu), 28.7 (*C*HMe$_2$), 28.6 (*C*HMe$_2$), 28.0 (*C*HMe$_2$), 27.7 (*C*HMe$_2$), 27.0 (Cy), 26.9 (Cy), 26.7 (CH*Me*$_2$), 26.1 (Cy), 25.9 (CH*Me*$_2$), 25.3 (HC(C(*Me*)NAr)$_2$), 25.2 (CH*Me*$_2$), 25.1 (CH*Me*$_2$), 24.9 (HC(C(*Me*)NAr)$_2$), 24.9 (CH*Me*$_2$), 24.8 (CH*Me*$_2$), 24.4 (CH*Me*$_2$), 23.8 (CH*Me*$_2$). Anal. calcd (%) for $Nb_1N_5C_{47}H_{70}\cdot0.5C_6H_{18}OSi_2$: C, 68.31; H, 9.06; N, 7.97. Found: C, 67.40; H, 9.18; N, 8.23. MP: dec. 136–161 ˚C.

(BDI)Nb(N^{t}Bu)(NCy)(CNCy) (3.8b): Compound **3.6** (10 mg, 0.012 mmol) and cyclohexylisocyanide (2.7 mg, 0.025 mmol) were dissolved in C$_6$D$_6$ (0.4 mL) in a 4 mL vial and transferred to a J. Young NMR tube. The solution was heated at 60 ˚C for 3 h, resulting in a color change from red to orange. A ^{1}H NMR spectrum indicated clean conversion to **3.8b** and dicyclohexylcarbodiimide. **^{1}H NMR (400 MHz, C$_6$D$_6$, 293 K):** δ 7.29–7.16 (m, 3H, Ar), 7.10–6.96 (m, 3H, Ar), 5.06 (s, 1H, *H*C(C(Me)NAr)$_2$), 4.48 (m, 1H, NbNCy C*H*), 4.13 (sep, 1H, C*H*Me$_2$), 3.81 (sep, 1H, C*H*Me$_2$), 3.58 (sep, 1H, C*H*Me$_2$), 3.53 (sep, 1H, C*H*Me$_2$), 2.88 (m, 1H, CNCy C*H*), 2.48 (br d, 1H, Cy), 2.09 (br d, 1H, Cy), 1.90–0.67 (m, 20H, Cy), 1.75 (d, 3H, CH*Me*$_2$), 1.72 (s, 3H, HC(C(*Me*)NAr)$_2$), 1.68 (s, 3H, HC(C(*Me*)NAr)$_2$), 1.62 (d, 3H, CH*Me*$_2$), 1.50 (d, 3H, CH*Me*$_2$), 1.41 (d, 6H, CH*Me*$_2$), 1.36 (d, 3H, CH*Me*$_2$), 1.30 (d, 3H, CH*Me*$_2$), 1.23 (d, 3H, CH*Me*$_2$), 1.12 (s, 9H, ^{t}Bu).

(BDI)NbH(NH^{t}Bu)(N^{t}Bu) (3.9): Compound **3.2** (200 mg, 0.30 mmol) was added to a 25 mL Schlenk tube and dissolved in 2 mL HMDSO to give a nearly saturated orange solution. The flask was evacuated under reduced pressure for 5 s, and the headspace was backfilled with H_2. The solution was left at room temperature for 1 day, resulting in a slight lightening of the color. Storage at -40 ˚C for 5 days yielded yellow-orange crystals of **3.9**. The crystals were isolated and residual solvent was removed under vacuum Yield: 91 mg, 41%. *Generation in solution*: Compound **3.2** (10 mg, 0.015 mmol) was dissolved in C$_6$D$_6$ (0.4 ml) in a 4 mL vial to give an orange-yellow solution and then transferred to a J. Young NMR tube and sealed. The solution was degassed with two freeze-pump-thaw cycles. With ca. 95% of the length of the tube submerged in liquid N_2, the

tube was evacuated under reduced pressure for 5 s, and the headspace was backfilled with 1 atm H_2. The tube was sealed, and then allowed to warm to room temperature. Upon thawing, the solution rapidly changed color from orange-yellow to a lighter yellow-orange. **^{1}H NMR (500 MHz, C_6D_6, 293 K):** δ 9.09 (br s, 1H, Nb-*H*) 7.80 (s, 1H, N-H) 7.24-7.07 (m, 6H, Ar), 5.02 (s, 1H, *H*C(C(Me)NAr)$_2$), 3.56 (sep, 2H, C*H*Me$_2$), 3.46 (sep, 2H, C*H*Me$_2$), 1.62 (s, 6H, HC(C(*Me*)NAr)$_2$), 1.50 (d, 6H, CH*Me*$_2$), 1.37 (d, 6H, CH*Me*$_2$), 1.25 (s, 9H, NbN^{t}Bu), 1.23 (d, 6H, CH*Me*$_2$), 1.21 (d, 6H, CH*Me*$_2$), 1.06 (s, 9H, NbN(H)^{t}Bu). **^{13}C{^{1}H} NMR (600 MHz, C_6D_6, 293 K):** δ 166.2 (HC(*C*(Me)NAr)$_2$), 152.0 (Ar), 145.3 (Ar), 142.1 (Ar), 125.9 (Ar), 124.7 (Ar), 124.3 (Ar), 101.0 (H*C*(C(Me)NAr)$_2$), 67.2 (C_α, NbN(H)^{t}Bu), 56.5 (C_α, NbN^{t}Bu), 33.3 (C_β, NbN(H)^{t}Bu), 33.1 (C_β, NbN^{t}Bu), 28.7 (*C*HMe$_2$), 28.6 (*C*HMe$_2$), 25.3 (CH*Me*$_2$), 25.2 (CH*Me*$_2$), 25.1 (CH*Me*$_2$), 25.0 (CH*Me*$_2$), 24.9 (HC(C(*Me*)NAr)$_2$). FT-IR (KBr, nujol, cm^{-1}): 3344 (sharp, w, N-H stretch), 3323 (sharp, w, N-H stretch), 1652 (broad, m, Nb-H stretch). Anal. calcd (%) for $Nb_1N_4C_{37}H_{61}$: C, 67.87; H, 9.39; N, 8.56. Found: C, 67.69; H, 9.33; N, 8.47.

(BDI)NbH(NH^{t}Bu)(NAr) (3.10): Compound **3.4** (10 mg, 0.013 mmol) was dissolved in C_6D_6 (0.4 ml) in a 4 mL vial to give a red solution and then transferred to a J. Young NMR tube and sealed. The solution was degassed with two freeze-pump-thaw cycles. With ca. 95% of the length of the tube submerged in liquid N_2, the tube was evacuated under reduced pressure for 5 s, and the headspace was backfilled with 1 atm H_2. The tube was sealed, and then allowed to warm to room temperature. Upon thawing, the solution lightened in color. **^{1}H NMR (400 MHz, C_6D_6, 293 K):** δ 9.43 (br s, 1H, Nb-*H*) 8.66 (s, 1H, N-H) 7.19–6.95 (m, 9H, Ar), 5.24 (s, 1H, *H*C(C(Me)NAr)$_2$), 4.26 (br s, 1H, C*H*Me$_2$), 4.08 (br s, 1H, C*H*Me$_2$), 3.83 (sep, 1H, C*H*Me$_2$), 3.38 (sep, 1H, C*H*Me$_2$), 3.25 (sep, 1H, C*H*Me$_2$), 3.21 (sep, 1H, C*H*Me$_2$), 1.71 (s, 3H, HC(C(*Me*)NAr)$_2$), 1.69 (s, 3H, HC(C(*Me*)NAr)$_2$), 1.37–1.30 (m, 18H, CH*Me*$_2$), 1.25 (d, 3H, CH*Me*$_2$), 1.17–1.09 (m, 12H, CH*Me*$_2$), 1.02 (d, 3H, CH*Me*$_2$), 0.82 (s, 9H, ^{t}Bu). **^{13}C{^{1}H} NMR (600 MHz, C_6D_6, 293 K):** δ 166.8 (HC(*C*(Me)NAr)$_2$), 166.1 (HC(*C*(Me)NAr)$_2$), 153.3 (Ar), 149.0 (Ar), 144.4 (Ar), 142.5 (Ar), 141.5 (Ar), 140.6 (Ar), 140.4 (Ar), 126.6 (Ar), 125.7 (Ar), 125.6 (Ar), 125.1 (Ar), 124.3 (Ar), 124.0 (Ar), 123.8 (Ar), 123.7 (Ar), 122.5 (Ar), 101.8 (H*C*(C(Me)NAr)$_2$), 57.1 (C_α, ^{t}Bu), 32.1 (C_β, ^{t}Bu), 29.9 (*C*HMe$_2$), 29.2 (*C*HMe$_2$), 28.4 (*C*HMe$_2$), 28.2 (*C*HMe$_2$), 27.9 (*C*HMe$_2$), 27.9 (*C*HMe$_2$), 26.1 (CH*Me*$_2$), 25.9 (CH*Me*$_2$), 25.8 (CH*Me*$_2$), 25.5 (CH*Me*$_2$), 25.0 (CH*Me*$_2$), 25.0 (HC(C(*Me*)NAr)$_2$), 24.8 (HC(C(*Me*)NAr)$_2$), 24.6 (CH*Me*$_2$), 24.5 (CH*Me*$_2$), 24.2 (CH*Me*$_2$), 24.1 (CH*Me*$_2$), 24.0 (CH*Me*$_2$), 23.9 (CH*Me*$_2$) 23.8 (CH*Me*$_2$).

(BDI)NbH(N[SiH$_2$Ph]^{t}Bu)(N^{t}Bu) (3.11): Compound **3.2** (220 mg, 0.34 mmol) was dissolved in 10 mL hexane in a 20 mL vial to give an orange solution. Phenylsilane (42 μL, 0.34 mmol) was added in one portion using a micropipette, resulting in an immediate color change to yellow. The solution was left at room temperature for 15 min, and then the volatile materials were removed under vacuum, leaving a yellow powder. The residue was extracted with hexane and the resulting solution was concentrated. The solution was stored at -40 ˚C overnight, yielding **3.11** as a pale yellow microcrystalline powder. The powder was isolated and residual solvent was removed under vacuum. Yield: 220 mg, 85% over 2 crops. X-ray suitable crystals were obtained by recrystallization from a concentrated HMDSO solution at -40 °C. **^{1}H NMR (600 MHz, C_6D_6, 293 K):** δ 9.15 (br s, 1H, Nb-*H*), 8.19 (br d, 2H, SiH$_2$*Ph*), 7.37–7.08 (br m, 9H, Ar/SiH$_2$*Ph*), 6.06 (br d, 1H, Si*H*$_2$Ph), 5.56 (br d, 1H, Si*H*$_2$Ph), 4.94 (s, 1H, *H*C(C(Me)NAr)$_2$), 4.42 (sep, 1H, C*H*Me$_2$),

4.29 (br sep, 1H, C*H*Me$_2$), 3.22 (br sep, 1H, C*H*Me$_2$), 3.17 (br sep, 1H, C*H*Me$_2$), 1.86 (br d, 3H, CH*Me*$_2$), 1.65–0.80 (br m, 45H, CH*Me*$_2$/HC(C(*Me*)NAr)$_2$/^{t}Bu). **^{1}H NMR (500 MHz, C$_7$D$_8$, 253 K):** δ 9.05 (br s, 1H, Nb-*H*) 8.16 (d, 2H, SiH$_2$*Ph*), 7.26 (t, 3H, SiH$_2$*Ph*), 7.19 (m, 2H, Ar), 7.15–7.03 (m, 4H, Ar/SiH$_2$*Ph*), 6.02 (d, 1H, Si*H*$_2$Ph, ^{2}J = 9.1 Hz), 5.53 (d, 1H, Si*H*$_2$Ph, ^{2}J = 9.1 Hz), 4.88 (s, 1H, *H*C(C(Me)NAr)$_2$), 4.40 (sep, 1H, C*H*Me$_2$), 4.26 (sep, 1H, C*H*Me$_2$), 3.16 (sep, 1H, C*H*Me$_2$), 3.11 (sep, 1H, C*H*Me$_2$), 1.83 (d, 3H, CH*Me*$_2$), 1.59 (d, 3H, CH*Me*$_2$), 1.57 (s, 3H, HC(C(*Me*)NAr)$_2$), 1.53 (s, 3H, HC(C(*Me*)NAr)$_2$), 1.42 (d, 3H, CH*Me*$_2$), 1.40 (s, 9H, NbN^{t}Bu), 1.29–1.17 (m, 9H, CH*Me*$_2$), 1.09 (d, 3H, CH*Me*$_2$), 1.08 (d, 3H, CH*Me*$_2$), 0.78 (s, 9H, NbN(Si)^{t}Bu). **^{13}C{^{1}H} NMR (500 MHz, C$_7$D$_8$, 253 K):** δ 166.2 (HC(*C*(Me)NAr)$_2$), 165.9 (HC(*C*(Me)NAr)$_2$), 152.1 (Ar), 147.1 (Ar), 145.3 (Ar), 143.4 (Ar), 142.1 (Ar), 137.9 (Ar), 135.6 (Ar), 129.4 (Ar), 128.5 (Ar), 127.5 (Ar), 126.8 (Ar), 126.1 (Ar), 126.0 (Ar), 124.5 (Ar), 123.5 (Ar), 101.3 (H*C*(C(Me)NAr)$_2$), 71.0 (C$_\alpha$, NbN(Si)^{t}Bu), 58.6 (C$_\alpha$, NbN^{t}Bu), 32.8 (C$_\beta$, Nb^{t}Bu), 29.8 (C$_\beta$, NbN(Si)^{t}Bu), 28.8 (*C*HMe$_2$), 28.4 (*C*HMe$_2$), 28.1 (*C*HMe$_2$), 27.9 (*C*HMe$_2$), 26.4 (CH*Me*$_2$), 25.9 (CH*Me*$_2$), 25.9 (CH*Me*$_2$), 25.3 (CH*Me*$_2$), 25.2 (HC(C(*Me*)NAr)$_2$), 25.1 (CH*Me*$_2$), 25.0 (CH*Me*$_2$), 24.9 (CH*Me*$_2$), 24.5 (HC(C(*Me*)NAr)$_2$), 24.4 (CH*Me*$_2$). FT-IR (KBr, nujol, cm^{-1}): 2204 (sharp, s, Si-H stretch), 2130 (sharp, s, Si-H stretch), 2103 (sharp, s, Si-H stretch), 1667 (broad, m, Nb-H stretch). Anal. calcd (%) for $Nb_1Si_1N_4C_{43}H_{67}$: C, 67.87; H, 8.87; N, 7.36. Found: C, 68.02; H, 8.77; N, 7.41. MP: dec. 120–143 ˚C.

(BDI)NbH(N[SiH$_2$^{n}Bu]^{t}Bu)(N^{t}Bu) (3.12): Compound **3.2** (180 mg, 0.28 mmol) was added to a 50 mL Schlenk flask and dissolved in 5 mL toluene to give an orange solution. Phenylsilane (36 μL, 0.28 mmol) was added using a micropipette, resulting in an immediate color change to orange-yellow. The solution was left at room temperature overnight, then the volatile materials were removed under vacuum leaving an orange-yellow residue. The residue was extracted with HMDSO and the resulting solution was concentrated. The solution was stored at -40 ˚C overnight, yielding pale yellow crystals of **3.12**. The crystalline material was isolated and residual solvent was removed under vacuum. Yield: 160 mg, 75% over two crops. **^{1}H NMR (600 MHz, C$_6$D$_6$, 293 K):** δ 8.65 (br s, 1H, Nb-*H*) 8.19, 7.28–7.07 (br m, 6H, Ar), 5.34 (br s, 1H, Si*H*$_2$^{n}Bu), 5.01 (br s, 1H, Si*H*$_2$^{n}Bu), 4.92 (s, 1H, *H*C(C(Me)NAr)$_2$), 4.30 (br m, 1H, C*H*Me$_2$), 4.22 (br m, 1H, C*H*Me$_2$), 3.19 (br m, 2H, C*H*Me$_2$), 1.80–0.80 (br m, 57H, CH*Me*$_2$/HC(C(*Me*)NAr)$_2$/^{t}Bu/^{n}Bu). FT-IR (KBr, nujol, cm^{-1}): 2178 (sharp, m, Si-H stretch), 2092 (sharp, s, Si-H stretch), 1667 (broad, m, Nb-H stretch). MP: 148–168 ˚C.

(BDI)NbH(N[BO$_2$C$_6$H$_{12}$]^{t}Bu)(N^{t}Bu) (3.13): Compound **3.2** (210 mg, 0.32 mmol) was dissolved in 5 mL hexane in a 20 mL vial to give an orange solution. Pinacolborane (49 μL, 0.32 mmol) was added using a micropipette, resulting in an immediate color change to yellow. The solution was left at room temperature for 3 h, and then filtered through a pad of Celite. The volatile materials were removed under vacuum, leaving a yellow residue. The residue was extracted with a hexane/HMDSO mixture and the resulting solution was concentrated. The solution was stored at -40 ˚C overnight, yielding **3.13** as a yellow microcrystalline powder. The powder was isolated and residual solvent was removed under vacuum. Yield: 97 mg, 39%. X-ray suitable crystals were obtained by recrystallization from a concentrated HMDSO solution at -40 °C. **^{1}H NMR (600 MHz, C$_6$D$_6$, 293 K):** δ 10.01 (s, 1H, Nb-*H*), 7.26–7.13 (m, 6H, Ar) 5.11 (s, 1H, *H*C(C(Me)NAr)$_2$), 3.63 (sep, 1H, C*H*Me$_2$), 3.52 (sep, 1H, C*H*Me$_2$), 3.32 (sep, 1H, C*H*Me$_2$), 3.25 (sep, 1H, C*H*Me$_2$), 1.69

(s, 3H, HC(C(*Me*)NAr)$_2$), 1.65 (s, 3H, HC(C(*Me*)NAr)$_2$), 1.63 (d, 3H, CH*Me*$_2$), 1.61 (d, 3H, CH*Me*$_2$), 1.54 (s, 9H, NbN^{t}Bu), 1.45 (d, 3H, CH*Me*$_2$), 1.44 (d, 3H, CH*Me*$_2$), 1.29 (d, 3H, CH*Me*$_2$), 1.23 (d, 3H, CH*Me*$_2$), 1.21 (d, 3H, CH*Me*$_2$), 1.16 (d, 3H, CH*Me*$_2$), 1.14 (s, 6 H, BPin C*H*$_3$), 1.13 (s, 6 H, BPin C*H*$_3$), 1.11 (s, 9H, NbN(B)^{t}Bu). **^{13}C{^{1}H} NMR (400 MHz, C$_6$D$_6$, 293 K):** δ 165.5 (CH(*C*(Me)NAr)$_2$), 163.8 (CH(*C*(Me)NAr)$_2$), 153.2 (Ar), 150.0 (Ar), 144.0 (Ar), 142.5 (Ar), 142.2 (Ar), 142.0 (Ar), 126.3 (Ar), 125.8 (Ar), 125.3 (Ar), 125.1 (Ar), 123.9 (Ar), 123.6 (Ar), 103.7 (*C*H(C(Me)NAr)$_2$), 82.4 (C$_\alpha$, NbN^{t}Bu), 56.2 (C$_\alpha$, NbN(B)^{t}Bu), 35.4 (C$_\beta$, NbN^{t}Bu), 33.3 (C$_\beta$, NbN(B)^{t}Bu), 29.1 (*C*HMe$_2$), 28.9 (*C*HMe$_2$), 28.0 (*C*HMe$_2$), 27.4 (*C*HMe$_2$), 26.8 (CH*Me*$_2$), 26.4 (CH*Me*$_2$), 26.0 (HC(C(*Me*)NAr)$_2$), 25.8 (HC(C(*Me*)NAr)$_2$), 25.7 (CH*Me*$_2$), 25.6 (CH*Me*$_2$), 25.4 (CH*Me*$_2$), 25.0 (BPin *C*H$_3$), 24.8 (CH*Me*$_2$), 24.6 (CH*Me*$_2$), 24.4 (CH*Me*$_2$), 24.2 (BPin *C*H$_3$). FT-IR (KBr, nujol, cm^{-1}): 1662 (broad, m, Nb-H stretch). Anal. calcd (%) for $NbO_2N_4BC_{43}H_{72}$: C, 66.15; H, 9.30; N, 7.18. Found: C, 65.97; H, 9.42; N, 7.08. MP: dec. 142–148 ˚C.

(BDI)Nb(OC(H)O)(N[SiH$_2$^{n}Bu]^{t}Bu)(N^{t}Bu) (3.14): Compound **3.12** (190 mg, 0.26 mmol) was added to a 100 mL Schlenk flask and dissolved in 10 mL toluene to give a pale yellow solution. The flask was evacuated under reduced pressure for 5 s, and the headspace was backfilled with CO_2, resulting in a slight lightening of the color. The solution was stirred at room temperature overnight, and then the volatile materials were removed under vacuum, leaving a yellow residue. The residue was extracted with pentane and the resulting solution was concentrated. The solution was stored at -40 ˚C overnight, yielding pale yellow crystals of **3.14**. The crystalline material was isolated and residual solvent was removed under vacuum. Yield: 95 mg, 48% over two crops. ^{1}H NMR (400 MHz, C_6D_6, 293 K) δ 7.86 (s, 1H, OC*HO*), 7.22–7.11 (m, 5H, Ar), 7.07 (dd, 1H, Ar), 5.51 (m, 1H, Si*H*$_2$^{n}Bu), 5.13 (s, 1H, *H*C(C(Me)NAr)$_2$), 5.06 (m, 1H, Si*H*$_2$^{n}Bu), 4.11 (sep, 1H, C*H*Me$_2$), 3.67 (sep, 1H, C*H*Me$_2$), 2.96 (sep, 1H, C*H*Me$_2$), 2.95 (sep, 1H, C*H*Me$_2$), 1.65–0.99 (m, 6H, ^{n}Bu C*H*$_2$), 1.64 (d, 3H, CH*Me*$_2$), 1.61 (s, 3H, HC(C(*Me*)NAr)$_2$), 1.61 (s, 3H, HC(C(*Me*)NAr)$_2$), 1.58 (d, 3H, CH*Me*$_2$), 1.56 (d, 3H, CH*Me*$_2$), 1.48 (s, 9H, NbN^{t}Bu), 1.37 (d, 3H, CH*Me*$_2$), 1.25 (d, 3H, CH*Me*$_2$), 1.23 (d, 3H, CH*Me*$_2$), 1.08 (br s, 9H, NbN(Si)^{t}Bu), 1.04 (d, 3H, CH*Me*$_2$), 1.04 (d, 3H, CH*Me*$_2$), 0.92 (t, 3H, ^{n}Bu C*H*$_2$). FT-IR (KBr, nujol, cm^{-1}): 2182 (s, Si-H stretch), 2098 (s, Si-H stretch), 1649 (s, C=O stretch). Anal. calcd (%) for $NbSiO_2N_4C_{42}H_{71}$: C, 64.26; H, 9.12; N, 7.14. Found: C, 64.10; H 9.30; N, 7.03. MP: dec. 123–143 ˚C.

(BDI)Nb(OC(H)O)(N[BO$_2$C$_6$H$_{12}$]^{t}Bu)(N^{t}Bu) (3.15): Compound **3.13** (160 mg, 0.20 mmol) was added to a 100 mL Schlenk flask and dissolved in 10 mL hexane to give a yellow solution. The flask was evacuated under reduced pressure for 5 s, and the headspace was backfilled with CO_2, resulting in a slight lightening of the color. The solution was stirred at room temperature overnight, and then the volatile materials were removed under vacuum, leaving a yellow residue. The residue was extracted with HMDSO and the resulting solution was concentrated. The solution was stored at -40 ˚C overnight, yielding yellow crystals of **3.15**. The crystalline material was isolated and residual solvent was removed under vacuum. Yield: 57 mg, 35% over three crops. **^{1}H NMR (400 MHz, C$_6$D$_6$, 293 K):** δ 8.60 (s, 1H, NbOC*HO*), 7.28–7.11 (m, 5H, Ar), 7.06 (dd, 1H, Ar), 5.16 (s, 1H, *H*C(C(Me)NAr)$_2$), 4.15 (sep, 1H, C*H*Me$_2$), 3.78 (sep, 1H, C*H*Me$_2$), 2.95 (sep, 1H, C*H*Me$_2$), 2.90 (sep, 1H, C*H*Me$_2$), 1.67 (s, 3H, HC(C(*Me*)NAr)$_2$), 1.60 (s, 3H, HC(C(*Me*)NAr)$_2$), 1.59 (d, 3H, CH*Me*$_2$), 1.57 (s, 9H, NbN^{t}Bu), 1.53 (d, 3H, CH*Me*$_2$), 1.29 (s, 9H, NbN(B)^{t}Bu), 1.26 (d, 3H, CH*Me*$_2$), 1.24 (d, 3H, CH*Me*$_2$), 1.21 (s, 6H, BPin C*H*$_3$), 1.20 (d, 3H, CH*Me*$_2$), 1.19 (d, 3H, CH*Me*$_2$),

1.13 (s, 6H, BPin C*H*$_3$), 1.06 (d, 3H, CH*Me*$_2$), 1.04 (d, 3H, CH*Me*$_2$). **^{13}C{^{1}H} NMR (600 MHz, C_6D_6, 293 K):** δ 169.0 (CH(*C*(Me)NAr)$_2$), 166.2 (CH(*C*(Me)NAr)$_2$), 164.9 (NbO*C*HO), 149.1 (Ar), 148.6 (Ar), 145.8 (Ar), 144.4 (Ar), 143.7 (Ar), 140.5 (Ar), 127.3 (Ar), 126.4 (Ar), 125.7 (Ar), 125.0 (Ar), 124.6 (Ar), 123.8 (Ar), 103.9 (*C*H(C(Me)NAr)$_2$), 82.4 (C_α, NbN^{t}Bu), 58.2 (C_α, NbN(B)^{t}Bu), 32.6 (C_β, NbN^{t}Bu), 28.9 (*C*HMe$_2$), 28.8 (*C*HMe$_2$), 27.9 (*C*HMe$_2$), 27.8 (*C*HMe$_2$), 26.9 (CH*Me*$_2$), 26.6 (HC(C(*Me*)NAr)$_2$), 26.5 (C_α, NbN(B)^{t}Bu), 26.3 (HC(C(*Me*)NAr)$_2$), 26.3 (CH*Me*$_2$), 25.9 (CH*Me*$_2$), 25.9 (CH*Me*$_2$), 25.8 (CH*Me*$_2$), 25.5 (CH*Me*$_2$), 25.4 (CH*Me*$_2$), 25.0 (BPin *C*H$_3$), 24.8 (BPin *C*H$_3$), 24.5 (CH*Me*$_2$). FT-IR (KBr, nujol, cm^{-1}): 1661 (s, C=O stretch). Anal. calcd (%) for $NbO_4N_4BC_{44}H_{72}$: C, 64.26; H, 9.12; N, 7.14. Found: C, 63.89; H 8.87; N, 6.71. MP: 113–138 ˚C.

(BDI)Nb(N^{t}Bu)(NH^{t}Bu)(CC^{t}Bu) (3.16): Compound **3.2** (130 mg, 0.20 mmol) was added to a 100 mL Schlenk flask and dissolved in 10 mL toluene to give an orange solution. *Tert*-butylacetylene (25 μL, 0.20 mmol) was added using a microsyringe. The solution was heated at 60 ˚C for 15 h, resulting in a color change from orange to pale yellow. The volatile materials were removed under vacuum, leaving a pale yellow powder. The residue was extracted with hexane and the resulting solution was filtered through a pad of Celite and concentrated. The solution was stored at -40 ˚C overnight, yielding **3.16** as a pale yellow crystalline solid. The crystalline material was isolated and residual solvent was removed under vacuum. Yield: 85 mg, 56% over 2 crops. X-ray suitable crystals were obtained by recrystallization from a concentrated hexane solution at -40 °C. A 1.9:1 ratio of **3.16a** to **3.16b** was observed by ^{1}H NMR spectroscopy at 293 K, while a 1.4:1 ratio was observed at 253 K. **^{1}H NMR (600 MHz, C_6D_6, 293 K):** Compound **3.16a**: δ 7.67 (br s, 1H, N-*H*), 7.30–7.05 (br m, 6H, Ar), 5.06 (br s, 1H, *H*C(C(Me)NAr)$_2$), 3.66 (br m, 2H, C*H*Me$_2$), 3.06 (br m, 1H, C*H*Me$_2$), 2.88 (br m, 1H, C*H*Me$_2$), 1.69–0.94 (br m, 57H, CH*Me*$_2$/HC(C(*Me*)NAr)$_2$/^{t}Bu). Compound **3.16b**: δ 8.65 (br s, 1H, N-*H*), 7.30–7.05 (br m, 6H, Ar), 5.03 (br s, 1H, *H*C(C(Me)NAr)$_2$), 4.19 (br m, 1H, C*H*Me$_2$), 3.93 (br m, 1H, C*H*Me$_2$), 3.14 (br m, 2H, C*H*Me$_2$), 1.83 (br m, 3H, CH*Me*$_2$),1.69–0.94 (br m, 54H, CH*Me*$_2$/HC(C(*Me*)NAr)$_2$/^{t}Bu). **^{1}H NMR (500 MHz, C_7D_8, 253 K):** Compound **3.16a**: δ 7.57 (s, 1H, N-*H*), 7.22–7.04 (m, 6H, Ar), 4.98 (s, 1H, *H*C(C(Me)NAr)$_2$), 3.61 (sep, 1H, C*H*Me$_2$), 3.60 (sep, 1H, C*H*Me$_2$), 3.01 (sep, 1H, C*H*Me$_2$), 2.80 (sep, 1H, C*H*Me$_2$), 1.59–0.95 (m, 57H, CH*Me*$_2$/HC(C(*Me*)NAr)$_2$/^{t}Bu). Compound **3.16b**: δ 8.67 (s, 1H, N-*H*), 7.30–7.05 (m, 6H, Ar), 4.95 (s, 1H, *H*C(C(Me)NAr)$_2$), 4.19 (sep, 1H, C*H*Me$_2$), 3.89 (sep, 1H, C*H*Me$_2$), 3.10 (sep, 2H, C*H*Me$_2$), 1.83 (d, 3H, CH*Me*$_2$),1.69–0.94 (m, 54H, CH*Me*$_2$/HC(C(*Me*)NAr)$_2$/^{t}Bu). **^{1}H NMR (500 MHz, C_7D_8, 333 K):** δ 7.85 (br s, 1H, N-*H*), 7.19–6.70 (br m, 6H, Ar), 5.09 (s, 1H, *H*C(C(Me)NAr)$_2$), 3.88–2.60 (br m, 4H, C*H*Me$_2$), 1.65–0.85 (br m, 57H, CH*Me*$_2$/HC(C(*Me*)NAr)$_2$/^{t}Bu). **^{13}C{^{1}H} NMR (500 MHz, C_7D_8, 253 K):** δ 167.7 (HC(*C*(Me)NAr)$_2$), 166.8 (HC(*C*(Me)NAr)$_2$), 165.9 (HC(*C*(Me)NAr)$_2$), 165.5 (HC(*C*(Me)NAr)$_2$), 154.5 (Ar), 152.5 (Ar), 151.9 (Ar), 150.9 (Ar), 143.2 (Ar), 142.6 (Ar), 141.6 (Ar), 141.3 (Ar), 141.1 (Ar), 140.7 (Ar), 140.4 (Ar), 128.5 (Ar), 127.6 (Ar), 126.2 (Ar), 126.1 (Ar), 125.9 (Ar), 124.7 (Ar), 124.0 (Ar), 123.8 (Ar), 123.6 (Ar), 123.0 (Ar), 122.8 (Ar), 101.2 (H*C*(C(Me)NAr)$_2$), 100.9 (H*C*(C(Me)NAr)$_2$), 71.5 (C_α, ^{t}Bu), 66.1 (C_α, ^{t}Bu), 57.9 (C_α, ^{t}Bu), 57.1 (C_α, ^{t}Bu), 33.7 (C_β, ^{t}Bu), 32.3 (C_β, ^{t}Bu), 31.7 (C_β, ^{t}Bu), 31.5 (C_β, ^{t}Bu), 31.3 (C_β, ^{t}Bu), 30.0 (C_β, ^{t}Bu), 29.5 (*C*HMe$_2$), 29.2 (*C*HMe$_2$), 28.8 (*C*HMe$_2$), 28.5 (*C*HMe$_2$), 28.4 (*C*HMe$_2$), 28.0 (*C*HMe$_2$), 27.4 (*C*HMe$_2$), 26.8 (*C*H$_3$), 26.7 (*C*H$_3$), 26.4 (*C*H$_3$), 26.2 (*C*H$_3$), 26.1 (*C*H$_3$), 25.8 (*C*H$_3$), 25.7 (*C*H$_3$), 25.6 (*C*H$_3$), 25.5 (*C*H$_3$), 25.4 (*C*H$_3$), 25.2 (*C*H$_3$), 25.1 (*C*H$_3$), 25.1 (*C*H$_3$), 24.9 (*C*H$_3$), 24.8 (*C*H$_3$), 24.5 (*C*H$_3$), 24.3

(*C*H$_3$), 23.9 (*C*H$_3$), 23.7 (*C*H$_3$). FT-IR (KBr, nujol, cm^{-1}): 3318 (sharp, w, N-H), 2080 (s, C≡C stretch). Anal. calcd (%) for $NbN_4C_{42}H_{66}$: C, 70.07; H, 9.24; N, 7.78. Found: C, 70.34; H 8.88; N, 7.80. MP: dec. 190–209 ˚C.

(κ^1-BDI)Nb(N^{t}Bu)(NH^{t}Bu)(SCPh$_3$) (3.17): Compound **3.2** (140 mg, 0.22 mmol) was dissolved in 5 mL toluene in a 20 mL vial to give an orange solution. In a separate vial, triphenylmethanethiol (61 mg, 0.22 mmol) was dissolved in 3 mL toluene. The triphenylmethanethiol solution was added to the solution of **3.2**, resulting in a slight lightening of the solution color. The solution was left at room temperature for 16 h, and then the volatile materials were removed under vacuum, leaving a yellow residue. The residue was extracted with HMDSO and the resulting solution was concentrated. The solution was stored at -40 ˚C overnight, yielding **3.17** as a pale yellow microcrystalline powder. The powder was isolated and residual solvent was removed under vacuum. Yield: 120 mg, 60% over two crops. X-ray suitable crystals were obtained by recrystallization from a concentrated HMDSO solution at -40 °C. **^{1}H NMR (400 MHz, C$_6$D$_6$, 293 K):** δ 7.62 (m, 6H, SC*Ph*$_3$), 7.29–7.05 (m, 6H, Ar), 7.09 (t, 6H, SC*Ph*$_3$), 6.99 (t, 3H, SC*Ph*$_3$), 6.24 (s, 1H, N-*H*), 4.66 (s, 1H, *H*C(C(Me)NAr)$_2$), 3.84 (sep, 1H, C*H*Me$_2$), 3.31 (sep, 1H, C*H*Me$_2$), 2.94 (sep, 1H, C*H*Me$_2$), 2.85 (sep, 1H, C*H*Me$_2$), 2.51 (s, 3H, HC(C(*Me*)NAr)$_2$), 1.69 (d, 3H, CH*Me*$_2$), 1.49 (d, 3H, CH*Me*$_2$), 1.38 (d, 3H, CH*Me*$_2$), 1.31 (s, 3H, HC(C(*Me*)NAr)$_2$), 1.29 (d, 3H, CH*Me*$_2$), 1.25 (d, 3H, CH*Me*$_2$), 1.20 (s, 9H, NbN^{t}Bu), 1.16 (d, 3H, CH*Me*$_2$), 1.13 (d, 3H, CH*Me*$_2$), 1.11 (d, 3H, CH*Me*$_2$), 1.03 (s, 9H, NbN(H)^{t}Bu). **^{13}C{^{1}H} NMR (600 MHz, C$_6$D$_6$, 293 K):** δ 165.0 (CH(*C*(Me)NAr)$_2$), 153.1 (Ar), 150.5 (Ar), 149.7 (Ar), 148.6 (Ar), 148.0 (Ar), 144.0 (Ar), 142.7 (Ar), 137.0 (Ar), 136.1 (Ar), 131.0 (SC*Ph*$_3$), 130.4 (Ar), 128.7 (Ar), 127.9 (SC*Ph*$_3$), 126.8 (SC*Ph*$_3$), 126.7 (Ar), 124.5 (Ar), 123.3 (Ar), 123.2 (Ar), 123.0 (Ar), 102.5 (*C*H(C(Me)NAr)$_2$), 73.5 (S*C*Ph$_3$), 69.0 (C$_\alpha$, NbN(H)^{t}Bu), 57.5 (C$_\alpha$, NbN^{t}Bu), 34.5 (C$_\beta$, NbN^{t}Bu), 31.3 (C$_\beta$, NbN(H)^{t}Bu), 28.7 (*C*HMe$_2$), 28.6 (*C*HMe$_2$), 28.5 (*C*HMe$_2$), 28.4 (*C*HMe$_2$), 26.3 (CH*Me*$_2$), 26.1 (CH*Me*$_2$), 25.3 (CH*Me*$_2$), 24.4 (CH*Me*$_2$), 23.9 (CH*Me*$_2$), 23.4 (CH*Me*$_2$), 23.2 (CH*Me*$_2$), 23.0 (CH(C(*Me)*NAr)$_2$), 22.9 (CH*Me*$_2$), 22.1 (CH(C(*Me)*NAr)$_2$). Anal calcd (%) for $NbSN_4C_{56}H_{75}$: C, 72.39, H, 8.14; N, 6.03. Found: C, 72.28; H, 7.91; N, 5.95. MP: dec. 169–178 °C.

[(BDI)Nb(N^{t}Bu)(μ-S)]$_2$ (3.18): Compound **3.2** (100 mg, 0.15 mmol) was dissolved in 6 mL benzene in a 20 mL vial to give an orange solution. Carbon disulfide (9.2 μL, 0.15 mmol) was added using a microsyringe, resulting in an immediate color change from orange to red. The solution was left at room temperature for 16 h, resulting in precipitation of **3.18** as red crystalline blocks. Yield: 65 mg, 69%. **^{1}H NMR (400 MHz, C$_6$D$_6$, 293 K):** δ 7.37–6.95 (m, 12H, Ar), 5.07 (s, 2H, *H*C(C(Me)NAr)$_2$), 3.79 (sep, 4H, C*H*Me$_2$), 2.99 (sep, 4H, C*H*Me$_2$), 1.54 (d, 12H, CH*Me*$_2$), 1.51 (s, 18H, NbN^{t}Bu), 1.47 (s, 12H, HC(C(*Me*)NAr)$_2$), 1.43 (d, 12H, CH*Me*$_2$), 1.24 (d, 12H, CH*Me*$_2$), 1.10 (d, 12H, CH*Me*$_2$). Compound **3.18** was not sufficiently soluble in common NMR solvents to obtain solution ^{13}C NMR data. Anal. calcd (%) for $Nb_2S_2N_6C_{66}H_{100}$: C, 64.58; H, 8.21; N, 6.85. Found: C, 64.42; H, 8.53; N, 6.62.

[(BDI)Nb(N^{t}Bu)(μ-O$_2$CN(^{t}Bu)CO$_2$)]$_2$ (3.19): Compound **3.2** (200 mg, 0.31 mmol) was added to a 100 mL Schlenk flask and dissolved in 25 mL benzene to give an orange solution. The flask was evacuated under reduced pressure for 5 s, and the headspace was backfilled with CO_2, resulting in an immediate color change from orange to yellow. The solution was stirred at room temperature

overnight. The volatile materials were removed under vacuum, leaving a yellow-orange powder. The residue was extracted with toluene and the resulting solution was concentrated. The solution was stored at -40 ˚C overnight, yielding yellow-orange crystals of **3.19**. The crystalline material was isolated and residual solvent was removed under vacuum. Yield: 180 mg, 76% over three crops. **^{1}H NMR (400 MHz, C_6D_6, 293 K):** δ 7.22–7.14 (m, 6H, Ar), 7.07–7.03 (m, 6H, Ar), 5.36 (s, 2H, *H*C(C(Me)NAr)$_2$), 3.99 (br sep, 4H, C*H*Me$_2$), 3.00 (br s, 4H, C*H*Me$_2$), 1.77 (br s, 12H, CH*Me*$_2$), 1.64 (br s, 12H, HC(C(*Me*)NAr)$_2$), 1.61 (s, 18H, NbN^{t}Bu), 1.40 (d, 12H, CH*Me*$_2$), 1.27 (br d, 12H, CH*Me*$_2$), 1.07 (d, 12H, CH*Me*$_2$), 0.85 (s, 18H O_2CN^tBu). **^{1}H NMR (400 MHz, $CDCl_3$, 293 K):** δ 7.16 (d, 4H, Ar), 7.07 (t, 4H, Ar), 6.99 (d, 4H, Ar), 5.64 (s, 2H, *H*C(C(Me)NAr)$_2$), 3.76 (sep, 4H, C*H*Me$_2$), 2.82 (br sep, 4H, C*H*Me$_2$), 1.82 (s, 12H, HC(C(*Me*)NAr)$_2$), 1.43 (br s, 12H, CH*Me*$_2$), 1.29 (s, 18H, NbN^{t}Bu), 1.17 (d, 12H, CH*Me*$_2$), 1.15 (br d, 12H, CH*Me*$_2$), 0.99 (d, 12H, CH*Me*$_2$), 0.44 (s, 18H O_2CN^tBu). **^{13}C{^{1}H} NMR (400 MHz, $CDCl_3$, 293 K):** δ 168.3 (CH(*C*(Me)NAr)$_2$), 147.6 (Ar), 144.0 (Ar), 143.3 (Ar), 126.2 (Ar), 125.1 (Ar), 123.6 (Ar), 104.7 (*C*H(C(Me)NAr)$_2$), 70.3 (C_α, NbN^{t}Bu), 54.3 (C_α, O_2CN^tBu), 31.5 (C_β, NbN^{t}Bu), 28.2 (*C*HMe$_2$), 28.2 (C_β, O_2CN^tBu), 28.1 (*C*HMe$_2$), 26.4 (CH(C(*Me*)NAr)$_2$), 26.2 (CH*Me*$_2$), 25.5 (CH*Me*$_2$), 25.4 (CH*Me*$_2$), 24.5 (CH*Me*$_2$). FT-IR (KBr, nujol, cm^{-1}): 1720 (s, C=O stretch). Anal. calcd (%) for $Nb_2O_8N_8C_{78}H_{118}$: C, 63.23; H, 8.03; N, 7.56. Found: C, 63.26; H, 7.92; N, 7.60. MP: dec. 178–228 ˚C.

(BDI)Nb(NAr)(N(^{t}Bu)CO_2) (3.20): Compound **3.4** (1.8 g, 2.4 mmol) was added to a 1000 mL Schlenk flask and dissolved in 100 mL hexane to give a red solution. The flask was evacuated under reduced pressure for 10 s, and the headspace was backfilled with CO_2. The solution was stirred at room temperature for 10 min, resulting in a lightening of the solution color and precipitation of a red powder. The powder was collected on a fritted funnel and washed with hexane (3 x 25 mL), and then extracted with diethyl ether. Upon dissolution of the residue in diethyl ether, red crystalline material began forming at room temperature. The solution was stored at -40 ˚C overnight, yielding additional red crystals of **3.20**. The crystalline material was isolated and residual solvent was removed under vacuum. Yield: 1.0 g, 53% over three crops. **^{1}H NMR (600 MHz, C_6D_6, 293 K):** δ 7.19–6.87 (br m, 9H, Ar), 5.51 (s, 1H, *H*C(C(Me)NAr)$_2$), 4.46 (br s, 1H, C*H*Me$_2$), 4.14 (br s, 1H, C*H*Me$_2$), 3.23 (br s, 1H, C*H*Me$_2$), 2.87 (br s, 1H, C*H*Me$_2$), 2.83 (br s, 1H, C*H*Me$_2$), 2.73 (br s, 1H, C*H*Me$_2$), 1.73 (br s, 3H, HC(C(*Me*)NAr)$_2$), 1.63–1.53 (br m, 6H, CH*Me*$_2$/HC(C(*Me*)NAr)$_2$), 1.39 (br s, 3H, CH*Me*$_2$), 1.29–1.03 (br m, 30H, CH*Me*$_2$/^{t}Bu), 0.95 (br s, 3H, CH*Me*$_2$), 0.85 (br s, 3H, CH*Me*$_2$), 0.64 (br s, 3H, CH*Me*$_2$). **^{1}H NMR (500 MHz, C_7D_8, 233 K):** δ 7.17–6.82 (m, 9H, Ar), 5.51 (s, 1H, *H*C(C(Me)NAr)$_2$), 4.46 (br sep, 1H, C*H*Me$_2$), 4.08 (br sep, 1H, C*H*Me$_2$), 3.09 (br sep, 1H, C*H*Me$_2$), 2.82 (br sep, 1H, C*H*Me$_2$), 2.75 (br sep, 1H, C*H*Me$_2$), 2.65 (br sep, 1H, C*H*Me$_2$), 1.68 (s, 3H, HC(C(*Me*)NAr)$_2$), 1.57 (br d, 3H, CH*Me*$_2$), 1.47 (s, 3H, HC(C(*Me*)NAr)$_2$), 1.36 (br d, 3H, CH*Me*$_2$), 1.33–1.08 (br m, 21H, CH*Me*$_2$/^{t}Bu), 1.02 (br d, 3H, CH*Me*$_2$), 1.01 (br d, 3H, CH*Me*$_2$), 0.93 (br d, 3H, CH*Me*$_2$), 0.77 (br d, 3H, CH*Me*$_2$) 0.56 (br d, 3H, CH*Me*$_2$). **^{13}C{^{1}H} NMR (500 MHz, C_7D_8, 233 K):** δ 170.1 (HC(*C*(Me)NAr)$_2$), 165.8 (HC(*C*(Me)NAr)$_2$), 160.6 (N*C*O$_2$), 154.4 (Ar), 148.8 (Ar), 145.1 (Ar), 144.9 (Ar), 143.1 (Ar), 141.4 (Ar), 141.3 (Ar), 140.5 (Ar), 132.5 (Ar), 129.4 (Ar), 126.9 (Ar), 126.1 (Ar), 125.7 (Ar), 124.2 (Ar), 123.7 (Ar), 123.0 (Ar), 122.3 (Ar), 104.5 (H*C*(C(Me)NAr)$_2$), 57.7 (C_α, ^{t}Bu), 31.2 (*C*HMe$_2$), 30.7 (C_β, Nb^{t}Bu), 29.2 (*C*HMe$_2$), 28.2 (HC(C(*Me*)NAr)$_2$), 28.2 (*C*HMe$_2$), 28.0 (*C*HMe$_2$), 27.7 (*C*HMe$_2$), 27.2 (*C*HMe$_2$), 26.9 (CH*Me*$_2$), 26.6 (CH*Me*$_2$), 26.0 (CH*Me*$_2$), 25.7 (CH*Me*$_2$), 25.2

(CH*Me*$_2$), 25.0 (CH*Me*$_2$), 24.9 (CH*Me*$_2$), 24.4 (CH*Me*$_2$), 23.9 (CH*Me*$_2$), 23.7 (HC(C(*Me*)NAr)$_2$), 22.4 (CH*Me*$_2$), 21.3 (CH*Me*$_2$). Anal. calcd (%) for $Nb_1O_2N_4C_{46}H_{67}\cdot C_4H_{10}O$: C, 68.63; H, 8.87; N, 6.40. Found: C, 68.59; H, 8.72; N, 6.79. MP: dec. 135–152 ˚C.

[(BDI)Nb(NAr)(μ-CO$_3$)]$_2$ (3.21): Compound **3.4** (250 mg, 0.33 mmol) was added to a 100 mL Schlenk flask and dissolved in 10 mL toluene to give a red solution. The flask was evacuated under reduced pressure for 5 s, and the headspace was backfilled with CO_2. The solution was stirred at 60 ˚C under N_2 atmosphere for 5 h, resulting in a lightening of the solution color. The volatile materials were removed under vacuum, leaving a red residue. The residue was extracted with HMDSO and the resulting solution was concentrated. The solution was stored at -40 ˚C overnight, yielding red crystals of **3.21**. The crystalline material was isolated and residual solvent was removed under vacuum. Yield: 98 mg, 40% over three crops. **^{1}H NMR (400 MHz, C$_6$D$_6$, 293 K):** δ 7.19 (d, 2H, Ar), 7.13 (d, 2H, Ar), 7.12–7.04 (m, 10H, Ar), 7.00 (d, 2H, Ar), 6.92 (t, 2H, Ar), 5.56 (s, 2H, *H*C(C(Me)NAr)$_2$), 4.50 (sep, 2H, C*H*Me$_2$), 4.19 (sep, 2H, C*H*Me$_2$), 3.68 (sep, 2H, C*H*Me$_2$), 3.39 (sep, 2H, C*H*Me$_2$), 2.92 (sep, 2H, C*H*Me$_2$), 2.83 (sep, 2H, C*H*Me$_2$), 1.78 (s, 6H, HC(C(*Me*)NAr)$_2$), 1.75 (s, 6H, HC(C(*Me*)NAr)$_2$), 1.44 (d, 6H, CH*Me*$_2$), 1.25–1.15 (m, 15H, CH*Me*$_2$), 1.09 (d, 6H, CH*Me*$_2$), 1.06–1.00 (m, 24H, CH*Me*$_2$), 0.98 (d, 6H, CH*Me*$_2$). **^{13}C{^{1}H} NMR (600 MHz, C$_6$D$_6$, 293 K):** δ 168.6 (HC(*C*(Me)NAr)$_2$), 168.2 (HC(*C*(Me)NAr)$_2$), 166.5 (*C*O$_3$), 152.2 (Ar), 149.6 (Ar), 146.9 (Ar), 144.8 (Ar), 144.7 (Ar), 144.4 (Ar), 143.0 (Ar), 142.2 (Ar), 142.2 (Ar), 127.4 (Ar), 127.0 (Ar), 126.7 (Ar), 125.2 (Ar), 124.8 (Ar), 124.7 (Ar), 124.0 (Ar), 123.2 (Ar), 121.7 (Ar), 105.9 (*C*H(C(Me)NAr)$_2$), 28.8 (*C*HMe$_2$), 28.7 (*C*HMe$_2$), 28.5 (*C*HMe$_2$), 28.4 (*C*HMe$_2$), 28.3 (*C*HMe$_2$), 28.1 (*C*HMe$_2$), 27.3 (CH*Me*$_2$), 27.2 (CH*Me*$_2$), 26.6 (CH*Me*$_2$), 26.5 (CH(C(*Me*)NAr)$_2$), 26.5 (CH*Me*$_2$), 26.1 (CH*Me*$_2$), 26.0 (CH*Me*$_2$), 25.8 (CH*Me*$_2$), 25.7 (CH(C(*Me*)NAr)$_2$), 25.5 (CH*Me*$_2$), 25.0 (CH*Me*$_2$), 24.7 (CH*Me*$_2$), 24.4 (CH*Me*$_2$), 24.2 (CH*Me*$_2$). Anal. calcd (%) for $Nb_2O_6N_6C_{84}H_{116}\cdot 2C_6H_{18}OSi_2$: C, 63.48; H, 8.43; N, 4.63. Found: C, 63.45; H, 8.68; N, 4.63. MP: dec. 171–215 ˚C.

(BDI)Nb(NAr)(O)(Py) (3.22): Compound **3.20** (300 mg, 0.34 mmol) was added to a 50 mL Schlenk flask and dissolved in 10 mL toluene to give a red solution. Pyridine (0.55 mL, 6.9 mmol) was added to the solution of **3.20**. The solution was stirred at 60 ˚C for 2 h, resulting in a color change from red to orange. The volatile materials were removed under vacuum, leaving an orange residue. The residue was triturated with hexane, and then extracted with toluene. The resulting solution was concentrated and then stored at -40 ˚C overnight, yielding orange crystals of **3.22**. The crystalline material was isolated and residual solvent was removed under vacuum. Yield: 59 mg, 22% over two crops. **^{1}H NMR (600 MHz, C$_6$D$_6$, 293 K):** δ 8.33 (br s, 2H, Py), 7.32–6.82 (m, 9H, Ar), 6.56 (br s, 1H, Py), 6.17 (br s, 2H, Py), 5.19 (s, 1H, *H*C(C(Me)NAr)$_2$), 4.68 (br s, 1H, C*H*Me$_2$), 4.26 (br s, 1H, C*H*Me$_2$), 3.52 (br sep, 4H, C*H*Me$_2$), 1.70 (s, 6H, HC(C(*Me*)NAr)$_2$), 1.65–0.83 (m, 36H, CH*Me*$_2$). MP: dec. 143–152 ˚C. **^{13}C{^{1}H} NMR (600 MHz, C$_6$D$_5$Br, 293 K):** δ 167.7 (HC(*C*(Me)NAr)$_2$), 157.8 (Ar), 153.4 (Ar), 152.0 (Py), 149.5 (Ar), 144.3 (Ar), 141.9 (Ar), 137.9 (Ar), 136.9 (Py), 129.3 (Ar), 128.6 (Ar), 126.1 (Ar), 125.7 (Ar), 124.6 (Ar), 123.5 (Py), 122.7 (Ar), 99.6 (*C*H(C(Me)NAr)$_2$), 29.4 (*C*HMe$_2$), 28.1 (*C*HMe$_2$), 25.9 (CH(C(*Me*)NAr)$_2$), 25.3 (CH*Me*$_2$), 25.0 (CH*Me*$_2$), 24.8 (CH*Me*$_2$). Anal. calcd (%) for $Nb_1O_1N_4C_{46}H_{63}$: C, 70.75; H, 8.13; N, 7.17. Found: C, 70.18; H, 7.77; N, 6.72. MP: dec. 143–152 ˚C.

(κ^1-BDI)Nb(Py)(NAr)-(μ-O)$_2$-(NAr)Nb(BDI) (3.23): Compound **3.22** (10 mg, 0.013 mmol) was dissolved in C_6D_6 (0.4 mL) in a 4 mL vial and transferred to a J. Young NMR tube. The solution was heated at 60 ˚C for 24 h, resulting in a color change from orange to yellow. A ^{1}H NMR spectrum indicated clean conversion to **3.23**. The volatile materials were removed under vacuum, leaving a yellow residue. The residue was extracted with diethyl ether and the resulting solution was concentrated and then stored at -40 ˚C overnight, yielding yellow crystals of **3.23**. **^{1}H NMR (600 MHz, C_6D_6, 293 K):** δ 8.86 (br s, 2H, Py), 7.31–6.87 (m, 18H, Ar/Py), 6.84 (t, 1H, Ar), 6.60 (br d, 2H, Py), 5.50 (s, 1H, κ^2-BDI *H*C(C(Me)NAr)$_2$), 4.50 (s, 1H, κ^1-BDI *H*C(C(Me)NAr)$_2$), 4.35 (sep, 1H, C*H*Me$_2$), 4.00 (br sep, 2H, C*H*Me$_2$), 3.92 (br sep, 1H, C*H*Me$_2$), 3.76 (sep, 1H, C*H*Me$_2$), 3.27 (br sep, 1H, C*H*Me$_2$), 3.04 (br sep, 1H, C*H*Me$_2$), 3.03 (br sep, 1H, C*H*Me$_2$), 2.82 (br sep, 1H, C*H*Me$_2$), 2.78 (br sep, 1H, C*H*Me$_2$), 2.71 (br sep, 2H, C*H*Me$_2$), 2.66 (s, 3H, κ^1-BDI HC(C(*Me*)NAr)$_2$), 1.64 (s, 3H, κ^2-BDI HC(C(*Me*)NAr)$_2$), 1.61 (s, 3H, κ^2-BDI HC(C(*Me*)NAr)$_2$), 1.54 (br d, 3H, CH*Me$_2$*), 1.51 (br d, 3H, CH*Me$_2$*), 1.48 (br d, 3H, CH*Me$_2$*), 1.39 (br d, 3H, CH*Me$_2$*), 1.32 (br d, 3H, CH*Me$_2$*), 1.31–1.11 (br m, 30H, CH*Me$_2$*), 1.29 (s, 3H, κ^1-BDI HC(C(*Me*)NAr)$_2$), 1.06 (br d, 3H, CH*Me$_2$*), 1.05 (br d, 3H, CH*Me$_2$*), 0.93 (br d, 3H, CH*Me$_2$*), 0.89 (br d, 3H, CH*Me$_2$*), 0.87 (br d, 3H, CH*Me$_2$*), 0.67 (br d, 3H, CH*Me$_2$*), 0.64 (br d, 3H, CH*Me$_2$*), 0.59 (br d, 3H, CH*Me$_2$*), 0.20 (br d, 3H, CH*Me$_2$*). **^{13}C{^{1}H} NMR (600 MHz, C_6D_6, 293 K):** δ 169.5 (κ^2-BDI HC(*C*(Me)NAr)$_2$), 169.0 (κ^2-BDI HC(*C*(Me)NAr)$_2$), 165.3 (κ^1-BDI HC(*C*(Me)NAr)$_2$), 157.8 (κ^1-BDI HC(*C*(Me)NAr)$_2$), 154.3 (Ar), 154.1 (Ar), 151.0 (Py), 149.4 (Ar), 149.0 (Ar), 146.6 (Ar), 145.2 (Ar), 144.7 (Ar), 144.5 (Ar), 144.3 (Ar), 143.6 (Ar), 143.3 (Ar), 141.9 (Ar), 141.6 (Ar), 139.9 (Ar), 137.9 (Ar), 137.1 (Ar), 136.6 (Ar), 129.3 (Ar), 128.6 (Ar), 128.0 (Ar), 127.6 (Ar), 127.4 (Ar), 126.9 (Ar), 126.4 (Ar), 126.0 (Ar), 125.7 (Ar), 124.5 (Py), 124.1 (Ar), 123.7 (Ar), 123.6 (Ar), 123.5 (Py), 123.4 (Ar), 123.0 (Ar), 122.9 (Ar), 122.5 (Ar), 122.4 (Ar), 122.0 (Ar), 105.6 (κ^2-BDI *C*H(C(Me)NAr)$_2$), 104.0 (κ^1-BDI *C*H(C(Me)NAr)$_2$), 29.8 (*C*HMe$_2$), 29.6 (*C*HMe$_2$), 28.8 (*C*HMe$_2$), 28.7 (*C*HMe$_2$), 28.5 (*C*HMe$_2$), 28.4 (*C*HMe$_2$), 28.3 (*C*HMe$_2$), 28.3 (*C*HMe$_2$), 28.1 (*C*HMe$_2$), 28.0 (*C*HMe$_2$), 28.0 (*C*HMe$_2$), 27.7 (CH*Me$_2$*), 27.1 (κ^2-BDI CH(C(*Me*)NAr)$_2$), 27.0 (κ^2-BDI CH(C(*Me*)NAr)$_2$), 26.9 (CH*Me$_2$*), 26.5 (CH*Me$_2$*), 26.2 (CH*Me$_2$*), 25.9 (CH*Me$_2$*), 25.8 (CH*Me$_2$*), 25.7 (CH*Me$_2$*), 25.5 (CH(C(*Me*)NAr)$_2$), 25.3 (CH*Me$_2$*), 25.1 (CH*Me$_2$*), 24.9 (CH*Me$_2$*), 24.7 (CH*Me$_2$*), 24.3 (CH*Me$_2$*), 23.9 (CH*Me$_2$*), 23.8 (κ^1-BDI CH(C(*Me*)NAr)$_2$), 23.6 (CH*Me$_2$*), 23.5 (CH*Me$_2$*), 23.1 (κ^1-BDI CH(C(*Me*)NAr)$_2$), 22.3 (CH*Me$_2$*).

(BDI)Nb(NAr)(O)(DMAP) (3.24): Compound **3.20** (200 mg, 0.25 mmol) was dissolved in 3 mL benzene in a 20 mL vial to give a red solution. In a separate vial, 4-dimethylaminopyridine (DMAP) (33 mg, 0.27 mmol) was dissolved in 2 mL benzene. The DMAP solution was added to the solution of **3.20**. The solution was left at room temperature for 3 days, resulting in a slow color change from red to orange-yellow and precipitation of a yellow powder. The volatile materials were removed under vacuum, leaving an orange-yellow residue. The residue was washed with hexane (3 x 10 mL), and residual solvent was removed under vacuum to give **3.24** as a yellow powder. Yield: 126 mg, 61%. X-ray suitable crystals were obtained by recrystallization via slow cooling of a concentrated solution in benzene from 60 °C to room temperature. **^{1}H NMR (600 MHz, $CDCl_3$, 293 K):** δ 7.90 (d, 2H, DMAP), 7.17 (t, 1H, Ar), 7.13 (d, 1H, Ar), 7.08 (d, 1H, Ar), 7.07 (d, 1H, Ar), 6.96 (d, 1H, Ar), 6.92 (t, 1H, Ar), 6.89 (d, 1H, Ar), 6.74 (t, 1H, Ar), 6.63 (d, 1H, Ar), 5.92 (d, 2H, DMAP), 5.35 (s, 1H, *H*C(C(Me)NAr)$_2$), 4.22 (sep, 1H, C*H*Me$_2$), 3.98 (sep, 1H, C*H*Me$_2$), 3.54 (sep, 1H, C*H*Me$_2$), 3.34 (sep, 1H, C*H*Me$_2$), 3.14 (sep, 1H, C*H*Me$_2$), 2.99 (sep, 1H,

C*H*Me$_2$), 2.93 (s, 6H, DMAP C*H*$_3$), 1.92 (s, 3H, HC(C(*Me*)NAr)$_2$), 1.73 (s, 3H, HC(C(*Me*)NAr)$_2$), 1.48 (d, 3H, CH*Me*$_2$), 1.28 (d, 3H, CH*Me*$_2$), 1.25 (d, 3H, CH*Me*$_2$), 1.19 (d, 3H, CH*Me*$_2$), 1.18 (d, 3H, CH*Me*$_2$), 1.17 (d, 3H, CH*Me*$_2$), 1.03 (d, 3H, CH*Me*$_2$), 0.99 (d, 3H, CH*Me*$_2$), 0.98 (d, 3H, CH*Me*$_2$), 0.97 (d, 3H, CH*Me*$_2$), 0.88 (d, 3H, CH*Me*$_2$), 0.51 (d, 3H, CH*Me*$_2$). **^{13}C{^{1}H} NMR (600 MHz, C$_6$D$_5$Br, 293 K):** δ 167.2 (HC(*C*(Me)NAr)$_2$), 166.2 (HC(*C*(Me)NAr)$_2$), 153.4 (DMAP), 153.3 (Ar), 152.8 (Ar), 151.5 (DMAP), 147.1 (Ar), 144.7 (Ar), 143.8 (Ar), 142.5 (Ar), 141.4 (Ar), 140.9 (Ar), 137.1 (Ar), 125.7 (Ar), 125.4 (Ar), 125.2 (Ar), 124.6 (Ar), 123.8 (Ar), 123.0 (Ar), 122.8 (Ar), 121.4 (Ar), 121.3 (Ar), 104.8 (DMAP), 99.3 (*C*H(C(Me)NAr)$_2$), 38.3 (DMAP *C*H$_3$), 29.8 (*C*HMe$_2$), 28.6 (*C*HMe$_2$), 27.7 (*C*HMe$_2$), 27.6 (*C*HMe$_2$), 27.5 (*C*HMe$_2$), 26.9 (*C*HMe$_2$), 25.9 (CH(C(*Me*)NAr)$_2$), 25.6 (CH*Me*$_2$), 25.4 (CH(C(*Me*)NAr)$_2$), 25.4 (CH*Me*$_2$), 25.3 (CH*Me*$_2$), 25.2 (CH*Me*$_2$), 25.0 (CH*Me*$_2$), 24.9 (CH*Me*$_2$), 24.8 (CH*Me*$_2$), 24.2 (CH*Me*$_2$), 24.1 (CH*Me*$_2$), 23.5 (CH*Me*$_2$), 22.5 (CH*Me*$_2$), 15.6 (CH*Me*$_2$). Anal. calcd (%) for $Nb_1O_1N_5C_{48}H_{68}$: C, 69.97; H, 8.32; N, 8.50. Found: C, 70.35; H, 8.26; N, 8.26. MP: dec. 219–236 ˚C.

(BDI)NbH(O[SiH$_2$Ph])(NAr) (3.25a): Compound **3.22** (10 mg, 0.012 mmol) was suspended in C$_6$D$_6$ (0.4 mL) in a 4 mL vial. Phenylsilane (1.6 μL, 0.013 mmol) was added by microsyringe, resulting in immediate dissolution of the suspended solid and a slight lightening of the solution color. The resulting solution was transferred to a J. Young NMR tube. A ^{1}H NMR spectrum indicated clean conversion to **3.25a** and free DMAP. **^{1}H NMR (400 MHz, C$_6$D$_6$, 293 K):** δ 11.20 (br s, 1H, Nb-*H*), 7.34 (d, 2H, SiH$_2$*Ph*), 7.18–6.95 (m, 12H, Ar/SiH$_2$*Ph*), 5.19 (s, 1H, *H*C(C(Me)NAr)$_2$), 5.14 (d, 1H, Si*H*$_2$Ph, ^{2}J = 16 Hz), 4.99 (d, 1H, Si*H*$_2$Ph, ^{2}J = 16 Hz), 3.98 (sep, 2H, C*H*Me$_2$), 3.59 (sep, 1H, C*H*Me$_2$), 3.56 (sep, 1H, C*H*Me$_2$), 3.17 (br sep, 1H, C*H*Me$_2$), 3.14 (sep, 1H, C*H*Me$_2$), 1.63 (s, 3H, HC(C(*Me*)NAr)$_2$), 1.60 (s, 3H, HC(C(*Me*)NAr)$_2$), 1.33 (d, 3H, CH*Me*$_2$), 1.29–1.11 (m, 30H, CH*Me*$_2$), 1.07 (d, 3H, CH*Me*$_2$).

(BDI)NbH(O[SiHPh$_2$])(NAr) (3.25b): Compound **3.22** (10 mg, 0.012 mmol) was suspended in C$_6$D$_6$ (0.4 mL) in a 4 mL vial. Diphenylsilane (2.5 μL, 0.013 mmol) was added by microsyringe, resulting in immediate dissolution of the suspended solid and a slight lightening of the solution color. The resulting solution was transferred to a J. Young NMR tube. A ^{1}H NMR spectrum indicated clean conversion to **3.25b** and free DMAP. **^{1}H NMR (600 MHz, C$_6$D$_6$, 293 K):** δ 11.32 (br s, 1H, Nb-*H*), 7.45 (d, 2H, SiH*Ph*$_2$), 7.30 (d, 2H, SiH*Ph*$_2$), 7.21–6.95 (m, 15H, Ar/SiH*Ph*$_2$), 5.55 (s, 1H, Si*H*Ph$_2$), 5.20 (s, 1H, *H*C(C(Me)NAr)$_2$), 3.96 (br s, 2H, C*H*Me$_2$), 3.60 (br sep, 1H, C*H*Me$_2$), 3.57 (br sep, 1H, C*H*Me$_2$), 3.09 (br sep, 1H, C*H*Me$_2$), 3.08 (br sep, 1H, C*H*Me$_2$), 1.64 (s, 3H, HC(C(*Me*)NAr)$_2$), 1.58 (s, 3H, HC(C(*Me*)NAr)$_2$), 1.39–0.93 (m, 36H, CH*Me*$_2$).

(BDI)NbH(O[SiMe$_2$Ph])(NAr) (3.25c): Compound **3.22** (10 mg, 0.012 mmol) was suspended in C$_6$D$_6$ (0.4 mL) in a 4 mL vial. Dimethylphenylsilane (2.0 μL, 0.013 mmol) was added by microsyringe, resulting in dissolution of the suspended solid and a slight lightening of the solution color within 5 min. The resulting solution was transferred to a J. Young NMR tube. A ^{1}H NMR spectrum indicated clean conversion to **3.25c** and free DMAP. **^{1}H NMR (600 MHz, C$_6$D$_6$, 293 K):** δ 11.02 (br s, 1H, Nb-*H*), 7.33 (d, 2H, SiMe$_2$*Ph*), 7.21–6.97 (m, 12H, Ar/SiMe$_2$*Ph*), 5.21 (s, 1H, *H*C(C(Me)NAr)$_2$), 4.01 (br sep, 1H, C*H*Me$_2$), 3.92 (br sep, 1H, C*H*Me$_2$), 3.61 (sep, 1H, C*H*Me$_2$), 3.55 (sep, 1H, C*H*Me$_2$), 3.08 (br sep, 1H, C*H*Me$_2$), 3.07 (br sep, 1H, C*H*Me$_2$), 1.64 (s,

3H, HC(C(*Me*)NAr)$_2$), 1.60 (s, 3H, HC(C(*Me*)NAr)$_2$), 1.36–1.02 (m, 36H, CH*Me*$_2$), 0.15 (s, 3H, Si*Me*$_2$Ph), 0.12 (s, 3H, Si*Me*$_2$Ph).

(BDI)Nb(OCHN^{t}Bu)(O[SiMe$_2$Ph])(NAr) (3.26): Compound **3.20** (200 mg, 0.25 mmol) was dissolved in 4 mL benzene in a 20 mL vial to give a red solution. In a separate vial, dimethylphenylsilane (29 mg, 0.25 mmol) was dissolved in 2 mL benzene. The silane solution was added to the solution of **3.20**. The solution was left at room temperature for 40 h, resulting in a slow color change from red to yellow. The volatile materials were removed under vacuum, leaving a yellow residue. The residue was extracted with hexane and the resulting solution was concentrated and then stored at -40 ˚C overnight, yielding yellow crystals of **3.26**. The crystalline material was isolated and residual solvent was removed under vacuum. Yield: 94 mg, 41%. **^{1}H NMR (600 MHz, C$_6$D$_6$, 293 K):** δ 11.02 (br s, 1H, Nb-*H*), 7.88 (d, 2H, SiMe$_2$*Ph*), 7.29 (t, 2H, SiH*Ph*$_2$), 7.24 (tt, 1H, Ar), 7.13 (t, 1H, Ar), 7.09 (dd, 1H, Ar), 7.07–7.00 (m, 5H, Ar), 6.98 (dd, 1H, Ar), 6.93 (t, 1H, SiMe$_2$*Ph*), 6.33 (s, 1H, OC*H*N^{t}Bu), 5.33 (s, 1H, *H*C(C(Me)NAr)$_2$), 4.16 (sep, 1H, C*H*Me$_2$), 3.98 (sep, 1H, C*H*Me$_2$), 3.65 (sep, 1H, C*H*Me$_2$), 3.36 (sep, 1H, C*H*Me$_2$), 2.93 (sep, 1H, C*H*Me$_2$), 2.81 (sep, 1H, C*H*Me$_2$), 1.60 (s, 6H, HC(C(*Me*)NAr)$_2$), 1.33 (d, 3H, CH*Me*$_2$), 1.31 (d, 3H, CH*Me*$_2$), 1.27 (d, 3H, CH*Me*$_2$), 1.26 (d, 3H, CH*Me*$_2$), 1.23 (d, 3H, CH*Me*$_2$), 1.14 (d, 3H, CH*Me*$_2$), 1.15 (s, 9H, ^{t}Bu), 1.13 (d, 3H, CH*Me*$_2$), 1.08 (d, 3H, CH*Me*$_2$), 1.03 (d, 3H, CH*Me*$_2$), 0.99 (d, 3H, CH*Me*$_2$), 0.98 (d, 3H, CH*Me*$_2$), 0.87 (d, 3H, CH*Me*$_2$), 0.34 (s, 3H, Si*Me*$_2$Ph), 0.25 (s, 3H, Si*Me*$_2$Ph). **^{13}C{^{1}H} NMR (600 MHz, C$_6$D$_6$, 293 K):** δ 167.8 (HC(*C*(Me)NAr)$_2$), 167.7 (HC(*C*(Me)NAr)$_2$), 154.8 (O*C*HN^{t}Bu), 153.0 (Ar), 151.5 (Ar), 150.7 (Ar), 145.0 (Ar), 143.3 (Ar), 142.7 (Ar), 141.5 (Ar), 141.1 (Ar), 141.1 (Ar), 139.6 (Ar), 135.3 (SiMe$_2$*Ph*), 129.1 (Ar), 127.6 (SiMe$_2$*Ph*), 127.5 (Ar), 126.7 (Ar), 126.4 (Ar), 126.0 (Ar), 125.4 (Ar), 124.8 (Ar), 124.8 (SiMe$_2$*Ph*), 123.9 (Ar), 123.2 (Ar), 122.3 (Ar), 102.8 (H*C*(C(Me)NAr)$_2$), 52.8 (C$_\alpha$, ^{t}Bu), 31.0 (C$_\beta$, ^{t}Bu), 29.7 (*C*HMe$_2$), 29.4 (*C*HMe$_2$), 28.3 (*C*HMe$_2$), 28.1 (*C*HMe$_2$), 28.0 (*C*HMe$_2$), 27.8 (*C*HMe$_2$), 26.4 (HC(C(*Me*)NAr)$_2$), 26.2 (HC(C(*Me*)NAr)$_2$), 25.6 (CH*Me*$_2$), 25.5 (CH*Me*$_2$), 25.2 (CH*Me*$_2$), 25.1 (CH*Me*$_2$), 25.0 (CH*Me*$_2$), 25.0 (CH*Me*$_2$), 24.9 (CH*Me*$_2$), 24.8 (CH*Me*$_2$), 24.6 (CH*Me*$_2$), 24.2 (CH*Me*$_2$), 24.1 (CH*Me*$_2$), 23.7 (CH*Me*$_2$), 1.1 (Si*Me*$_2$Ph), 0.6 (Si*Me*$_2$Ph). Anal. calcd (%) for $Nb_1O_2N_4C_{54}H_{79}$: C, 69.20; H, 8.50; N, 5.98. Found: C, 69.28; H, 8.30; N, 5.90. MP: 205–210 ˚C.

(BDI$^\#$)Nb(NAr)(O$_2$CNH(^{t}Bu)) (3.27): Compound **3.20** (10 mg, 0.012 mmol) was dissolved in C$_6$D$_6$ (0.4 mL) in a J. Young NMR tube. The solution was heated at 60 ˚C for 5 h. A ^{1}H NMR spectrum indicated conversion to **3.27**. **^{1}H NMR (400 MHz, C$_6$D$_6$, 293 K):** δ 7.33 (dd, 1H, Ar), 7.27–7.03 (m, 5H, Ar), 6.91–6.80 (m, 3H, Ar), 5.46 (s, 1H, *H*C(C(Me)NAr)), 4.51 (s, 1H, N-*H*), 3.95 (sep, 1H, C*H*Me$_2$), 3.88 (sep, 1H, C*H*Me$_2$), 3.75 (sep, 1H, C*H*Me$_2$), 3.74 (sep, 1H, C*H*Me$_2$), 3.69 (s, 1H, C*H*$_2$), 3.53 (s, 1H, C*H*$_2$), 3.36 (sep, 1H, C*H*Me$_2$), 3.33 (sep, 1H, C*H*Me$_2$), 1.70 (s, 3H, HC(C(*Me*)NAr)), 1.64 (d, 3H, CH*Me*$_2$), 1.53 (d, 3H, CH*Me*$_2$), 1.47 (d, 3H, CH*Me*$_2$), 1.44 (d, 3H, CH*Me*$_2$), 1.35 (d, 3H, CH*Me*$_2$), 1.30 (d, 3H, CH*Me*$_2$), 1.16 (d, 3H, CH*Me*$_2$), 1.01 (d, 6H, CH*Me*$_2$), 0.98 (s, 9H, ^{t}Bu), 0.87 (d, 6H, CH*Me*$_2$), 0.77 (d, 3H, CH*Me*$_2$).

(BDI)Nb(NAr)(N(^{t}Bu)CO$_2$B(C$_6$F$_5$)$_3$) (3.28): Compound **3.20** (200 mg, 0.25 mmol) was dissolved in 5 mL benzene in a 20 mL vial to give a red solution. In a separate vial, tris(perfluorophenyl)borane (130 mg, 0.25 mmol) was dissolved in 5 mL benzene. The borane solution was added to the solution of **3.20**, resulting in an immediate color change from red to

purple. The solution was left at room temperature for 5 min, and then the volatile materials were removed under vacuum, leaving a purple powder. The residue was extracted with diethyl ether and the resulting solution was concentrated and then stored at -40 ˚C overnight, yielding purple crystals of **3.28**. Yield: 150 mg, 45%. **^{1}H NMR (600 MHz, C_6D_6, 293 K):** δ 7.33 (t, 1H, Ar), 7.11–7.06 (m, 2H, Ar), 6.97 (d, 1H, Ar), 6.91–6.81 (m, 5H, Ar), 5.59 (s, 1H, *H*C(C(Me)NAr)$_2$), 4.09 (sep, 1H, C*H*Me$_2$), 3.73 (sep, 1H, C*H*Me$_2$), 2.91 (sep, 1H, C*H*Me$_2$), 2.48 (br m, 2H, C*H*Me$_2$), 2.34 (sep, 1H, C*H*Me$_2$), 1.58 (d, 3H, CH*Me*$_2$), 1.50 (s, 3H, HC(C(*Me*)NAr)$_2$), 1.41 (s, 3H, HC(C(*Me*)NAr)$_2$), 1.35 (d, 3H, CH*Me*$_2$), 1.08 (d, 3H, CH*Me*$_2$), 1.06–1.02 (m, 12H, CH*Me*$_2$/^{t}Bu), 0.99 (d, 3H, CH*Me*$_2$), 0.95 (d, 3H, CH*Me*$_2$), 0.82 (d, 3H, CH*Me*$_2$) 0.80 (d, 3H, CH*Me*$_2$), 0.74 (d, 3H, CH*Me*$_2$), 0.70 (d, 3H, CH*Me*$_2$) 0.31 (d, 3H, CH*Me*$_2$). **^{13}C{^{1}H} NMR (600 MHz, C_6D_6, 293 K):** δ 172.3 (N*C*O$_2$), 168.2 (HC(*C*(Me)NAr)$_2$), 167.4 (HC(*C*(Me)NAr)$_2$), 156.0 (Ar), 151.6 (Ar), 149.4 (C_6F_5), 147.8 (C_6F_5), 145.6 (Ar), 144.4 (Ar), 144.0 (Ar), 142.2 (Ar), 142.1 (Ar), 140.9 (Ar), 138.1 (C_6F_5), 136.4 (C_6F_5), 131.4 (Ar), 129.0 (Ar), 128.5 (Ar), 127.9 (Ar), 125.9 (Ar), 124.4 (Ar), 123.9 (Ar), 123.5 (Ar), 122.7 (Ar), 107.4 (H*C*(C(Me)NAr)$_2$), 57.8 (C_α, ^{t}Bu), 32.5 (*C*HMe$_2$), 30.5 (C_β, Nb^{t}Bu), 29.4 (*C*HMe$_2$), 29.0 (HC(C(*Me*)NAr)$_2$), 28.8 (*C*HMe$_2$), 27.9 (*C*HMe$_2$), 27.9 (CH*Me*$_2$), 27.4 (*C*HMe$_2$), 27.0 (*C*HMe$_2$), 26.7 (CH*Me*$_2$), 26.3 (CH*Me*$_2$), 25.9 (CH*Me*$_2$), 25.5 (CH*Me*$_2$), 25.0 (CH*Me*$_2$), 24.9 (HC(C(*Me*)NAr)$_2$), 24.5 (CH*Me*$_2$), 24.3 (CH*Me*$_2$), 23.7 (CH*Me*$_2$), 23.7 (CH*Me*$_2$), 22.9 (CH*Me*$_2$), 22.3 (CH*Me*$_2$). Anal. calcd (%) for $Nb_1F_{15}O_2N_4C_{64}H_{67}$: C, 58.55; H, 5.14; N, 4.27. Found: C, 58.41; H, 5.18; N, 4.37. MP: 185–195 ˚C.

X-Ray Crystallographic Studies: Single crystals of **3.5, 3.6, 3.8a, 3.9, 3.11, 3.13, 3.14, 3.15, 3.16, 3.17, 3.18, 3.19, 3.20, 3.21, 3.23, 3.24, 3.26** and **3.28** were coated in Paratone-N oil, mounted on a Kaptan loop, transferred to a Bruker APEX CCD area detector,[106] centered in the beam, and cooled by a nitrogen flow low-temperature apparatus that had been previously calibrated by a thermocouple placed at the same position as the crystal. Preliminary orientation matrices and cell constants were determined by collection of 36 10 s frames, followed by spot integration and least-squares refinement. An arbitrary hemisphere of data was collected, and the raw data were integrated using SAINT.[107] Cell dimensions reported were calculated from all reflections with $I >$ 10 (Table 1). The data were corrected for Lorentz and polarization effects, but no correction for crystal decay was applied. An empirical absorption correction based on comparison of redundant and equivalent reflections was applied using SADABS.[108] Structures were solved by direct methods with the aid of successive difference Fourier maps and were refined against all data using the SHELXTL 5.0 software package.[109] Thermal parameters for all non-hydrogen atoms were refined anisotropically. The PLATON/SQUEEZE procedure[110] was used to remove extraneous electron density due to highly disordered toluene solvent in the structure of compound **3.19**. ORTEP diagrams were created using the ORTEP-3 software package[111] and Mercury.[112]

Table 3.1 Crystallographic data for compounds **3.5**, **3.6** and **3.8a**.

Compound	**3.5**	**3.6**	**3.8a**
Empirical formula	$C_{47}H_{64}N_7Nb$	$C_{45}H_{72}N_7Nb$	$C_{44}H_{70}N_5Nb$
Formula weight (amu)	819.96	804.00	761.96
Wavelength (Å)	0.71073	0.71073	0.71073
Space group	*P*bca	*P*bca	$P2_1/n$
a (Å)	13.720(1)	20.5536(5)	17.6899(8)
b (Å)	17.223(1)	18.1156(4)	12.1612(6)
c (Å)	37.278(2)	23.8915(6)	20.3860(9)
α (°)	90	90	90
β (°)	90	90	92.995(2)
γ (°)	90	90	90
V ($Å^3$)	8809.1(7)	8915.4(4)	4379.7(4)
Z	8	8	4
ρ_{calcd} (g/cm^3)	1.237	1.198	1.156
μ (mm^{-1})	0.313	0.308	0.308
F_{000} (e^-)	3488	3456	1640
Crystal size (mm^3)	.13 x .08 x .06	.12 x .08 x .06	.12 x .12 x .10
Theta min / max (˚)	1.092 / 25.394	1.705 / 25.372	1.486 / 25.376
Reflections collected	63316	38627	42990
R_{int}	0.0660	0.0697	0.0494
T_{max} / T_{min}	0.7452 / 0.6685	0.7452 / 0.6986	0.7452 / 0.6865
Data / restr. / param.	8104 / 0 / 509	8169 / 0 / 491	8036 / 0 / 467
GoF	1.043	1.023	1.047
R_1 / wR_2 (I>2σ(I))	0.0352 / 0.0780	0.0436 / 0.1040	0.0448 / 0.1136
R_1 / wR_2 (all data)	0.0510 / 0.0863	0.0712 / 0.1201	0.0547 / 0.1202
Res. peak / hole ($e^-/Å^3$)	0.464 / -0.395	0.664 / -0.404	1.919 / -0.762

Table 3.2 Crystallographic data for compounds **3.9**, **3.11** and **3.13**.

Compound	**3.9**	**3.11 · HMDSO**	**3.13**
Empirical formula	$C_{37}H_{61}N_4Nb$	$C_{49}H_{85}N_4NbOSi_3$	$C_{43}H_{72}BN_4NbO_2$
Formula weight (amu)	654.80	923.38	780.76
Wavelength (Å)	0.71073	0.71073	0.71073
Space group	$P2_1/c$	P-1	P-1
a (Å)	13.322(5)	10.6684(3)	9.897(2)
b (Å)	12.754(5)	12.8523(4)	11.357(2)
c (Å)	21.266(5)	21.1721(7)	21.303(4)
α (°)	90	101.451(2)	90.045(6)
β (°)	91.766(5)	103.695(1)	101.926(5)
γ (°)	90	103.100(1)	113.572(6)
V (Å^3)	3612(2)	2647.7(1)	2138.1(8)
Z	4	2	2
ρ_{calcd} (g/cm^3)	1.204	1.158	1.213
μ (mm^{-1})	0.362	0.331	0.320
F_{000} (e$^-$)	1408	996	840
Crystal size (mm^3)	.20 x .20 x .12	.13 x .07 x .05	.08 x .06 x .05
Theta min / max (˚)	1.529 / 25.496	1.688 / 25.483	0.981 / 25.379
Reflections collected	70529	46576	18471
R_{int}	0.0615	0.0709	0.0456
T_{max} / T_{min}	0.7452 / 0.6810	0.7452 / 0.6936	0.7452 / 0.6836
Data / restr. / param.	6652 / 0 / 436	9696 / 0 / 557	7562 / 6 / 485
GoF	1.090	1.026	1.066
R_1 / wR_2 (I>2σ(I))	0.0660 / 0.1485	0.0476 / 0.0880	0.0757 / 0.2051
R_1 / wR_2 (all data)	0.0694 / 0.1500	0.0771 / 0.0995	0.0843 / 0.2186
Res. peak / hole (e$^-$/Å^3)	1.210 / -1.496	1.117 / -0.912	1.888 / -0.707

Table 3.3 Crystallographic data for compounds **3.14**, **3.15**, **3.16**, and **3.17**.

Compound	**3.14**	**3.15**	**3.16**	**3.17**
Empirical formula	$C_{42}H_{71}N_4NbO_2Si$	$C_{44}H_{72}BN_4NbO_4$	$C_{43}H_{69}N_4Nb$	$C_{56}H_{75}N_4NbS$
Formula weight (amu)	785.02	824.77	734.93	929.17
Wavelength (Å)	0.71073	0.71073	0.71073	0.71073
Space group	$P2_1/n$	Pn	$Pbca$	P-1
a (Å)	10.650(1)	12.5350(5)	19.517(2)	13.4066(4)
b (Å)	24.638(2)	17.4460(8)	18.796(2)	13.5108(4)
c (Å)	16.578(1)	20.5667(8)	22.580(3)	14.4569(4)
α (°)	90	90	90	101.715(1)
β (°)	97.111(3)	96.552(2)	90	96.702(2)
γ (°)	90	90	90	90.848(2)
V ($Å^3$)	4316.8(5)	4468.3(3)	8283(2)	2544.5(1)
Z	4	4	8	2
ρ_{calcd} (g/cm^3)	1.208	1.226	1.179	1.213
μ (mm^{-1})	0.344	0.313	0.323	0.317
F_{000} (e^-)	1688	1768	3168	992
Crystal size (mm^3)	.08 x .05 x .05	.10 x .06 x .06	.12 x .08 x .08	.08 x .06 x .05
Theta min / max (˚)	1.488 / 25.428	1.167 / 25.392	1.754 / 25.407	1.449 / 25.426
Reflections collected	9146	8187	142121	57967
R_{int}	0.0361	0.0586	0.0671	0.0478
T_{max} / T_{min}	0.7452 / 0.7031	0.7452 / 0.7242	0.7452 / 0.7100	0.7452 / 0.7047
Data / restr. / param.	9146 / 0 / 477	8187 / 2 / 1013	7601 / 0 / 456	9328 / 0 / 575
GoF	1.119	1.021	1.065	1.043
R_1 / wR_2 ($I>2\sigma(I)$)	0.0336 / 0.0948	0.0386 / 0.0839	0.0427 / 0.0916	0.0330 / 0.0785
R_1 / wR_2 (all data)	0.0396 / 0.0995	0.0520 / 0.0916	0.0540 / 0.0968	0.0417 / 0.0836
Flack parameter	-	0.08(3)	-	-
Res. peak / hole ($e^-/Å^3$)	0.630 / -0.421	0.609 / -0.365	1.022 / -0.712	0.469 / -0.357

Table 3.4 Crystallographic data for compounds **3.18**, **3.19**, **3.20**, and **3.21**.

Compound	**3.18**	**3.19 · C_7H_8**	**3.20 · Et_2O**	**3.21 · 2 HMDSO**
Empirical formula	$C_{66}H_{100}N_6NbS_2$	$C_{85}H_{126}N_8Nb_2O_8$	$C_{50}H_{77}N_4NbO_3$	$C_{48}H_{76}N_3NbO_4Si_2$
Formula weight (amu)	1227.45	524.58	875.06	908.2
Wavelength (Å)	0.71073	0.71073	0.71073	0.71073
Space group	*C*2/c	*P*2_1/c	*C*c	*P*-1
a (Å)	22.292(5)	17.141(2)	18.1386(6)	13.329(1)
b (Å)	14.181(5)	25.100(3)	13.7454(5)	15.658(1)
c (Å)	22.910(5)	22.772(3)	19.8912(7)	24.934(2)
α (°)	90	90	90	76.581(4)
β (°)	117.461(5)	111.348(5)	106.288(1)	81.666(4)
γ (°)	90	90	90	83.559(4)
V (Å^3)	6426(3)	9125(2)	4760.3(3)	4991.7(8)
Z	4	4	4	4
ρ_{calcd} (g/cm^3)	1.269	1.146	1.221	1.208
μ (mm^{-1})	0.465	0.304	0.297	0.332
F_{000} (e^-)	2608	3352	1880	1944
Crystal size (mm^3)	.70 x .40 x .10	.06 x .06 x .04	.12 x .08 x .05	.14 x .12 x .10
Theta min / max (˚)	1.767 / 25.380	1.257 / 25.415	1.888 / 25.370	1.341 / 25.499
Reflections collected	70667	71870	27774	85486
R_{int}	0.0312	0.0843	0.0524	0.1465
T_{max} / T_{min}	0.7452 / 0.7023	0.7452 / 0.6712	0.7452 / 0.7071	0.7452 / 0.6683
Data / restr. / param.	5882 / 0 / 356	16734 / 0 / 961	7825 / 2 / 542	18439 / 0 / 1085
GoF	1.045	0.978	1.048	1.011
R_1 / wR_2 (I>2σ(I))	0.0228 / 0.0586	0.0491 / 0.0993	0.0325 / 0.0770	0.0602 / 0.1596
R_1 / wR_2 (all data)	0.0244 / 0.0598	0.0830 / 0.1087	0.0347 / 0.0784	0.0848 / 0.1706
Flack parameter	-	-	-0.04(2)	-
Res. peak / hole (e^-/Å^3)	0.600 / -0.315	0.503 / -0.525	0.623 / -0.372	1.731 / -1.010

Table 3.5 Crystallographic data for compounds **3.23**, **3.24**, **3.26**, and **3.28**.

Compound	**3.23 · 1½ Et_2O**	**3.24 · ½ C_7H_8**	**3.26**	**3.28 · Et_2O**
Empirical formula	$C_{92.5}H_{135}N_7Nb_2O_{3.5}$	$C_{51}H_{71}N_5NbO$	$C_{54}H_{79}N_4NbO_2Si$	$C_{68}H_{77}BF_{15}N_4NbO_3$
Formula weight (amu)	1586.89	863.03	937.21	908.2
Wavelength (Å)	0.71073	0.71073	0.71073	0.71073
Space group	$P2_1/n$	P-1	$P2_1/n$	$P2_1/c$
a (Å)	17.639(1)	11.665(1)	12.629(2)	22.223(2)
b (Å)	20.811(1)	12.637(1)	21.336(4)	24.338(2)
c (Å)	25.088(2)	17.247(1)	19.715(4)	24.561(2)
α (°)	90	81.664(2)	90	90
β (°)	100.667(1)	85.819(3)	92.431(4)	91.576(3)
γ (°)	90	68.744(2)	90	90
V ($Å^3$)	9050(1)	2343.6(2)	5307(2)	13279(2)
Z	4	2	4	8
ρ_{calcd} (g/cm^3)	1.165	1.223	1.173	1.388
μ (mm^{-1})	0.303	0.298	0.290	0.272
F_{000} (e^-)	3396	922	2008	5744
Crystal size (mm^3)	.18 x .12 x .10	.16 x .12 x .12	.12 x .10 x .08	.14 x .06 x .04
Theta min / max (˚)	1.280 / 25.359	1.194 / 25.469	1.407 / 25.389	1.507 / 25.427
Reflections collected	83162	31429	59328	63293
R_{int}	0.0546	0.0396	0.0530	0.1107
T_{max} / T_{min}	0.7452 / 0.6621	0.7452 / 0.7049	0.7452 / 0.6620	0.7452 / 0.5545
Data / restr. / param.	16411 / 3 / 968	8583 / 0 / 539	9689 / 0 / 578	24253 / 0 / 1695
GoF	1.059	1.065	1.042	0.969
R_1 / wR_2 ($I>2\sigma(I)$)	0.0473 / 0.1178	0.0288 / 0.0716	0.0451 / 0.1023	0.0689 / 0.1719
R_1 / wR_2 (all data)	0.0688 / 0.1305	0.0312 / 0.0732	0.0574 / 0.1083	0.1241 / 0.1956
Res. peak / hole ($e^-/Å^3$)	1.248 / -0.933	0.624 / -0.337	0.914 / -0.257	0.941 / -1.599

Notes and References

(1) Nugent, W. A.; Mayer, J. M. *Metal-ligand multiple bonds*; Wiley, 1988.
(2) Grubbs, R. H. *Tetrahedron* **2004**, *60* (34), 7117.
(3) Nugent, W. A.; Haymore, B. L. *Coord. Chem. Rev.* **1980**, *31*, 123.
(4) Kolb, H. C.; VanNieuwenhze, M. S.; Sharpless, K. B. *Chem. Rev.* **1994**, *94* (8), 2483.
(5) Cummins, C. C.; Baxter, S. M.; Wolczanski, P. T. *J. Am. Chem. Soc.* **1988**, *110*, 8731.
(6) Walsh, P. J.; Hollander, F. J.; Bergman, R. G. *J. Am. Chem. Soc.* **1988**, *110*, 8729.
(7) Duncan, A. P.; Bergman, R. G. *Chem. Rec.* **2002**, *2* (6), 431.

(8) Hazari, N.; Mountford, P. *Acc. Chem. Res.* **2005**, *38* (11), 839.
(9) Krska, S. W.; Zuckerman, R. L.; Bergman, R. G. *J. Am. Chem. Soc.* **1998**, *120* (45), 11828.
(10) Zuckerman, R. L.; Krska, S. W.; Bergman, R. G. *J. Am. Chem. Soc.* **2000**, *122* (5), 751.
(11) Meyer, K. E.; Walsh, P. J.; Bergman, R. G. *J. Am. Chem. Soc.* **1994**, *116* (6), 2669.
(12) Meyer, K. E.; Walsh, P. J.; Bergman, R. G. *J. Am. Chem. Soc.* **1995**, *117* (3), 974.
(13) Walsh, P. J.; Baranger, A. M.; Bergman, R. G. *J. Am. Chem. Soc.* **1992**, *114*, 1708.
(14) Li, Y.; Shi, Y.; Odom, A. L. *J. Am. Chem. Soc.* **2004**, *126* (6), 1794.
(15) Odom, A. L.; McDaniel, T. J. *Acc. Chem. Res.* **2015**.
(16) Baranger, A. M.; Walsh, P. J.; Bergman, R. G. *J. Am. Chem. Soc.* **1993**, *115* (7), 2753.
(17) Anderson, L. L.; Arnold, J.; Bergman, R. G. *Org. Lett.* **2004**, *6*, 2519.
(18) Pohlki, F.; Doye, S. *Chem. Soc. Rev.* **2003**, *32* (2), 104.
(19) Ruck, R. T.; Zuckerman, R. L.; Krska, S. W.; Bergman, R. G. *Angew. Chem. Int. Ed. Engl.* **2004**, *43* (40), 5372.
(20) Basuli, F.; Aneetha, H.; Huffman, J. C.; Mindiola, D. J. *J. Am. Chem. Soc.* **2005**, *127* (51), 17992.
(21) Davis-Gilbert, Z. W.; Yao, L. J.; Tonks, I. A. *J. Am. Chem. Soc.* **2016**, *138* (44), 14570.
(22) Nguyen, A. I.; Zarkesh, R. a.; Lacy, D. C.; Thorson, M. K.; Heyduk, A. F. *Chem. Sci.* **2011**, *2* (1), 166.
(23) Gilbert, Z. W.; Hue, R. J.; Tonks, I. A. *Nat. Chem.* **2016**, *8* (1), 63.
(24) Cavaliere, V. N.; Crestani, M. G.; Pinter, B.; Pink, M.; Chen, C.-H.; Baik, M.-H.; Mindiola, D. J. *J. Am. Chem. Soc.* **2011**, *133* (28), 10700.
(25) Crestani, M. G.; Hickey, A. K.; Gao, X.; Pintér, B.; Cavaliere, V. N.; Ito, J.-I.; Chen, C.-H.; Mindiola, D. J. *J. Am. Chem. Soc.* **2013**, *135*, 14754.
(26) La Pierre, H. S.; Arnold, J.; Toste, F. D. *Angew. Chemie Int. Ed.* **2011**, *50*, 3900.
(27) Gianetti, T. L.; La Pierre, H. S.; Arnold, J. *Eur. J. Inorg. Chem.* **2013**, *2013* (22–23), 3771.
(28) Sousa, S. C. A.; Cabrita, I.; Fernandes, A. C. *Chem. Soc. Rev.* **2012**, *41* (17), 5641.
(29) Du, G.; Abu-Omar, M. *Curr. Org. Chem.* **2008**, *12* (14), 1185.
(30) Kennedy-Smith, J. J.; Nolin, K. A.; Gunterman, H. P.; Toste, F. D. *J. Am. Chem. Soc.* **2003**, *125* (14), 4056.
(31) Nolin, K. A.; Krumper, J. R.; Pluth, M. D.; Bergman, R. G.; Toste, F. D. *J. Am. Chem. Soc.* **2007**, *129* (47), 14684.
(32) Fernandes, A. C.; Fernandes, J. A.; Almeida Paz, F. A.; Romão, C. C. *Dalt. Trans.* **2008**, *125* (47), 6686.
(33) Smeltz, J. L.; Boyle, P. D.; Ison, E. A. *Organometallics* **2012**, *31* (17), 5994.
(34) Huang, L.; Wei, H. *New J. Chem.* **2014**, *38* (11), 5421.
(35) Chong, C. C.; Kinjo, R. *ACS Catal.* **2015**, *5* (6), 3238.
(36) Chu, J.; Lu, E.; Chen, Y.; Leng, X. *Organometallics* **2013**, *32* (5), 1137.
(37) Chu, J.; Han, X.; Kefalidis, C. E.; Zhou, J.; Maron, L.; Leng, X.; Chen, Y. *J. Am. Chem. Soc.* **2014**.
(38) Polse, J. L.; Andersen, R. A.; Bergman, R. G. *J. Am. Chem. Soc.* **1998**, *120* (51), 13405.
(39) Hanna, T. E.; Keresztes, I.; Lobkovsky, E.; Bernskoetter, W. H.; Chirik, P. J. *Organometallics* **2004**, *23* (14), 3448.
(40) Blake, R. E.; Antonelli, D. M.; Henling, L. M.; Schaefer, W. P.; Hardcastle, K. I.; Bercaw, J. E. *Organometallics* **1998**, *17* (4), 718.
(41) Toomey, H. E.; Pun, D.; Veiros, L. F.; Chirik, P. J. *Organometallics* **2008**, *27*, 872.
(42) Ren, W.; Zhou, E.; Fang, B.; Zi, G.; Fang, D.-C.; Walter, M. D. *Chem. Sci.* **2014**, *5* (8),

3165.
(43) Zhou, E.; Ren, W.; Hou, G.; Zi, G.; Fang, D.-C.; Walter, M. D. *Organometallics* **2015**, 150702125911008.
(44) Carney, M. J.; Walsh, P. J.; Hollander, F. J.; Bergman, R. G. *J. Am. Chem. Soc.* **1989**, *111* (23), 8751.
(45) Carney, M. J.; Walsh, P. J.; Hollander, F. J.; Bergman, R. G. *Organometallics* **1992**, *11* (2), 761.
(46) Polse, J. L.; Andersen, R. A.; Bergman, R. G. *J. Am. Chem. Soc.* **1995**, *117* (19), 5393.
(47) Carney, M. J.; Walsh, P. J.; Bergman, R. G. *J. Am. Chem. Soc.* **1990**, *112* (17), 6426.
(48) Howard, W. A.; Trnka, T. M.; Waters, M.; Parkin, G. *J. Organomet. Chem.* **1997**, *528* (1), 95.
(49) Kortman, G. D.; Orr, M. J.; Hull, K. L. *Organometallics* **2015**, *34* (6), 1013.
(50) Nguyen, T. T.; Kortman, G. D.; Hull, K. L. *Organometallics* **2016**, *35* (11), 1713.
(51) Howard, W. A.; Waters, M.; Parkin, G. *J. Am. Chem. Soc.* **1993**, *115* (11), 4917.
(52) Sweeney, Z. K.; Polse, J. L.; Bergman, R. G.; Andersen, R. A. *Organometallics* **1999**, *18*, 5502.
(53) Hanna, T. E.; Lobkovsky, E.; Chirik, P. J. *Inorg. Chem.* **2007**, *46* (7), 2359.
(54) Blake, R. E.; Antonelli, D. M.; Henling, L. M.; Schaefer, W. P.; Hardcastle, K. I.; Bercaw, J. E. *Organometallics* **1998**, *17* (4), 718.
(55) Gountchev, T. I.; Tilley, T. D. *J. Am. Chem. Soc.* **1997**, *119*, 12831.
(56) Tomson, N. C.; Arnold, J.; Bergman, R. G. *Organometallics* **2010**, *29*, 2926.
(57) Obenhuber, A. H.; Gianetti, T. L.; Bergman, R. G.; Arnold, J. *Chem. Commun.* **2014**, *51*, 1278.
(58) De With, J.; Horton, A. D.; Orpen, A. G. *Organometallics* **1993**, *12* (5), 1493.
(59) Cundari, T. R. *Organometallics* **1994**, *13* (8), 2987.
(60) Kriegel, B. M.; Bergman, R. G.; Arnold, J. *J. Am. Chem. Soc.* **2016**, *138* (1), 52.
(61) Obenhuber, A. H.; Gianetti, T. L.; Berrebi, X.; Bergman, R. G.; Arnold, J. *J. Am. Chem. Soc.* **2014**, *136* (8), 2994.
(62) Hohloch, S.; Kriegel, B. M.; Bergman, R. G.; Arnold, J. *Dalt. Trans.* **2016**, *45* (40), 15725.
(63) Tomson, N. C.; Yan, A.; Arnold, J.; Bergman, R. G. *J. Am. Chem. Soc.* **2008**, *130*, 11262.
(64) Tomson, N. C.; Arnold, J.; Bergman, R. G. *Organometallics* **2010**, *29*, 5010.
(65) Tomson, N. C.; Arnold, J.; Bergman, R. G. *Dalton Trans.* **2011**, *40* (30), 7718.
(66) Gianetti, T. L.; Tomson, N. C.; Arnold, J.; Bergman, R. G. *J. Am. Chem. Soc.* **2011**, *133*, 14904.
(67) Gianetti, T. L.; Nocton, G.; Minasian, S. G.; Tomson, N. C.; Kilcoyne, A. L. D.; Kozimor, S. A.; Shuh, D. K.; Tyliszczak, T.; Bergman, R. G.; Arnold, J. *J. Am. Chem. Soc.* **2013**, *135* (8), 3224.
(68) Gianetti, T. L.; Bergman, R. G.; Arnold, J. *Chem. Sci.* **2014**, *5* (6), 2517.
(69) Gianetti, T. L.; Nocton, G.; Minasian, S. G.; Kaltsoyannis, N.; Kilcoyne, A. L. D.; Kozimor, S. A.; Shuh, D. K.; Tyliszczak, T.; Bergman, R. G.; Arnold, J. *Chem. Sci.* **2015**, *6* (2), 993.
(70) Heyduk, A. F.; Blackmore, K. J.; Ketterer, N. a; Ziller, J. W. *Inorg. Chem.* **2005**, *44* (3), 468.
(71) Addison, A. W.; Rao, T. N.; Reedijk, J.; van Rijn, J.; Verschoor, G. C. *J. Chem. Soc. Dalt. Trans.* **1984**, 1349.
(72) Burger, B. J.; Santarsiero, B. D.; Trimmer, M. S.; Bercaw, J. E. *J. Am. Chem. Soc.* **1988**, *110* (10), 3134.

(73) Figueroa, J. S.; Cummins, C. C. *J. Am. Chem. Soc.* **2003**, *125* (14), 4020.
(74) Dorogov, K. Y.; Churakov, A. V.; Kuzmina, L. G.; Howard, J. A. K.; Nikonov, G. I. *Eur. J. Inorg. Chem.* **2004**, *2004* (4), 771.
(75) Ziegler, J. A.; Bergman, R. G.; Arnold, J. *Dalt. Trans.* **2016**, *45* (32), 12661.
(76) Okuniewski, A.; Rosiak, D.; Chojnacki, J.; Becker, B. *Polyhedron* **2015**, *90*, 47.
(77) Blake, A. J.; McInnes, J. M.; Mountford, P.; Nikonov, G. I.; Swallow, D.; Watkin, D. J. *J. Chem. Soc. Dalt. Trans.* **1999**, *42* (3), 379.
(78) Guiducci, A. E.; Cowley, A. R.; Skinner, M. E. G.; Mountford, P. *J. Chem. Soc. Dalt. Trans.* **2001**, 1392.
(79) Guiducci, A. E.; Boyd, C. L.; Mountford, P. *Organometallics* **2006**, *25*, 1167.
(80) Guiducci, A. E.; Boyd, C. L.; Clot, E.; Mountford, P. *Dalton Trans.* **2009**, 5960.
(81) Tiong, P. J.; Nova, A.; Groom, L. R.; Schwarz, A. D.; Selby, J. D.; Schofield, a. D.; Clot, E.; Mountford, P. *Organometallics* **2011**, *30* (5), 1182.
(82) Boyd, C. L.; Clot, E.; Guiducci, A. E.; Mountford, P. *Organometallics* **2005**, *24* (10), 2347.
(83) Boyd, C. L.; Toupance, T.; Tyrrell, B. R.; Ward, B. D.; Wilson, C. R.; Cowley, A. R.; Mountford, P. *Organometallics* **2005**, *24*, 309.
(84) Hsu, S.-H.; Chang, J.-C.; Lai, C.-L.; Hu, C.-H.; Lee, H. M.; Lee, G.-H.; Peng, S.-M.; Huang, J.-H. *Inorg. Chem.* **2004**, *43*, 6786.
(85) Drew, M. G. B.; Rice, D. A.; Williams, D. M. *J. Chem. Soc. Dalt. Trans.* **1985**, No. 3, 417.
(86) Skripkin, Y. V.; Eremenko, I. .; Pasynskii, A. A.; Struchkov, Y. T.; Shklover, V. E. *J. Organomet. Chem.* **1984**, *267* (3), 285.
(87) Chu, J.; Lu, E.; Liu, Z.; Chen, Y.; Leng, X.; Song, H. *Angew. Chem. Int. Ed. Engl.* **2011**, *50* (33), 7677.
(88) Wigley, D. E. *Prog. Inorg. Chem.* **1994**, *42*, 239.
(89) Muñiz, K. *Chem. Soc. Rev.* **2004**, *33* (3), 166.
(90) Muñiz, K.; Iesato, A.; Nieger, M. *Chemistry* **2003**, *9* (22), 5581.
(91) Travia, N. E.; Xu, Z.; Keith, J. M.; Ison, E. A.; Fanwick, P. E.; Hall, M. B.; Abu-Omar, M. M. *Inorg. Chem.* **2011**, *50* (20), 10505.
(92) Vaughan, W. M.; Abboud, K. A.; Boncella, J. M. *J. Organomet. Chem.* **1995**, *485* (1), 37.
(93) Parkin, G. In *Progress in Inorganic Chemistry*; Karlin, K. D., Ed.; John Wiley & Sons, Inc.: Hoboken, NJ, USA, 1997; pp 1–165.
(94) Cahill, R.; Cookson, R. C.; Crabb, T. A. *Tetrahedron* **1969**, *25* (19), 4681.
(95) Kilgore, U. J.; Basuli, F.; Huffman, J. C.; Mindiola, D. J. *Inorg. Chem.* **2005**, *45*, 487.
(96) Fox, A. R.; Cummins, C. C. *J. Am. Chem. Soc.* **2009**, *131* (16), 5716.
(97) Camp, C.; Grant, L. N.; Bergman, R. G.; Arnold, J. *Chem. Commun.* **2016**, *52*, 5538.
(98) Fuller, A.-M.; Hughes, D. L.; Jones, G. A.; Lancaster, S. J. *Dalt. Trans.* **2012**, *41* (18), 5599.
(99) Bottaro, J. C.; Penwell, P. E.; Schmitt, R. J. *Synth. Commun.* **1997**, *27* (8), 1465.
(100) Barral, K.; Moorhouse, A. D.; Moses, J. E. *Org. Lett.* **2007**, *9* (9), 1809.
(101) Demko, Z. P.; Sharpless, K. B. *Angew. Chemie Int. Ed.* **2002**, *41* (12), 2110.
(102) Frauhiger, B. E.; White, P. S.; Templeton, J. L. *Organometallics* **2012**, *31* (1), 225.
(103) Feldman, J.; Mclain, S. J.; Parthasarathy, A.; Marshall, W. J.; Calabrese, J. C.; Arthur, S. D. *Organometallics* **1997**, *16*, 1514.
(104) Budzelaar, P. H. M.; van Oort, A. B.; Orpen, A. G. *Eur. J. Inorg. Chem.* **1998**, 1485.
(105) Sundermeyer, J.; Putterlik, J.; Foth, M.; Field, J.; Ramesar, N. *Chem. Ber.* **1994**, *127*, 1201.
(106) SMART: Area-Detector Software Package; Bruker Analytical X-ray Systems, Inc.: Madison, WI, 2001-2003.

(107) SAINT: SAX Area-Detector Integration Program; Bruker Analytical X-ray Systems Inc.: Madison, WI, 2003.
(108) SADABS: Bruker-Nonius Area Detector Scaling and Absorption; Bruker Analytical X-ray Systems, Inc.: Madison, WI, 2003.
(109) Sheldrick, G. M. *Acta Crystallogr. Sect. A* **2008**, *64*, 112.
(110) Spek, A. L. *Acta Crystallogr. Sect. D Biol. Crystallogr.* **2009**, *65* (2), 148.
(111) Farrugia, L. J. *Journal of Applied Crystallography*. International Union of Crystallography October 1, 1997, p 565.
(112) Macrae, C. F.; Bruno, I. J.; Chisholm, J. A.; Edgington, P. R.; McCabe, P.; Pidcock, E.; Rodriguez-Monge, L.; Taylor, R.; van de Streek, J.; Wood, P. A. *J. Appl. Crystallogr.* **2008**, *41* (2), 466.

Chapter 4

Insertion and Reductive Elimination Reactions of a Cyclometallated Tantalum Hydride Complex

Introduction

Low-valent complexes of tantalum and niobium undergo a variety of unusual stoichiometric reactions with both organic and inorganic substrates. For example, such species have been shown to promote C-C couplings,[1–5] activations of N_2 and other small molecules,[6–11] atom and group transfer reactions,[12,13] and cleavages of strong C-H, and C-N bonds.[14–16] Despite their rich stoichiometric chemistry, the use of early metal d^2 complexes in catalytic applications remains underdeveloped, largely due to the relative thermodynamic stability of high-valent early transition metal species.

A fundamentally different strategy to carry out catalytic reductive and oxidative bond-forming and bond-breaking reactions using early transition metals exploits redox non-innocent supporting ligands.[17–26] A variety of ligands typically incorporating oxygen, nitrogen, or sulfur donors within conjugated frameworks have been employed; however, ligands involving carbon donors are scarce in comparison. Transition metal alkylidenes incorporated into conjugated π systems are well primed to support redox behavior, yet only a handful of conjugated alkylidene-containing metallacycles have been reported in the literature, and those that have been reported have only been studied in the context of olefin metathesis catalysts.[27,28]

We recently reported that the niobium(V) complex (BDI)Nb(N^{t}Bu)Me_2 (BDI = N,N'-diaryl-β-diketiminate, aryl = 2,6-^{i}Pr$_2$-C_6H_3)[29,30] undergoes hydrogenolysis under 1 atm H_2, releasing two equivalents of CH_4 and generating new niobium compounds.[31–35] Depending on solvent used for this reaction, a remarkable variety of low-, mid-, and high-valent niobium species have been isolated, including η^6-arene inverted sandwich complexes,[32] a catalyst precursor for alkyne semihydrogenation,[33,36] and a complex that activates C-F bonds of fluorinated aromatics.[34] Our studies suggest that a three-coordinate Nb(III) complex is formed as an intermediate, which then undergoes divergent reactivity to give the isolated reaction products. While the three-coordinate intermediate has not been directly observed, following the hydrogenolysis of (BDI)Nb(N^{t}Bu)Me_2 by ^{1}H NMR has shown the appearance and subsequent disappearance of another intermediate, which we believe may play an important role in these reactions.[34] Although isolation of this reactive intermediate has eluded us, it has been characterized in solution as a cyclometallated niobium hydride complex. This species likely exists in equilibrium with a three-coordinate Nb(III) complex, as has been observed in a related niobium system.[9,37,38]

Here we describe the synthesis and reactivity of an analogous cyclometallated tantalum hydride complex, and assess its utility as an isolable synthon for trivalent tantalum species. Depending on the π-acid that the hydride complex reacts with, we observe either reductive elimination leading to low-valent tantalum complexes, or insertion chemistry to form a product bearing a unique redox-active alkylidene-containing metallacycle.

Results and discussion

Treatment of (BDI)Ta(N^{t}Bu)Me_2 (**4.1**)[39] with 1 – 4 atm of H_2 for 15 h at room temperature in either hexane or toluene solution resulted in a slow color change from pale yellow to yellow-orange. Cooling a concentrated solution in hexane afforded complex **2** in up to 80% yield as a pale yellow microcrystalline solid (Scheme 4.1). The ^{1}H NMR spectrum of **2** showed the presence of

two diastereoisomers (**4.2a** and **4.2b**), differing in orientation at the methine position of the cyclometallated isopropyl group (Figure 4.1). The two isomers are generated in a 4:1 ratio (80% **4.2a**), but are isolated in variable ratios depending on crystallization conditions (i.e. temperature and ratio of **4.2a** to **4.2b** present in solution). Heating a solution of **4.2** in C_6D_6 under 1 atm H_2 at 40 ˚C for 24 h results in formation of a 3.5:1 equilibrium mixture of **4.2a** and **4.2b** (78% **4.2a**), which does not change with further heating at 40 ˚C. The major isomer (**4.2a**) is obtained in up to 94% diastereomeric purity by successive crystallizations from hexane.

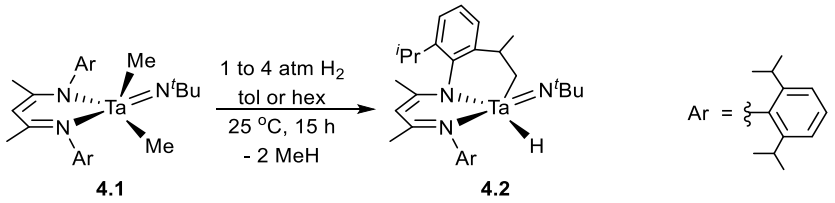

Scheme 4.1 Synthesis of cyclometallated Ta(V) hydride complex **4.2**.

According to ^{1}H NMR and ^{13}C NMR spectroscopies **4.2a** and **4.2b** are both *C*$_1$ symmetric. Notably, **4.2a** and **4.2b** show sharp singlets at 20.9 and 20.5 ppm, respectively, assigned to the Ta-*H*. Such highly downfield shifts for Ta(V) hydride species have precedent in the literature.[40–43] The ^{1}H NMR spectrum of **4.2a** also displays a characteristic doublet of doublet of quartets at 3.1 ppm, corresponding to the methine proton of the cyclometallated isopropyl group; this feature results from coupling to each of the diastereotopic protons of the Ta bound methylene, as well as the unactivated methyl group. Compound **4.2b** shows an analogous signal at 4.5 ppm. The diastereotopic methylene protons of **4.2a** appear as a doublet of doublets of doublets at 1.6 ppm (^{2}J = 16 Hz, ^{3}J = 3.6 Hz, ^{3}J(Ta-*H*) = 1.8 Hz) and a doublet of doublets at 0.9 ppm (^{2}J = 16 Hz, ^{3}J = 11 Hz), while the analogous protons of **4.2b** appear as a doublet of doublet of doublets at 2.4 ppm (^{2}J = 16 Hz, ^{3}J = 3.7 Hz, ^{3}J(Ta-*H*) = 1.2 Hz) and a doublet of doublets at 0.7 ppm (^{2}J = 16 Hz, ^{3}J = 4.9 Hz). The vicinal coupling constants of the methylene protons are consistent with the dihedral angles predicted for the structures shown for **4.2a** and **4.2b** in Figure 4.1.[44,45] Cyclometallation of the same BDI ligand to give similar NMR spectral features has been observed by Piers in a related scandium complex.[46–48] A single absorption at 1779 cm^{-1} in the FT-IR spectrum confirms the presence of a terminal tantalum hydride.[49,50]

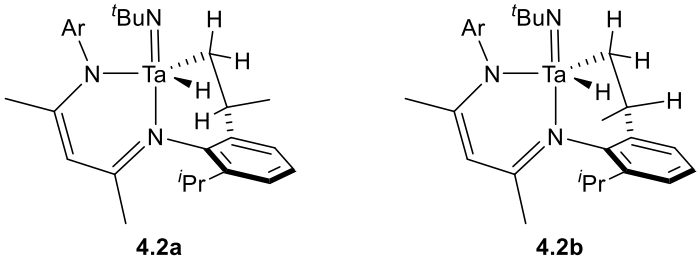

Figure 4.1 Structures of the major (**4.2a**) and minor (**4.2b**) diastereoisomers of **4.2**.

Compound **4.2a** was characterized in the solid-state by X-ray crystallography (Figure 4.2). The structure shows a distorted trigonal bipyramidal geometry (τ = 0.87)[51] with the imido group and one of the BDI nitrogens in the apical positions. The crystallographic data was of sufficient quality

to locate and refine the hydride isotropically; the Ta-H(1) distance is 1.93(4) Å, which is within the typical range for tantalum hydride species.[52]

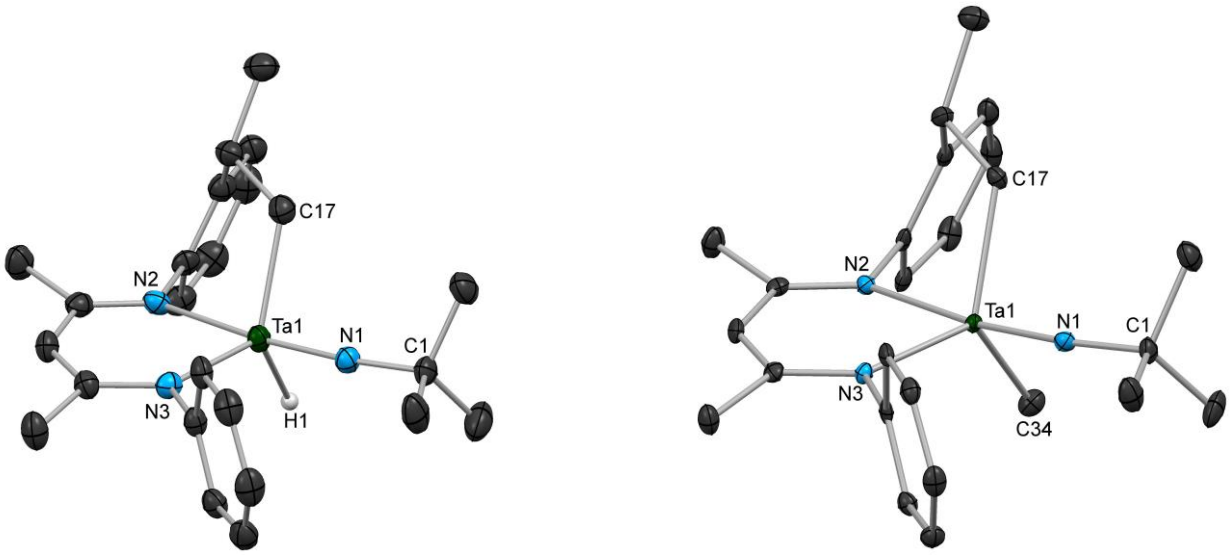

Figure 4.2 Molecular structures of **4.2a** (left) and **4.3** (right) determined by X-ray diffraction. Selected hydrogen atoms and ^{i}Pr groups are omitted for clarity; thermal ellipsoids are set at the 50% probability level. For **4.2a** (left), selected bond lengths (Å): Ta(1)-H(1) 1.93(4), Ta(1)-N(1) 1.787(3), Ta(1)-N(2) 2.234(4), Ta(1)-N(3) 2.092(4), Ta(1)-C(17) 2.186(5); selected bond angles (˚): N(3)-Ta(1)-H(1) 117(1), C(17)-Ta(1)-H(1) 117(1), N(3)-Ta(1)-C(17) 121.0(2), N(1)-Ta(1)-N(2) 173.4(1), C(1)-N(1)-Ta(1) 171.8(3). For **4.3** (right), Selected bond lengths (Å): Ta(1)-C(34) 2.172(2), Ta(1)-N(1) 1.785(2), Ta(1)-N(2) 2.300(2), Ta(1)-N(3) 2.102(2), Ta(1)-C(17) 2.184(2); selected bond angles (˚): N(3)-Ta(1)-C(34) 120.5(9), C(17)-Ta(1)-C(34) 115.7(1), N(3)-Ta(1)-C(17) 119.8(8), N(1)-Ta(1)-N(2) 173.1(1), C(1)-N(1)-Ta(1) 170.2(2).

Two mechanistic hypotheses can be proposed for the formation of **4.2** from **4.1** (Scheme 4.2). In either case, the methyl hydride intermediate **4.A** is first generated by σ-bond metathesis of **1** with H_2, with concomitant release of methane. In Path **I**, **4.A** then undergoes reductive elimination to release a second equivalent of methane and generate the three-coordinate Ta(III) intermediate **4.B**, which is finally trapped as **4.2** via intramolecular oxidative addition. This mechanism is analogous to that proposed for generation of Nb(III) species from hydrogenolysis of (BDI)Nb(N^{t}Bu)Me_2.[32] It is noteworthy that in the niobium case, the analog to the cyclometallated hydride species **4.2** is observed as an intermediate by ^{1}H NMR, but undergoes facile further reactions. In Path **II**, **4.A** undergoes a second σ-bond metathesis step rather than reductive elimination to release methane and form tantalum dihydride intermediate **4.C**. Compound **4.C** then undergoes another, intramolecular σ-bond metathesis to give **4.2**.

A deuterium labelling experiment was carried out in order to gain more insight into the reaction mechanism. Assuming Path **I**, reaction of **4.1** with D_2 would selectively give the Ta-*H* derivative of **4.2** accompanied by formation of CH_3D, while assuming Path **II**, the reaction would preferentially give the Ta-*D* derivative of **4.2** accompanied by formation of CH_3D and HD at early conversion; upon build-up of HD, however, some amount of CH_4 and Ta-*H* **4.2** would also be formed. Elucidation of the operant mechanism is significantly complicated by the observation (via

^{2}H NMR spectroscopy) that the deuterium label is exchanged into all of the isopropyl methyl groups – and to a lesser extent into all of the isopropyl methine groups – indicating that the cyclometallation (a) is reversible under H_2 atmosphere and (b) occurs at both the methyl and methine positions. Hence, a mixture of Ta-*H* **4.2** and Ta-*D* **4.2** is observed, along with production of CH_3D, HD and CH_4. At early conversion (~2 h reaction time) a strong preference for Ta-*D* **4.2** over Ta-*H* (11:1) is observed, which at first glance appears to give preference to Path **II**. However, this does not rule out Path **I**, as it is possible that **4.2** undergoes facile hydride exchange with D_2 via σ-bond metathesis at a significantly faster rate than **4.2** is produced. In fact, the fastest rates for σ-bond metathesis observed in the literature are for exchange of a hydride with H_2, rather than those involving alkyl groups or other heteroatoms.[53,54] Deuterium scrambling is also observed when isolated **4.2** is exposed to D_2.

The progress of the reaction of **4.1** with H_2 was monitored by ^{1}H NMR spectroscopy. A peak that grew in at 22.0 ppm subsequently disappeared upon complete conversion of starting material to product, suggesting the presence of a tantalum hydride intermediate (See Figure A# in Appendix #). This resonance, as well as a singlet at 5.2 integrating to 1 H (BDI backbone C-*H*) and another singlet at 0.7 ppm integrating to 3 H (Ta-C*H*$_3$) can be assigned to methyl hydride intermediate **4.A** (Scheme 4.2).

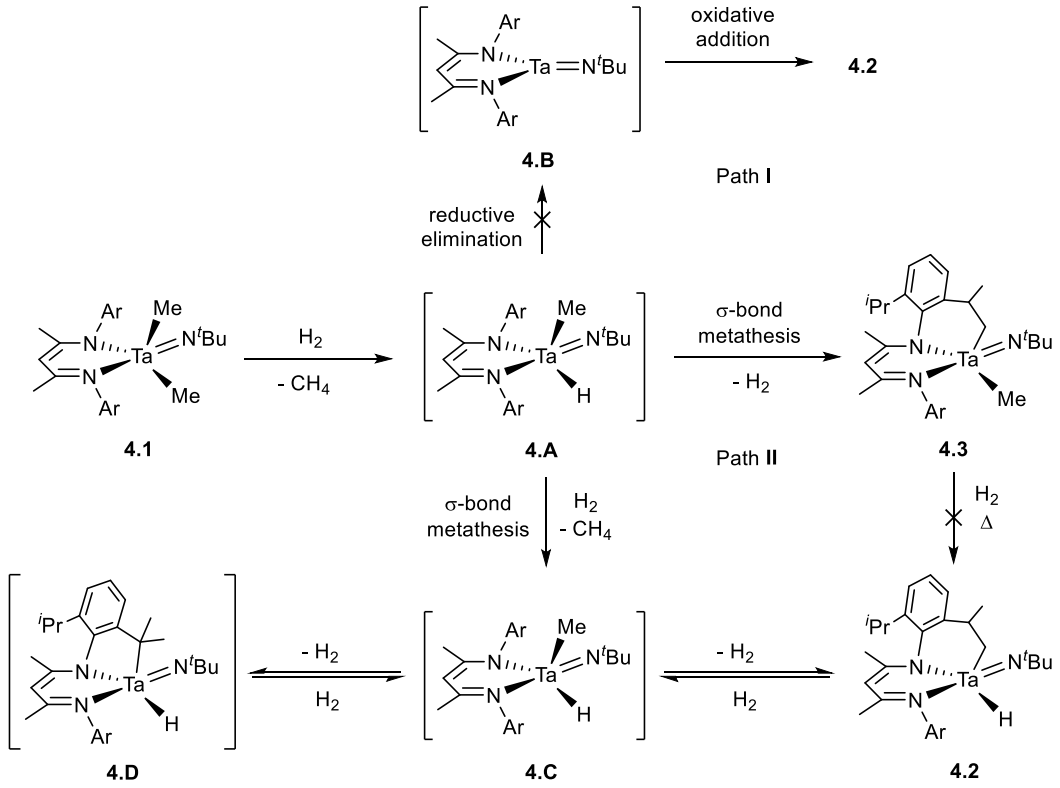

Scheme 4.2 Mechanistic hypothesis for conversion of conversion of **4.1** to **4.2**.

In addition to **4.2** and **4.A**, another species forms during the course of the hydrogenolysis reaction which has been identified as the cyclometallated methyl complex **4.3**. Unlike **4.A**, the quantity of **4.3** only increases throughout the reaction and remains constant once all of the starting

material is depleted, indicating that it is not an intermediate in the formation of **4.2**, but rather a side-product. Compound **4.3** could not be isolated from this reaction, but has been isolated in pure form by a different route (see below, Scheme 4.3). Notably, the **4.3**:**4.2** product ratio observed is highly dependent on the concentration of H_2 present in solution. When the reaction is carried out by introducing H_2 to an NMR tube at room temperature, the ratio of **4.3**:**4.2** is *ca.* eight-fold higher than that observed from a reaction in which H_2 is introduced to an NMR tube cooled to -196 ˚C. Surprisingly, exposure of pure **4.3** to H_2 does not convert **4.3** to **4.2**, even at temperatures up to 100 ˚C, at which point significant thermal decomposition is observed. Additionally, no exchange of D_2 into the BDI ligand is observed when **4.3** is exposed to 1 atm D_2.

The observations that the ratio of **4.3** to **4.2** is dependent on H_2 concentration and that **4.3** does not convert to **4.2** are consistent with Path **II** in Scheme 2. Hence, Path **II** depicts the most likely mechanistic pathway. After initial production of intermediate **4.A**, intramolecular σ-bond metathesis to form **4.3** is competitive with σ-bond metathesis with H_2 to form the transient intermediate **4.C** at lower H_2 concentration. Intermediate **4.C** exists in equilibrium with both **4.2** and **4.D**, explaining the incorporation of the deuterium label into the ligand. Conversion from **4.C** to **2** likely proceeds by intramolecular σ-bond metathesis, but may occur by reductive elimination of H_2 followed by oxidative addition of the C-H bond.

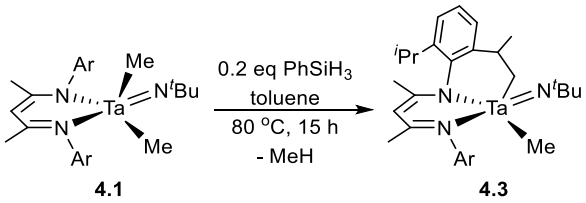

Scheme 4.3 Synthesis of compound **4.3** from **4.1**.

Compound **4.3** is observed as one of several products formed on heating a solution of **4.1** in C_6D_6, and can be generated cleanly by heating **4.1** in the presence of a catalytic quantity of phenylsilane (Scheme 4.3). As expected, the ^{1}H NMR spectrum is quite similar to that of compound **4.2**. Unlike **4.2**, however, **4.3** is observed and isolated as only a single diastereoisomer, with a geometry analogous to that of **4.2a**. Compound **4.3** has been crystallographically characterized; its structure is shown in Figure 4.2. Like **4.2**, **4.3** is a distorted trigonal bipyramid (τ = 0.88). Bond angles and lengths are nearly identical between **4.2** and **4.3**, implying similar electronic structures.

Heating **4.2** to reflux in toluene under N_2 atmosphere for 15 h results in an orange solution from which orange crystals of **4.4** can be isolated (Scheme 4.4). Compound **4.4** is observed as the major product in an NMR tube reaction, although several other unidentified minor products are also formed. In contrast to **4.2**, the BDI ligand in **4.4** has been C-H activated at *both* isopropyl methine positions rather than a single isopropyl methyl position, resulting in a symmetric molecule. Work to elucidate the mechanism of this unusual transformation is ongoing. We have previously reported that the niobium homolog of **4.4** is isolated via the room temperature reaction of $BDINbMe_2$ with 1 atm of H_2 in hexane.[34] Like the niobium derivative, **4.4** displays C_s symmetry in its ^{1}H NMR spectrum, exhibiting a septet integrating for two protons corresponding to the

isopropyl methines, as well as two singlets and two doublets, each integrating for six protons, corresponding to the isopropyl methyl units.

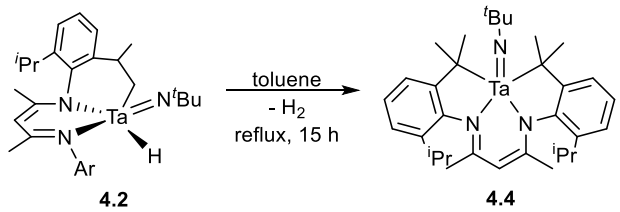

4.2 4.4

Scheme 4.4 Thermal conversion of **4.2** to **4.4**.

Adding DMAP to **4.2** in hexane results in the precipitation of a pale yellow powder, which has been identified as the six-coordinate DMAP adduct, compound **4.5** (Scheme 4.5). The ^{1}H NMR spectrum exhibits dynamic behavior, with broad signals for all of the DMAP aryl protons, three of the isopropyl methine protons, and one of the isopropyl methyl groups at room temperature. The Ta-*H* resonance appears as a broad singlet at 17.6 ppm, 3.3 ppm upfield from that of the Ta-*H* in **4.2a**. Upon warming to 60 ˚C, the aromatic DMAP signals and isopropyl methyl signals become sharp doublets, the methine signals sharpen into two overlapping septets and a doublet of doublet of quartets, and the hydride signal sharpens and shifts downfield to 19.1 ppm, indicating that the dynamic process occurs rapidly on the NMR timescale at 60 ˚C.

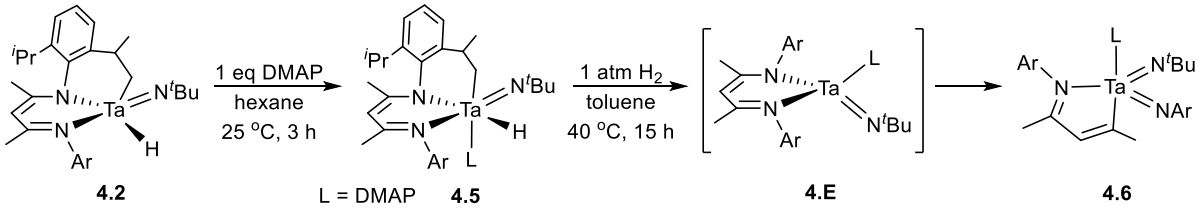

4.2 L = DMAP 4.5 4.E 4.6

Scheme 4.5 Reactivity of **4.2** with a sigma donating DMAP ligand.

Compound **4.5** shows a $\nu_{Ta\text{-}H}$ band in the IR spectrum at 1714 cm^{-1}, some 65 cm^{-1} lower in energy than that observed for **4.2**, indicating weakening of the Ta-H bond upon coordination of DMAP. The apparent decrease in Ta-H bond strength can be attributed to an increase in electron density at the Ta center associated with coordination of DMAP. The X-ray crystal structure of **4.5** is shown in Figure 4.3. The hydride was located in the Fourier difference map and refined isotropically. The Ta-H bond length is 1.74(4) Å, almost 0.2 Å shorter than that seen in **4.2**, but still within the range typically observed for Ta-H bonds. The geometry is significantly distorted from octahedral presumably due to a combination of geometric constraints imposed by the cyclometallated ligand and the considerable steric hindrance near the metal center. In particular, the DMAP ligand bends toward the hydride ligand to avoid steric repulsion between the DMAP ligand and the aryl groups, so that the angle N(4)-Ta-H(1) is only 69.3(1)˚. In comparison with **4.2**, the tantalum alkyl and hydride units are brought much closer in proximity (C(17)-Ta-H(1) = 87.7(1)˚), so less geometric reorganization is required to access a reductive elimination transition state. Hence, **4.5** seemed to be an attractive candidate for generating Ta(III) species via C-H reductive elimination.

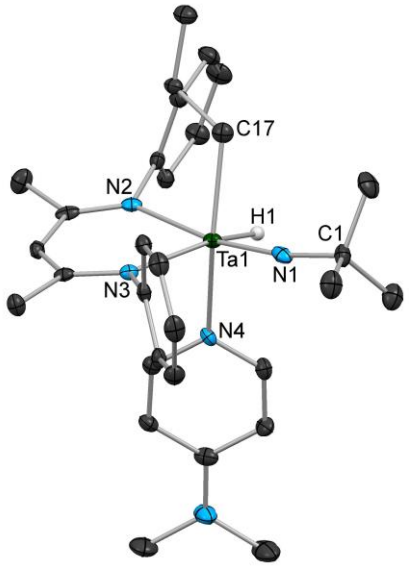

Figure 4.3 Molecular structure of **4.5** determined X-ray diffraction. Selected hydrogen atoms, ^{i}Pr groups, and two co-crystallized benzene molecules are omitted for clarity; thermal ellipsoids are set at the 50% probability level. Selected bond lengths (Å): Ta(1)-H(1) 1.74(4), Ta(1)-N(1) 1.788(3), Ta(1)-N(2) 2.301(3), Ta(1)-N(3) 2.167(3), Ta(1)-N(4) 2.299(3), Ta(1)-C(17) 2.216(4). Selected bond angles (˚): N(3)-Ta(1)-N(4) 89.9(1), N(4)-Ta(1)-H(1) 69.3(1), H(1)-Ta(1)-C(17) 87.7(1), N(3)-Ta(1)-C(17) 108.3(1), N(1)-Ta(1)-H(1) 95.5(1), N(1)-Ta(1)-N(3) 104.8(1), N(2)-Ta(1)-N(3) 82.5(1), N(2)-Ta(1)-H(1) 79.7(1), C(1)-N(1)-Ta(1) 169.7(3).

Gentle heating of a solution of **4.5** at 40 ˚C under 1 atm H_2 for 15 h results in a color change to red-orange. Concentration and cooling in hexane yields compound **4.6** as an orange crystalline solid (Scheme 4.5). The ^{1}H NMR spectrum of **4.6** no longer shows a singlet between 5 and 6 ppm corresponding to the BDI backbone methine proton but instead contains a new singlet at 7.0 ppm, corresponding to the monoazabutadiene (MAD) backbone methine proton.[35] Additionally, the NMR spectrum shows only three distinct isopropyl methine resonances, with one integrating for two protons and the others each integrating for one, consistent with a system in which one aryl group is capable of free rotation on the NMR timescale and the other is not. The observations that all four isopropyl methine protons are represented as septets, and that there is no longer a singlet at high field corresponding to a tantalum hydride are also consistent with a system in which the C-H metallation has been reversed. Our groups and others have observed analogous degradation of the BDI ligand, which proceeds through reductive C-N cleavage in d^2 early transition metal complexes.[35,55] Hence, compound **4.E** is likely an intermediate species in the formation of **4.6**.

Conversion of **4.5** to **4.6** appears to be catalyzed by H_2. Although heating a solution of **4.5** at 80 ˚C under N_2 for 15 h results in conversion to a complex mixture containing **4.6** as the major product, the same reaction under H_2 goes cleanly to **4.6** at 40 ˚C overnight, or within 60 h at room temperature. This may be explained by the formation of a tantalum dihydride intermediate from σ-bond metathesis of **4.5** with H_2, which then reductively eliminates H_2 to generate intermediate **4.E**. Finally, **4.E** undergoes fast, irreversible reductive C-N cleavage to give **4.6**.

Stirring **4.5** under 1 atm of D_2 converts it to the monodeuteride derivative **4.5-d** with negligible incorporation of deuterium into the BDI ligand, as evidenced by the disappearance of the Ta-H signal in the ^{1}H NMR spectrum. Isolated **4.5-d** under a N_2 atmosphere also only exchanges a minimal amount (~3%) of deuterium into the ligand isopropyl methyls within 24 h at room temperature. These results show that under either H_2 or N_2 atmosphere, the system does not readily establish an equilibrium between **4.E** and **4.5** via reductive elimination and oxidative addition, and that under H_2, **4.5** also does not readily establish an equilibrium with a dihydride complex via σ-bond metathesis. This implies that conversion to **4.6** is much faster than regeneration of **4.5**.

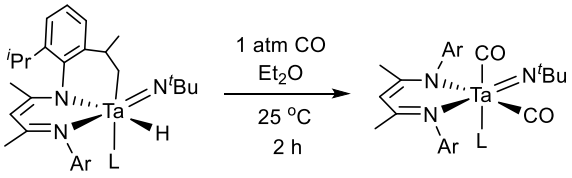

4.5 **4.7**

Scheme 4.6 Reductive elimination to generate a six-coordinate Ta(III) dicarbonyl complex.

Introduction of CO to an Et_2O solution of **4.5** resulted in an immediate color change to red-brown. The product, compound **4.7**, was obtained as red crystals from a toluene/hexane mixture (Scheme 4.6). The ^{1}H NMR spectrum of **4.7** shows C_1 symmetry, with four distinct septets corresponding to the isopropyl methine protons, again indicating that reductive elimination of the C-H activated methyl group has occurred. We have reported the pyridine adduct of a Nb(III) dicarbonyl analog, which shows similar spectral features at low temperature.[31] However, the niobium analog displays C_{2v} symmetry at higher temperature, likely due to facile decoordination and exchange of pyridine. In the case of compound **4.7**, decoordination of the more strongly bound DMAP is much slower than the NMR timescale at room temperature. The ν_{CO} of **4.7** in the IR spectrum are at 1949 and 1845 cm^{-1}, also similar to those reported for the niobium analog. Adding CO to **4.5** in the presence of a large excess of DMAP does not slow the progress of the reaction, indicating that it does not proceed by dissociative displacement of DMAP by CO. Hence, in order to form **4.7**, a molecule of CO coordinates to make a 7-coordinate complex, so that the reductive elimination is promoted by backbonding to CO that begins to develop at the transition state. After reductive elimination, a second equivalent of CO binds to the trivalent tantalum center to give **4.7**.

The strong coordination of the DMAP ligand in **4.7** limits its reactivity toward substrates such as alkynes. Hence, we hoped to access more reactive Ta(III) species by preparing a 5-coordinate, base-free derivative of **4.7**. Addition of CO to a hexane solution of **4.2** at room temperature resulted in conversion to an intractable mixture of products. However, addition of CO to a solution of **4.2** in hexane cooled to -77 ˚C, followed by slow warming to room temperature, resulted in relatively clean conversion to the five-coordinate dicarbonyl complex **4.8**, which was isolated as green crystals in 55% yield (Scheme 4.7). It is possible that insertion of CO into the Ta-H bond competes with reductive elimination at higher temperature, leading to a mixture of products when CO was added at room temperature. In fact, **4.2** undergoes clean insertion reactivity with some other unsaturated substrates (see below). Upon addition of DMAP, compound **4.8** is converted cleanly to compound **4.7**. Like the Nb derivative, compound **4.8** has C_{2v} symmetry in solution, exhibiting

only a single septet integrating to four isopropyl methine protons in the ^{1}H NMR spectrum.[31] The ^{1}H NMR spectrum contains sharp resonances under N_2 at room temperature, but contains broad resonances under CO, likely due to facile CO exchange. Compound **4.8** shows ν_{CO} absorptions at 1975 and 1869 cm^{-1}; both are higher energy than the corresponding absorptions in compound **4.7**, indicating less back-donation is present in **4.8** than in **4.7** due to decreased electron density at the tantalum center in **4.8** relative to **4.7**. The absorptions are also lower in energy than for the niobium analog (1988 and 1893 cm^{-1}), indicating more back-bonding in the tantalum system, consistent with the more reducing nature of tantalum (III) relative to niobium (III). Reductive elimination to form **4.8** may be induced by initial coordination of a molecule of CO to **4.2**. The resulting intermediate then has a vacant coordination site to bind a second equivalent of CO, further stabilizing the d^2 metal center.

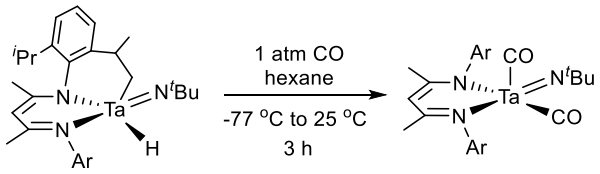

4.2 **4.8**

Scheme 4.7 Reductive elimination at low temperature to generate a 5-coordinat Ta(III) dicarbonyl complex.

Addition of one equivalent of 2,6-dimethylphenylisocyanide to a solution of cyclometallated tantalum hydride complex **4.2** at low temperature followed by allowing the resulting solution to warm to room temperature resulted in a slight darkening of the solution color from pale yellow to yellow. The product was isolated as a yellow microcrystalline solid and identified as the η^2-iminoformyl complex **4.9** (Scheme 4.8). Unlike carbon monoxide, which promoted reductive elimination to give the Ta(III) dicarbonyl complex **4.8**, the isocyanide instead inserts into the Ta-H bond to give **4.9**. Insertions of carbon monoxide or isocyanides into early metal hydrides are very well precedented,[56,57] but the stark contrast in outcomes for reactions with carbon monoxide and isocyanide in this case was surprising.

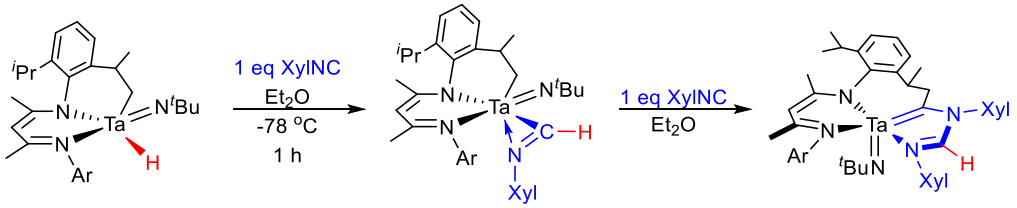

4.2 **4.9** **4.10**

Scheme 4.8 Insertion of 2,6-dimethylphenylisocyanide to give compounds **4.9** and **4.10**.

Like compound **4.2**, **4.9** was isolated as a mixture of two diastereoisomers: **4.9a** (major) and **4.9b** (minor), which could not be fully separated by recrystallization due to their nearly identical solubility profiles. The two isomers gave distinct ^{1}H NMR spectra consistent with completely dissymmetric molecules. The iminoformyl methine signals for **4.9a** and **4.9b** were observed as singlets at 10.37 and 10.39 ppm, respectively. A doublet of doublets with ^{2}J = 15 Hz and ^{3}J = 12

Hz corresponding to a diastereotopic proton in the Ta-bound methylene group of **4.9a** appeared at 2.66 ppm; the other diastereotopic methylene proton signal for **4.9a** (1.86 ppm) as well as both of the signals for **4.9b** (3.05 and 1.85 ppm) were also observed, but overlapped with other signals, preventing determination of the geminal and vicinal coupling constants.

Compound **4.9** was structurally characterized using X-ray diffraction; a representation of the molecular structure is shown in Figure 4.4**.** The single crystal of **4.9** that was subjected to X-ray crystallographic analysis co-crystallized as a nearly equal mixture of **4.9a** and **4.9b**; the co-crystallization of the two diastereomers manifested itself in the structural solution by disorder about the cyclometallated isopropyl group. This disorder was fully modeled, and considering the centroid of the C=N bond as occupying one coordination site when determining bond angles about the tantalum center, the geometry of **4.9** can be described as distorted trigonal bipyramidal (τ = 0.84) with the imido group and one BDI nitrogen in the apical positions, similar to **4.2**. The Ta-C(17) bond distance is 2.216(6) Å, identical to the distance observed for compound **4.2**. The Ta-C(34) and Ta-N(4) distances of 2.149(6) Å and 2.187(5) Å are consistent with the distances reported for related η^2-iminoformyl complexes.[56]

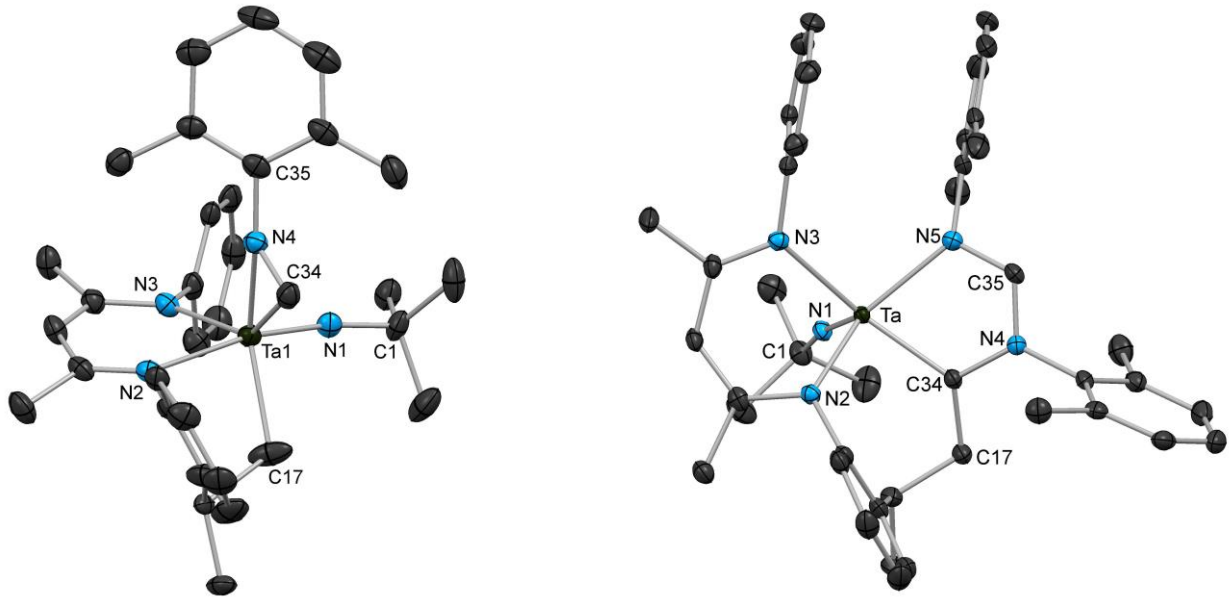

Figure 4.4 Molecular structures of **4.9a** (left) and **4.10** (right) as determined by X-ray diffraction. Hydrogen atoms and ^{i}Pr groups are omitted for clarity; thermal ellipsoids are set at the 50 % probability level. For **4.9a** (left), selected bond lengths (Å): Ta-N(1) 1.783(5), Ta-N(2) 2.333(4), Ta-N(3) 2.139(4), Ta-N(4) 2.187(5), Ta-C(34) 2.149(6), Ta-C(17) 2.216(6), N4-C34 1.266(7); selected bond angles (˚): Ta-N(1)-C(1) 171.7(4), Ta-N(4)-C(35) 156.1(4), N(1)-Ta-N(2) 170.2(2), N(1)-Ta-N(3) 100.8(2), N(3)-Ta-C(34) 135.9(2), N(3)-Ta-C(17) 116.1(3), C(34)-Ta-C(17) 101.8(2), N(4)-Ta-C(34) 34.0(2). For **4.10** (right), selected bond lengths (Å): Ta-N(1) 1.787(2), Ta-N(2) 2.124(2), Ta-N(3) 2.308(2), Ta-N(5) 2.192(2), Ta-C(34) 2.082(3), C(34)-N(4) 1.410(3), N(4)-C(35) 1.339(3), C(35)-N(5) 1.338(4), C(34)-C(17) 1.507(4); selected bond angles (˚): Ta-N(1)-C(1) 169.6(2), N(1)-Ta-N(5) 119.94(9), N(2)-Ta-N(5) 137.83(8), N(3)-Ta-C(34) 155.41(9).

Upon addition of a second equivalent of 2,6-dimethylphenylisocyanide, the color of a solution of **4.9** immediately changed to dark green-blue. Likewise, adding two equivalents of 2,6-dimethylisocyanide to a solution of **4.2** at room temperature resulted in a color change from pale yellow to the same dark green-blue color. In both cases, ^{1}H NMR spectroscopy indicated clean conversion to a single new product, which was isolated as dark green blocks and identified as the Ta(V) amidinylidene, **4.10** (Scheme 4.8). Formation of **4.10** from **4.9** results from insertion of isocyanide into the tantalum-carbon bond, followed by coupling of the two equivalents of isocyanide. While insertion reactions of unsaturated substrates such as CO and isocyanides into metal alkyls or metal hydrides often lead to C-C bond formation between two inserted substrates leading to metal enediolates or enediamides, coupling to form a C-N bond is quite unusual, and formation of a metallaimidazole structural motif by coupling of isocyanides has not been previously reported. The constrained geometry imposed by the cyclometallated nature of the supporting BDI ligand likely prohibits C-C bond formation, so that the iminoformyl and iminoacyl groups resulting from insertion of isocyanide into the Ta-H and Ta-C bond, respectively, couple via the usually less favorable C-N bond formation. Several examples of related M(CNCN) metallacycles incorporating Fischer-type carbenes in late transition metal and low-valent mid transition metal systems have been reported, but **4.10** is the first example of an alkylidene with this structural motif.

In contrast to compound **4.9** which was generated and isolated as a mixture of diastereoisomers, the ^{1}H NMR spectrum of **4.10** indicated the presence of only a single compound. Resonances corresponding to the BDI backbone methine and tantalaimidazolyl methine both appeared as singlets in the ^{1}H NMR spectrum at 5.31 and 5.52 ppm, respectively. The ^{1}H NMR spectrum also displays two well resolved doublets of doublets at 5.18 ppm (^{2}J = 15 Hz, ^{3}J = 12 Hz) and 2.38 ppm (^{2}J = 15 Hz, ^{3}J = 3.6 Hz) corresponding to the methylene protons and a doublet of quartet of doublets at 4.16 ppm corresponding to the adjacent methine group. The substantial difference in chemical shift for the two methylene protons is likely a consequence of their differing proximities to flanking 2,6-dimethylphenyl groups in the compound rather than any significant difference in electron density.

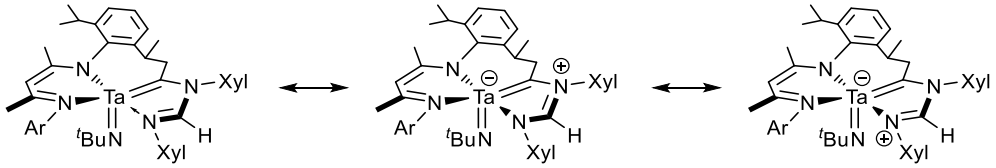

Scheme 4.9 Resonance contributors to the overall structure of **4.10**.

The solid-state structure of compound **4.10** (Figure 4.4, right) shows a distorted square-based pyramidal geometry about the tantalum center (τ = 0.29) with the imido group in the apical position. Notably, the tantalaimidazole ring is nearly planar; the tantalum center is only slightly displaced from the N-C-N-C plane, with dihedral angles of N(4)-C(35)-N(5)-Ta = 11.5˚ and C(35)-N(4)-C(34)-Ta = 14.4˚. The N(4)-C(35) and N(5)-C(35) distances of 1.339(3) and 1.338(4) Å, respectively, are effectively identical and are intermediate between single and double bonds. Moreover, the Ta-N(5) distance is 2.192(2) Å, intermediate between typical distances for Ta-N dative bonds and covalent single bonds. Taken together, this indicates a significant contribution

from a charge separated resonance structure, as shown is Scheme 4.9. A strong trans influence exerted by C(34) in comparison to N(5) can be observed from the large difference between the short N(2)-Ta distance of 2.124(2) Å and long N(3)-Ta distance of 2.308(2) Å.

Transition metal complexes supported by 4-membered π-conjugated organic fragments, such as enediolates, enediamides, and quinones, are well known to support up to two reversible ligand-based redox events, which has been utilized extensively in catalysis and molecular electronics.[17,18,58] While a small number of alkylidene-containing metallacycles based on rhenium[27] and molybdenum[28] have been reported, their redox chemistry has not been explored.[59] Hence, we set out to investigate the electrochemistry of **4.10**. As shown in Figure 4.5, a cyclic voltammetry study showed two oxidation waves with E_{pa} of -1.04 and -0.16 V, respectively, relative to the $Fc^{0/+}$ redox couple. While the second oxidation did not appear to be at all reversible, the first wave appeared at least quasi-reversible based on the full scan, and a second scan focusing on only this redox process (Figure 4.5, right) showed that this was an electrochemically reversible redox process with $E_{1/2}$ at -1.08 V. A plot of i_{pa} versus the square root of scan rate from 10 to 1000 mV/s was linear, further confirming that the electrochemical process was reversible (see below, Figure 4.9).

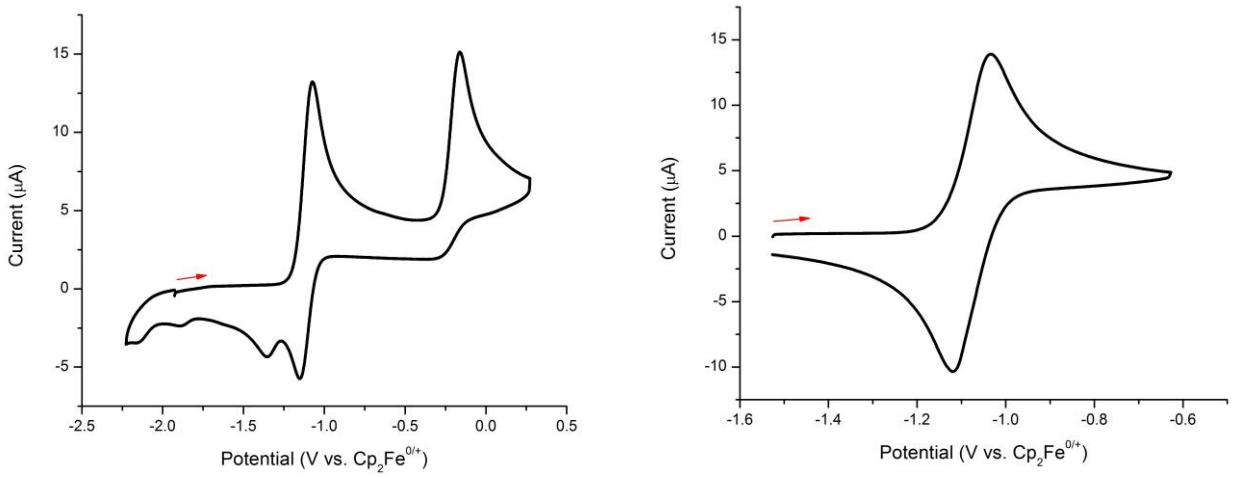

Figure 4.5 Cyclic voltammogram of complex **4.10** in dichloromethane at 100 mV/s: left, scan over a 2 V potential range showing two oxidation events; right, scan over a 1 V potential range showing reversible one-electron oxidation process.

Since the electrochemical data demonstrated that compound **4.10** could be oxidized twice, we set out to chemically access and isolate the products of both one- and two-electron oxidation. Treatment of **4.10** with one equivalent of $AgB(C_6F_5)_4$ in Et_2O resulted in a color change from dark green to dark brown and precipitation of silver metal. Upon workup, compound **4.11**, the product of one-electron oxidation of **4.10**, was isolated as brown crystals in 37% yield (Scheme 4.10). Formation of **4.11** likely results from removal of one electron from the redox non-innocent amidinylidene ligand. Upon addition of an equivalent of cobaltocene, a solution of compound **4** in THF changed color from brown back to dark green. A ^1H NMR spectrum of the crude reaction mixture showed conversion back to compound **4.10** with formation of cobaltocenium, confirming the chemical reversibility of the transformation from **4.10** to **4.11**.

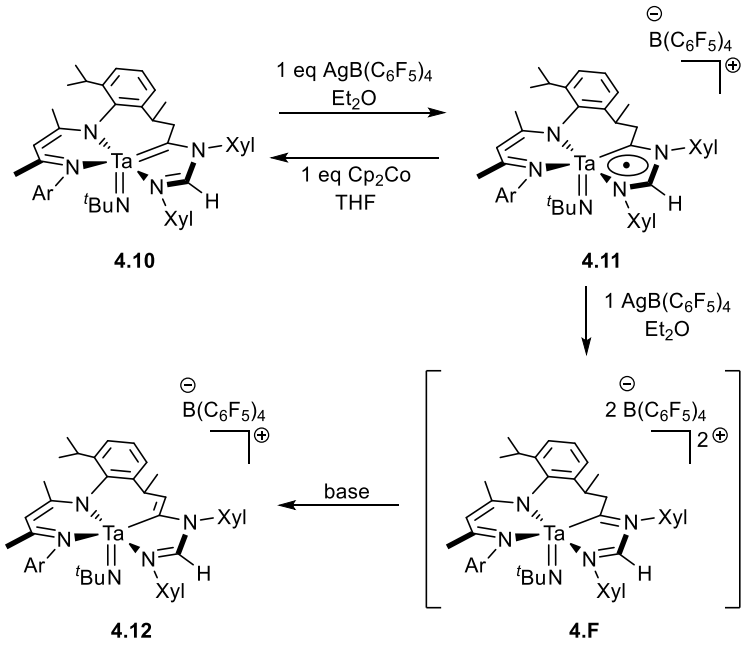

Scheme 4.10 Reversible one-electron and irreversible two-electron chemical oxidation of **4.10**.

Compound **4.11** is paramagnetic and only broad features were observed in the ^{1}H NMR spectrum; regardless, the chemical structure was readily established by single crystal X-ray diffraction, as shown in Figure 4.6. As expected based on the cyclic voltammetry data, the molecular structure of the cationic portion of **4.11** is quite similar to that of **4.10** (τ = 0.40). The most significant difference in metrical parameters between **4.10** and **4.11** is an increase in Ta-C(34) bond distance from 2.082(3) Å to 2.203(3) Å upon oxidation of **4.10** to **4.11**, consistent with weakening of the Ta-C π-bond. While the change is much less pronounced, the C(34)-N(4) and C(35)-N(5) bonds both shorten from 1.410(3) Å to 1.380(4) Å and 1.338(4) Å to 1.306(3) Å, respectively, while the Ta-N(5) and N(4)-C(35) distances remain essentially consistent between the two structures. Notably, the TaCNCN metallacycle becomes much more planar upon oxidation from **4.10** to **4.11**; the dihedral angles for **4.11** are N(4)-C(35)-N(5)-Ta = 3.3˚ and C(35)-N(4)-C(34)-Ta = 6.6˚, compared to 11.5˚ and 14.4˚ for **4.10**.

Since the tantalum center in compound **4.10** was already in the Ta(V) oxidation state prior to oxidation to **4.11**, the spin density of the unpaired electron in **4.11** was expected to reside predominantly on the ligand. An X-band EPR spectrum taken in room-temperature THF solution showed an isotropic 10-line pattern (Figure 4.7). A simulation of the EPR spectrum indicated that the splitting pattern resulted from hyperfine coupling to ^{181}Ta (S = 7/2, A^{181}Ta = 38 G) and both ^{14}N nuclei within the metallacycle (S = 1, A^{14}N(1) = 15 G, A^{14}N(2) = 6 G). The coupling to tantalum is weak compared to that reported for Ta(IV) radicals in the literature, consistent with the majority of the spin density being located within the CNCN framework.

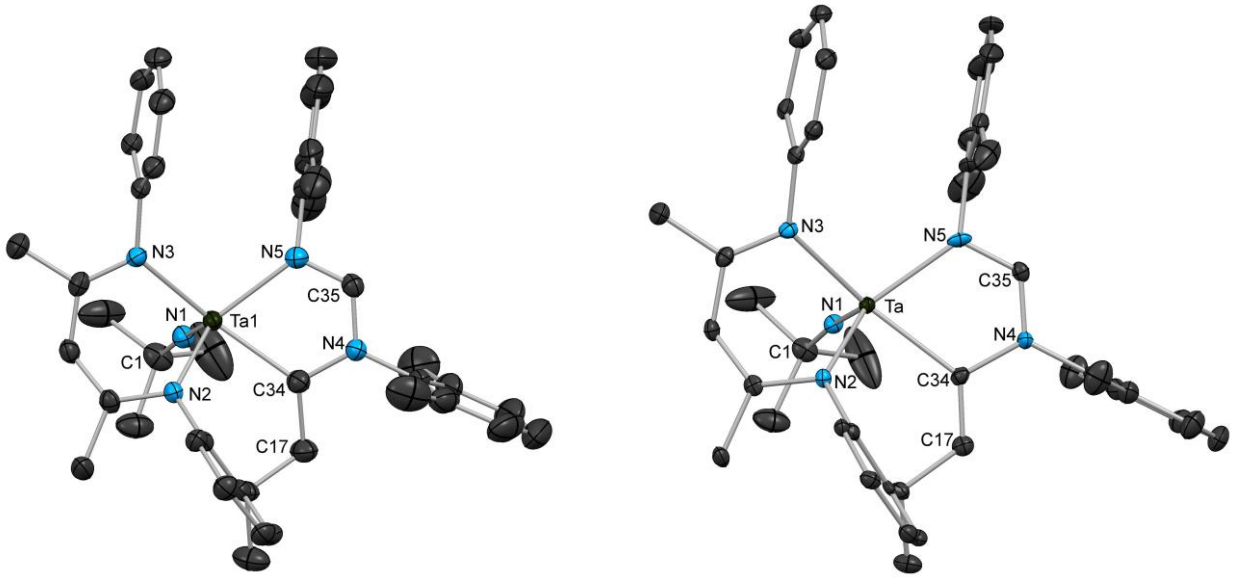

Figure 4.6 Molecular structures of the cationic portions of **4.11** (left) and **4.12** (right) as determined X-ray diffraction. Hydrogen atoms, ^{i}Pr groups, $B(C_6F_5)_4^-$ counterions, and co-crystallized molecules of diethyl ether are omitted for clarity; thermal ellipsoids are set at the 50 % probability level. For **4.11** (left), selected bond lengths (Å): Ta-N(1) 1.751(2), Ta-N(2) 2.081(2), Ta-N(3) 2.223(2), Ta-N(5) 2.195(2), Ta-C(34) 2.203(3), C(34)-N(4) 1.380(4), N(4)-C(35) 1.353(3), C(35)-N(5) 1.306(3), C(34)-C(17) 1.505(4); selected bond angles (˚): Ta-N(1)-C(1) 174.3(2), N(1)-Ta-N(5) 113.5(1), N(2)-Ta-N(5) 138.18(9), N(3)-Ta-C(34) 162.05(9). For **4.12** (right), selected bond lengths (Å): Ta-N(1) 1.748(3), Ta-N(2) 2.075(2), Ta-N(3) 2.231(2), Ta-N(5) 2.182(3), Ta-C(34) 2.250(3), C(34)-N(4) 1.434(4), N(4)-C(35) 1.319(4), C(35)-N(5)1.330(4), C(34)-C(17) 1.342(4); selected bond angles (˚): Ta-N(1)-C(1) 171.9(2), N(1)-Ta-N(5) 108.5(1), N(2)-Ta-N(5) 141.71(9), N(3)-Ta-C(34) 162.1(1).

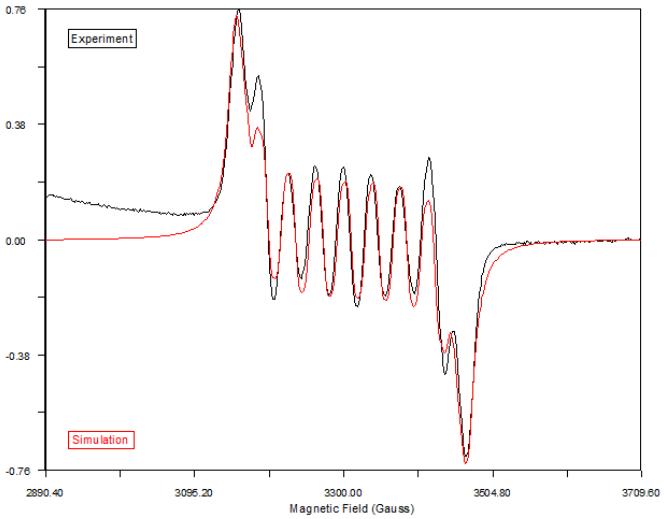

Figure 4.7 X-band EPR spectrum of **4.11** taken at room temperature in THF solution (black line) and simulation (red line). Hyperfine coupling constants: A^{181}Ta = 38 G, A^{14}N(1) = 15 G, A^{14}N(2) = 6 G.

Since the cyclic voltammogram (Figure 4.5) showed a second, irreversible oxidation, a solution of compound **4.10** in THF was exposed to two equivalents of $Ag(BC_6F_5)$, which resulted in a color change to yellow rather than brown and precipitation of silver metal, indicating formation of a different product from **4.11**. Upon workup, the diamagnetic Ta(V) product **4.12** was isolated as a yellow crystalline solid in 59% yield (Scheme 4.10). Compound **4.12** forms from a second one-electron oxidation of the tantalacycle to give the dicationic intermediate **4.F**, which readily converts to **4.12** by deprotonation of the methylene group. While the base responsible for this deprotonation event was not determined, intermediate **4.F** is likely very acidic due to its dicationic nature, and could be deprotonated by an adventitious source.

Unlike **4.11**, compound **4.12** is diamagnetic and displays sharp peaks at room temperature in its ^{1}H NMR spectrum. Since the methylene group has been deprotonated, compound **4.12** no longer contains a pair of characteristic methylene protons. Instead, the single vinylic methine proton resonates as a doublet at 5.76 ppm, and the adjacent methine proton resonates as a quintet at 4.56 ppm. The BDI backbone methine signal appears as a singlet at 6.31 ppm, 1 ppm downfield from the corresponding signal for **4.10**; this downfield shift is characteristic of conversion from a neutral to a cationic BDI complex, and has been observed in other Nb and Ta systems. The signal corresponding to the amidinyl methine proton also appears quite deshielded at 7.32 ppm, nearly 2 ppm downfield from the corresponding signal for compound **4.10**, consistent with a considerable buildup of positive charge within the TaCNCN metallacycle.

The solid-state structure of **4.12** again shows a distorted square-based pyramidal geometry for the cationic portion of **4.12** ($\tau = 0.34$), analogous to that of **4.10** and **4.11** (Figure 4.6, right). The Ta-C(34) bond distance increases 2.203(3) Å to 2.250(3) Å upon oxidation of **4.11** to **4.12**; while this change is less significant than the change observed upon conversion from **4.10** to **4.11**, the distance is consistent with a Ta-C single bond. The TaCNCN ring in compound **4.12** is planar (N(4)-C(35)-N(5)-Ta = 0.1˚ and C(35)-N(4)-C(34)-Ta = 0.3˚) and C(17) is also essentially coplanar with the tantalacycle (C(35)-N(4)-C(34)-C(17) = 4.5˚). Moreover, the C(17)-C(34) distance has decreased from 1.505(4) Å to 1.342(4) Å, consistent with the presence of a C-N double bond, further confirming the molecular structure of **4.12**.

In order to gain further understanding of the changes in electronic structure associated with one-electron oxidation of **4.10** to **4.11**, DFT calculations were carried out on both compounds using the PBE functional with Grimme's D3 corrections for dispersion forces. The geometries were optimized from the X-ray crystal structures, and the metrical parameters for both optimized compounds correlated well with the metrical parameters observed experimentally. The planarization of the tantalacycle upon converting from **4.10** (N(4)-C(35)-N(5)-Ta = 17.4˚ and C(35)-N(4)-C(34)-Ta = 20.0˚) to **4.11** (N(4)-C(35)-N(5)-Ta = 8.5˚ and C(35)-N(4)-C(34)-Ta = 11.2˚) is also reproduced in the calculations, although both calculated structures are less planar than their analogous experimental solid-state structures. As in the solid-state structures, the most significant change in bond distances between **4.10** and **4.11** is observed for the Ta-C bond. Upon converting from **4.10** to **4.11**, the distance increases from 2.082(3) Å (exp) or 2.091 Å (calc) to 2.203(3) Å (exp) or 2.216 Å (calc). This is consistent with the majority of the electron density due to the one-electron oxidation being removed from the HOMO of **4.10**, which is primarily

composed of a π-bonding interaction between the tantalum center and the coordinating carbon atom (Figure 4.8, left). Moreover, the Mulliken spin-density of the radical cation species **4.11** correlates very well with this orbital, consistent with the unpaired electron primarily residing on the Ta-bound carbon, but also being delocalized throughout the TaCNCN ring (Figure 4.8, right). The calculated spin density is also consistent with the relatively weak hyperfine coupling to the tantalum atom and the two nitrogen atoms in the ring observed in the EPR spectrum.

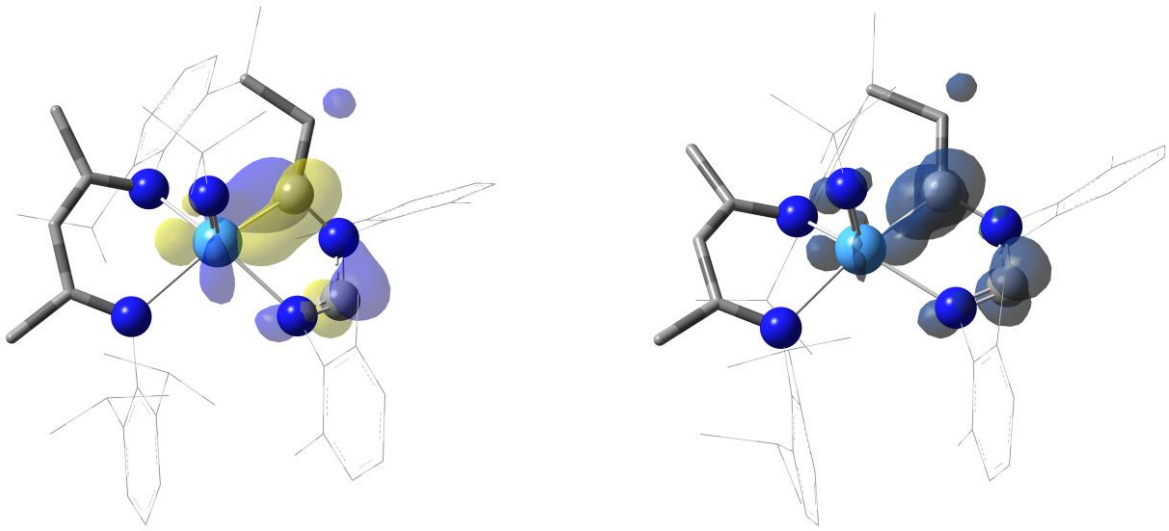

Figure 4.8 GaussView renderings of DFT calculated HOMO of **4.10** (left, isovalue = 0.06), and Mulliken spin density of **4.11** (right, blue = α, green = β, isovalue = 0.005).

Table 4.1 Partial atomic charges and electron spin density on selected atoms in **4.10** and **4.11** calculated using Mulliken, NPA, and QTAIM approaches.

	ATOM	MULLIKEN CHARGE	NPA CHARGE	QTAIM CHARGE	MULLIKEN SPIN	QTAIM SPIN
4.10	Ta	+0.04	+1.80	+2.19		
	C(Ta-*C*)	-0.26	-0.33	-0.12		
	N(Ta-C-*N*-C)	-0.11	-0.42	-1.17		
	C(Ta-C-N-*C*)	+0.13	+0.22	+0.88		
	N(Ta-*N*-C-N)	-0.37	-0.74	-1.17		
	N(imido)	-0.20	-0.89	-1.18		
	N(BDI)	-0.35	-0.70	-1.15		
	N'(BDI)	-0.32	-0.66	-1.17		
4.11	Ta	+0.28	+2.05	+2.28	+0.21	+0.14
	C(Ta-*C*)	-0.22	-0.13	+0.05	+0.49	+0.41
	N(Ta-C-*N*-C)	-0.11	-0.43	-1.17	-0.05	+0.02
	C(Ta-C-N-*C*)	+0.21	+0.32	+0.97	+0.22	+0.17
	N(Ta-*N*-C-N)	-0.35	-0.71	-1.21	+0.05	+0.01
	N(imido)	-0.15	-0.87	-1.13	+0.05	+0.05
	N(BDI)	-0.37	-0.73	-1.16	-0.01	+0.01
	N'(BDI)	-0.35	-0.68	-1.19	0.00	+0.01

Atomic charges and spin densities for optimized structures of **4.10** and **4.11** are summarized in Table 4.1. Using Mulliken, NPA, and QTAIM approaches, the atomic charges for the tantalum atom and two carbon atoms within the tantalaimidazole ring change most significantly between **4.10** and **4.11**, while most of the other charges remain fairly constant between the two compounds, again consistent with removal of electron density from the HOMO shown in Figure 4.8, left. Mulliken and QTAIM approaches produce similar results for the spin density in **4.11**, both consistent with most of the spin being localized on the tantalum center and two carbon atoms, as depicted in Figure 4.8, right.

We have previously found that the niobium (III) complex (BDI)Nb(N^{t}Bu)(CO)$_2$ catalyzes the semihydrogenation of internal alkynes to *cis*-alkenes via a mechanism involving oxidative addition and reductive elimination steps at the niobium center.[33] In the absence of dihydrogen, the niobium dicarbonyl complex reacted with diphenylacetylene to generate the isolable complex (BDI)Nb(N^{t}Bu)(CO)(PhCCPh) that was best described as a Nb(V) metallacyclopropene complex, but also had considerable Nb(III) η^2-alkyne character.[31,33] Hence, having isolated the analogous tantalum (III) dicarbonyl complex (BDI)Ta(N^{t}Bu)(CO)$_2$ (**4.8**), we set out to investigate its reactivity toward internal alkyne substrates.

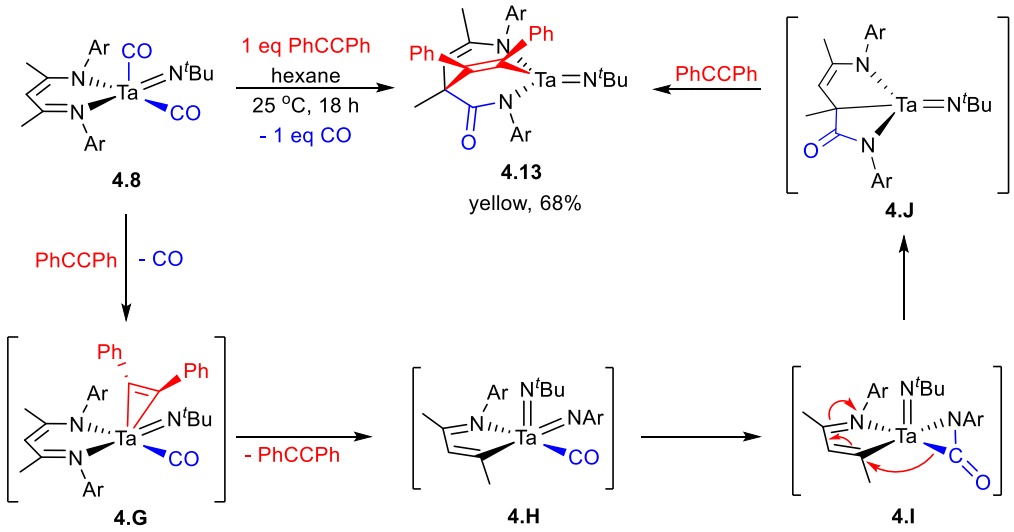

Scheme 4.11 Reaction of tantalum (III) dicarbonyl complex with diphenylacetylene.

In contrast to the niobium system, the tantalum dicarbonyl complex did not catalyze hydrogenation of alkynes. Moreover, rather than forming a metallacyclopropene complex, tantalum dicarbonyl complex **4.8** reacted with an equivalent of diphenylacetylene to give Ta(V) complex **4.13**, which was isolated as yellow crystals in 68% yield (Scheme 4.11). In **4.13**, both the alkyne and one of the carbonyl ligands of **4.8** have formed new C-C single bonds to the same BDI backbone carbon, thus implicating a monoazadiene (MAD) tantalum bis(imido) complex resulting from reductive C-N cleavage of the BDI ligand as an intermediate in the transformation. We have observed similar transformations involving insertion chemistry following reductive C-N cleavage in the niobium system.[60] A plausible mechanism for formation of **4.13** is shown in Scheme 4.11. Alkyne first displaces CO to give metallacyclopropene intermediate **4.G**. Unlike the niobium analog which was an isolable compound, **4.G** is unstable toward reductive C-N cleavage, which results in transformation to MAD tantalum bis(imido) intermediate **4.H**. The remaining carbonyl

ligand adds across the arylimido group to generate η^2-isocyanate complex **4.I**, which then rearranges as shown to give **4.J**. Finally, alkyne inserts into the Ta-C bond of **4.J** to give the observed product. The solid-state structure of **4.13** (Figure 4.9) showed a nearly tetrahedral geometry about the tantalum center (τ_4' = 0.92)[61] and bond distances consistent with covalent single bonds between both of the nitrogens originating from the BDI ligand (Ta-N(2) = 2.006(2) Å, Ta-N(3) = 2.014(2) Å), as well as the vinylic carbon (Ta-C(36) = 2.105(2) Å).

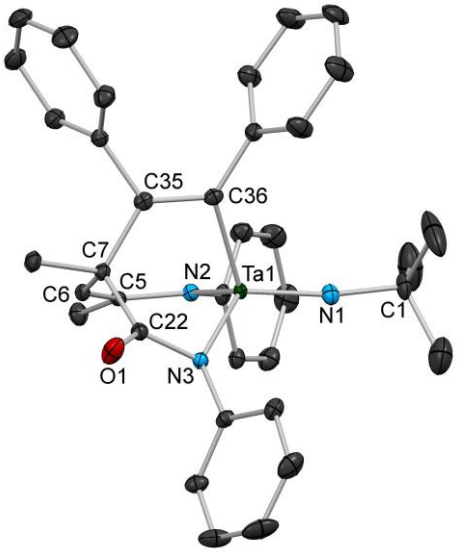

Figure 4.9 Molecular structure of **4.13** as determined by X-ray diffraction. Hydrogen atoms and ^{i}Pr groups are omitted for clarity; thermal ellipsoids are set at the 50 % probability level. Selected bond lengths (Å): Ta-N(1) 1.755(2), Ta-N(2) 2.006(2), Ta-N(3) 2.014(2), Ta-C(36) 2.105(2), C(35)-C(36) 1.352(3); selected bond angles (˚): N(1)-Ta-N(2) 109.53(7), N(1)-Ta-N(3) 116.70(7), N(1)-Ta-C(36) 110.19(7), N(2)-Ta-N(3) 111.36(6), N(2)-Ta-C(36) 105.83(7), N(3)-Ta-C(36) 102.51(7), Ta-N(1)-C(1) 170.7(2).

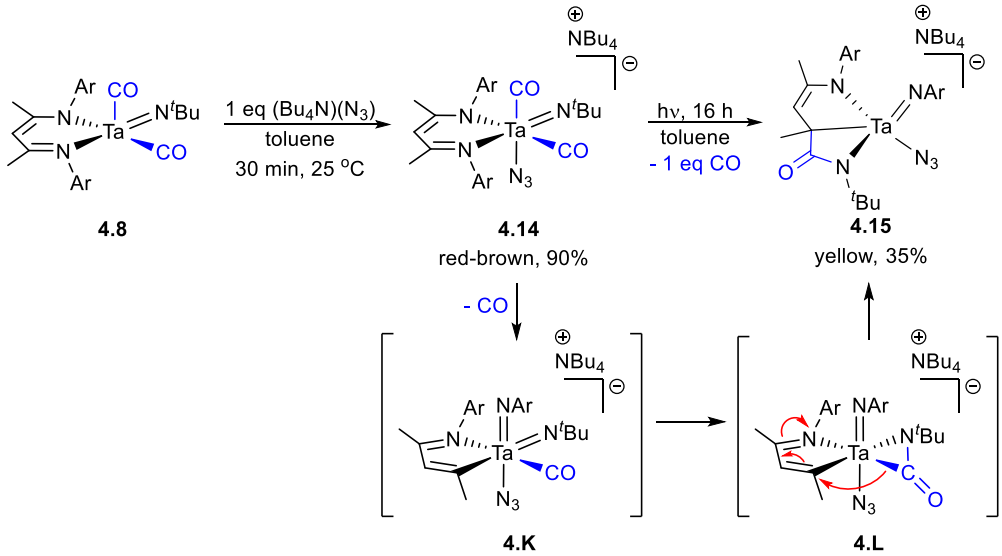

Scheme 4.12 Synthesis and photolytic reaction of a Ta(III) dicarbonyl azide anionic complex.

Since terminal nitride functionalities are scarce in group 5 chemistry[62–68] and a tantalum terminal nitride complex has yet to be reported, we considered **4.8** as a potential source of low-valent tantalum to target high-valent tantalum nitrido complexes. Addition of tetrabutylammonium azide to **4.8** resulted in an immediate color change to red-brown. Upon workup of the reaction, the 6-coordinate azide adduct **4.14** was isolated in 90% yield (Scheme 4.12) and characterized by ^{1}H NMR spectroscopy and X-Ray crystallography. The X-Ray crystal structure (Figure A.2, left) showed a distorted octahedral geometry with a long Ta-N(4) bond distance of 2.235(2) Å and a bent Ta-N(4)-N(5) angle of 132.7(2)˚, likely due to the trans influence of the carbonyl ligand and the fact that **4.14** is already an 18 electron complex without any π-donation from the azido ligand.

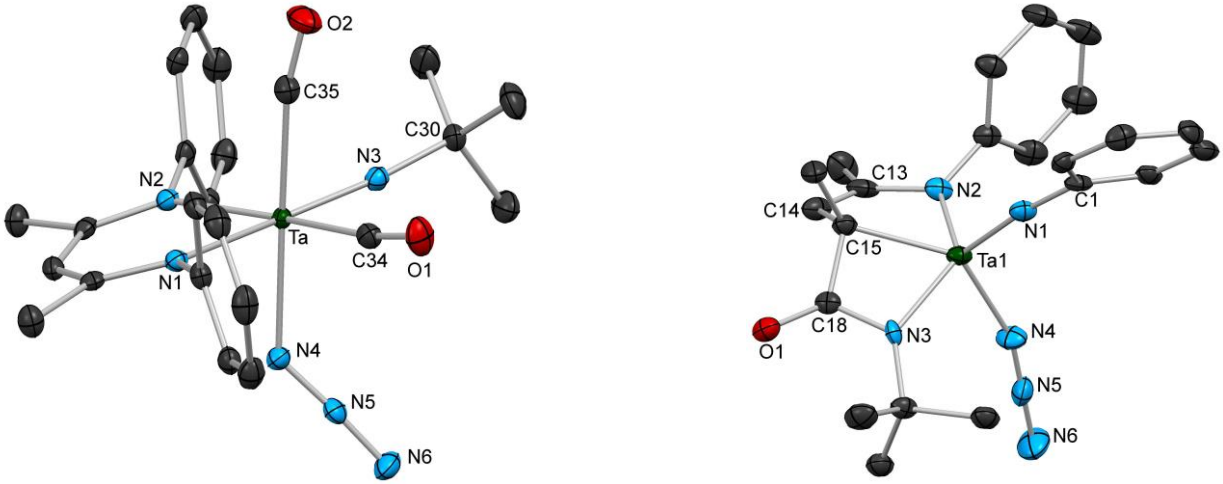

Figure 4.10 Molecular structures of **4.14** (left) and **4.15** (right) as determined by X-ray diffraction. Hydrogen atoms, ^{i}Pr groups, tetrabutylammonium counterions, a co-crystallized molecule of diethyl in **4.14** and a second crystallographically inequivalent molecule of **4.15** are omitted for clarity; thermal ellipsoids are set at the 50 % probability level. For **4.14**, selected bond lengths (Å): Ta-N(1) 2.297(2), Ta-N(2) 2.234(2), Ta-N(3) 1.816(2), Ta-N(4) 2.235(2), Ta-C(34) 2.088(3), Ta-C(35) 2.082(3); selected bond angles (˚): N(1)-Ta-N(3) 169.75(8), N(2)-Ta-C(34) 168.25(9), N(4)-Ta-C(35) 177.18(9), Ta-N(3)-C(30) 171.0(2), Ta-C(34)-O(1) 172.6(2), Ta-C(35)-O(2) 169.1(2), Ta-N(4)-N(5) 132.7(2), N(4)-N(5)-N(6) 176.6(2). For **4.15**, selected bond lengths (Å): Ta(1)-N(1) 1.789(6), Ta(1)-N(2) 2.024(6), Ta(1)-N(3) 2.139(6), Ta(1)-N(4) 2.074(6), Ta(1)-C(15) 2.209(7); selected bond angles (˚): N(2)-Ta(1)-N(3) 132.8(2), N(4)-Ta(1)-C(15) 135.8(2), N(1)-Ta(1)-N(2) 108.2(2), N(2)-Ta(1)-C(15) 79.4(3), N(3)-Ta(1)-C(15) 62.9(2), Ta(1)-N(1)-C(1) 173.0(5), Ta(1)-N(4)-N(5) 161.9(6), N(4)-N(5)-N(6) 178.2(9).

Group 5 transition metal azido complexes have been shown to release dinitrogen and generate terminal nitrido complexes upon either heating or exposure to UV light.[64,69] While heating a solution of **4.14** resulted in conversion to a complex mixture of products, photo-activation of **4.14** resulted in relatively clean conversion to Ta(V) complex **4.15**, which was isolated as yellow crystals in 35% yield. Rather than promoting release of dinitrogen, UV light influenced release of carbon monoxide from **4.14** to generate a reactive Nb(III) center which ultimately rearranged to give **4.15**, leaving the azido ligand intact. The reaction to give **4.15** likely proceeds by the mechanism shown in Scheme 4.12, which is related to the mechanism for transformation of **4.8** into **4.13**. Initial photolysis of a metal-CO bond induces reductive C-N cleavage of the BDI ligand

to give MAD bis(imido) intermediate **4.K**. The remaining carbonyl ligand adds across the now reactive *tert*-butylimido group to generate η^2-isocyanate complex **4.L**, which then rearranges to give **4.15**. The solid-state structure of **4.15** showed a five-coordinate geometry that was highly constrained by the tridentate N-C-N ligand, and thus could not be well described as square-based pyramidal or trigonal bipyramidal (Figure 4.10, right). Notably, the Ta-N(4) distance was 2.074(6) Å and the Ta-N(4)-N(5) angle was 161.9(6)˚, indicating a much stronger π-component to the interaction between the azido ligand and the tantalum center than was observed for **4.14**.

Summary and Conclusions

The cyclometallated hydride **4.2** was generated in high yield via reaction of the tantalum dimethyl precursor **4.1** with H_2. This reaction most likely proceeds by successive σ-bond metathesis steps with H_2, leading to a tantalum dihydride intermediate. In contrast, reaction of the analogous niobium dimethyl precursor with H_2 was shown to generate trivalent complexes; these Nb(III) species are likely generated via a cyclometallated niobium hydride intermediate analogous to **4.2**. Likewise, compound **4.2** could be used as an isolable precursor for accessing Ta(III) species. Coordination of a σ-donating DMAP ligand to **4.2**, followed by reaction with CO at room temperature, afforded the six-coordinate Ta(III) dicarbonyl complex **4.7** via reductive elimination, while the analogous highly reducing five-coordinate Ta(III) dicarbonyl complex **4.8** could be accessed directly from **4.2** when CO was added at low temperature. Hence, these results give credence to the proposal that the niobium analog of **4.2** is an intermediate in accessing Nb(III) chemistry, and provide a synthetic platform for accessing low valent tantalum chemistry. Compound **4.8** has been utilized in further transformations with elemental phosphorus,[70] as well as azides and alkynes and promises to be a useful starting material for future Ta(III) chemistry.

Instead of promoting reductive elimination, 2,6-dimethylphenylisocyanide reacted with **4.2** via migratory insertion to give **4.10**, a product containing a unique metallaimidazole ring. Compound **4.10** could be reversibly oxidized by one electron either electrochemically or chemically to give the tantalum radical cation species **4.11**. DFT calculations, as well as X-ray crystallographic and EPR spectroscopic data were consistent with the electron being removed from an orbital primarily composed of Ta-C π-bonding character, but also delocalized over the tantalaimidazole ring. We hope to further investigate the utility of amidinylidenes and related π-conjugated alkylidene ligands as electron reservoirs in early transition metal chemistry.

Experimental

General Considerations: Unless otherwise noted, all reactions were performed using standard Schlenk line techniques or in an MBraun inert atmosphere glove box under an atmosphere of nitrogen (<1 ppm O_2/H_2O). Glassware and Celite were stored in an oven at ca. 160˚ C. Molecular sieves (4 Å) were activated by heating to 200 °C overnight under vacuum prior to storage in a glovebox. Hexane, n-pentane, diethyl ether, dichloromethane, toluene, and THF were purified by passage through columns of activated alumina and degassed. Pyridine and ^{t}BuNH$_2$ were distilled from CaH_2. Deuterated solvents were vacuum-transferred from sodium/benzophenone and degassed with three freeze-pump-thaw cycles. NMR spectra were recorded on Bruker AV-600, AVB-400, AVQ-400, AV-500, and DRX-500 spectrometers. ^{1}H and ^{13}C{^{1}H} chemical shifts are

given relative to residual solvent peaks. Proton and carbon NMR assignments were routinely confirmed by ^{1}H-^{1}H (COSY and NOESY) and ^{1}H-^{13}C (HSQC and HMBC) experiments. FT-IR samples were prepared as Nujol mulls and were taken between KBr disks using a Nicolet iS10 FT-IR spectrometer. Melting points were determined using an OptiMelt automated melting point system. $TaCl_5$ was purified by sublimation. $AgB(C_6F_5)_4$,[71] HBDI,[72] Li(BDI)•OEt_2,[73] Ta(N^tBu)Cl_3Py_2,[74] and (BDI)Ta(N^tBu)Me_2 (**4.1**)[39] (BDI = ArNC(Me)CHC(Me)NAr, Ar = 2,6-diisopropylphenyl) were prepared using the literature procedures. H_2 was obtained from Airgas or PraxAir, and D_2 was obtained from Liquid Carbonic or Cambridge Isotope Laboratories. All other reagents were acquired from commercial sources and used as received. Elemental analyses were determined either at the College of Chemistry, University of California, Berkeley or at the School of Human Sciences, Science Center, London Metropolitan University. LR-EI-MS data was obtained at the QB3/Chemistry Mass Spectrometry Facility, University of California, Berkeley. X-ray structural determinations were performed at CHEXRAY, University of California, Berkeley on SMART APEX I and SMART APEX II QUAZAR diffractometers.

{ArNC(Me)CHC(Me)N[2-(CHMeCH$_2$)-6-^{i}Pr-C$_6$H$_3$]}Ta(N^{t}Bu)H (4.2a, 4.2b): Hexane (150 mL) was added to a 500 mL Teflon-sealed flask containing **4.1** (5.06 g, 7.23 mmol) at room temperature, resulting in a pale yellow solution. Under static vacuum, ca. 80% of the volume of the flask was submerged in a Dewar flask filled with liquid nitrogen until the solution was completely frozen. With the reaction flask still submerged in the Dewar flask, the reaction flask was placed under dynamic vacuum for ca. 30 s, and then filled with 1 atm H_2, sealed, and allowed to come to room temperature. Upon warming, the color of the solution started to become deeper yellow. The solution was stirred vigorously overnight at room temperature resulting in a yellow-orange solution. The volatile materials were removed under vacuum, and the residue was extracted with hexane and the combined hexane extracts were transferred to a Schlenk tube via cannula. The solution was concentrated and stored at -40 ˚C overnight, giving a mixture of compounds **4.2a** and **4.2b** as pale yellow microcrystals. The solid was isolated and residual solvent was removed under vacuum (3.87 g, 80%, 3 crops, 8:1 ratio of **4.2a** to **4.2b** in 1st crop, 4:1 ratio in 2nd crop, 3:1 ratio in 3rd crop). A 15:1 ratio of **4.2a** to **4.2b** was obtained by recrystallization of material that had been isolated as a 1st crop of crystals from hexane at 15 ˚C. The ratio of **4.2a** to **4.2b** was determined by integrating the Ta-*H* peaks for the two compounds in the ^{1}H NMR spectrum relative to one another. X-ray quality crystals were grown from slow evaporation of benzene; data were collected on a crystal containing only **4.2a**. **^{1}H NMR (600 MHz, C$_6$D$_6$, 293 K)** Compound **4.2a**: δ 20.89 (s, 1H, Ta*H*), 7.15-7.04 (m, 6H, Ar), 5.50 (s, 1H, *H*C(C(Me)NAr)$_2$), 3.20 (sep, 1H, C*H*Me$_2$), 3.08 (ddq, 1H, MeC*H*CH$_2$Ta), 2.83 (sep, 1H, C*H*Me$_2$), 2.75 (sep, 1H, C*H*Me$_2$), 1.83 (s, 3H, HC(C(*Me*)NAr)$_2$), 1.60 (ddd, 1H, MeCHC*H*$_2$Ta, ^{2}J = 16 Hz, ^{3}J = 3.6 Hz, ^{3}J(Ta-*H*) = 1.8 Hz),[75] 1.57 (s, 3H, HC(C(*Me*)NAr)$_2$), 1.52 (d, 3H, CH*Me*$_2$), 1.42 (d, 3H, CH*Me*$_2$), 1.40 (d, 3H, *Me*CHCH$_2$Ta), 1.36 (d, 3H, CH*Me*$_2$), 1.20 (d, 3H, CH*Me*$_2$), 1.11 (d, 3H, CH*Me*$_2$), 1.09 (s, 9H, ^{t}Bu), 1.03 (d, 3H, CH*Me*$_2$), 0.97 (dd, 1H, MeCHC*H*$_2$Ta, ^{2}J = 16 Hz, ^{3}J = 11 Hz). Compound **4.2b**:[76] δ 20.52 (s, 1H, Ta*H*), 7.15-7.04 (m, 6H, Ar), 5.46 (s, 1H, *H*C(C(Me)NAr)$_2$), 4.48 (ddq, 1H, MeC*H*CH$_2$Ta), 3.18 (1H, C*H*Me$_2$), 2.88 (1H, C*H*Me$_2$), 2.78 (1H, C*H*Me$_2$), 2.37 (ddd, 1H, MeCHC*H*$_2$Ta, ^{2}J = 16 Hz, ^{3}J = 3.7 Hz, ^{3}J(Ta-*H*) = 1.2 Hz), 1.85 (s, 3H, HC(C(*Me*)NAr)$_2$), 1.54 (s, 3H, HC(C(*Me*)NAr)$_2$), 1.50 (3H, CH*Me*$_2$), 1.42 (3H, CH*Me*$_2$), 1.29 (d, 3H, CH*Me*$_2$), 1.19 (3H, CH*Me*$_2$), 1.13-1.08 (m, 15H, *Me*CHCH$_2$Ta/CH*Me*$_2$/^{t}Bu) 1.02 (d, 3H, CH*Me*$_2$), 0.70 (dd, 1H,

MeCHC*H*$_2$Ta, ^{2}J = 16 Hz, ^{3}J = 4.9 Hz). **^{13}C{^{1}H} NMR (600 MHz, C$_6$D$_6$, 293 K)** Compound **4.2a**: δ 167.9 (HC(*C*(Me)NAr)$_2$), 163.2 (HC(*C*(Me)NAr)$_2$), 150.4 (Ar), 145.2 (Ar), 142.9 (Ar), 141.4 (Ar), 140.7 (Ar), 140.5 (Ar), 126.8 (Ar), 126.4 (Ar), 124.4 (Ar), 124.4 (Ar), 123.9 (Ar), 121.7 (Ar), 103.9 (H*C*(C(Me)NAr)$_2$), 82.7 (MeCH*C*H$_2$Ta), 62.7 (C$_\alpha$, ^{t}Bu), 35.2 (Me*C*HCH$_2$Ta), 33.5 (C$_\beta$, ^{t}Bu), 28.8 (*C*HMe$_2$), 28.5 (*C*HMe$_2$), 28.3 (*C*HMe$_2$), 25.9 (HC(C(*Me*)NAr)$_2$), 25.3 (CH*Me*$_2$), 25.3 (CH*Me*$_2$), 25.1 (CH*Me*$_2$), 24.9 (CH*Me*$_2$), 24.3 (CH*Me*$_2$), 24.1 (CH*Me*$_2$), 23.6 (CH*Me*$_2$), 23.5 (HC(C(*Me*)NAr)$_2$). Anal. calcd (%) for Ta$_1$N$_3$C$_{33}$H$_{50}$ (15:1 ratio of **4.2a** to **4.2b**): C, 59.18; H, 7.53; N, 6.27. Found: C, 58.80; H, 7.78; N, 6.30. FT-IR (KBr, nujol, cm^{-1}): 1779 (m, Ta-H stretch). MP: dec. 151–159 ˚C. LR-EI-MS: *m/z* calcd for Ta$_1$N$_3$C$_{33}$H$_{50}$: 669, found: 669.

{ArNC(Me)CHC(Me)N[2-(CHMeCH$_2$)-6-^{i}Pr-C$_6$H$_3$]}Ta(N^{t}Bu)(Me) (4.3): Compound **4.1** (200 mg, 0.286 mmol) was added to a 100 mL flask and dissolved in 25 mL toluene. PhSiH$_3$ (71 µL, 0.58 mmol) was added using a micropipette. The solution was stirred at 80 ˚C for 15 h, resulting in a color change from pale yellow to orange. The volatile materials were removed under vacuum and the residue was triturated with hexane, resulting in an orange powder. The powder was extracted with hexane and the resulting solution was cannula filtered and concentrated. The solution was stored at -40 ˚C overnight, yielding pale yellow crystals of **4.3**. The crystals were isolated and residual solvent was removed under vacuum (130 mg, 65%, 2 crops). X-ray quality crystals were grown from slow evaporation of benzene. Under otherwise identical conditions, the same product was observed by ^{1}H NMR spectroscopy using a sub-stoichiometric quantity of PhSiH$_3$ (0.2 eq). **^{1}H NMR (600 MHz, C$_6$D$_6$, 293 K):** δ 7.21-7.11 (m, 4H, Ar), 7.05 (m, 2H, Ar), 5.45 (s, 1H, *H*C(C(Me)NAr)$_2$), 3.16 (sep, 1H, C*H*Me$_2$), 2.97 (m, 2H, C*H*Me$_2$/MeC*H*CH$_2$Ta), 2.83 (sep, 1H, C*H*Me$_2$), 1.79 (s, 3H, HC(C(*Me*)NAr)$_2$), 1.74 (dd, 1H, TaC*H*$_2$, ^{2}J = 16 Hz, ^{3}J = 3.5 Hz), 1.56 (s, 3H, HC(C(*Me*)NAr)$_2$), 1.49 (d, 3H, CH*Me*$_2$), 1.48 (d, 3H, CH*Me*$_2$), 1.46 (d, 3H, *Me*CHCH$_2$Ta), 1.33 (d, 3H, CH*Me*$_2$), 1.17 (d, 3H, CH*Me*$_2$), 1.15 (dd, 1H, TaC*H*$_2$, ^{2}J = 16 Hz, ^{3}J = 12 Hz), 1.11 (d, 3H, CH*Me*$_2$), 1.07 (s, 9H, ^{t}Bu), 1.02 (d, 3H, CH*Me*$_2$), 0.36 (s, 3H, Ta*Me*). **^{13}C{^{1}H} NMR (600 MHz, C$_6$D$_6$, 293 K):** δ 168.5 (HC(*C*(Me)NAr)$_2$), 163.0 (HC(*C*(Me)NAr)$_2$), 151.6 (Ar), 145.0 (Ar), 144.1 (Ar), 141.7 (Ar), 141.5 (Ar), 140.6 (Ar), 126.4 (Ar), 126.3 (Ar), 124.9 (Ar), 124.2 (Ar), 124.2 (Ar), 121.8 (Ar), 103.2 (H*C*(C(Me)NAr)$_2$), 78.8 (Ta*C*H$_2$), 63.5 (C$_\alpha$, ^{t}Bu), 52.3 (Ta*Me*), 35.7 (Me*C*HCH$_2$Ta), 31.5 (C$_\beta$, ^{t}Bu), 28.6 (*C*HMe$_2$) , 28.5 (*C*HMe$_2$), 28.0 (*C*HMe$_2$), 26.1 (HC(C(*Me*)NAr), 25.5 (*Me*CHCH$_2$Ta), 25.4 (CH*Me*$_2$), 25.0 (CH*Me*$_2$), 24.8 (CH*Me*$_2$), 24.8 (CH*Me*$_2$), 24.7 (HC(C(*Me*)NAr), 24.6 (CH*Me*$_2$), 24.3 (CH*Me*$_2$). Anal. calcd (%) for Ta$_1$N$_3$C$_{34}$H$_{52}$: C, 59.72; H, 7.67; N, 6.15. Found: C, 59.53; H, 7.48; N, 5.98. MP: dec. 220–227 ˚C.

[κ^4-CNNC-BDI]Ta(N^{t}Bu) (4.4): Compound **4.2** (160 mg, 0.239 mmol) was added to a 100 mL flask and dissolved in 25 mL toluene. The solution was stirred at 120 ˚C for 15 h, resulting in a color change from pale yellow to orange. The volatile materials were removed under vacuum and the residue was triturated with hexane, resulting in an orange powder. 10 mL of hexane was added to the powder, resulting in a suspension. Toluene was added slowly and the suspension was gently heated until all of the powder dissolved. The solution was stored at -40 ˚C overnight, yielding orange crystals of **4.4**. The crystals were isolated and residual solvent was removed under vacuum (27 mg, 17%). **^{1}H NMR (600 MHz, C$_6$D$_6$, 293 K):** δ 7.39 (t, 2H, Ar), 7.26 (d, 2H, Ar), 7.03 (d, 2H, Ar), 5.15 (s, 1H, *H*C(C(Me)NAr)$_2$), 2.83 (sep, 2H, C*H*Me$_2$), 2.50 (s, 6H, 1.76 (s, 6H, HC(C(*Me*)NAr)$_2$), 1.95 (s, 6H, TaC*Me*$_2$), 1.46 (s, 6H, TaC*Me*$_2$), 1.22 (d, 6H, CH*Me*$_2$), 0.93 (d, 6H,

CH*Me*$_2$), 0.70 (s, 9H, ^{t}Bu). **^{13}C{^{1}H} NMR (600 MHz, C$_6$D$_6$, 293 K):** δ 166.0 (HC(*C*(Me)NAr)$_2$), 149.0 (Ar), 139.7 (Ar), 139.6 (Ar), 129.3 (Ar), 123.0 (Ar), 122.1 (Ar), 103.9 (H*C*(C(Me)NAr)$_2$), 72.1 (Ta*C*Me$_2$), 66.5 (C$_\alpha$, ^{t}Bu), 33.5 (C$_\beta$, ^{t}Bu), 28.3 (*C*HMe$_2$), 28.0 (HC(C(*Me*)NAr)$_2$), 26.0 (TaC*Me*$_2$), 24.9 (CH*Me*$_2$), 21.2 (TaC*Me*$_2$) 20.9 (CH*Me*$_2$). Anal. calcd (%) for Ta$_1$N$_3$C$_{33}$H$_{48}$: C, 59.36; H, 7.25; N, 6.29. Found: C, 59.23; H, 7.33; N, 6.19. MP: dec. 229–235 ˚C.

{ArNC(Me)CHC(Me)N[2-(CHMeCH$_2$)-6-^{i}Pr-C$_6$H$_3$]}Ta(N^{t}Bu)(DMAP)H (4.5): Compound **4.2** (200 mg, 0.299 mmol) was added to a 20 mL vial and dissolved in 8 mL hexane. In a separate 20 mL vial, 4-dimethylaminopyridine (36.4 mg, 0.299 mmol) was dissolved in 12 mL hexane. The two solutions were mixed, resulting in a color change from pale yellow to yellow-brown. Upon standing at room temperature for 3 h, **4.5** precipitated as a pale yellow powder; the powder was filtered off and washed with 10 mL hexane, and residual solvent was removed under vacuum (154 mg, 65%). **^{1}H NMR (500 MHz, C$_6$D$_6$, 293 K):** δ 17.58 (br s, 1H, Ta-*H*), 8.45 (br s, 2H, DMAP), 7.27 (d, 1H, Ar), 7.20 (t, 1H, Ar), 7.18 (t, 1H, Ar), 7.14 (m, 1H, Ar), 7.12 (m, 1H, Ar), 7.10 (m, 1H, Ar), 5.77 (d, 2H, DMAP), 5.47 (s, 1H, *H*C(C(Me)NAr)$_2$), 3.34 (br m, 1H, MeC*H*CH$_2$Ta), 3.18 (sep, 1H, C*H*(Me)$_2$), 3.06 (br m, 1H, C*H*(Me)$_2$), 2.96 (br m, 1H, C*H*(Me)$_2$), 2.05 (s, 6H, DMAP), 1.86 (s, 3H, HC(C(*Me*)NAr)$_2$), 1.82 (m, 1H, TaC*H*$_2$), 1.74 (s, 3H, HC(C(*Me*)NAr)$_2$), 1.69 (d, 3H, *Me*CHCH$_2$Ta), 1.62 (d, 3H, CH*Me*$_2$), 1.44 (dd, 1H, TaC*H*$_2$, ^{2}J = 15 Hz, ^{3}J = 3.8 Hz), 1.24 (d, 3H, CH*Me*$_2$), 1.20 (d, 3H, CH*Me*$_2$), 1.17 (s, 9H, ^{t}Bu), 1.17 (br m, 3H, CH*Me*$_2$), 1.14 (d, 3H, CH*Me*$_2$), 0.73 (br d, 3H, CH*Me*$_2$). **^{1}H NMR (500 MHz, C$_6$D$_6$, 333 K):** δ 19.1 (s, 1H, Ta-*H*), 8.42 (d, 2H, DMAP), 7.19-7.08 (m, 6H, Ar), 5.98 (d, 2H, DMAP), 5.49 (s, 1H, *H*C(C(Me)NAr)$_2$), 3.18 (ddq, 1H, MeC*H*CH$_2$Ta), 3.08 (sep, 1H, C*H*(Me)$_2$), 3.03 (sep, 1H, C*H*(Me)$_2$), 2.95 (sep, 2H, C*H*(Me)$_2$), 2.22 (s, 6H, DMAP), 1.86 (s, 3H, HC(C(*Me*)NAr)$_2$), 1.68 (s, 3H, HC(C(*Me*)NAr)$_2$), 1.55 (d, 3H, CHCH$_2$Ta), 1.53 (d, 3H, CH*Me*$_2$), 1.48 (dd, 1H, TaC*H*$_2$, ^{2}J = 15 Hz, ^{3}J = 3.6 Hz), 1.36 (br dd, 1H, TaC*H*$_2$, ^{2}J = 15 Hz, ^{3}J = 13 Hz), 1.31 (d, 3H, CH*Me*$_2$), 1.23 (d, 3H, CH*Me*$_2$), 1.16 (d, 3H, CH*Me*$_2$), 1.10 (d, 3H, CH*Me*$_2$), 1.09 (s, 9H, ^{t}Bu), 1.01 (d, 3H, CH*Me*$_2$). **^{13}C{^{1}H} NMR (500 MHz, C$_6$D$_6$, 293 K):** δ 166.2 (HC(*C*(Me)NAr)$_2$), 162.5 (HC(*C*(Me)NAr)$_2$), 154.0 (Ar), 151.4 (Ar), 143.8 (Ar), 142.7 (Ar), 142.3 (Ar), 140.3 (Ar), 125.8 (Ar), 124.9 (Ar), 124.4 (Ar), 124.0 (Ar), 122.9 (Ar), 121.1 (DMAP), 105.6 (DMAP), 103.0 (H*C*(C(Me)NAr)$_2$), 81.5 (Ta*C*H$_2$), 63.3 (C$_\alpha$, ^{t}Bu), 38.3 (Me, DMAP), 36.1 (Me*C*HCH$_2$Ta), 33.1 (C$_\beta$, ^{t}Bu), 28.8 (*C*HMe$_2$), 28.4 (*C*HMe$_2$), 28.2 (*C*HMe$_2$), 26.0 (*Me*CHCH$_2$Ta), 25.9 (HC(C(*Me*)NAr)$_2$), 25.6 (CH*Me*$_2$), 25.2 (CH*Me*$_2$), 25.1 (CH*Me*$_2$), 24.5 (CH*Me*$_2$), 24.4 (CH*Me*$_2$), 24.0 (HC(C(*Me*)NAr)$_2$), 23.5 (CH*Me*$_2$). Anal. calcd (%) for Ta$_1$N$_5$C$_{40}$H$_{60}$: C, 60.67; H, 7.64; N, 8.84. Found: C, 60.74; H, 7.69; N, 8.47. FT-IR (KBr, nujol, cm^{-1}): 1714 (m, Ta-H stretch). MP: dec. 112–124 ˚C.

{ArNC(Me)CHC(Me)N[2-(CHMeCH$_2$)-6-^{i}Pr-C$_6$H$_3$]}Ta(N^{t}Bu)(DMAP)D (4.5-d): Compound **4.5** (123 mg, 0.155 mmol) was added to a 100 mL flask and dissolved in 10 mL benzene. While stirring the solution, the flask was evacuated under reduced pressure for 10 s, and the headspace was backfilled with 1 atm D$_2$. The solution was stirred at room temperature for 2 h, and then the volatile materials were removed under vacuum to give **4.5-d** as a pale yellow powder. The powder was washed with 10 mL hexane and residual solvent was removed under vacuum. ^{1}H NMR spectroscopy showed the disappearance of the Ta-*H* peak at 17.58 ppm, and otherwise contained a ^{1}H NMR spectrum identical to that of **4.5**.

(MAD)Ta(N^{t}Bu)(NAr)(DMAP) (4.6): Compound **4.2** (220 mg, 0.328 mmol) and DMAP (40.0 mg, 0.328 mmol) were added to a 100 mL flask and dissolved in 25 mL toluene, giving a light brown solution. While stirring the solution, the flask was evacuated under reduced pressure for ca. 30 s, and the headspace was backfilled with 1 atm H_2. The solution immediately changed color from light brown to orange-red upon addition of H_2. The solution was stirred at 40 ˚C for 15 h. The volatile materials were removed under vacuum and the residue was triturated with hexane, resulting in a red-orange powder. The powder was extracted with hexane and the resulting solution was concentrated and stored at -80 ˚C overnight, yielding orange crystals of **4.6**. The crystals were isolated and residual solvent was removed under vacuum (105 mg, 40%, 2 crops). **^{1}H NMR (500 MHz, C$_6$D$_6$, 293 K):** δ 8.12 (d, 2H, DMAP), 7.42 (d, 2H, Ta=N*Ar*), 7.04 (t, 1H, Ta=N*Ar*), 7.01 (m, 2H, *H*C(C(Me)NAr)(CMe)/C=N*Ar*), 6.88 (t, 1H, C=N*Ar*), 6.68 (d, 1H, C=N*Ar*), 5.33 (d, 2H, DMAP), 4.91 (sep, 2H, C*H*(Me)$_2$ of Ta=N*Ar*), 3.85 (sep, 1H, C*H*(Me)$_2$ of C=N*Ar*), 3.10 (sep, 1H, C*H*(Me)$_2$ of C=N*Ar*), 3.01 (s, 3H, (HC(C(Me)NAr)(C*Me*)), 1.77 (s, 6H, DMAP), 1.65 (m, 12H, ^{t}Bu/HC(C(*Me*)NAr)(CMe)), 1.62 (d, 6H, CH*Me*$_2$ of Ta=N*Ar*), 1.53 (d, 3H, CH*Me*$_2$ of C=N*Ar*), 1.40 (d, 6H, CH*Me*$_2$ of Ta=N*Ar*), 1.11 (d, 3H, CH*Me*$_2$ of C=N*Ar*), 1.04 (d, 3H, CH*Me*$_2$ of C=N*Ar*), 0.96 (d, 3H, CH*Me*$_2$ of C=N*Ar*) **^{13}C{^{1}H} NMR (600 MHz, C$_6$D$_6$, 293 K):** δ 186.4 (HC(*C*(Me)NAr)(CMe)), 155.0 (HC(C(Me)NAr)(*C*Me)), 153.5 (Ar), 153.2 (DMAP), 145.8 (Ar), 143.0 (Ar), 142.1 (Ar), 141.6 (Ar), 131.3 (H*C*(C(Me)NAr)(CMe)), 126.0 (C=N*Ar*), 123.9 (C=N*Ar*), 123.3 (C=N*Ar*), 122.2 (Ta=N*Ar*), 119.4 (Ta=N*Ar*), 105.1 (DMAP), 63.8 (C$_\alpha$, ^{t}Bu), 37.9 (Me of DMAP), 35.4 (C$_\beta$, ^{t}Bu), 33.8 (HC(C(Me)NAr)(C*Me*)), 28.9 (*C*HMe$_2$ of C=N*Ar*), 27.8 (*C*HMe$_2$ of C=N*Ar*), 27.1 (*C*HMe$_2$ of Ta=N*Ar*), 25.1 (CH*Me*$_2$ of Ta=N*Ar*), 25.0 (CH*Me*$_2$ of C=N*Ar*), 24.9 (CH*Me*$_2$ of C=N*Ar*), 24.6 (CH*Me*$_2$ of Ta=N*Ar*), 24.5 (CH*Me*$_2$ of C=N*Ar*), 23.6 (CH*Me*$_2$ of C=N*Ar*), 23.0 (HC(C(*Me*)NAr)(CMe)). Anal. calcd (%) for $Ta_1N_5C_{40}H_{60}$: C, 60.67; H, 7.64; N, 8.84. Found: C, 60.46; H, 7.48; N, 8.71. MP: dec. 175–191 ˚C.

(BDI)Ta(N^{t}Bu)(CO)$_2$(DMAP) (4.7): Compound **4.5** (295 mg, 0.440 mmol) and DMAP (54 mg, 0.44 mmol) were added to a 100 mL flask and dissolved in 30 mL diethyl ether, giving a light brown solution. While the solution was being stirred, the flask was evacuated under reduced pressure for ca. 5 s, and the headspace was backfilled with 1 atm CO. The solution immediately changed color from light brown to dark red-brown upon addition of CO. The reaction mixture was stirred at room temperature for 2 h, and then the volatiles were removed under reduced pressure, giving a red-brown powder. The powder was re-dissolved in diethyl ether and filtered. Ether was then removed once again under reduced pressure to give a red-brown powder. The powder was extracted with toluene and the resulting solution was concentrated by slowly adding hexane until precipitate began to form. The solution was stored at -40 ˚C overnight, yielding red crystals of **4.7**. The crystals were isolated and residual solvent was removed under vacuum (161 mg, 44%, 3 crops). **^{1}H NMR (600 MHz, C$_6$D$_6$, 293 K):** δ 9.01 (br s, 1H, DMAP), 8.21 (br s, 1H, DMAP), 7.30 (dd, 1H, Ar), 7.24-7.19 (m, 3H, Ar), 7.12 (dd, 1H, Ar), 7.09 (dd, 1H, Ar), 5.88 (br s, 1H, DMAP), 5.79 (br s, 1H, DMAP), 5.33 (s, 1H, *H*C(C(Me)NAr)$_2$), 3.85 (sep, 1H, C*H*Me$_2$), 3.15 (sep, 1H, C*H*Me$_2$), 3.11 (sep, 1H, C*H*Me$_2$), 2.95 (sep, 1H, C*H*Me$_2$), 2.68 (sep, 1H, C*H*Me$_2$), 2.09 (s, 6H, DMAP), 2.03 (s, 3H, HC(C(*Me*)NAr)$_2$), 1.86 (s, 3H, HC(C(*Me*)NAr)$_2$), 1.82 (d, 3H, CH*Me*$_2$), 1.68 (d, 3H, CH*Me*$_2$), 1.33 (d, 3H, CH*Me*$_2$), 1.18 (d, 3H, CH*Me*$_2$), 1.09 (d, 3H, CH*Me*$_2$), 1.07 (d, 2H, CH*Me*$_2$), 1.06 (s, 9H, ^{t}Bu), 1.04 (s, 3H, CH*Me*$_2$), 0.97 (s, 3H, CH*Me*$_2$). **^{13}C{^{1}H} NMR (400 MHz, C$_6$D$_6$, 293 K):** δ 165.3 (HC(*C*(Me)NAr)$_2$), 162.6 (HC(*C*(Me)NAr)$_2$), 154.0 (Ar), 149.7

(Ar), 149.6 (Ar), 144.3 (Ar), 143.8 (Ar), 142.0 (Ar), 141.8 (Ar), 126.0 (Ar), 125.8 (Ar), 124.1 (Ar), 123.9 (Ar), 123.6 (Ar), 123.5 (Ar), 105.7 (DMAP), 96.7 (H*C*(C(Me)NAr)$_2$), 65.4 (C$_\alpha$, ^{t}Bu), 38.3 (DMAP Me), 31.1 (C$_\beta$, ^{t}Bu), 29.2 (*C*HMe$_2$), 28.8 (*C*HMe$_2$), 28.5 (*C*HMe$_2$), 28.3 (*C*HMe$_2$), 25.8 (CH*Me*$_2$), 25.7 (CH*Me*$_2$), 25.7 (HC(C(*Me*)NAr)$_2$), 25.6 (HC(C(*Me*)NAr)$_2$), 25.4 (CH*Me*$_2$), 25.2 (CH*Me*$_2$), 25.1 (CH*Me*$_2$), 25.0 (CH*Me*$_2$), 24.9 (CH*Me*$_2$), 24.7 (CH*Me*$_2$). Anal. calcd (%) for $Ta_1O_2N_5C_{41}H_{60}$: C, 58.91; H, 7.24; N, 8.38. Found: C, 58.79; H, 7.40; N, 8.29. FT-IR (KBr, nujol, cm^{-1}): 1949 (s), 1845 (s). MP: dec. 185–195 ˚C.

(BDI)Ta(N^{t}Bu)(CO)$_2$ (4.8): Compound 4.**2** (241 mg, 0.360 mmol) was added to a 100 mL flask and dissolved in 25 mL hexane. The solution was cooled to -77 ˚C, and then the flask was evacuated under reduced pressure for ca. 5 s with stirring. The headspace was then refilled with 1 atm CO. The solution was allowed to slowly come to room temperature with stirring over 3 h, resulting in a color change from pale yellow to brown. The solution was then cannula filtered and concentrated, and then stored at -40 ˚C overnight, yielding green crystals of **4.8**. The crystals were isolated and residual solvent was removed under vacuum (145 mg, 55%). **^{1}H NMR (500 MHz, C$_6$D$_6$, 293 K):** δ 7.18 (dd, 2H, Ar), 7.10 (m, 4H, Ar), 5.43 (s, 1H, *H*C(C(Me)NAr)$_2$), 2.91 (sep, 4H, C*H*Me$_2$), 1.76 (s, 6H, HC(C(*Me*)NAr)$_2$), 1.48 (d, 12H, CH*Me*$_2$), 1.11 (d, 12H, CH*Me*$_2$), 0.82 (s, 9H, ^{t}Bu). **^{13}C{^{1}H} NMR (600 MHz, C$_6$D$_6$, 293 K):** δ 165.9 (HC(*C*(Me)NAr)$_2$), 148.9 (Ar), 141.8 (Ar), 126.7 (Ar), 124.0 (Ar), 102.4 (H*C*(C(Me)NAr)$_2$), 66.5 (C$_\alpha$, ^{t}Bu), 31.3 (C$_\beta$, ^{t}Bu), 28.9 (*C*HMe$_2$), 25.4 (CH*Me*$_2$), 24.7 (HC(C(*Me*)NAr)$_2$), 24.5 (CH*Me*$_2$). Anal. calcd (%) for $Ta_1O_2N_3C_{35}H_{50}$: C, 57.92; H, 6.94; N, 5.79. Found: C, 57.88; H, 7.11; N, 5.68. FT-IR (KBr, nujol, cm^{-1}): 1975 (s), 1959 (s), 1869 (s). MP: dec. 181–187 ˚C.

{ArNC(Me)CHC(Me)N[2-(CHMeCH$_2$)-6-^{i}Pr-C$_6$H$_3$]}(η^2-N(Xyl)CH)Ta(N^{t}Bu) (4.9a, 4.9b): Diethyl ether (60 mL) was added to a 100 mL flask containing **4.2** (276 mg, 0.412 mol), resulting in a pale yellow solution. Diethyl ether (20 mL) was added to a separate 100 mL flask containing 2,6-dimethylphenylisocyanide (52 mg, 0.40 mmol), resulting in a colorless solution. The resulting solutions were both cooled to -80 ˚C with stirring, and then the isocyanide solution was transferred to the flask containing **4.2** via cannula. The solution was stirred at -80˚ C for 30 minutes, and then allowed to warm to room temperature. Upon warming to room temperature, the solution became darker yellow. The solution was stirred at room temperature for 2 h. The volatile materials were removed under vacuum, and the resulting pale yellow-green residue was extracted with hexanes (75 mL) and the resulting solution was filtered and concentrated. The solution was stored at -40 ˚C for 1 week to give **4.9a** and **4.9b** as a pale yellow microcrystalline powder, which was isolated and residual solvent was removed under vacuum. X-ray quality crystals were obtained from slow evaporation of benzene solvent. Yield: 169 mg, 52% over 3 crops in ~3:1 ratio of **4.9a** to **4.9b**. **^{1}H NMR (600 MHz, C$_6$D$_6$)** Compound **4.9a**: δ 10.37 (s, 1H, TaC(NXyl)*H*), 7.34 (d, 1H, Ar), 7.20 (t, 1H, Ar), 7.16-7.01 (m, 4H, Ar), 6.95 (d, 1H, Xyl), 6.87 (t, 1H, Xyl), 6.80 (d, 1H, Xyl), 5.28 (s, 1H, *H*C(C(Me)NAr)$_2$), 3.56 (sep, 1H, C*H*Me$_2$), 3.17 (sep, 1H, C*H*Me$_2$), 3.08 (m, 1H, MeC*H*CH$_2$Ta), 2.66 (dd, 1H, TaC*H*$_2$, ^{2}J = 15 Hz, ^{3}J = 12 Hz), 2.54 (sep, 1H, C*H*Me$_2$), 2.39 (s, 3H, Xyl), 1.86 (m, 1H, TaC*H*$_2$), 1.84 (s, 3H, Xyl), 1.71 (d, 3H, *Me*CHCH$_2$Ta), 1.67 (s, 3H, HC(C(*Me*)NAr)$_2$), 1.62 (s, 3H, HC(C(*Me*)NAr)$_2$), 1.58 (d, 3H, CH*Me*$_2$), 1.20 (d, 3H, CH*Me*$_2$), 1.13 (d, 3H, CH*Me*$_2$), 1.07 (d, 3H, CH*Me*$_2$), 0.92 (s, 9H, ^{t}Bu), 0.80 (d, 3H, CH*Me*$_2$), 0.63 (d, 3H, CH*Me*$_2$). Compound **4.9b**: δ 10.39 (s, 1H, TaC(NXyl)*H*), 7.22 (d, 1H, Ar), 7.16-7.01 (m, 5H, Ar),

6.95 (m, 1H, Xyl), 6.87 (m, 1H, Xyl), 6.79 (m, 1H, Xyl), 5.23 (s, 1H, *H*C(C(Me)NAr)$_2$), 4.77 (m, 1H, MeC*H*CH$_2$Ta), 3.52 (sep, 1H, C*H*Me$_2$), 3.25 (sep, 1H, C*H*Me$_2$), 3.05 (m, 1H, TaC*H*$_2$), 2.55 (m, 1H, C*H*Me$_2$), 2.36 (s, 3H, Xyl), 1.85 (m, 1H, TaC*H*$_2$), 1.84 (s, 3H, Xyl), 1.65 (s, 2H, HC(C(*Me*)NAr)$_2$), 1.55 (d, 3H, CH*Me*$_2$), 1.26 (d, 3H, *Me*CHCH$_2$Ta), 1.20 (d, 3H, CH*Me*$_2$), 1.13 (d, 3H, CH*Me*$_2$), 1.09 (d, 3H, CH*Me*$_2$), 0.94 (s, 9H, ^{t}Bu), 0.77 (d, 3H, CH*Me*$_2$), 0.58 (d, 3H, CH*Me*$_2$). **^{13}C{^{1}H} NMR (600 MHz, C$_6$D$_6$)** Compound **4.9a**: δ 167.3 (HC(*C*(Me)NAr)$_2$), 162.6 (HC(*C*(Me)NAr)$_2$), 152.2 (Ar), 146.8 (Ar), 145.2 (Xyl), 144.9 (Ar), 142.6 (Ar), 142.2 (Ar), 139.5 (Ar), 132.0 (Xyl), 130.3 (Xyl), 129.6 (Xyl), 128.7 (Xyl), 126.2 (Xyl), 126.0 (Ar), 125.7 (Ar), 124.8 (Ar), 124.0 (Ar), 123.7 (Ar), 121.6 (Ar), 104.2 (H*C*(C(Me)NAr)$_2$), 73.8 (Ta*C*H$_2$), 64.2 (C$_\alpha$, ^{t}Bu), 36.4 (Me*C*HCH$_2$Ta), 32.4 (C$_\beta$, ^{t}Bu), 28.4 (*C*HMe$_2$) , 27.9 (*C*HMe$_2$), 27.1 (*C*HMe$_2$), 25.9 (HC(C(*Me*)NAr), 25.5 (CH*Me*$_2$), 25.5 (CH*Me*$_2$), 25.3 (CH*Me*$_2$), 24.9 (CH*Me*$_2$), 24.7 (CH*Me*$_2$), 24.2 (CH*Me*$_2$), 24.2 (CH*Me*$_2$), 23.9 (HC(C(*Me*)NAr), 19.2 (Xyl), 18.3 (Xyl). Anal. calcd (%) for Ta$_1$N$_4$C$_{42}$H$_{59}$: C, 62.99; H, 7.43; N, 7.00. Found: C, 62.60; H, 7.36; N, 6.66. MP: dec. 151–159 ˚C.

{ArNC(Me)CHC(Me)N[2-(CHMeCH$_2$CN(Xyl)C(H)N(Xyl))-6-^{i}Pr-C$_6$H$_3$]}Ta(N^{t}Bu) (4.10): Diethyl ether (100 mL) was cooled to -80 ˚C, and then added to a 200 mL Schlenk flask containing **4.2** (600 mg, 0.896 mmol) and 2,6-dimethylphenylisocyanide (247 mg, 1.88 mmol), resulting in a pale yellow-green solution. The solution was stirred for 2 h at room temperature. As the solution warmed to room temperature, it became progressively dark green-blue. The volatile materials were removed under vacuum, and the residue was extracted with hexanes (3 x 50 mL) and filtered to give a dark green-blue filtrate. The solution was concentrated and stored at -40 ˚C overnight, yielding **4.10** as a dark green crystalline solid, which was isolated and residual solvent was removed under vacuum. Yield: 506 mg, 61% over two crops. Alternatively, **4.10** can be prepared from the reaction of **4.9** with one equivalent of 2,6-dimethylphenylisocyanide. **^{1}H NMR (400 MHz, C$_6$D$_6$):** δ 7.13-7.01 (m, 5H, Ar), 6.95 (d, 1H, Xyl), 6.85 (t, 1H, Xyl), 6.82 (t, 1H, Xyl), 6.76 (m, 2H, Ar and Xyl), 6.68 (d, 1H, Xyl), 6.59 (d, 1H, Xyl), 5.52 (s, 1H, Ta=CN(Xyl)C*H*N(Xyl)), 5.31 (s, 1H, *H*C(C(Me)NAr)$_2$), 5.18 (dd, 1H, Ta=CC*H*$_2$CH(Me)Ar, ^{2}J = 15 Hz, ^{3}J = 3.6 Hz), 4.16 (dqd, 1H, Ta=CCH$_2$C*H*(CH$_3$)Ar, ^{3}J(CH$_2$) = 12 Hz, ^{3}J(CH$_3$) = 7.0 Hz, ^{3}J(CH$_2$)' = 3.6 Hz), 3.38 (sep, 1H, C*H*Me$_2$), 3.02 (m, 2H, C*H*Me$_2$), 2.47 (s, 3H, Xyl), 2.35 (dd, 1H, Ta=CC*H*$_2$CH(CH$_3$)Ar, ^{2}J = 15 Hz, ^{3}J = 12 Hz , 1.98 (s, 3H, Xyl), 1.66 (s, 3H, HC(C(*Me*)NAr)$_2$), 1.62 (s, 3H, Xyl), 1.61 (s, 9H, ^{t}Bu), 1.56 (s, 3H, HC(C(*Me*)NAr)$_2$), 1.46 (d, 3H, Ta=CCH$_2$CH(*Me*)Ar), 1.33 (d, 3H, CH*Me*$_2$), 1.29 (s, 3H, Xyl), 1.23 (d, 3H, CH*Me*$_2$), 1.22 (d, 3H, CH*Me*$_2$), 1.14 (d, 3H, CH*Me*$_2$), 1.07 (d, 3H, CH*Me*$_2$), 0.86 (d, 3H, CH*Me*$_2$). ^{13}CNMR (500 MHz, C$_6$D$_6$): 170.7 (HC(*C*(Me)NAr)$_2$), 167.4 (HC(*C*(Me)NAr)$_2$), 151.7 (Ar), 149.6 (Ar), 149.0 (Xyl), 141.8 (Ar), 141.5 (Ta=*C*), 141.3 (Ar), 140.4 (Ar), 136.7 (Xyl), 135.7 (Xyl), 135.1 (Xyl), 133.0 (Ar or Xyl), 132.8 (Ta=CN(Xyl)*C*HN(Xyl)), 128.7 (Xyl), 128.4 (Ar or Xyl), 128.2 (Ar or Xyl) 128.0 (Xyl), 127.8 (Ar), 127.7 (Xyl) 127.4 (Xyl), 125.9 (Ar or Xyl), 125.3 (Ar), 124.5 (Xyl), 124.2 (Xyl), 123.9 (Ar), 123.6 (Ar), 122.7 (Ar), 107.3 (H*C*(C(Me)NAr)$_2$), 68.6 (C$_\alpha$, ^{t}Bu), 46.6 (Ta=C*C*H$_2$CH(CH$_3$)Ar), 36.3 (Ta=CCH$_2$*C*H(CH$_3$)Ar), 34.9 (C$_\beta$, ^{t}Bu), 28.7 (*C*HMe$_2$), 28.4 (*C*HMe$_2$), 28.1 (*C*HMe$_2$), 26.8 (HC(C(*Me*)NAr)$_2$), 26.7 (CH*Me*$_2$), 26.2 (CH*Me*$_2$), 25.6 (CH*Me*$_2$), 25.3 (CH*Me*$_2$), 24.4 (CH*Me*$_2$), 24.4 (HC(C(*Me*)NAr)$_2$), 23.3 (CH*Me*$_2$), 20.7 (Xyl), 20.3 (Xyl), 19.2 (CH*Me*$_2$), 18.2 (Xyl), 16.7 (Xyl). Anal. calcd (%) for Ta$_1$N$_5$C$_{51}$H$_{68}$: C, 65.72; H, 7.35; N, 7.51. Found: C, 65.97; H, 7.68; N, 7.21. MP: dec. 154–176 ˚C.

[{ArNC(Me)CHC(Me)N[2-(CHMeCH$_2$CN(Xyl)C(H)N(Xyl))-6-^{i}Pr-C$_6$H$_3$]}Ta(N^{t}Bu)][B(C$_6$F$_5$)$_4$] (4.11): Diethyl ether (5 mL) was added to **4.10** (100 mg, 0.11 mmol) in a 20 mL scintillation vial, resulting in a dark green-blue solution. In a separate 20 mL scintillation vial, AgB(C$_6$F$_5$)$_4$·Et$_2$O (120 mg, 0.14 mmol) was dissolved in diethyl ether (5 mL). Both vials were cooled to -40 ˚C, and the Ag^+ solution was transferred to the solution of **4.10** while stirring. The color of the solution changed from dark green to dark brown with a dark precipitate, and the solution was stirred while being allowed to warm to room temperature for 10 minutes. The suspension was filtered through a pad of Celite to remove silver metal. Upon standing at room temperature, **4.11** began to precipitate from the diethyl ether solution as a dark brown crystalline solid. The suspension was stored at -40 ˚C overnight, resulting in the formation of additional crystals, which were isolated and residual solvent was removed under vacuum. Yield: 66 mg, 37%. No peaks were observed in the ^{1}H NMR or ^{13}C NMR spectra of **4.11** due to its paramagnetism. Anal. calcd (%) for Ta$_1$F$_{20}$N$_5$C$_{75}$B$_1$H$_{68}$: C, 55.91; H, 4.25; N, 4.35. Found: C, 55.85 H, 4.31; N, 4.27. MP: dec. 143–173 ˚C.

[{ArNC(Me)CHC(Me)N[2-(CHMeCHCN(Xyl)C(H)N(Xyl))-6-^{i}Pr-C$_6$H$_3$]}Ta(N^{t}Bu)][B(C$_6$F$_5$)$_4$] (4.12): Diethyl ether (5 mL) was added to **4.10** (100 mg, 0.11 mmol) in a 20 mL scintillation vial, resulting in a dark green-blue solution. In a separate 20 mL scintillation vial, AgB(C$_6$F$_5$)$_4$·Et$_2$O (250 mg, 0.29 mmol) was dissolved in diethyl ether (5 mL). Both vials were cooled to -40 ˚C, and the Ag^+ solution was transferred to the solution of **4.10** while stirring. The color of the solution changed from dark green to dark brown to yellow with a dark precipitate, and the solution was stirred while being allowed to warm to room temperature for 10 minutes. The suspension was filtered through a pad of Celite to remove silver metal. Upon standing at room temperature, **4.12** began to precipitate from the diethyl ether solution as a yellow crystalline solid. The suspension was stored at -40 ˚C overnight, resulting in the formation of additional crystals, which were isolated and residual solvent was removed under vacuum. Yield: 106 mg, 59%. **^{1}H NMR (600 MHz, CDCl$_3$):** δ 7.32 (s, 1H, TaCN(Xyl)C*H*N(Xyl)), 7.22-7.07 (m, 7H, Ar), 6.97 (d, 2H, Ar), 6.82 (t, 1H, Ar), 6.73 (d, 1H, Ar), 6.45 (d, 1H, Ar), 6.31 (s, 1H, *H*C(C(Me)NAr)$_2$), 5.76 (d, 1H, TaCC*H*=CH(Me)Ar), 4.56 (quint, 1H, TaCCH=C*H*(CH$_3$)Ar), 2.90 (sep, 1H, C*H*Me$_2$), 2.68 (sep, 1H, C*H*Me$_2$), 2.65 (sep, 1H, C*H*Me$_2$), 2.44 (s, 3H, Xyl), 2.25 (s, 3H, Xyl), 2.02 (s, 3H, HC(C(*Me*)NAr)$_2$), 1.96 (s, 3H, HC(C(*Me*)NAr)$_2$), 1.68 (s, 3H, Xyl), 1.62 (s, 3H, Xyl), 1.43 (d, 3H, TaCCH=CH(*Me*)Ar), 1.42 (s, 3H, Xyl), 1.38 (d, 3H, CH*Me*$_2$), 1.34 (s, 9H, ^{t}Bu), 1.17 (s, 3H, Xyl), 1.14 (d, 3H, CH*Me*$_2$), 1.10 (d, 3H, CH*Me*$_2$), 1.01 (d, 3H, CH*Me*$_2$), 0.95 (d, 3H, CH*Me*$_2$). **^{13}C{^{1}H} NMR (600 MHz, CDCl$_3$):** 190.6 (Ta*C*N(Xyl)CHN(Xyl)), 176.4 (HC(*C*(Me)NAr)$_2$), 163.6 (TaCN(Xyl)*C*HN(Xyl)), 161.0 (HC(*C*(Me)NAr)$_2$), 145.9 (Ar), 144.8 (Ar), 149.0 (Xyl), 143.0 (Ar), 141.6 (Ar), 141.3 (Ar), 140.6 (Ar), 140.2 (Ar), 135.6 (Ar), 135.5 (Ar), 135.3 (Ar), 133.6 (Ar), 132.6 (Ar), 130.2 (Ar), 130.0 (Ar), 129.3 (Ar) 129.2 (Ar), 129.0 (Ar), 128.7 (Ar) 128.2 (Ar), 127.9 (Ar), 125.0 (Ar), 124.9 (Ar), 124.7 (Ar), 122.3 (Ar), 108.0 (H*C*(C(Me)NAr)$_2$), 71.9 (C$_\alpha$, ^{t}Bu), 36.6 (TaCCH=*C*H(CH$_3$)Ar), 32.8 (C$_\beta$, ^{t}Bu), 29.7 (HC(C(*Me*)NAr)$_2$), 29.4 (*C*HMe$_2$), 29.2 (*C*HMe$_2$), 28.6 (*C*HMe$_2$), 26.3 (CH*Me*$_2$), 25.7 (CH*Me*$_2$), 25.5 (HC(C(*Me*)NAr)$_2$), 25.5 (CH*Me*$_2$), 24.8 (CH*Me*$_2$), 24.0 (CH*Me*$_2$), 23.5 (CH*Me*$_2$), 20.7 (Xyl), 19.6 (Xyl), 17.7 (Xyl), 16.6 (CH*Me*$_2$), 16.0 (Xyl). Anal. calcd (%) for Ta$_1$F$_{20}$N$_5$C$_{75}$B$_1$H$_{67}$: C, 55.95; H, 4.19; N, 4.35. Found: C, 55.88 H, 4.10; N, 4.27. MP: dec. 190–240 ˚C.

{ArNC(Me)C(H)C(Me)(C(Ph)=C(Ph))C(O)NAr}Ta(N^{t}Bu) (4.13): Compound **4.8** (200 mg, 0.27 mmol) and diphenylacetylene (48 mg, 0.27 mmol) were dissolved in 10 mL hexane in a 20 mL vial. The resulting solution was left at room temperature for 18 h, resulting in a slow color change from green to yellow. The solution was concentrated and stored at -40 ˚C overnight, yielding yellow crystals of **4.13**. Yield: 160 mg, 68% over two crops. X-ray suitable crystals were obtained by recrystallization from a concentrated *n*-pentane solution at -40 °C. **^{1}H NMR (600 MHz, C$_6$D$_6$, 293 K):** δ 7.26 (dd, 1H, Ar or Ph), 7.22–7.18 (m, 2H, Ar/Ph), 7.18–7.07 (m, 6H, Ar/Ph), 7.03 (t, 2H, Ph), 6.99 (dd, 1H, Ar or Ph), 6.94 (m, 1H, Ar or Ph), 6.89–6.81 (m, 3H, Ar/Ph), 4.57 (s, 1H, *H*C(C(Me)NAr)), 4.02 (sep, 1H, C*H*Me$_2$), 3.41 (sep, 1H, C*H*Me$_2$), 3.13 (sep, 1H, C*H*Me$_2$), 2.90 (sep, 1H, C*H*Me$_2$), 1.87 (s, 3H, HC(C(*Me*)C(O)NAr)), 1.64 (d, 3H, CH*Me*$_2$), 1.57 (s, 3H, HC(C(*Me*)NAr)), 1.41 (d, 3H, CH*Me*$_2$), 1.40 (d, 3H, CH*Me*$_2$), 1.38 (d, 3H, CH*Me*$_2$), 1.35 (d, 3H, CH*Me*$_2$), 1.34 (d, 3H, CH*Me*$_2$), 1.10 (d, 3H, CH*Me*$_2$), 0.93 (br d, 3H, CH*Me*$_2$), 0.79 (s, 9H, ^{t}Bu). **^{13}C{^{1}H} NMR (600 MHz, C$_6$D$_6$, 293 K):** δ 210.4 (HC(C(Me)*C*(O)NAr), 174.7 (HC(*C*(Me)NAr)), 150.0 (Ar or Ph or Ph*C*=*C*Ph), 146.2 (Ar or Ph or Ph*C*=*C*Ph), 145.3 (Ar or Ph or Ph*C*=*C*Ph), 145.2 (Ar or Ph or Ph*C*=*C*Ph), 143.7 (Ar or Ph or Ph*C*=*C*Ph), 143.6 (Ar or Ph or Ph*C*=*C*Ph), 143.3 (Ar or Ph or Ph*C*=*C*Ph), 143.1 (Ar or Ph or Ph*C*=*C*Ph), 142.9 (Ar or Ph or Ph*C*=*C*Ph), 140.9 (Ar or Ph or Ph*C*=*C*Ph), 129.9 (Ar or Ph), 129.4 (Ar or Ph), 128.7 (Ar or Ph), 128.5 (Ar or Ph), 127.4 (Ar or Ph), 127.2 (Ph), 127.2 (Ar or Ph), 127.0 (Ar or Ph), 125.8 (Ph), 124.1 (Ar or Ph), 123.9 (Ar or Ph), 123.5 (Ar or Ph), 123.5 (Ar or Ph), 102.0 (H*C*(C(Me)NAr)), 69.9 (HC(*C*(Me)C(O)NAr)), 52.9 (C$_\alpha$, ^{t}Bu), 33.3 (HC(C(*Me*)C(O)NAr)), 32.6 (C$_\beta$, ^{t}Bu), 30.3 (*C*HMe$_2$), 29.4 (*C*HMe$_2$), 29.0 (*C*HMe$_2$), 28.5 (*C*HMe$_2$), 26.3 (CH*Me*$_2$), 25.4 (CH*Me*$_2$), 25.4 (CH*Me*$_2$), 24.5 (CH*Me*$_2$), 24.4 (CH*Me*$_2$), 24.3 (CH*Me*$_2$), 24.0 (CH*Me*$_2$), 23.9 (HC(C(*Me*)NAr)), 23.6 (CH*Me*$_2$). Anal. calcd (%) for Ta$_1$O$_1$N$_3$C$_{48}$H$_{60}$: C, 65.82; H, 6.90; N, 4.80. Found: C, 65.75; H, 6.79; N, 4.87. MP: dec. 112–140 ˚C.

[(BDI)Ta(N^{t}Bu)(CO)$_2$N$_3$][^{n}Bu$_4$N] (4.14): Compound **4.8** (400 mg, 0.55 mmol) was dissolved in 5 mL toluene in a 20 mL vial. In a separate vial, tetrabutylammonium azide (160 mg, 0.55 mmol) was dissolved in 5 mL toluene. The azide solution was added to the solution of **4.8**, resulting in an immediate color change from green to red. The solution was left at room temperature for 30 minutes, and then the volatile materials were removed under vacuum, leaving a red residue. The residue was triturated with hexane, and then extracted with diethyl ether. The resulting red solution was concentrated and stored at -40 ˚C overnight, yielding red crystals of **4.14**. Yield: 500 mg, 90% over two crops. **^{1}H NMR (600 MHz, C$_6$D$_6$, 293 K):** δ 7.40 (dd, 2H, Ar), 7.29 (dd, 2H, Ar), 7.19 (t, 2H, Ar), 4.98 (s, 1H, *H*C(C(Me)NAr)$_2$), 4.64 (br s, 2H, C*H*Me$_2$), 4.06 (sep, 2H, C*H*Me$_2$), 2.31 (m, 8H, NC*H*$_2$CH$_2$CH$_2$CH$_3$), 1.81 (s, 6H, HC(C(*Me*)NAr)$_2$), 1.79 (d, 6H, CH*Me*$_2$), 1.71 (br d, 6H, CH*Me*$_2$), 1.59 (br s, 9H, ^{t}Bu), 1.48 (br d, 6H, CH*Me*$_2$), 1.38 (d, 6H, CH*Me*$_2$), 0.98–0.83 (m, 16H, NCH$_2$C*H*$_2$C*H*$_2$CH$_3$), 0.72 (t, 12H, NCH$_2$CH$_2$CH$_2$C*H*$_3$). **^{13}C{^{1}H} NMR (600 MHz, C$_6$D$_6$, 293 K):** δ 165.1 (HC(*C*(Me)NAr)$_2$), 152.2 (Ar), 144.3 (Ar), 143.3 (Ar), 124.7 (Ar), 124.4 (Ar), 123.8 (Ar), 99.7 (H*C*(C(Me)NAr)$_2$), 64.8 (C$_\alpha$, ^{t}Bu), 58.3 (N*C*H$_2$CH$_2$CH$_2$CH$_3$), 33.3 (C$_\beta$, ^{t}Bu), 29.1 (*C*HMe$_2$), 28.2 (*C*HMe$_2$), 26.1 (CH*Me*$_2$), 25.9 (CH*Me*$_2$), 25.7 (CH*Me*$_2$), 25.7 (CH*Me*$_2$), 25.1 (HC(C(*Me*)NAr)$_2$), 23.7 (NCH$_2$*C*H$_2$CH$_2$CH$_3$), 19.6 (NCH$_2$CH$_2$*C*H$_2$CH$_3$), 13.7 (NCH$_2$CH$_2$CH$_2$*C*H$_3$). Anal. calcd (%) for Ta$_1$O$_2$N$_7$C$_{51}$H$_{86}$: C, 60.63; H, 8.58; N, 9.71. Found: C, 60.40; H, 8.43; N, 9.79. MP: dec. 114–126 ˚C.

[{ArNC(Me)C(H)C(Me)C(O)NAr}Ta(N^{t}Bu)N$_3$][^{n}Bu$_4$N] (4.15): Compound **4.14** (200 mg, 0.20 mmol) was dissolved in 20 mL toluene in a 100 mL Schlenk flask to give a red solution. The solution was irradiated with UV light in a photo-reactor under N_2 atmosphere for 16 h, resulting in a color change from red to orange. The volatile materials were removed under vacuum, leaving an orange residue. The residue was triturated with hexane, and then extracted with toluene. The resulting orange solution was concentrated and stored at -40 ˚C overnight, yielding yellow crystals of **4.15**. Yield: 68 mg, 35% over two crops. X-ray suitable crystals were obtained by recrystallization from a concentrated diethyl ether solution at -40 °C. **^{1}H NMR (600 MHz, C$_6$D$_6$, 293 K):** δ 7.30 (dd, 1H, Ar), 7.19–7.15 (m, 3H, Ar), 7.13 (dd, 1H, Ar), 6.91 (t, 1H, Ar), 5.69 (s, 1H, *H*C(C(Me)NAr)), 4.30 (sep, 1H, C*H*Me$_2$), 4.17 (sep, 1H, C*H*Me$_2$), 4.15 (sep, 2H, C*H*Me$_2$), 2.72–2.67 (m, 11H, HC(C(*Me*)C(O)NAr)/NC*H*$_2$CH$_2$CH$_2$CH$_3$), 1.85 (d, 3H, CH*Me*$_2$), 1.81 (s, 9H, ^{t}Bu), 1.72 (s, 3H, HC(C(*Me*)NAr)), 1.51 (d, 6H, CH*Me*$_2$), 1.47 (d, 3H, CH*Me*$_2$), 1.31 (d, 6H, CH*Me*$_2$), 1.30 (d, 3H, CH*Me*$_2$), 1.20 (d, 3H, CH*Me*$_2$), 1.17–1.10 (m, 16H, NCH$_2$C*H*$_2$C*H*$_2$CH$_3$), 0.88 (t, 12H, NCH$_2$CH$_2$CH$_2$C*H*$_3$). **^{13}C{^{1}H} NMR (600 MHz, C$_6$D$_6$, 293 K):** δ 154.4 (HC(*C*(Me)NAr)), 147.0 (Ar), 146.7 (Ar), 145.3 (Ar), 143.3 (Ar), 126.1 (Ar), 124.0 (Ar), 123.7 (Ar), 121.9 (Ar), 120.5 (Ar), 111.7 (H*C*(C(Me)NAr)), 71.0 (HC(*C*(Me)C(O)NAr)), 58.7 (N*C*H$_2$CH$_2$CH$_2$CH$_3$), 53.4 (C$_\alpha$, ^{t}Bu), 30.6 (C$_\beta$, ^{t}Bu), 28.2 (*C*HMe$_2$), 28.1 (*C*HMe$_2$), 27.8 (*C*HMe$_2$), 25.7 (CH*Me*$_2$), 25.5 (HC(C(*Me*)C(O)NAr)), 25.4 (CH*Me*$_2$), 25.3 (CH*Me*$_2$), 25.0 (CH*Me*$_2$), 24.1 (CH*Me*$_2$), 24.1 (NCH$_2$*C*H$_2$CH$_2$CH$_3$), 24.1 (CH*Me*$_2$), 20.0 (NCH$_2$CH$_2$*C*H$_2$CH$_3$), 18.5 (HC(C(*Me*)NAr)), 13.9 (NCH$_2$CH$_2$CH$_2$*C*H$_3$). Anal. calcd (%) for Ta$_1$O$_1$N$_7$C$_{50}$H$_{86}$: C, 61.14; H, 8.83; N, 9.98. Found: C, 61.47; H, 8.96; N, 9.80. MP: 148–156 ˚C.

Cyclic Voltammetry Studies: Electrochemical data were obtained with a BASi Epsilon potentiostat at room temperature using a glassy carbon working electrode, a platinum counter electrode, and a silver wire floating reference electrode. Cyclic voltammograms were recorded in a glovebox at room temperature in dichloromethane solution containing 0.1 M [^{n}Bu$_4$N][PF$_6$] as the supporting electrolyte and 0.001M of **4.10**. All potentials were referenced against a [Cp$_2$Fe]0/+ internal standard.

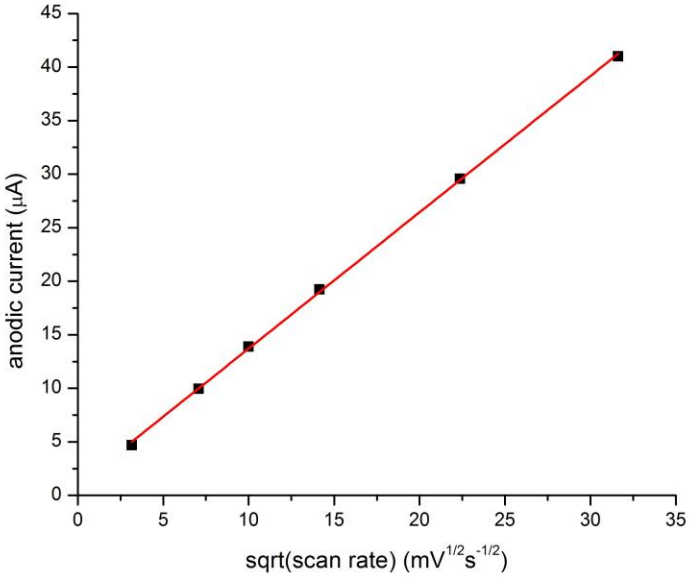

Figure 4.11 Plot (R^2 = 0.9996) of i_{pa} vs. sqrt(scan rate) from 10 to 1000 mV/s for **4.10**.

EPR Measurements: Solution EPR spectra were obtained with a Varian E-12 spectrometer, an EIP-547 microwave frequency counter, and a Varian E-500 gaussmeter, which was calibrated using 2,2-diphenyl-1-picrylhydrazyl (DPPH, g¼ 2.0036). The spectral simulations were performed with EasySpin.[77]

DFT Calculations: Structures were calculated using the Gaussian09 suite of programs.[78] Self-consistent field computations were performed with tight convergence criteria on ultrafine grids, while geometry optimizations were converged to tight geometric convergence criteria for all compounds. The PBE pure functional[79,80] with Grimme's D3 corrections for dispersion forces[81] was used throughout this computational study. The light atoms (H, C and N) were treated with Dunning's correlation consistent polarized valence double zeta basis,[82] while the tantalum atom was treated with a Stuttgart/Dresden ECP pseudopotential (SDD).[83,84] QTAIM analyses were performed with AIMAll Version 16.01.09.[85]

X-Ray Crystallographic Studies: Single crystals of **4.2a**, **4.3**, **4.5**, **4.9**, **4.10**, **4.11**, **4.12**, **4.13**, **4.14** and **4.15** were coated in Paratone-N oil, mounted on a Kaptan loop, transferred to a Bruker APEX CCD area detector,[86] centered in the beam, and cooled by a nitrogen flow low-temperature apparatus that had been previously calibrated by a thermocouple placed at the same position as the crystal. Preliminary orientation matrices and cell constants were determined by collection of 36 10 s frames, followed by spot integration and least-squares refinement. An arbitrary hemisphere of data was collected, and the raw data were integrated using SAINT.[87] Cell dimensions reported were calculated from all reflections with $I > 10$ (Table 1). The data were corrected for Lorentz and polarization effects, but no correction for crystal decay was applied. An empirical absorption correction based on comparison of redundant and equivalent reflections was applied using SADABS.[88] Structures were solved by direct methods with the aid of successive difference Fourier maps and were refined against all data using the SHELXTL 5.0 software package.[89] Thermal

parameters for all non-hydrogen atoms were refined anisotropically. ORTEP diagrams were created using the ORTEP-3 software package[90] and Mercury.[91]

Table 4.2 Crystallographic data for compounds **4.2a**, **4.3** and **4.5**.

Compound	**4.2a · ½ C_6H_6**	**4.3 · ½ C_6H_6**	**4.5 · C_6H_6**
Empirical formula	$C_{36}H_{53}N_3Ta$	$C_{37}H_{55}N_3Ta$	$C_{46}H_{66}N_5Ta$
Formula weight (amu)	708.76	722.79	869.99
Wavelength (Å)	0.71073	0.71073	0.71073
Space group	*P*-1	*P*-1	$P2_1/n$
a (Å)	9.1595(3)	9.0824(5)	11.413(5)
b (Å)	11.4603(4)	11.2781(6)	17.448(5)
c (Å)	17.0518(6)	18.1047(9)	21.602(5)
α (°)	87.553(2)	74.765(2)	90
β (°)	81.957(2)	84.576(2)	97.815(5)
γ (°)	71.414(2)	73.290(2)	90
V (Å^3)	1679.9(1)	1713.4(2)	4262(2)
Z	2	2	4
ρ_{calcd} (g/cm^3)	1.401	1.401	1.356
μ (mm^{-1})	3.299	3.235	2.616
F_{000} (e$^-$)	726	742	1800
Crystal size (mm^3)	.10 x .06 x .06	.08 x .04 x .04	.06 x .04 x .04
Theta min / max (˚)	2.23 / 25.43	1.95 / 25.41	1.51 / 25.44
Reflections collected	32504	31904	57607
R_{int}	0.0337	0.0302	0.0466
T_{max} / T_{min}	0.7452 / 0.6457	0.8815 / 0.7818	0.9026 / 0.8588
Data / restr. / param.	6169 / 0 / 377	6289 / 0 / 383	7837 / 0 / 487
GoF	1.077	1.064	1.062
R_1 / wR_2 (I>2σ(I))	0.0310 / 0.0766	0.0184 / 0.0401	0.0287 / 0.0602
R_1 / wR_2 (all data)	0.0354 / 0.0793	0.0208 / 0.0409	0.0354 / 0.0627
Res. peak / hole (e$^-$/Å^3)	4.278 / -0.721	1.759 / -0.780	3.682 / -2.095

Table 4.3 Crystallographic data for compounds **4.9**, **4.10**, **4.11**, and **4.12**.

Compound	**4.9**	**4.10**	**4.11 · ½ Et_2O**	**4.12 · ½ Et_2O**
Empirical formula	$C_{42}H_{59}N_4Ta$	$C_{51}H_{68}N_5Ta$	$C_{77}H_{73}N_5O_{½}$ $BF_{20}Ta$	$C_{77}H_{72}N_5O_{½}$ $BF_{20}Ta$
Formula weight (amu)	800.88	932.05	1648.16	1647.15
Wavelength (Å)	0.71073	0.71073	0.71073	0.71073
Space group	$P2_12_12_1$	P-1	P-1	P-1
a (Å)	10.989(1)	11.0249(7)	13.596(2)	13.7780(7)
b (Å)	18.570(2)	12.2748(8)	16.095(2)	16.0261(9)
c (Å)	18.795(2)	17.777(1)	17.884(3)	17.5749(8)
α (°)	90	73.929(1)	96.674(8)	79.572(2)
β (°)	90	75.071(1)	112.279(5)	67.312(2)
γ (°)	90	83.673(1)	93.021(6)	86.219(2)
V ($Å^3$)	3835.4(6)	2231.7(2)	3576.8(9)	3521.6(3)
Z	4	2	2	2
ρ_{calcd} (g/cm^3)	1.387	1.387	1.530	1.553
μ (mm^{-1})	2.899	2.503	1.637	1.663
F_{000} (e^-)	1648	964	1664	1662
Crystal size (mm^3)	.14 x .10 x .04	.20 x .15 x .09	.12 x .08 x .06	.07 x .03 x .02
Theta min / max (˚)	1.54 / 25.36	1.73 / 25.41	1.62 / 25.45	1.60 / 25.40
Reflections collected	73304	8204	51203	72955
R_{int}	0.0581	0.0328	0.0419	0.0604
T_{max} / T_{min}	0.7452 / 0.5820	0.7452 / 0.6588	0.7452 / 0.6518	0.7452 / 0.6927
Data / restr. / param.	7015 / 0 / 459	8204 / 0 / 556	13089 / 0 / 980	12930 / 6 / 988
GoF	1.087	1.105	1.056	1.011
R_1 / wR_2 ($I>2\sigma(I)$)	0.0261 / 0.0572	0.0191 / 0.0564	0.0280 / 0.0578	0.0312 / 0.0570
R_1 / wR_2 (all data)	0.0289 / 0.0587	0.0198 / 0.0567	0.0348 / 0.0604	0.0424 / 0.0604
Flack parameter	0.50(1)	-	-	-
Res. peak / hole ($e^-/Å^3$)	2.480 / -0.798	0.940 / -1.059	0.632 / -0.680	1.229 / -0.565

Table 4.4 Crystallographic data for compounds **4.13**, **4.14** and **4.15**.

Compound	**4.13**	**4.14 · $C_4H_{10}O$**	**4.15**
Empirical formula	$C_{48}H_{60}N_3OTa$	$C_{55}H_{96}N_7O_3Ta$	$C_{50}H_{86}N_7OTa$
Formula weight (amu)	875.94	1084.33	982.20
Wavelength (Å)	0.71073	0.71073	0.71073
Space group	$P2_1/n$	*P*-1	*P*-1
a (Å)	11.795(5)	12.538(1)	15.846(1)
b (Å)	19.733(5)	12.866(1)	16.219(1)
c (Å)	18.398(5)	17.601(1)	21.967(1)
α (°)	90	93.269(3)	92.497(2)
β (°)	94.317(5)	92.588(3)	99.864(2)
γ (°)	90	90.765(3)	90.841(2)
V ($Å^3$)	4270(2)	2832.5(4)	5555.7(4)
Z	4	2	4
ρ_{calcd} (g/cm^3)	1.363	1.271	1.174
μ (mm^{-1})	2.612	1.986	2.016
F_{000} (e^-)	1800	1144	2064
Crystal size (mm^3)	.08 x .08 x .06	.12 x .10 x .10	.08 x .06 x .05
Theta min / max (˚)	1.52 / 25.39	1.16 / 25.45	0.94 / 25.40
Reflections collected	70000	80943	35443
R_{int}	0.0236	0.0217	0.0309
T_{max} / T_{min}	0.7452 / 0.5832	0.7452 / 0.6947	0.7452 / 0.6418
Data / restr. / param.	7830 / 0 / 491	10469 / 0 / 614	19494 / 0 / 1085
GoF	1.075	1.072	1.162
R_1 / wR_2 ($I>2\sigma(I)$)	0.0156 / 0.0378	0.0224 / 0.0583	0.0524 / 0.1268
R_1 / wR_2 (all data)	0.0166 / 0.0385	0.0232 / 0.0589	0.0737 / 0.1370
Res. peak / hole ($e^-/Å^3$)	0.957 / -0.423	4.172 / -0.929	2.902 / -1.119

Notes and References

(1) Bruck, A.; Copenhaver, A. S.; Wigley, D. E. *J. Am. Chem. Soc.* **1987**, *109*, 6525.
(2) Cotton, F. A.; Hall, W. T. *J. Am. Chem. Soc.* **1979**, *101*, 5094.
(3) Mclain, S. J.; Wood, C. D.; Schrock, R. R. *J. Am. Chem. Soc.* **1979**, *101*, 4558.
(4) Roskamp, E. J.; Pedersen, S. F. *J. Am. Chem. Soc.* **1987**, *109* (21), 6551.
(5) Labinger, J. A.; Schwartz, J. *J. Am. Chem. Soc.* **1975**, *97* (6), 1596.
(6) Fryzuk, M. D.; Kozak, C. M.; Bowdridge, M. R.; Patrick, B. O.; Rettig, S. J. *J. Am. Chem. Soc.* **2002**, *124* (28), 8389.

(7) LaPointe, R. E.; Wolczanski, P. T.; Mitchell, J. F. *J. Am. Chem. Soc.* **1986**, *108* (20), 6382.
(8) Neithamer, D. R.; LaPointe, R. E.; Wheeler, R. A.; Richeson, D. S.; Van Duyne, G. D.; Wolczanski, P. T. *J. Am. Chem. Soc.* **1989**, *111* (25), 9056.
(9) Figueroa, J. S.; Cummins, C. C. *Dalton Trans.* **2006**, 2161.
(10) Kilgore, U. J.; Yang, X.; Tomaszewski, J.; Huffman, J. C.; Mindiola, D. J. *Inorg. Chem.* **2006**, *45* (26), 10712.
(11) Hulley, E. B.; Wolczanski, P. T.; Lobkovsky, E. B. *Chem. Commun.* **2009**, 6412.
(12) Veige, A. S.; Slaughter, L. M.; Wolczanski, P. T.; Matsunaga, N.; Decker, S. A.; Cundari, T. R. *J. Am. Chem. Soc.* **2001**, *123* (26), 6419.
(13) Veige, A. S.; Kleckley, T. S.; Chamberlin, R. M.; Neithamer, D. R.; Lee, C. E.; Wolczanski, P. T.; Lobkovsky, E. B.; Glassey, W. V. *J. Organomet. Chem.* **1999**, *591*, 194.
(14) Kleckley, T. S.; Bennett, J. L.; Wolczanski, P. T.; Lobkovsky, E. B. *J. Am. Chem. Soc.* **1997**, *119* (1), 247.
(15) Gray, S. D.; Weller, K. J.; Bruck, M. A.; Briggs, P. M.; Wigley, D. E. *J. Am. Chem. Soc.* **1995**, *117*, 10678.
(16) Yu, J. S.; Fanwick, P. E.; Rothwell, I. P. *J. Am. Chem. Soc.* **1990**, *112* (22), 8171.
(17) Luca, O. R.; Crabtree, R. H. *Chem. Soc. Rev.* **2013**, *42* (4), 1440.
(18) Munhá, R. F.; Zarkesh, R. A.; Heyduk, A. F. *Dalton Trans.* **2013**, *42* (11), 3751.
(19) Nguyen, A. I.; Blackmore, K. J.; Carter, S. M.; Zarkesh, R. A.; Heyduk, A. F. *J. Am. Chem. Soc.* **2009**, *131* (9), 3307.
(20) Lu, F.; Zarkesh, R. A.; Heyduk, A. F. *Eur. J. Inorg. Chem.* **2012**, *2012* (3), 467.
(21) Zarkesh, R. A.; Ziller, J. W.; Heyduk, A. F. *Angew. Chem. Int. Ed. Engl.* **2008**, *47* (25), 4715.
(22) Nguyen, A. I.; Zarkesh, R. A.; Lacy, D. C.; Thorson, M. K.; Heyduk, A. F. *Chem. Sci.* **2011**, *2* (1), 166.
(23) Blackmore, K. J.; Lal, N.; Ziller, J. W.; Heyduk, A. F. *J. Am. Chem. Soc.* **2008**, *130*, 2728.
(24) Haneline, M. R.; Heyduk, A. F. *J. Am. Chem. Soc.* **2006**, *128* (26), 8410.
(25) Stanciu, C.; Jones, M. E.; Fanwick, P. E.; Abu-Omar, M. M. *J. Am. Chem. Soc.* **2007**, *129* (41), 12400.
(26) Tsurugi, H.; Saito, T.; Tanahashi, H.; Arnold, J.; Mashima, K. *J. Am. Chem. Soc.* **2011**, *133* (46), 18673.
(27) Toreki, R.; Vaughan, G. A.; Schrock, R. R.; Davis, W. M. *J. Am. Chem. Soc.* **1993**, *115* (1), 127.
(28) Townsend, E. M.; Kilyanek, S. M.; Schrock, R. R.; Müller, P.; Smith, S. J.; Hoveyda, A. H. *Organometallics* **2013**, *32* (16), 4612.
(29) Tomson, N. C.; Yan, A.; Arnold, J.; Bergman, R. G. *J. Am. Chem. Soc.* **2008**, *130*, 11262.
(30) Tomson, N. C.; Arnold, J.; Bergman, R. G. *Organometallics* **2010**, *29*, 2926.
(31) Tomson, N. C.; Arnold, J.; Bergman, R. G. *Organometallics* **2010**, *29*, 5010.
(32) Gianetti, T. L.; Nocton, G.; Minasian, S. G.; Tomson, N. C.; Kilcoyne, A. L. D.; Kozimor, S. A.; Shuh, D. K.; Tyliszczak, T.; Bergman, R. G.; Arnold, J. *J. Am. Chem. Soc.* **2013**, *135* (8), 3224.
(33) Gianetti, T. L.; Tomson, N. C.; Arnold, J.; Bergman, R. G. *J. Am. Chem. Soc.* **2011**, *133*, 14904.
(34) Gianetti, T. L.; Bergman, R. G.; Arnold, J. *J. Am. Chem. Soc.* **2013**, *135* (22), 8145.
(35) Obenhuber, A. H.; Gianetti, T. L.; Berrebi, X.; Bergman, R. G.; Arnold, J. *J. Am. Chem. Soc.* **2014**, *136* (8), 2994.

(36) Gianetti, T. L.; La Pierre, H. S.; Arnold, J. *Eur. J. Inorg. Chem.* **2013**, *2013* (22–23), 3771.
(37) Figueroa, J. S.; Cummins, C. C. *J. Am. Chem. Soc.* **2003**, *125* (14), 4020.
(38) Figueroa, J. S.; Piro, N. A.; Mindiola, D. J.; Fickes, M. G.; Cummins, C. C. *Organometallics* **2010**, *29* (21), 5215.
(39) Tomson, N. C.; Arnold, J.; Bergman, R. G. *Dalton Trans.* **2011**, *40* (30), 7718.
(40) Gountchev, T. I.; Tilley, T. D. *J. Am. Chem. Soc.* **1997**, *119*, 12831.
(41) Burckhardt, U.; Tilley, T. D. *J. Am. Chem. Soc.* **1999**, *121*, 6328.
(42) Burckhardt, U.; Casty, G. L.; Gavenonis, J.; Tilley, T. D. *Organometallics* **2002**, *21*, 3108.
(43) Hrobárik, P.; Hrobáriková, V.; Greif, A. H.; Kaupp, M. *Angew. Chem. Int. Ed. Engl.* **2012**, *51* (43), 10884.
(44) Karplus, M. *J. Chem. Phys.* **1959**, *30* (1), 11.
(45) Minch, M. J. *Concepts Magn. Reson.* **1994**, *6* (1), 41.
(46) Hayes, P. G.; Piers, W. E.; Lee, L. W. M.; Knight, L. K.; Parvez, M.; Elsegood, M. R. J.; Clegg, W. *Organometallics* **2001**, *20* (12), 2533.
(47) Knight, L. K.; Piers, W. E.; Fleurat-Lessard, P.; Parvez, M.; McDonald, R. *Organometallics* **2004**, *23* (9), 2087.
(48) Chu, T.; Piers, W. E.; Dutton, J. L.; Parvez, M. *Organometallics* **2012**, *32*, 1159.
(49) Kaesz, H. D.; Saillant, R. B. *Chem. Rev.* **1972**, *72* (3), 231.
(50) Rankin, M. A.; Cummins, C. C. *J. Am. Chem. Soc.* **2010**, *132* (29), 10021.
(51) Addison, A. W.; Rao, T. N.; Reedijk, J.; van Rijn, J.; Verschoor, G. C. *J. Chem. Soc. Dalt. Trans.* **1984**, 1349.
(52) Allen, F. H. *Acta Crystallogr. Sect. B Struct. Sci.* **2002**, *58* (3), 380.
(53) Thompson, M. E.; Baxter, S. M.; Bulls, A. R.; Burger, B. J.; Nolan, M. C.; Santarsiero, B. D.; Schaefer, W. P.; Bercaw, J. E. *J. Am. Chem. Soc.* **1987**, *109* (1), 203.
(54) Waterman, R. *Organometallics* **2013**.
(55) Basuli, F.; Kilgore, U. J.; Brown, D.; Huffman, J. C.; Mindiola, D. J. *Organometallics* **2004**, *23* (26), 6166.
(56) Durfee, L. D.; Rothwell, I. P. *Chem. Rev.* **1988**, *88*, 1059.
(57) Gómez, M. *Eur. J. Inorg. Chem.* **2003**, *2003* (20), 3681.
(58) Chirik, P. J.; Wieghardt, K. *Science* **2010**, *327* (5967), 794.
(59) Cui, P.; Iluc, V. M. *Chem. Sci.* **2015**, *6* (12), 7343.
(60) Obenhuber, A. H.; Gianetti, T. L.; Bergman, R. G.; Arnold, J. *Chem. Commun.* **2014**, *51*, 1278.
(61) Okuniewski, A.; Rosiak, D.; Chojnacki, J.; Becker, B. *Polyhedron* **2015**, *90*, 47.
(62) Mindiola, D. J.; Meyer, K.; Cherry, J.-P. F.; Baker, T. A.; Cummins, C. C. *Organometallics* **2000**, *19*, 1622.
(63) Figueroa, J. S.; Piro, N. A.; Clough, C. R.; Cummins, C. C. *J. Am. Chem. Soc.* **2006**, *128* (3), 940.
(64) Tran, B. L.; Pink, M.; Gao, X.; Park, H.; Mindiola, D. J. *J. Am. Chem. Soc.* **2010**, *132* (5), 1458.
(65) Critchlow, S. C.; Lerchen, M. E.; Smith, R. C.; Doherty, N. M. *J. Am. Chem. Soc.* **1988**, *110* (24), 8071.
(66) Johnson, C. E.; Kysor, E. A.; Findlater, M.; Jasinski, J. P.; Metell, A. S.; Queen, J. W.; Abernethy, C. D. *Dalton Trans.* **2010**, *39* (14), 3482.
(67) Groysman, S.; Villagrán, D.; Freedman, D. E.; Nocera, D. G. *Chem. Commun.* **2011**, *47* (37), 10242.

(68) Tran, B. L.; Pinter, B.; Nichols, A. J.; Konopka, F. T.; Thompson, R.; Chen, C.-H.; Krzystek, J.; Ozarowski, A.; Telser, J.; Baik, M.-H.; Meyer, K.; Mindiola, D. J. *J. Am. Chem. Soc.* **2012**, *134* (31), 13035.
(69) Camp, C.; Grant, L. N.; Bergman, R. G.; Arnold, J. *Chem. Commun.* **2016**, *52*, 5538.
(70) Camp, C.; Maron, L.; Bergman, R. G.; Arnold, J. *J. Am. Chem. Soc.* **2014**, *136* (50), 17652.
(71) Kuprat, M.; Lehmann, M.; Schulz, A.; Villinger, A. *Organometallics* **2010**, *29* (6), 1421.
(72) Feldman, J.; Mclain, S. J.; Parthasarathy, A.; Marshall, W. J.; Calabrese, J. C.; Arthur, S. D. *Organometallics* **1997**, *16*, 1514.
(73) Stender, M.; Wright, R. J.; Eichler, B. E.; Prust, J.; Olmstead, M. M.; Roesky, H. W.; Power, P. P. *J. Chem. Soc. Dalt. Trans.* **2001**, No. 23, 3465.
(74) Schmidt, S.; Sundermeyer, J. *J. Organomet. Chem.* **1994**, *472*, 127.
(75) The small coupling to Ta-H only served to broaden the Ta-H resonance at 20.9 ppm, and no COSY correlation was observed between the methylene and the hydride. However, coupling to the Ta-H was confirmed by a selective homonuclear decoupling experiment.
(76) Some resonances for **4.2b** were obscured by resonances of **4.2a**, preventing determination of multiplicities and chemical shifts.
(77) Stoll, S.; Schweiger, A. *J. Magn. Reson.* **2006**, *178* (1), 42.
(78) Frisch, M.; Trucks, G.; Schlegel, H.; Scuseria, G.; Robb, M.; Cheeseman, J.; Scalmani, G.; Barone, V.; Mennucci, B.; Petersson, G.; Nakatsuji, H.; Caricato, M.; Li, X.; Hratchian, H.; Izmaylov, A.; Bloino, J.; Zheng, G.; Sonnenberg, J.; Hada, M.; Ehara, M.; Toyota, K.; Fukuda, R.; Hasegawa, J.; Ishida, M.; Nakajima, T.; Honda, Y.; Kitao, O.; Nakai, H.; Vreven, T.; Montgomery, J.; Peralta, J.; Ogliaro, F.; Bearpark, M.; Heyd, J.; Brothers, E.; Kudin, K.; Staroverov, V.; Kobayashi, R.; Normand, J.; Raghavachari, K.; Rendell, A.; Burant, J.; Iyengar, S.; Tomasi, J.; Cossi, M.; Rega, N.; Millam, J.; Klene, M.; Knox, J.; Cross, J.; Bakken, V.; Adamo, C.; Jaramillo, J.; Gomperts, R.; Stratmann, R.; Yazyev, O.; Austin, A.; Cammi, R.; Pomelli, C.; Ochterski, J.; Martin, R.; Morokuma, K.; Zakrzewski, V.; Voth, G.; Salvador, P.; Dannenberg, J.; Dapprich, S.; Daniels, A.; Farkas; Foresman, J.; Ortiz, J.; Cioslowski, J.; Fox, D. *Gaussian 09, Revis. D.01, Gaussian, Inc., Wallingford CT* **2009**.
(79) Perdew, J. P.; Burke, K.; Ernzerhof, M. *Phys. Rev. Lett.* **1996**, *77* (18), 3865.
(80) Perdew, J. P.; Burke, K.; Ernzerhof, M. *Phys. Rev. Lett.* **1997**, *78* (7), 1396.
(81) Grimme, S.; Antony, J.; Ehrlich, S.; Krieg, H. *J. Chem. Phys.* **2010**, *132* (15), 154104.
(82) Dunning, T. H.; Hay, P. J.; Schaefer, H. F. In *Plenum, New York*; 1977; pp 1–27.
(83) Andrae, D.; Häußermann, U.; Dolg, M.; Stoll, H.; Preuß, H. *Theor. Chim. Acta* **1990**, *77* (2), 123.
(84) Martin, J. M. L.; Sundermann, A. *J. Chem. Phys.* **2001**, *114* (8).
(85) AIMAll (Version 16.10.31), Keith, T. A., TK Gristmill Software, Overland Park, KS, USA, 2016.
(86) SMART: Area-Detector Software Package; Bruker Analytical X-ray Systems, Inc.: Madison, WI, 2001-2003.
(87) SAINT: SAX Area-Detector Integration Program; Bruker Analytical X-ray Systems Inc.: Madison, WI, 2003.
(88) SADABS: Bruker-Nonius Area Detector Scaling and Absorption; Bruker Analytical X-ray Systems, Inc.: Madison, WI, 2003.
(89) Sheldrick, G. M. *Acta Crystallogr. Sect. A* **2008**, *64*, 112.
(90) Farrugia, L. J. *Journal of Applied Crystallography*. International Union of Crystallography

October 1, 1997, p 565.
(91) Macrae, C. F.; Bruno, I. J.; Chisholm, J. A.; Edgington, P. R.; McCabe, P.; Pidcock, E.; Rodriguez-Monge, L.; Taylor, R.; van de Streek, J.; Wood, P. A. *J. Appl. Crystallogr.* **2008**, *41* (2), 466.

Chapter 5

Group 5 Chemistry Supported by β-Diketiminate Ligands Bearing Mesityl and Dichlorophenyl Substituents

Introduction

The highly reducing nature of low-valent early transition metal complexes has been exploited to carry out a variety of challenging stoichiometric transformations, including reductive couplings to form new C-C bonds,[1–8] activation of small molecules, such as N_2 and CO_2,[9–21] and atom and group transfer reactions to generate reactive imido, oxo, alkylidene, and related multiply bonded fragments.[22–30] In contrast, catalytic reactions involving d^0-d^2 redox couples in early transition metals are quite rare,[31–35] but have recently become the focus of increased attention.[36–40] Recently, we published a series of reports on a niobium system supported by the combination of a sterically encumbering *β*-diketiminate ligand with 2,6-diisopropylphenyl N-substituents and a *tert*-butylimido ligand,[41–43] which not only demonstrates novel stoichiometric reactivity,[44–51] but also catalytic transformations, including alkyne semihydrogenation,[37,38] arene hydrodefluorination,[39] and nitrene transfer,[40] all using the Nb(III)-Nb(V) redox couple under relatively mild conditions.

The most successful approach for generating Nb(III) complexes using this system is reaction of Nb(V) dimethyl compounds with dihydrogen.[52–54] During the course of this research, we found that the dark purple Nb(IV)-Nb(IV) bis-*μ*-hydride complex $\{(BDI)Nb(N^tBu)(\mu\text{-}H)\}_2$ is generated in low yield (<1% to 21% depending on conditions).[45] While the chemistry of this compound was not studied beyond basic NMR and X-Ray characterization (due to its poor yield and poor solubility in organic solvents), related bridging niobium and tantalum hydride complexes studied by the Fryzuk and Kawaguchi groups have been shown to be reactive, readily eliminating dihydrogen in order to activate dinitrogen and other small molecules.[55–71] Moreover, related hydride-bridged dimers have also been amenable to reversible one-electron metal-based redox processes leading to mixed-valence complexes with interesting electronic structures.[72]

Prior to the studies discussed in this chapter, we had not yet investigated the influence of changing the electronic and steric profile of the BDI N-substituents on the reactivity of group 5 imido systems. Here, we discuss niobium and tantalum imido complexes supported by BDI ligands with 2,4,6-trimethylphenyl N-substituents (BDI^{Mes}) and 2,6-dichlorophenyl N-substituents (BDI^{Cl}) that are less sterically encumbering than 2,6-diisopropylphenyl substituents. These ligands were used by Schrock and coworkers to support related high-valent molybdenum imido alkylidene complexes used in olefin metathesis catalysis.[73,74] While the ready cleavage of aryl C-Cl bonds under reducing conditions presents a challenge in utilizing the BDI^{Cl} ligand in mid- and low-valent group V chemistry, the BDI^{Mes} ligand has proven useful for supporting mid-valent and mixed-valent dimeric niobium imido complexes. We discuss the unusual redox reactivity of these complexes and investigate their electronic structures as determined using NMR spectroscopy, EPR spectroscopy, X-Ray crystallography, and DFT calculations.

Results and Discussion

Compound **5.1** was isolated in 70% yield as a red crystalline solid from salt metathesis of $BDI^{Mes}Li\cdot THF$ with $Nb(N^tBu)Cl_3Py_2$. The room temperature ^1H NMR spectrum of **5.1** contains sharp signals consistent with a C_s symmetric molecule with shifts and multiplicities typical for early transition metal BDI systems. In contrast, the analogous system in which the BDI ligand exhibits much more sterically encumbering diisopropylphenyl substituents showed broad signals

at room temperature, which was attributed to facile pyridine dissociation.[43] Stronger coordination of pyridine to **5.1** likely explains the sharper peaks that are observed.

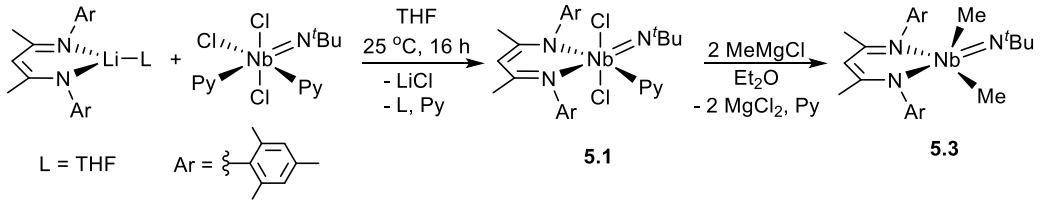

Scheme 5.1 Preparation of high-valent BDI^{Ar} niobium imido complexes.

Single crystal X-ray diffraction analysis of **5.1** indicates a distorted octahedral geometry about the niobium center with the two chlorides *trans* to one another (Figure 5.1, left). A large disparity between the Nb-N(1) (2.379(1) Å) and Nb-N(2) (2.096(1) Å) distances is consistent with the strong *trans* influence of the imido ligand. The Nb-N(1) distance is, however, noticeably shorter than the Nb-N(1) distance in the N-diisopropylphenyl derivative (2.420(2) Å), which may be a consequence of the less bulky flanking mesityl groups allowing for closer proximity of the BDI ligand to the Nb center.

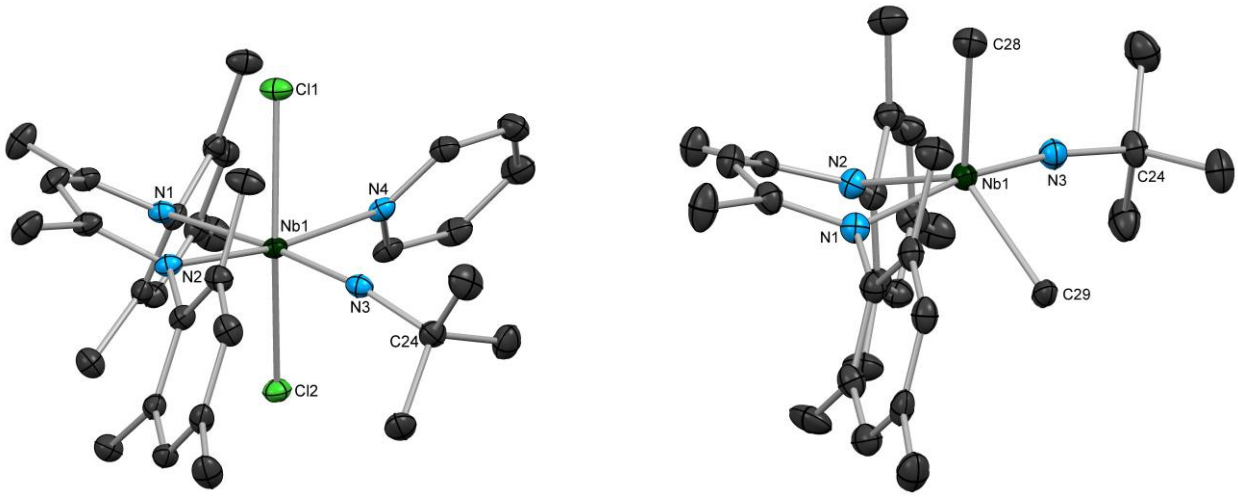

Figure 5.1 Molecular structures of **5.1** (left) and **5.2** (right) as determined by X-ray diffraction. Hydrogen atoms and a molecule of diethyl ether in **5.1** are omitted for clarity; thermal ellipsoids are set at the 50% probability level. For **5.1** (left), selected bond lengths (Å): Nb-N(1) 2.379(1), Nb-N(2) 2.096(1), Nb-N(3) 1.764(1), Nb-N(4) 2.380(1), Nb-Cl(1) 2.4314(4), Nb-Cl(2) 2.4339(4); selected bond angles (˚): Nb-N(3)-C(24) 165.4(1), Cl(1)-Nb-Cl(2) 162.7(2), N(1)-Nb-N(3) 173.50(5), N(2)-Nb-N(4) 170.99(5). For **5.2** (right), selected bond lengths (Å): Nb-N(1) 2.325(2), Nb-N(2) 2.116(2), Nb-N(3) 1.773(2), Nb-C(28) 2.190(2), Nb-C(29) 2.228(2); selected bond angles (˚): Nb-N(3)-C(24) 170.2(2), N(2)-Nb-C(28) 111.81(8), N(2)-Nb-C(29) 127.54(8), C(28)-Nb-C(29) 118.36(9), N(1)-Nb-N(3) 171.69(8).

Since niobium dimethyl complexes had proven useful as a starting material for accessing reactive low-valent niobium complexes,[42,45,52,53] a dialkyl complex containing the mesityl substituted BDI framework was targeted. The analogous dimethyl complex **5.2** was prepared by

reaction of **1** with methyl Grignard and isolated as orange-yellow crystalline material in 75% yield. The ^{1}H NMR spectrum of **5.2** indicates that it is C_s symmetric in solution and shows a slightly upfield shifted BDI backbone methine peak at 5.29 ppm (compared to the analogous resonance for compound **5.1** at 5.48 ppm). The X-ray crystal structure of **5.2** (Figure 5.1, left) shows a distorted trigonal bipyramidal geometry (τ_5 = 0.74)[75] with the imido group and one of the BDI nitrogen donors in the apical positions.

With the idea of accessing reactive Nb(III) species by hydrogenolysis of the methyl groups, a solution of **5.2** was exposed to 4 atm of H_2. The solution changed color from orange to purple, and a ^{1}H NMR spectrum indicated relatively clean conversion to a single new diamagnetic product. Bis-μ-hydride complex **5.3** was isolated as a deep purple microcrystalline powder in 77% yield upon stirring a solution of **5.2** in benzene under hydrogen atmosphere (Scheme 5.2).

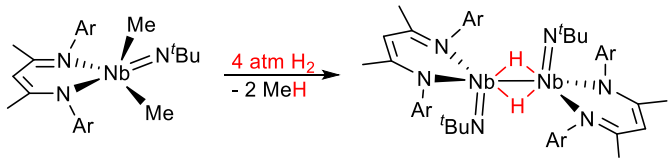

5.2 **5.3**

Scheme 5.2 Reaction of **5.2** with H_2 to generate diniobium(IV) bis-μ-hydride complex **5.3**.

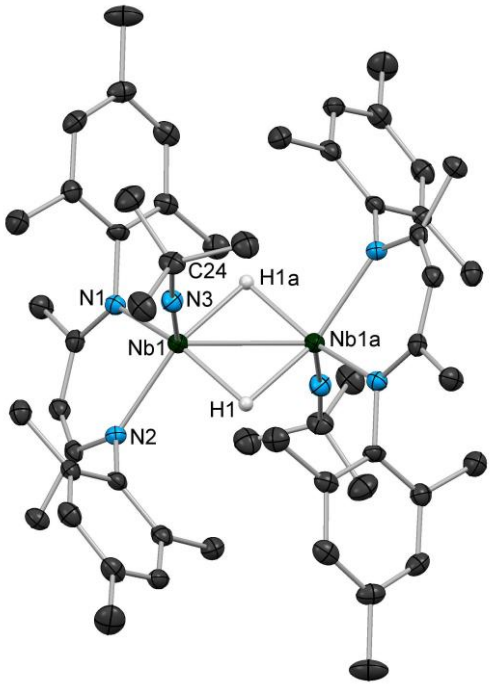

Figure 5.2. Molecular structure of **5.3** as determined by a single crystal X-ray diffraction study. Hydrogen atoms are omitted for clarity; thermal ellipsoids are set at the 50% probability level. Selected bond lengths (Å): Nb(1)-Nb(1a) 2.701(1), Nb(1)-H(1) 1.91(3), Nb(1)-H(1a) 1.95(3), Nb(1)-N(1) 2.206(3), Nb(1)-N(2) 2.204(3), Nb(1)-N(3) 1.775(3). Selected bond angles (˚): Nb(1)-N(3)-C(24) 175.4(2), N(1)-Nb(1)-H(1) 149.6(1) N(2)-Nb(1)-H(1a) 149.7(1), H(1)-Nb(1)-H(1a) 91.1(1).

DFT calculations on **5.3** using a B3LYP hybrid functional were carried out. The geometry was optimized starting from the atom coordinates in the solid-state crystal structure of **5.3**, and like the solid-state structure, the optimized geometry was C_{2h} symmetric with two equivalent Nb atoms related by an inversion center. As shown in Figure 5.3, the HOMO of **5.3** contains Nb(dz^2)-Nb(dz^2) σ-bonding character, as well as additional contribution to the σ-bonding character from the bridging hydride units and some contribution from the BDI π system. Overall, this DFT calculated picture of the HOMO lends credence to the formulation of **5.3** as a Nb-Nb σ-bonded complex.

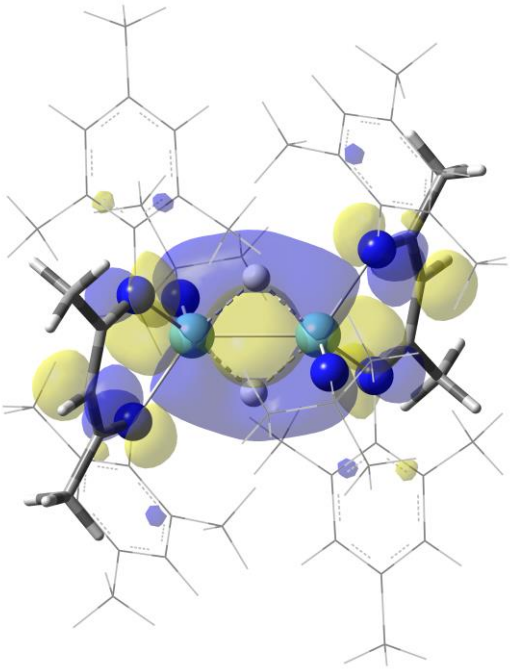

Figure 5.3 GaussView rendering of DFT calculated HOMO of **5.3** (isovalue = 0.02).

Since there are few examples of mixed-valent early transition metal complexes bridged by hydride ligands[72,76] (and none, to our knowledge, that contain niobium), we sought to access a mixed-valence Nb(IV)-Nb(V) species by one-electron oxidation of **5.3**. Oxidation with $AgB(C_6F_5)_4$ resulted in an immediate color change of a dimethoxyethane suspension of **5.3** from dark purple to dark green. After workup, dark green crystals of the dimeric bis-μ-imido complex **5.4a** were isolated in 43% yield. Similarly, the analogous $B(C_6H_5)_4$ salt **5.4b** could be prepared from $AgB(C_6H_6)_4$ in 41% yield.

Notably, **5.4** no longer contains bridging hydride ligands; the two niobium atoms are now bridged by the two imido moieties (Scheme 5.3). The one-electron oxidation presumably yields a reactive mixed valent hydride species that eliminates dihydrogen to give the formally Nb(III)-Nb(IV) imido bridged mixed-valent dimer **5.4**. Generation of H_2 was observed by ^{1}H NMR spectroscopy when following the conversion from **5.3** to **5.4**. The ^{1}H NMR spectrum of **5.4** displays only very broad features due to its paramagnetism.

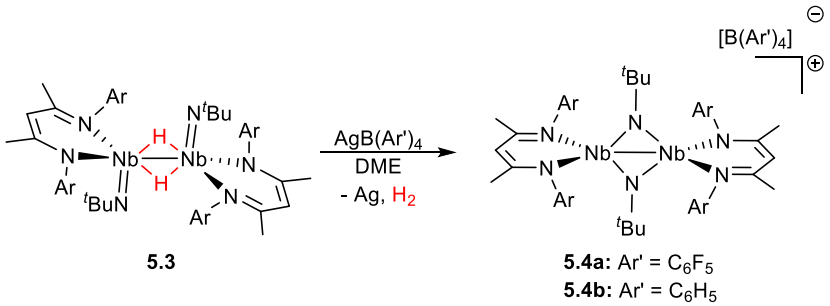

Scheme 5.3 Synthesis of mixed-valent diniobium complexes **5.4** from oxidation of **5.3**.

The molecular structure of the cationic portion of compound **5.4a** is shown in Figure 5.4. In analogy to compound **5.3**, the cationic portion of **5.4a** is C_{2h} symmetric so that only one half of the molecule appears in the asymmetric unit. The Nb-Nb distance is 2.717(1) Å, again within the normal range for a Nb-Nb single bond,[45,68,70,77–80] and slightly longer (0.016 Å) than the Nb-Nb distance in **5.3**. Ignoring the Nb-Nb interaction, the geometry of **5.4a** can be considered distorted tetrahedral at either niobium center (τ_4' = 0.85).[81]

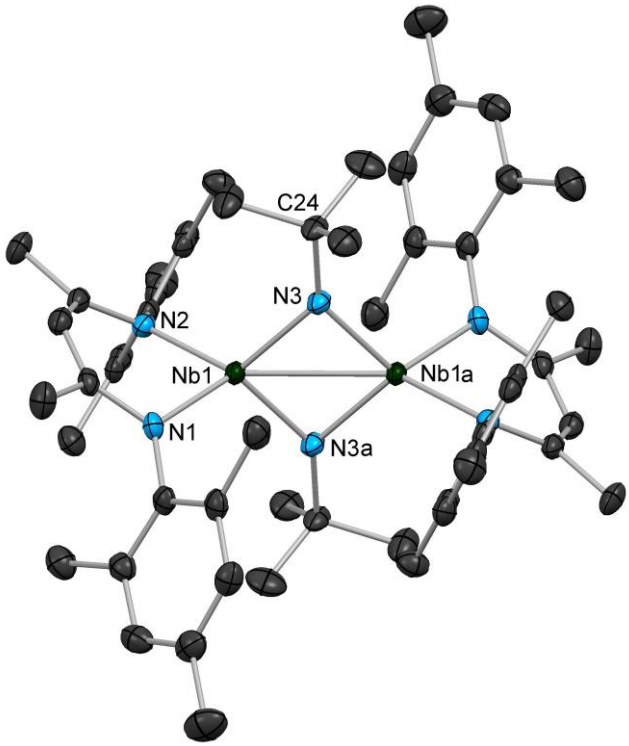

Figure 5.4. Molecular structure of the cationic portion of **5.4a** as determined by a single crystal X-ray diffraction study. One of two crystallographically inequivalent molecules of **5.4a** is shown. Hydrogen atoms, a $B(C_6F_5)_4$ counterion, and diethyl ether are omitted for clarity; thermal ellipsoids are set at the 50% probability level. Selected bond lengths (Å): Nb(1)-Nb(1a) 2.717(1), Nb(1)-N(1) 2.095(2), Nb(1)-N(2) 2.113(2), Nb(1)-N(3) 1.991(2), Nb(1)-N(3a) 1.974(2). Selected bond angles (˚): Nb(1)-N(3)-C(24) 132.1(2), N(1)-Nb(1)-N(3) 119.5(1), N(1)-Nb(1)-N(3a) 116.4(1), N(2)-Nb(1)-N(3) 120.21(9), N(2)-Nb(1)-N(3a) 117.7(1).

Although its formation was unexpected, very few examples of mixed-valent group 5 compounds containing direct metal-metal bonds have been reported,[72,76,82,83] with the majority of those being M(IV)-M(V) mixed-valent dimers, and none, to our knowledge, being M(III)-M(IV) dimers; as such, compound **5.4** represented an interesting target for further structural and reactivity studies. Both **5.3** and **5.4** are highly colored and thus absorb strongly in the visible range, as can be seen in their UV-Vis spectra (Figure 5.5). Upon conversion from **5.3** to **5.4**, the band in the visible region shifts from 580 nm to 650 nm, as can be observed qualitatively from a color change from dark purple to dark green. The absorption coefficients for the bands in the visible region for **5.3** and **5.4** are ~ 4000 $cm^{-1}mol^{-1}$ and ~ 3000 $cm^{-1}mol^{-1}$, respectively. Hence, they likely result from either metal-ligand, ligand-metal, or intervalence charge transfers, rather than Laporte forbidden d-d transitions. Additionally, **5.4** has a band in the NIR region centered at 1020 nm. TD-DFT calculations on **5.4** indicated that both the band centered at 650 nm and the band centered at 1020 nm (18028 cm^{-1}, f_{osc} = 0.106 and 11929 cm^{-1}, f_{osc} = 0.0381) can be tentatively assigned principally to LMCT transitions but the multiple nature of each transition does not allow for an accurate description without the help of more intensive calculations.[84] In addition to the bands in the visible region, both compounds display very intense bands in the ultraviolet region, which can likely be attributed to ligand-based π-π* transitions.

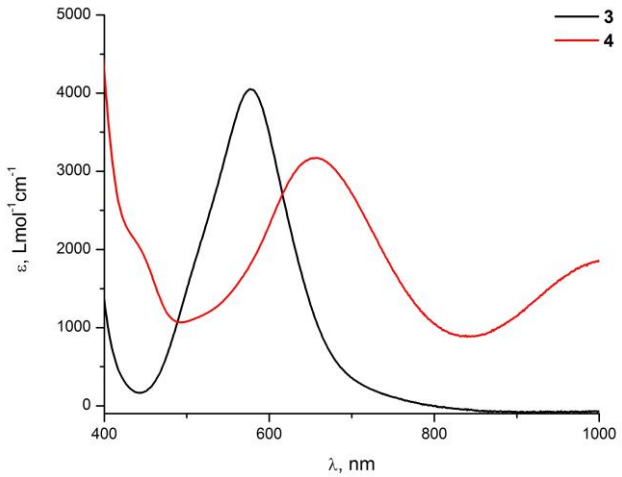

Figure 5.5. Ultraviolet-visible spectra of **5.3** (black trace) and **5.4** (red trace) in THF solution.

The electronic structure of complex **5.4** was further studied with X-band EPR spectroscopy, which revealed a multiline signal at a g value of 1.96 that displayed a slight dissymmetry. The spectrum was acquired in frozen THF solution at 77 K and did not change to a great extent within the temperature range from 4 K to 77 K. Only a very broad signal with unresolved hyperfine structure was observed in solution at room temperature. The EPR spectrum at 77 K along with a numerical simulation using the best parameters that fit the experimental data is presented in Figure 5.6. The mixed-valence diniobium complex **5.4** contains an unpaired electron spin (S = ½) where each ^{93}Nb possesses a 9/2 nuclear spin (100% natural abundance). Since the two niobium atoms share the unpaired electron spin density, the EPR spectrum was expected to be comprised of 19 lines (2nI+1). However, the observed spectrum is somewhat more complicated than a simple isotropic 19-line pattern; this is likely due to a combination of two effects: i) the spectral

simulations indicate the presence of a rhombic g-tensor with distinct values of the principal components g_x, g_y, and g_z, and ii) as suggested by the highly anisotropic and slightly different ^{93}Nb hyperfine coupling constants, the distribution of the electron spin density on the two niobium atoms is inequivalent. However, the differentiation between the two niobium atoms is not large and is about 13 MHz (4.6 G). Thus, the complex is best described as a Robin-Day class 3 mixed-valence complex with a delocalized unpaired electron.[85] Other mixed-valent formally Nb(IV)-Nb(V) compounds containing Nb-Nb interactions in the literature have either shown isotropic 19-line EPR spectra consistent with full delocalization of the lone electron over both metal centers (Robin-Day class 3),[83] or spectra in which no hyperfine coupling could be resolved.[82] Similarly, metal-metal bonded mixed-valent complexes of other transition metals in the literature either display EPR spectra consistent with equal delocalization over both metal centers[86,87] or do not display any discernable hyperfine coupling.[88–93]

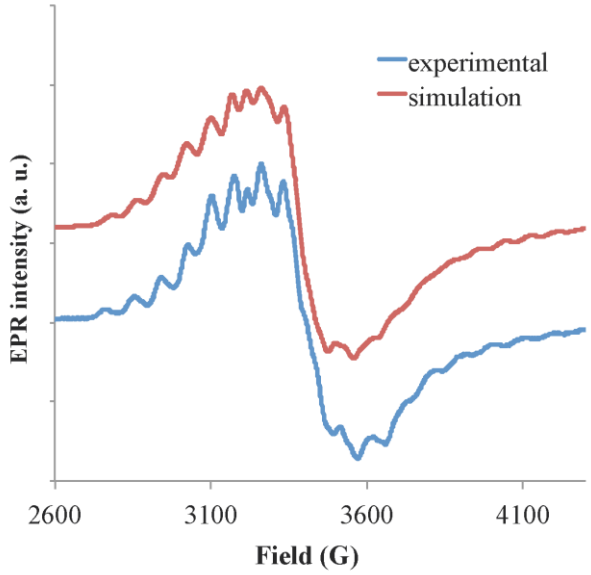

Figure 5.6. X-band EPR spectrum of **5.4** taken at 77 K in frozen THF solution (black line) and simulation (green line). Hyperfine coupling constants (MHz) and g tensor: A^{93}Nb(1) = [111, 48, 200], A^{93}Nb(2) = [115, 52, 234], g = [1.996, 1.969, 1.902].

DFT calculations using a B3LYP hybrid functional were carried out in order to better understand the electronic structure of **5.4**. Like compound **5.3**, the geometry of **5.4** was optimized from the solid-state structure, in which the two halves of the molecule were related by an inversion center. Using this functional, the inversion symmetry was maintained in geometry optimizations. GaussView representations of the spin density, as well as SOMO – 1 and SOMO orbitals are shown in Figure 5.7. The SOMO – 1 shows a Nb(dz^2)-Nb(dz^2) σ-bonding interaction similar to that observed in the HOMO of compound **5.3**. This molecular orbital also has bridging imido character, but this does not contribute to any great extent to the σ-bonding, in contrast to the bridging hydrides in **5.3**. The SOMO is predominantly metal dx^2-y^2 orbital based, with some contribution from the BDI π system. While the molecular orbital has equal contributions from both niobium centers, in contrast to the SOMO – 1, the interaction between the two metals is either nonbonding or weakly

δ-antibonding in nature. Hence, the calculated frontier orbitals of **5.4** are consistent with a Nb-Nb bond with at most a bond order of one; the slight lengthening of the Nb-Nb bond upon conversion from **5.3** to **5.4** may be a consequence of the δ-antibonding nature of the SOMO, but is more likely simply the result of **5.4** containing bridging imido ligands rather than bridging hydride ligands. As shown on the right side of Figure 5.7, the largest component of the spin density is distributed between the dx^2-y^2 orbitals of the two niobium centers, but a significant amount of the spin density is also delocalized over the bridging imido ligands and the BDI supporting ligands.

Calculations on **5.4** carried out using a PBE0 hybrid functional resulted in an optimized structure in which some of the metrical parameters, in particular the Nb-N(BDI) distances, are in better agreement with those in the X-ray crystal structure (See below, Table 5.1); however, unlike both the X-ray structure and the B3LYP-optimized structure, the PBE0-optimized structure no longer exhibits inversion symmetry. As would be expected for a structure exhibiting inversion symmetry, the spin density is evenly distributed over both halves of the molecule and EPR hyperfine constants calculated for both Nb centers are nearly equivalent in the B3LYP-optimized structure (See below, Table 5.2). However, the PBE0-optimized structure reflects subtle differences between the two niobium centers in both spin density and hyperfine constants, in accord with the slight differentiation in hyperfine coupling constants observed experimentally in the EPR spectrum taken at 77 K. The difference in the EPR hyperfine constants between the two niobium atoms ($\Delta A^{93}Nb_{Expt}$ = 14 G, $\Delta A^{93}Nb_{B3LYP}$ = 7 G, $\Delta A^{93}Nb_{PBE0}$ = 22 G) correlates well with the metrical observations described above.

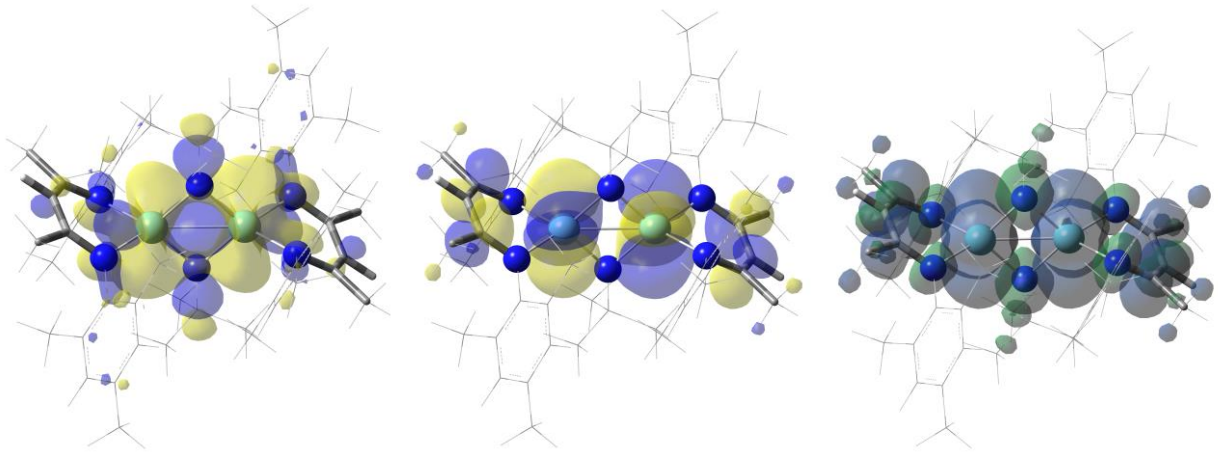

Figure 5.7. GaussView renderings of DFT calculated α SOMO – 1 (left) and SOMO (middle), and spin density (right, blue = α, green = β), of **5.4** (isovalue = 0.02).

It seemed plausible that one electron reduction of **5.4** could generate a reactive low-coordinate Nb(III) complex. It was found that **5.4** reacted instantaneously with an excess of potassium graphite in THF at -40 ˚C to generate a dark red solution from which compound **5.5** was isolated in 25% yield (Scheme 5.4). Compound **5.5** is a diamagnetic compound containing two distinct Nb(V) centers. Presumably, it forms by initial one-electron reduction of **5.4** to the symmetric Nb(III)-Nb(III) intermediate **5.A**, which then undergoes reductive C-N cleavage to generate intermediate **5.B**, which finally rearranges to the Nb(V)-Nb(V) product by two electron reduction

of the resulting monoazadiene ligand. This type of degradation pathway in which a nitrene fragment is transferred from a BDI ligand to a metal center is well known in low-valent early transition metal[52,54,94–99] and main group BDI systems;[100–104] however, systems in which the monoazadiene ligand rearranges to bridge two transition metal centers as a μ-carbene are, to our knowledge, unprecedented.

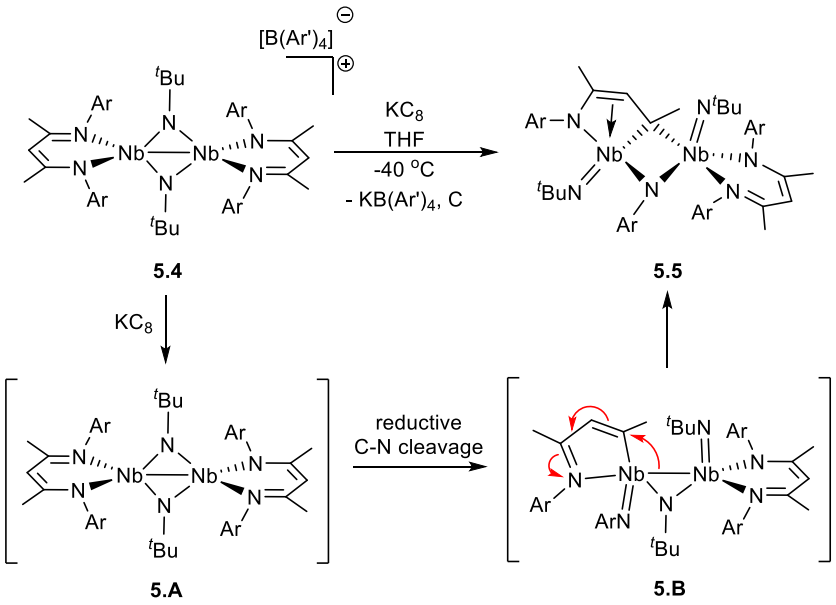

Scheme 5.4 Synthesis of Nb(V) dimer **5.5** from reduction of **5.4** and proposed mechanism.

The ^{1}H NMR spectrum of **5.5** exhibits sharp peaks and is consistent with a C_1-symmetric structure, containing twelve distinct mesityl methyl signals as well as four distinct BDI backbone methyl signals each integrating for three protons. Two different backbone methine singlets appear at 5.37 and 5.23 ppm, consistent with the low symmetry structure of **5**. The crystallographically-determined solid-state structure of **5.5** (Figure 5.8) reveals a significantly lengthened Nb-Nb distance of 3.0802(6) Å, in agreement with the lack of a significant Nb-Nb interaction, as expected for a d^0-d^0 system. The geometry about Nb(1) can be considered distorted square pyramidal (τ_5 = 0.28), while the geometry about Nb(2) (considering only the covalent bonds to N(4), C(30), N(5), and C(51)) is best considered distorted tetrahedral (τ_4' = 0.82). The N(4)-C(28), C(28)-C(29), and C(29)-C(30) distances are consistent with alternating single and double bonds as depicted in Scheme 5.4 and there appears to be a dative interaction between the C(28)-C(29) π-bond and the niobium center (Nb-C(28), 2.392(5) Å; Nb-C(29), 2.338(5) Å). Moreover, the Nb(1)-C(30) and Nb(2)-C(30) distances are 2.168(5) and 2.208(5) Å, consistent with C(30) behaving as a bridging μ-alkylidene group between the two niobium centers. The geometry about C(30) is, however, severely distorted from an ideal tetrahedron due to significant geometric constraints imposed in the complex; the smallest angle about C(30), Nb(2)-C(30)-C(29), is 77.4(3)˚, while the largest angle about C(30), Nb(1)-C(30)-C(29), is 145.7(3)˚. Curiously, although the Nb(1)-N(5) and Nb(2)-N(5) distances of 1.980(4) and 2.094(4) Å are consistent with the formulation of **5.5** as a μ-arylimido species, the Nb(1)-N(5)-C(42) bond angle is 161.6(3)˚, closer to values typically observed for terminal linear imido groups than for bridging imido groups. Notably, Nb(2) has a

relatively close contact with C(42), the *ipso* carbon of the arylimido group, of 2.507(5) Å, suggesting that the unusual geometry at the μ-imido group may at least in part be caused by an interaction between the *ipso* carbon and the relatively electron deficient (14 e^-) niobium center. Similar interactions with *ipso* carbons have been observed in other electron deficient early metal complexes.[105–108] However, another important factor that may drive the μ-imido moiety into this unusual geometry is the presence of the flanking mesityl groups on the intact BDI ligand, which would likely clash significantly with the aryl group if the imido moiety were more strongly bent.

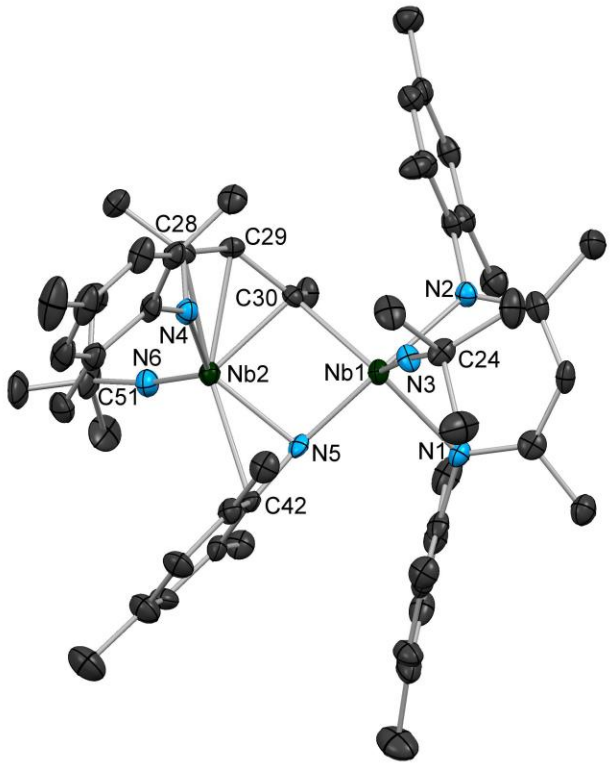

Figure 5.8 Molecular structure of **5.5** as determined by a single crystal X-ray diffraction study. Hydrogen atoms and a molecule of n-hexane are omitted for clarity; thermal ellipsoids are set at the 50% probability level. Selected bond lengths (Å): Nb(1)-Nb(2) 3.0802(6), Nb(1)-N(1) 2.218(4), Nb(1)-N(2) 2.301(4), Nb(1)-N(3) 1.754(4), Nb(1)-N(5) 1.9804, Nb(1)-C(30) 2.208(5), Nb(2)-N(4) 2.077(4), Nb(2)-N(5) 2.094(4), Nb(2)-N(6) 1.785(4), Nb(2)-C(30) 2.168(5), Nb(2)-C(28) 2.392(5), Nb(2)-C(29) 2.338(5), Nb(2)-C(42) 2.507(5), N(4)-C(28) 1.403(6), C(28)-C(29) 1.394(7), C(29)-C(30) 1.468(7), N(5)-C(42) 1.405(6). Selected bond angles (˚): Nb(1)-N(3)-C(24) 173.0(4), Nb(1)-N(5)-C(42) 161.6(3), Nb(2)-N(5)-C(42) 89.3(3), Nb(2)-N(6)-C(51) 169.7(4), Nb(1)-C(30)-Nb(2) 89.5(2), Nb(1)-N(5)-Nb(2) 98.2(2), N(1)-Nb(1)-C(30) 141.6(2), N(2)-Nb(1)-N(5) 158.4(2), N(4)-Nb(2)-N(5) 116.9(2), N(4)-Nb(2)-N(6) 123.4(2), N(4)-Nb(2)-C(30) 91.6(2), N(5)-Nb(2)-N(6) 118.2(2), N(5)-Nb(2)-C(30) 83.1(2), N(6)-Nb(2)-C(30) 106.5(2).

Reaction of Li(BDI^{Cl})·THF and M(N^tBu)Cl_3py_2 (M = Nb, Ta) in THF resulted in the formation of (BDI^{Cl})M(N^tBu)Cl_2py (**5.6**: M = Nb, **5.7**: M= Ta, BDI^{Cl} = HC(C(Me)NAr)$_2$, Ar = 2,6-Cl_2-C_6H_3), which were isolated from diethyl ether as red-orange and yellow-orange microcrystalline solids, respectively (Scheme 5.5). ^{1}H NMR spectroscopy indicated C_s symmetric solution structures

similar to the previously reported analogs (BDI^{Dipp})M(N^{t}Bu)Cl$_2$py (M = Nb, Ta). As in the BDI^{Dipp} complexes, the chemical shift of the tert-butyl imido protons (0.62 ppm) was upfield by around 1 ppm from that of the Nb(N^{t}Bu)Cl$_3$py$_2$ starting material. This could be attributed to the shielding effect imposed by the flanking aryl ring of the BDI in spatial proximity to the imido group. Additionally, the ^{1}H NMR shift of the singlet corresponding to the BDI backbone methine in both **5.6** and **5.7** is notably downfield compared to that of the BDI^{Dipp} analogs (5.51 vs. 5.34 ppm for Nb, 5.44 vs. 5.22 ppm for Ta). This indicated an electron-withdrawing effect of the dichloride substituents on the BDI aryl rings, which resulted in reduced electron donation from the ligand to the metal center and therefore deshielding of the backbone methines.

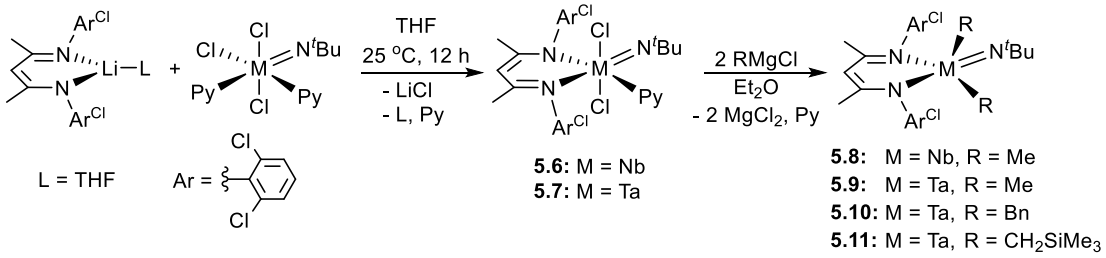

Scheme 5.5 Preparation of BDI^{Cl} niobium and tantalum imido dichloride and dialkyl complexes.

The room temperature ^{1}H NMR spectra of both **5.6** and **5.7** show a second set of broad peaks likely corresponding to geometric isomers (~12:1 ratio for **5.6a** to **5.6b** at room temperature; ~6:1 ratio of major isomer **5.7a** to minor isomer **5.7b** at room temperature). For both the Nb and Ta systems, the two sets of peaks show facile exchange by EXSY (10 ms at room temperature for **5.7** at room temperature), indicating that a fast equilibrium is established between the isomers at room temperature. ^{1}H NMR spectra collected at 80 ˚C show coalescence of the two sets of resonances into a single set of broad resonances due to a hastening of the dynamic process that interconverts the isomers relative to the NMR timescale. ^{1}H NMR spectra taken at -40 ˚C showed disappearance of the minor isomer, indicating an enthalpic preference for the major isomer. Similar fluxional behavior has been observed with analogous complexes supported by the BDI^{iPr} ligand, and can be attributed to a dissociative rearrangement involving decoordination and recoordination of the pyridine ligand.[43]

The molecular structures of **5.6** and **5.7**, along with selected bond lengths and angles, are shown in an ORTEP diagram in Figure 5.9. In the solid state, **5.6** and **5.7** exhibit distorted octahedral geometry with the chlorides oriented *trans* to one another, and the pyridine and imido group each oriented *trans* to one of the BDI nitrogens, analogous to the structures of the BDI^{Dipp} derivatives. The chlorides in **5.6** are considerably displaced towards the pyridine (Cl(5)-Nb-Cl(6) = 164.84(3)°), indicative of a weakened Nb-py binding interaction (Nb-N(4) = 2.348(2) Å). A similar effect is seen in **5.7** with the chloride ligands (Cl(5)-Ta-Cl(6) = 165.37(5)°) bent in towards the elongated Ta-py bond (Ta-N(4) = 2.302(5) Å).

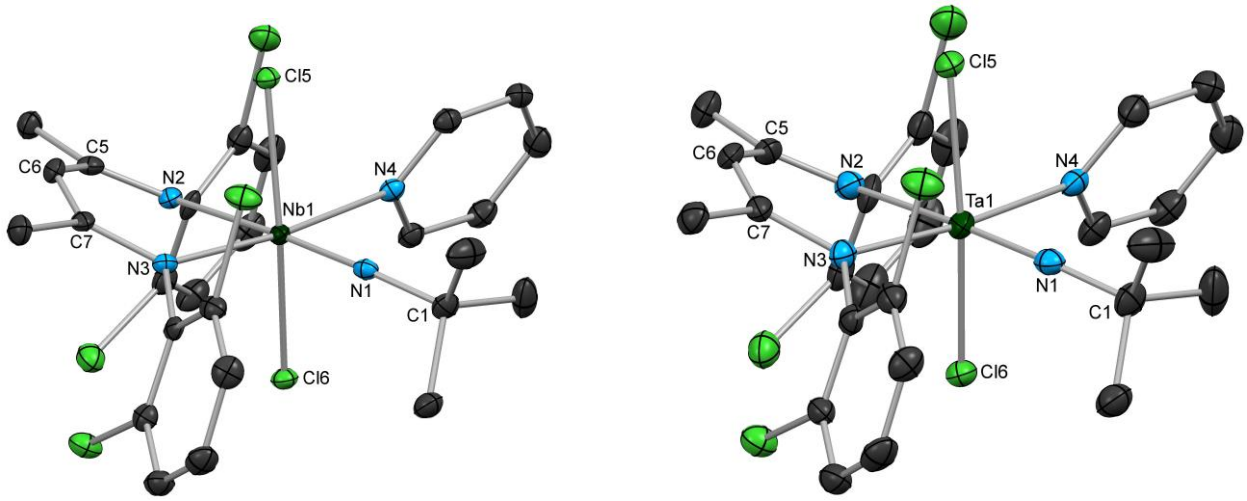

Figure 5.9 Molecular structures of **5.6** (left) and **5.7** (right) as determined by X-ray diffraction. Hydrogen atoms and a molecule of diethyl ether in each structure are omitted for clarity; thermal ellipsoids are set at the 50% probability level. For **5.6** (left), selected bond lengths (Å): Nb-N(1) = 1.770(2), Nb-N(2) = 2.372(2), Nb-N(3) = 2.104(2), Nb-N(4) = 2.348(2), Nb-Cl(5) = 2.3992(7), Nb-Cl(6) = 2.4368(7), N(2)-C(5) = 1.321(4), C(5)-C(6) = 1.421(4), C(6)-C(7) = 1.374(4), C(7)-N(3) = 1.375(4); selected bond angles (˚): N(1)-Nb-N(2) = 174.44(9), N(3)-Nb-N(4) = 170.81(9), Cl(5)-Nb-Cl(6) = 164.84(3), Nb-N(1)-C(1) = 167.5(2). For **5.7** (right), selected bond lengths (Å): Ta-N(1) = 1.794(5), Ta-N(2) = 2.359(5), Ta-N(3) = 2.111(5), Ta-N(4) = 2.302(5), Ta-Cl(5) = 2.3838(15), Ta-Cl(6) = 2.4140(15), N(2)-C(5) = 1.314(7), C(5)-C(6) = 1.413(8), C(6)-C(7) = 1.371(8), C(7)-N(3) = 1.377(7); selected bond angles (˚): N(1)-Ta-N(2) = 175.55(18), N(3)-Ta-N(4) = 171.27(16), Cl(5)-Ta-Cl(6) = 165.37(5), Ta-N(1)-C(1) = 167.4(4).

Addition of two equivalents of methyl magnesium chloride to a cooled solution of either **5.6** or **5.7** in Et_2O resulted in a rapid color change to pale yellow (Scheme 5.5). After evaporation of solvent and extraction with hexane, $(BDI^{Cl})M(N^tBu)Me_2$ (**5.8**: M = Nb, **5.9**: M = Ta) were isolated as pale yellow needles. Compounds **5.8** and **5.9** were somewhat thermally sensitive, decomposing into unidentified brown solids after several days at room temperature, but storage was possible for several months at -40 ˚C with no noticeable decomposition.

The ^{1}H NMR spectra of **5.8** and **5.9** in C_6D_6 each show one singlet integrating to six protons corresponding to the two methyl ligands at 0.99 ppm for **5.8** and 0.70 ppm for **5.9**. Moreover, the ^{1}H NMR spectra of **5.8** and **5.9** also show singlets integrating to six protons corresponding to the BDI backbone methyl groups at 1.70 ppm and 1.65 ppm, respectively, indicating C_s symmetry in solution. The molecular structures of **5.8** and **5.9** both show distorted trigonal bipyramidal geometries[75] (**5.8**: $\tau = 0.81$ **5.9**: $\tau = 0.80$) with the imido group and one BDI nitrogen in the apical positions (Figure 5.10). The bond lengths in the BDI ligand are closer to a fully delocalized structure than for **5.6** and **5.7**; in particular, the C-C bonds in the backbone have essentially identical lengths (1.384(5) vs. 1.397(5) Å). Distortion from ideal trigonal bipyramidal geometry is especially evident in the difference between the Nb-methyl bond lengths (2.178(3) vs. 2.208(3) Å) and Ta-methyl bond lengths (2.143(8) vs. 2.200(8) Å).

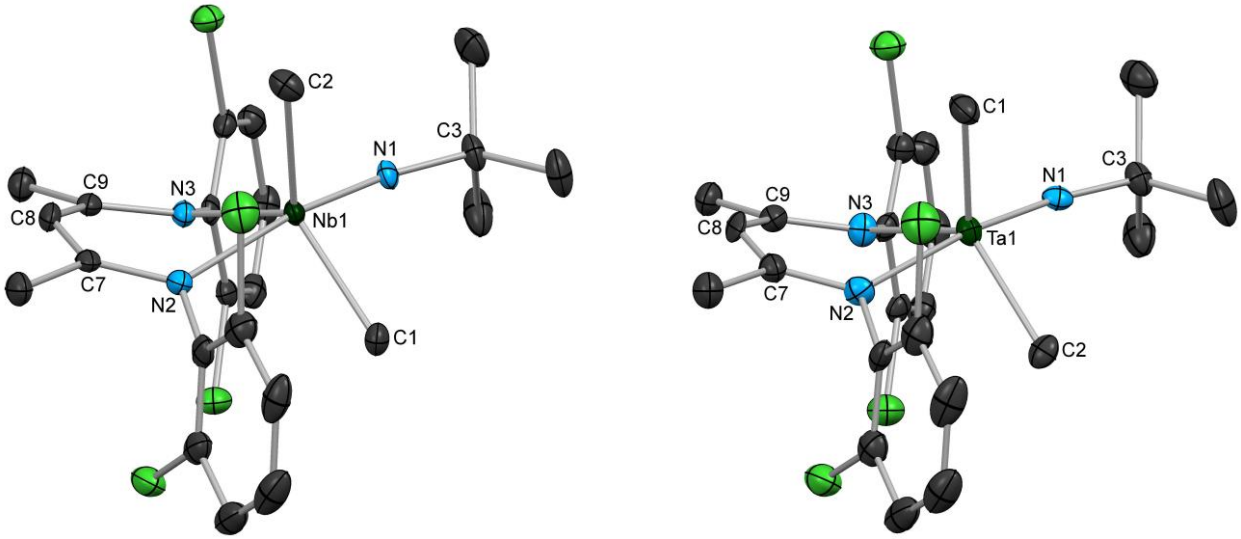

Figure 5.10 Molecular structures of **5.8** (left) and **5.9** (right) as determined by X-ray diffraction. Hydrogen atoms and a second crystallographically inequivalent molecule in each structure are omitted for clarity; thermal ellipsoids are set at the 50% probability level. For **5.8** (left), selected bond lengths (Å): Nb-N(1) = 1.772(3), Nb-N(2) = 2.328(3), Nb-N(3) = 2.115(3), Nb-C(1) = 2.208(3), Nb-C(2) = 2.178(3), N(2)-C(7) = 1.329(4), C(7)-C(8) = 1.397(5), C(8)-C(9) = 1.384(5), C(9)-N(3) = 1.365(4); selected bond angles (˚): N(1)-Nb-N(2) = 172.57(11), N(1)-Nb-N(3) = 98.50(11), N(1)-Nb-C(1) = 90.57(12), N(1)-Nb-C(2) = 97.05(13), N(2)-Nb-N(3) = 82.98(10), N(2)-Nb-C(1) = 82.63(11), N(2)-Nb-C(2) = 89.20(11), N(3)-Nb-C(1) = 124.17(11), N(3)-Nb-C(2) = 110.36(12), C(1)-Nb-C(2) = 123.03(13), C(3)-N(1)-Nb = 171.4(2). For **5.9** (right), selected bond lengths (Å): Ta-N(1) = 1.781(6), Ta-N(2) = 2.314(6), Ta-N(3) = 2.107(6), Ta-C(1) = 2.143(8), Ta-C(2) = 2.200(8), N(2)-C(7) = 1.333(10), C(7)-C(8) = 1.399(11), C(8)-C(9) = 1.388(11), C(9)-N(3) = 1.365(10); selected bond angles (˚): N(1)-Ta-N(2) = 173.1(3), N(1)-Ta-N(3) = 98.1(3), N(1)-Ta-C(1) = 97.6(3), N(1)-Ta-C(2) = 91.8(3), N(2)-Ta-N(3) = 82.8(2), N(2)-Ta-C(1) = 88.6(3), N(2)-Ta-C(2) = 82.1(3), N(3)-Ta-C(1) = 109.5(3), N(3)-Ta-C(2) = 125.2(3), C(1)-Ta-C(2) = 122.4(3), C(3)-N(1)-Ta = 171.2(6).

In addition to the dimethyl niobium and tantalum derivatives, dibenzyl and di(trimethylsilyl)methyl tantalum derivatives **5.10** and **5.11** were prepared via reaction of **2** with the respective Grignard reagents (Scheme 5.5). Characterization by ^{1}H NMR and ^{13}C NMR spectroscopies indicated C_s symmetry in solution. In contrast, previous attempts to prepare dibenzyl and di(trimethylsilyl)methyl derivatives from the (BDI$^{i\text{Pr}}$)M(N^{t}Bu)Cl$_2$Py precursors have been unsuccessful. Hence, the decrease in steric bulk around the metal center associated with changing the 2,6-diisopropyl substituents for 2,6-dichloride substituents allowed for the introduction of a wider range of alkyl ligands into the coordination sphere of the metal.

Treatment of compounds **5.6** – **5.11** with reducing reagents such as KC_8 or dihydrogen has led only to intractable mixtures of products. Based on previous results from our group in which low-valent group V complexes have been shown to readily activate aromatic C-X bonds (X = F, Cl),[39] it seems plausible that in-situ generated low-valent complexes either inter- or intramolecularly activate aromatic C-Cl bonds in the BDI^{Cl} ligand, leading to mixtures of products.

Summary and Conclusions

High-valent dichloride and dimethyl niobium *tert*-butylimido complexes supported by a BDI ligand bearing mesityl substituents, compounds **5.1** and **5.2**, were prepared and shown to exhibit structural features similar to those of previously described complexes featuring a BDI ligand with more sterically encumbering diisopropylphenyl substituents. Reaction of dimethyl complex **5.2** with dihydrogen led to generation of a bis-μ-hydrido Nb(IV)-Nb(IV) complex containing a metal-metal σ-bond in high yield. The analogous diisopropylphenyl-substituted BDI compound could only be isolated in low yield as a minor product in reactions of the dimethyl precursor with H_2 and exhibited relatively poor solubility in organic solvents, making **5.3** much more amenable to further reactivity studies. It was found that rather than giving a mixed-valent bis-μ-hydrido cation, one-electron oxidation of **5.3** resulted in release of dihydrogen to generate the imido-bridged mixed-valent Nb(III)-Nb(IV) dimer **5.4**. EPR spectroscopic measurements and DFT calculations were consistent with a symmetric structure for **5.4** containing a Nb-Nb single bond in which the unpaired electron is delocalized over both niobium centers. Rather than generating a neutral Nb(III) complex, one-electron reduction of **5.4** gave the high valent Nb(V)-Nb(V) dimer **5.5**, the product of reductive C-N cleavage followed by two-electron reduction of the resulting redox-active monoazadiene ligand. Interestingly, conversion from **5.3** to **5.4** effectively results from an oxidatively induced reductive elimination to generate a complex in an overall *lower* formal oxidation state than that of the starting material, while conversion from **5.4** to **5.5** results from a reductively induced overall four electron oxidation of the two niobium centers to give a complex with a *higher* formal oxidation state than that of the starting material.

Additionally, niobium and tantalum imido dichloride and dialkyl complexes were prepared in high yield by straightforward routes. Complexes **5.6 – 5.9** were characterized and shown to be mostly structurally analogous to a series of group 5 imido complexes supported by the diisopropylphenyl analog of the BDI ligand. Notably, the reduced steric bulk of the BDI^{Cl} ligand relative to the BDI^{iPr} analog allowed for the synthesis of tantalum dibenzyl and di(trimethylsilyl)methyl imido complexes **5.10** and **5.11**, while still providing enough support to avoid dimerization or decomposition. While the BDI^{Cl} ligand does not appear to be well-suited to stabilizing low-valent complexes, the ability of the BDI^{Cl} ligand to stabilize low-coordinate, cationic group 5 imido species remains a topic of interest.

Experimental

General Considerations: Unless otherwise noted, all reactions were performed using standard Schlenk line techniques or in an MBraun inert atmosphere glove box under an atmosphere of nitrogen (<1 ppm O_2/H_2O). Glassware and Celite were stored in an oven at ca. 140˚ C. Molecular sieves (4 Å) were activated by heating to 300 °C overnight under vacuum prior to storage in a glovebox. Hexane, diethyl ether, dichloromethane, benzene, toluene, pyridine, and THF were purified by passage through columns of activated alumina and degassed by sparging with nitrogen. $^tBuNH_2$ was distilled from CaH_2. Deuterated solvents were vacuum-transferred from sodium/benzophenone, degassed with three freeze-pump-thaw cycles, and stored over molecular sieves. NMR spectra were recorded on Bruker AV-600, AV-500, DRX-500, AVB-400, and AVQ-400 spectrometers. ^1H and $^{13}C\{^1H\}$ chemical shifts are given relative to residual solvent peaks.

Proton and carbon NMR assignments were routinely confirmed by ^{1}H-^{1}H (COSY) and ^{1}H-^{13}C (HSQC) experiments. Melting points were determined using an OptiMelt automated melting point system. $AgB(C_6F_5)_4$,[109] $AgB(C_6H_5)_4$,[110] KC_8,[111] $HBDI^{Ar}$,[112] $Li(BDI^{Ar})$•THF,[112] $HBDI^{Cl}$,[113] $Li(BDI^{Cl})$•THF,[113] and $py_2Cl_3Nb(N^tBu)$[114] were prepared using the literature procedures. All other reagents were acquired from commercial sources and used as received. Elemental analyses were carried out on the first crop of isolated material. Elemental analyses were determined either at the College of Chemistry, University of California, Berkeley or at the School of Human Sciences, Science Center, London Metropolitan University. X-ray structural determinations were performed at CHEXRAY, University of California, Berkeley on SMART APEX I and SMART APEX II QUAZAR diffractometers.

$(BDI^{Ar})Nb(N^tBu)Cl_2Py$ (5.1): THF (150 mL) was added to a solid mixture of $BDI^{Ar}Li(THF)$ (7.0 g, 17 mmol) and $Nb(N^tBu)Cl_3py_2$ (7.3 g, 17 mmol) in a 500 mL Schlenk flask to give a red solution. The solution was stirred at room temperature for 16 h, resulting in a dark red solution with a fine precipitate. The solvent was removed under vacuum to give a dark red residue, which was triturated with Et_2O (20 mL) and with hexane (2 x 20 mL). The residue was extracted with refluxing hexane using a Soxhlet apparatus, forming dark red crystals in the hexane extract as the extraction proceeded. Further crystals formed upon cooling to room temperature, and the dark red crystalline product was isolated and residual solvent was removed under vacuum. The solution was concentrated and cooled to -40 °C to yield a second crop. Yield: 7.7 g, 70%. **^{1}H NMR (400 MHz, C_6D_6, 293 K):** δ 8.82 (d, 2H, Py), 6.86 (s, 2H, Ar), 6.74 (t, 1H, Py), 6.60 (s, 2H, Ar), 6.32 (t, 2H, Py), 5.48 (s, 1H, *H*C(C(Me)NAr)$_2$), 2.71 (s, 6H, *o*-Me), 2.20 (s, 3H, *p*-Me), 2.18 (s, 3H, *p*-Me), 2.12 (s, 6H, *o*-Me), 1.56 (s, 6H, HC(C(*Me*)NAr)$_2$), 0.79 (s, 9H, ^{t}Bu). **^{13}C{^{1}H} NMR (400 MHz, C_6D_6, 293 K):** δ 171.0 (HC(*C*(Me)NAr)$_2$), 159.9 (HC(*C*(Me)NAr)$_2$), 154.3 (py), 137.7 (py), 134.8 (Ar), 133.7 (Ar), 133.4 (Ar), 133.0 (Ar), 129.8 (Ar), 129.0 (Ar), 122.6 (py), 107.2 (H*C*(C(Me)NAr)$_2$), 68.3 (C_α, ^{t}Bu), 28.9 (C_β, ^{t}Bu), 25.1 (HC(C(*Me*)NAr)$_2$), 24.5 (HC(C(*Me*)NAr)$_2$), 20.9 (*p*-Me), 20.7 (*o*-Me), 20.5 (*p*-Me), 19.64 (*o*-Me). Anal. calcd for $C_{32}H_{42}Cl_2N_4Nb$: C, 59.45; H, 6.55; N, 8.67. Found: C, 59.58; H, 6.67; N, 8.72. MP: dec. 165–190 ˚C.

$(BDI^{Ar})Nb(N^tBu)Me_2$ (5.2): Et_2O (200 mL) was added to **5.1** (5.5 g, 8.5 mmol) in a 500 mL Schlenk flask to give a red suspension. A solution of 3.0 M CH_3MgCl in THF (5.7 mL, 17 mmol) was added dropwise to the suspension of **5.1** at -72 °C with stirring, resulting in a color change from red to orange. After the addition was complete, the suspension was allowed to warm to room temperature with continued stirring. Upon warming to room temperature, the color of the solution became yellow-brown and a pale precipitate formed. After 10 minutes at room temperature, the solvent was removed under vacuum to give a yellow-brown residue. The residue was extracted with hexane, filtered, concentrated and stored at -40 °C overnight to give yellow block-like crystals of **5.2**, which were isolated and residual solvent was removed under vacuum. Yield: 3.3 g, 75%. **^{1}H NMR (400 MHz, C_6D_6, 293 K):** δ 6.83 (s, 4H, Ar), 5.29 (s, 1H, *H*C(C(Me)NAr)$_2$), 2.18 (s, 6H, *p*-Me), 2.15 (s, 12H, *o*-Me), 1.62 (s, 6H, HC(C(*Me*)NAr)$_2$), 1.14 ppm (s, 9H, ^{t}Bu), 0.82 (s, 6H, $NbMe_2$). **^{13}C{^{1}H} NMR (400 MHz, C_6D_6, 293 K):** δ 165.3 (HC(*C*(Me)NAr)$_2$), 151.2 (HC(*C*(Me)NAr)$_2$), 134.1 (Ar), 131.1 (Ar), 129.8 (Ar), 101.2 (H*C*(C(Me)NAr)$_2$), 64.8 (C_α, ^{t}Bu), 44.4 ($NbMe_2$), 30.6 (C_β, ^{t}Bu), 25.0 (HC(C(*Me*)NAr)$_2$), 20.9 (*p*-Me), 19.7 (*o*-Me). Anal. calcd for $C_{29}H_{44}N_3Nb$: C, 66.02; H, 8.41; N, 7.96. Found: C, 65.93; H, 8.50; N, 7.94. MP: dec. 141–155 ˚C.

{(BDI^{Ar})Nb(N^{t}Bu)(μ-H)}$_2$ (5.3): Benzene (5 mL) was added to **5.2** (250 mg, 0.48 mmol) in a Fischer-Porter tube, resulting in a yellow-orange solution. While stirring the solution, the headspace was evacuated and the vessel was pressurized with 60 psi H_2. The color of the solution immediately began to darken and became dark purple within 5 minutes. The solution was stirred for 14 h at room temperature, resulting in a purple-brown suspension with a fine purple precipitate. The headspace was evacuated and replaced with nitrogen, and the suspension was transferred to a Schlenk flask via cannula. The solvent was removed under vacuum to give a purple-brown residue, which was suspended in hexane, transferred to a Schlenk frit via cannula and washed further with hexane, leaving **5.3** as a purple microcrystalline powder which was collected on the frit. Residual solvent was removed under vacuum. X-Ray quality crystals of **5.3** were obtained from cooling a concentrated solution of **5.3** in toluene. Yield: 180 mg, 77%. **^{1}H NMR (600 MHz, C$_6$D$_6$, 293 K):** δ 6.94 (s, 4H, Ar), 6.76 (s, 4H, Ar), 5.15 (s, 2H, *H*C(C(Me)NAr)$_2$), 2.33 (s, 12H, *p*-Me), 2.05 (s, 12H, *o*-Me), 1.99 (s, 12H, *o*-Me), 1.66 ppm (s, 18H, ^{t}Bu), 1.62 (s, 12H, HC(C(*Me*)NAr)$_2$), -1.04 (br s, 2H, μ-H). **^{13}C{^{1}H} NMR (600 MHz, C$_6$D$_6$, 293 K):** δ 165.8 (HC(*C*(Me)NAr)$_2$), 145.8 (Ar), 133.1 (Ar), 132.2 (Ar), 131.9 (Ar), 130.4 (Ar), 128.9 (Ar), 99.5 (H*C*(C(Me)NAr)$_2$), 70.5 (C$_\alpha$, ^{t}Bu), 33.7 (C$_\beta$, ^{t}Bu), 23.1 (HC(C(*Me*)NAr)$_2$), 21.0 (*p*-Me), 20.1 (*o*-Me). Anal. calcd for $C_{54}H_{78}N_6Nb_2$: C, 65.05; H, 7.89; N, 8.43. Found: C, 64.96; H, 7.68; N, 8.33. MP: dec. 242–250 ˚C.

[{(BDI^{Ar})Nb(μ-N^{t}Bu)}$_2$][B(C$_6$F$_5$)$_4$] (5.4a): Compound **5.3** (220 mg, 0.22 mmol) was suspended in 10 mL dimethoxyethane in a 20 mL scintillation vial. AgB(C$_6$F$_5$)$_4$·Et$_2$O (0.26 g, 0.30 mmol) was dissolved in 5 mL dimethoxyethane in a separate 20 mL scintillation vial. Both vials were cooled to -40 ˚C, and the Ag^+ solution was transferred to the suspension of **3** by pipette while stirring. The color of the suspension changed from dark purple to dark brown to dark green with a dark precipitate within 1 minute, and the solution was allowed to stir while warming to room temperature for 20 minutes. The suspension was filtered through Celite to remove silver metal and the dark green filtrate was concentrated. Addition of 10 mL Et$_2$O to the concentrated DME solution resulted in precipitation of dark green crystals of **5.4a**. The suspension was stored at -40 ˚C overnight, resulting in the formation of additional crystals, which were isolated and residual solvent was removed under vacuum. Yield: 160 mg, 43%. **^{1}H NMR (400 MHz, C$_6$D$_5$Br, 293 K):** 6.1-5.2 (br s), 3.25-3.05 (br s), 2.8-1.3 (br s). Anal. calcd for $C_{78}H_{76}N_6B_1F_{20}Nb_2$: C, 55.96; H, 4.58; N, 5.02. Found: C, 55.69; H, 4.55; N, 4.85.

[{(BDI^{Ar})Nb(μ-N^{t}Bu)}$_2$][B(C$_6$H$_5$)$_4$] (5.4b): Compound **5.3** (200 mg, 0.20 mmol) and AgB(C$_6$F$_5$)$_4$·Et$_2$O (94 mg, 0.22 mmol) were suspended in 20 mL dimethoxyethane in a 20 mL scintillation vial. The suspension was stirred for six hours, during which time the color slowly changed from dark purple to dark brown to dark green with a dark precipitate. After the suspension was green, it was stirred for an additional 12 hours, then filtered through Celite to remove silver metal and concentrated. The concentrated DME solution was stored at -40 ˚C overnight to give dark green crystals of **5.4b**, which were isolated and residual solvent was removed under vacuum. Yield: 110 mg, 41%. **^{1}H NMR (400 MHz, C$_6$D$_6$, 293 K):** δ 8.17 (br s, BPh$_4$), 7.44 (br s, BPh$_4$), 7.28 (br s, BPh$_4$), 6.1-5.2 (br s), 3.25-3.05 (br s), 2.8-1.3 (br s). MP: dec. 189–205 ˚C.

(BDI^{Ar})Nb(N^{t}Bu)(μ-N(Ar))(μ-C(Me)C(H)C(Me)N(Ar))Nb(N^{t}Bu) (5.5): Compound **5.4b** (100 mg, 0.07 mmol) was dissolved in 3 mL THF in a 20 mL scintillation vial and cooled to -40 ˚C.

The solution was passed through a plug of KC_8 and Celite and the color of the solution instantaneously changed from dark green to dark red. The solvent was removed under vacuum to give a red oily residue, which was extracted with hexane and filtered through Celite to remove $KB(C_6H_5)_4$ and give a red solution (Note: even after extracting with copious amounts of hexane, the solid residue which was presumably mostly composed of $KB(C_6H_5)_4$ retained a red color). The solution was concentrated and stored at -40 °C overnight to give red crystals of **5.5**, which were isolated and residual solvent was removed under vacuum. Yield: 19 mg, 27%. **^{1}H NMR (400 MHz, C_6D_6, 293 K):** δ 7.22 (s, 1H, Ar), 6.96 (s, 1H, Ar), 6.94 (s, 1H, Ar), 6.93 (s, 1H, Ar), 6.88 (s, 1H, Ar), 6.84 (s, 1H, Ar), 6.82 (s, 1H, Ar), 6.63 (s, 1H, Ar), 5.29 (s, 1H, *H*C(C(Me)NAr), 5.15 (s, 1H, *H*C(C(Me)NAr), 3.01 (s, 3H, Ar C*H*$_3$), 2.43 (s, 3H, Ar C*H*$_3$), 2.41 (s, 3H, Ar C*H*$_3$), 2.34 (s, 3H, Ar C*H*$_3$), 2.29 (s, 3H, Ar C*H*$_3$), 2.27 (s, 3H, Ar C*H*$_3$), 2.24 (s, 3H, Ar C*H*$_3$), 2.23 (s, 3H, Ar C*H*$_3$), 2.21 (s, 3H, Ar C*H*$_3$), 2.16 (s, 3H, Ar C*H*$_3$), 2.07 (s, 3H, Ar C*H*$_3$), 2.05 (s, 3H, HC(C(*Me*)NAr)), 1.96 (s, 3H, HC(C(*Me*)(Nb)$_2$)), 1.79 (s, 3H, HC(C(*Me*)NAr)), 1.56 (s, 3H, HC(C(*Me*)NAr)), 1.48 (s, 3H, Ar C*H*3), 1.23 (s, 9H, ^{t}Bu), 0.77 (s, 9H, ^{t}Bu). **^{13}C{^{1}H} NMR (600 MHz, C_6D_6, 293 K):** δ 167.8 (HC(*C*(Me)NAr)), 165.7 (HC(*C*(Me)NAr)), 165.7 (HC(*C*(Me)NAr)), 151.4 (Ar), 150.5 (Ar), 145.9 (Ar), 144.0 (Ar), 139.3 (Ar), 135.8 (Ar), 134.5 (Ar), 134.2 (Ar), 134.1 (Ar), 134.0 (Ar), 133.9 (Ar), 133.5 (Ar), 132.8 (Ar), 132.0 (Ar), 131.9 (Ar), 130.8 (Ar), 130.4 (Ar), 130.2 (Ar), 130.1 (Ar), 129.7 (Ar), 129.7 (Ar), 129.4 (Ar), 129.1 (Ar), 128.8 (HC(*C*(Me)(Nb)$_2$)), 104.2 (H*C*(C(Me)NAr), 100.2 (H*C*(C(Me)NAr), 69.9 (C$_\alpha$, ^{t}Bu), 67.9 (C$_\alpha$, ^{t}Bu), 32.9 (C$_\beta$, ^{t}Bu), 32.6 (C$_\beta$, ^{t}Bu), 28.2 (Ar *C*H$_3$), 25.1 (HC(C(*Me*)NAr), 23.8 (HC(C(*Me*)(Nb)$_2$)), 23.7 (HC(C(*Me*)NAr), 23.6 (HC(C(*Me*)NAr), 21.4 (Ar *C*H$_3$), 21.1 (Ar *C*H$_3$), 21.0 (Ar *C*H$_3$), 21.0 (Ar *C*H$_3$), 20.9 (Ar *C*H$_3$), 20.8 (Ar *C*H$_3$), 20.4 (Ar *C*H$_3$), 20.3 (Ar *C*H$_3$), 20.1 (Ar *C*H$_3$), 19.8 (Ar *C*H$_3$), 19.2 (Ar *C*H$_3$). Anal. calcd for $C_{54}H_{76}N_6Nb_2$: C, 65.18; H, 7.70; N, 8.45. Found: C, 63.73; H, 7.52; N, 7.88. MP: dec. 163–170 ˚C.

(BDI^{Cl})Nb(N^{t}Bu)Cl$_2$Py (5.6): Nb(N^{t}Bu)Cl$_3$py$_2$ (1.21 g, 2.83 mmol, 1.0 equiv.) was dissolved in 40 mL of THF and cooled to 0 °C. In a separate flask, Li(BDI^{Cl})·THF (1.32 g, 2.83 mmol, 1.0 equiv.) was dissolved in 30 mL of THF and added slowly to the metal solution, which immediately turned orange. The solution was stirred room temperature for 18 h, resulting in a color change to bright red. The volatile materials were removed under vacuum to afford a red-orange solid. Soxhlet extraction with Et_2O produced red-orange microcrystals of **5.6**. The solid was isolated and residual solvent was removed under vacuum. Yield: 1.16 g, 59%. **^{1}H NMR (500 MHz, C_6D_6, 293K)** Compound **5.6a**: δ 9.01 (d, 2H, py), 7.1-6.3 (br m, 9H, py/Ar), 5.51 (br s, 1H, *H*C(C(Me)NAr)$_2$), 1.69 (s, 6H, HC(C(*Me*)NAr)$_2$), 0.83 (br s, 9H, N^t*Bu*). ^{1}H NMR (500 MHz, C_7D_8, 293K) Compound **5.6a**: δ 8.93 (br d, 2H, py), 6.9-6.8 (br m, 4H, py/Ar), 6.48 (br m, 3H, py/Ar), 6.37 (br m, 2H, py/Ar), 5.43 (s, 1H, *H*C(C(Me)NAr)$_2$), 1.66 (br s, 6H, HC(C(*Me*)NAr)$_2$), 0.77 (br s, 9H, ^{t}Bu). **^{1}H NMR (500 MHz, C_7D_8, 253K)** Compound **5.6a**: δ 8.90 (d, 2H, py), 6.90 (d, 2H, Ar), 6.76 (d, 2H, Ar), 6.72 (t, 1H, py), 6.43 (t, 1H, Ar), 6.37 (t, 1H, Ar), 6.26 (t, 2H, py), 5.41 (s, 1H, *H*C(C(Me)NAr)$_2$), 1.63 (s, 6H, HC(C(*Me*)NAr)$_2$), 0.77 (s, 9H, ^{t}Bu). ^{1}H NMR (500 MHz, $CDCl_3$, 293K) Compound **5.6a**: δ 8.79 (d, 2H, py), 7.74 (t, 1H, py), 7.35 (m, 2H, py/Ar), 7.13 (m, 5H, py/Ar), 7.00 (t, 1H, Ar), 5.68 (s, 1H, *H*C(C(Me)NAr)$_2$), 1.85 (s, 3H, HC(C(*Me*)NAr)$_2$), 1.76 (s, 3H, HC(C(*Me*)NAr)$_2$), 0.62 (s, 9H, ^{t}Bu). **^{13}C{^{1}H} NMR (125.8 MHz, C_6D_6, 293K)** Compound **5.6a**: δ 164.68 (C, HC(*C*(Me)NAr)$_2$), 161.68 (C, HC(*C*(Me)NAr)$_2$), 153.98 (CH, py), 150.48 (Ar), 144.90 (Ar), 138.65 (Ar), 133.13 (Ar), 132.79 (Ar), 128.99 (Ar), 128.14 (Ar), 126.81 (Ar), 125.96

(Ar), 123.38 (CH, py), 106.36 (CH, H*C*(C(Me)NAr)$_2$), 77.36 (C$_\alpha$, ^{t}Bu), 28.78 (C$_\beta$, ^{t}Bu), 25.70 (CH$_3$, HC(C(*Me*)NAr)$_2$), 24.40 (CH$_3$, HC(C(*Me*)NAr)$_2$). Anal. calcd (%) for $Nb_1Cl_6N_4C_{26}H_{27}$: C, 44.54; H, 4.03; N, 8.00. Found: C, 45.67; H, 4.00; N, 7.67. MP: dec. 195–228 ˚C.

(BDI^{Cl})Ta(N^{t}Bu)Cl$_2$Py (5.7): Ta(N^{t}Bu)Cl$_3$Py$_2$ (12.8 g, 24.8 mmol, 1.0 equiv.) and Li(BDI^{Cl}) (11.6 g, 24.8 mmol, 1.0 equiv.) were added to a 500 mL flask and dissolved in 300 mL THF. The solution was stirred at 60 ˚C for 15 h, resulting in a color change from light yellow to yellow-orange. The volatile materials were removed under vacuum and the residue was triturated with diethyl ether, resulting in a yellow-orange powder. The solid was extracted into diethyl ether and filtered using a Soxhlet apparatus. During the extraction, a yellow-orange solid began to precipitate. The flask containing the product was allowed to cool to room temperature, sealed under nitrogen, and stored at -40 ˚C overnight, yielding **5.7** as a yellow-orange microcrystalline solid. The solid was isolated and residual solvent was removed under vacuum. Yield: 16.4 g, 84%. **^{1}H NMR (500 MHz, C$_6$D$_6$, 293 K)** Compound **5.7a**: δ 9.06 (d, 2H, Py), 7.09 (d, 2H, Ar), 6.81 (d, 2H, Ar), 6.79 (t, 1H, Py), 6.49 (t, 1H, Ar), 6.38 (t, 1H, Ar), 6.31 (t, 2H, Py), 5.44 (s, 1H, *H*C(C(Me)NAr)$_2$), 1.68 (s, 3H, HC(C(*Me*)NAr)$_2$), 1.67 (s, 3H, HC(C(*Me*)NAr)$_2$), 0.86 (s, 9H, ^{t}Bu). Compound **5.7b**: 8.84 (br m, 2H, Py), 7.01-6.90 (m, 6H, Ar/Py), 6.67 (br m, 2H, Ar/Py), 6.42 (t, 1H, Ar/Py), 5.34 (s, 1H, *H*C(C(Me)NAr)$_2$), 1.66 (br s, 6H, HC(C(*Me*)NAr)$_2$), 1.48 (br s, 9H, ^{t}Bu). **^{1}H NMR (500 MHz, C$_6$D$_6$, 350 K):** δ 8.85 (br s, 2H, Py), 7.1-6.3 (br m, 9H, Ar/Py), 5.39 (s, 1H, *H*C(C(Me)NAr)$_2$), 1.67 (s, 6H, HC(C(*Me*)NAr)$_2$), 1.13 (br s, 9H, ^{t}Bu). **^{13}C{^{1}H} NMR (500 MHz, CDCl$_3$, 293 K)** Compound **5.7a**: δ 172.9 (HC(*C*(Me)NAr)$_2$), 162.7 (HC(*C*(Me)NAr)$_2$), 153.9 (Ar/Py), 149.6 (Ar/Py), 144.7 (Ar/Py), 138.8 (Ar/Py), 133.8 (Ar/Py), 133.4 (Ar/Py), 129.0 (Ar/Py), 128.2 (Ar/Py), 126.8 (Ar/Py), 126.1 (Ar/Py), 123.5 (Ar/Py), 106.2 (H*C*(C(Me)NAr)$_2$), 64.8 (C$_\alpha$, ^{t}Bu), 30.8 (C$_\beta$, ^{t}Bu), 25.8 (HC(C(*Me*)NAr)$_2$), 24.7 (HC(C(*Me*)NAr)$_2$). Anal. calcd (%) for $Ta_1Cl_6N_4C_{26}H_{27}$: C, 39.57; H, 3.45; N, 7.10. Found: C, 39.18; H, 3.41; N, 6.90. MP: dec. 226–252 ˚C.

(BDI^{Cl})Nb(N^{t}Bu)Me$_2$ (5.8): MeMgCl (1.0 mL of 3.0 M soln. in THF, 3.28 mmol, 1.95 equiv.) was added dropwise to a stirred suspension of **5.6** (1.15 g, 1.64 mmol, 1.0 equiv.) in 50 mL of Et$_2$O at -78 °C. The reaction mixture was allowed to warm to room temperature, resulting in a color change from light red to pale yellow-brown. After 30 min., the volatile materials were removed by vacuum and the residue was extracted with hexane and filtered through Celite. The clear yellow filtrate was concentrated and stored at -40 °C overnight, resulting in formation of pale yellow needles of **5.8**. The solid was isolated and residual solvent was removed under vacuum. Yield: 250 mg, 27%. **^{1}H NMR (500 MHz, C$_6$D$_6$, 293K):** δ 7.01 (d, 4H, Ar), 6.44 (t, 2H, Ar), 5.29 (s, 1H, *H*C(C(Me)NAr)$_2$), 1.70 (s, 6H, HC(C(*Me*)NAr)$_2$), 1.16 (s, 9H, ^{t}Bu), 0.99 (s, 6H, Nb*Me*$_2$). ^{13}C{^{1}H} NMR (125.8 MHz, C$_6$D$_6$, 293K): δ 167.07 (C, HC(*C*(Me)NAr)$_2$), 149.93 (C, HC(*C*(Me)NAr)$_2$), 131.99 (Ar), 128.83 (Ar), 128.61 (Ar), 128.35 (Ar), 126.19 (Ar), 101.79 (CH, H*C*(C(Me)NAr)$_2$), 65.22 (C$_\alpha$, N^{t}Bu), 46.63 (CH$_3$, Nb*Me*$_2$), 30.67 (C$_\beta$, ^{t}Bu), 24.91 (CH$_3$, HC(C(*Me*)NAr)$_2$). Anal. calcd (%) for $Nb_1Cl_4N_3C_{23}H_{28}$: C, 47.53; H, 4.86; N, 7.23. Found: C, 47.51; H, 4.89; N, 6.93. MP: 138–142 ˚C.

(BDI^{Cl})Ta(N^{t}Bu)Me$_2$ (5.9): Compound **5.7** (1.69 g, 2.14 mmol, 1 equiv.) was added to a 100 mL flask and dissolved in 25 mL Et$_2$O. MeMgCl (1.4 mL of 3.0 M soln. in THF, 4.17 mmol, 1.95 equiv.) was added dropwise at 0 ˚C with stirring, resulting in a color change from yellow-orange

to light yellow and formation of a white precipitate. The volatile materials were removed under vacuum. The residue was extracted with hexane and filtered through Celite to give a clear yellow solution. The solution was concentrated and stored at -40 ˚C overnight, yielding pale yellow needles of **5.9**. The solid was isolated and residual solvent was removed under vacuum. Yield: 0.931 g, 65% over two crops. **^{1}H NMR (500 MHz, C_6D_6, 293 K):** δ 7.00 (d, 4H, Ar), 6.42 (t, 2H, Ar), 5.27 (s, 1H, *H*C(C(Me)NAr)$_2$), 1.65 (s, 6H, HC(C(*Me*)NAr)$_2$), 1.18 (s, 9H, ^{t}Bu), 0.70 (s, 6H, Ta*Me*$_2$). **^{13}C{^{1}H} NMR (600 MHz, C_6D_6, 293 K):** δ 167.2 (HC(*C*(Me)NAr)$_2$), 149.7 (Ar), 132.2 (Ar), 128.8 (Ar), 126.5 (Ar), 103.5 (H*C*(C(Me)NAr)$_2$), 64.0 (C_α, ^{t}Bu), 56.5 (Ta*Me*$_2$), 32.1 (C_β, ^{t}Bu), 25.0 (HC(C(*Me*)NAr)$_2$). Anal. calcd (%) for $Ta_1Cl_4N_3C_{23}H_{28}$: C, 41.28; H, 4.22; N, 6.28. Found: C, 41.40; H, 4.11; N, 6.13. MP: 148–151 ˚C.

(BDI^{Cl})Ta(N^{t}Bu)Bn$_2$ (5.10) Compound **5.7** (50 mg, 0.063 mmol, 1.0 eq) was added to a 20 mL vial and dissolved in 5 mL THF. BnMgCl (86.6 μL of 1.5 M soln. in THF, 0.130 mmol, 2.05 eq) was added at -40 °C with stirring, resulting in a color change from yellow-orange to orange-red. The solution was stirred for 30 min at room temperature, and then the volatile materials were removed under vacuum. The residue was triturated with hexane and then extracted with hexane and filtered through Celite to give an orange-red solution. The solution was concentrated and stored at -40 ˚C overnight, yielding orange needles of **5.10**. The solid was isolated and residual solvent was removed under vacuum. Yield: 12 mg, 23%. **^{1}H NMR (600 MHz, C_6D_6, 293 K):** δ 7.22-7.15 (m, 8H, Ar), 6.94 (d, 4H, Ar), 6.87 (t, 2H, Ar), 6.34 (t, 2H, Ar), 5.39 (s, 1H, *H*C(C(Me)NAr)$_2$), 2.55 (d, 2H, Ta(C*H*$_2$Ph)$_2$, ^{2}J = 12 Hz), 2.28 (d, 2H, Ta(C*H*$_2$Ph)$_2$, ^{2}J = 12 Hz) 1.68 (s, 6H, HC(C(*Me*)NAr)$_2$), 0.57 (s, 9H, ^{t}Bu). **^{13}C{^{1}H} NMR (600 MHz, C_6D_6, 293 K):** δ 149.7 (Ar), 132.3 (Ar), 129.1 (Ar), 128.2 (Ar), 128.1 (Ar), 126.8 (Ar), 123.2 (Ar), 104.1 (H*C*(C(Me)NAr)$_2$), 85.6 (Ta(*C*H$_2$Ph)$_2$), 64.8 (C_α, ^{t}Bu), 32.0 (C_β, ^{t}Bu), 25.5 (HC(C(*Me*)NAr)$_2$).

(BDI^{Cl})Ta(N^{t}Bu)(CH$_2$SiMe$_3$)$_2$ (5.11) Compound **5.7** (50 mg, 0.063 mmol, 1.0 eq) was added to a 20 mL vial and dissolved in 5 mL THF. BnMgCl (97.5 μL of 1.3 M soln. in THF, 0.130 mmol, 2.05 eq) was added at -40 °C with stirring. Upon warming to room temperature, the solution changed color from yellow-orange to pale yellow. The solution was stirred for 30 min at room temperature, and then the volatile materials were removed under vacuum. The residue was triturated with hexane and then extracted with hexane and filtered through Celite to give an orange-red solution. The solution was concentrated and stored at -40 ˚C overnight, yielding pale yellow needles of **5.11**. The solid was isolated and residual solvent was removed under vacuum. Yield: 31 mg, 60% over 2 crops. **^{1}H NMR (600 MHz, C_6D_6, 293 K):** δ 7.02 (d, 4H, Ar), 6.46 (t, 2H, Ar), 5.33 (s, 1H, *H*C(C(Me)NAr)$_2$), 1.62 (br s, 6H, HC(C(*Me*)NAr)$_2$), 1.40 (d, 2H, Ta(C*H*$_2$SiMe$_3$)$_2$, ^{2}J = 9.8 Hz), 1.26 (s, 9H, ^{t}Bu), 1.05 (d, 2H, Ta(C*H*$_2$SiMe$_3$)$_2$, ^{2}J = 9.8 Hz), 0.21 (s, 18H, Ta(CH$_2$Si*Me*$_3$)$_2$). **^{13}C{^{1}H} NMR (600 MHz, C_6D_6, 293 K):** δ 132.6 (Ar), 129.4 (Ar), 126.6 (Ar), 104.8 (H*C*(C(Me)NAr)$_2$), 69.0 (Ta(*C*H$_2$SiMe$_3$)$_2$), 64.7 (C_α, ^{t}Bu), 32.6 (C_β, ^{t}Bu), 25.3 (HC(C(*Me*)NAr)$_2$), 4.0 (Ta(CH$_2$Si*Me*$_3$)$_2$.

EPR Measurements: The EPR spectra were obtained on a custom-designed continuous-wave (*cw*)/pulsed X-band Bruker Elexsys 580 EPR spectrometer. The variable-temperature *cw* EPR measurements were performed with a dual-mode resonator ER 4116-DM (Bruker BioSpin, Billerica, MA) that was equipped with a continuous-flow helium E900 cryostat (Oxford

Instruments, Oxfordshire, U.K.) for acquisition temperatures between 4-77 K. The operating frequency of the ER 4116-DM resonator in the perpendicular mode was 9.38 GHz. The spectra were acquired under non-saturating conditions with a modulation frequency of 100 kHz and modulation amplitude of 4 G. A sample of **5.4** was dissolved in THF under anaerobic conditions, transferred to a 4 mm J. Young quartz EPR tube (Wilmad Labglass, Vineland, NJ) and rapidly frozen at 77 K. The spectral simulations were performed with EasySpin.[115] The numerical simulations of the EPR spectrum of a frozen solution of **5.4** at 77 K included a rhombic g tensor (g_x = 1.996, g_y = 1.969, g_z = 1.902) for the unpaired electron spin (S = ½) and individual hyperfine tensors for the interaction of the electron spin (S = ½) with the ^{93}Nb nuclear spin(s) (I = 9/2) (^{93}Nb(1) (MHz): A_x = 111, A_y = 48, A_z = 200 and A^{93}Nb(2) (MHz): A_x = 115, A_y = 52, A_z = 234).

DFT Calculations: Calculations using B3LYP hybrid functionals[116] were performed using the Gaussian09 suite of programs.[117] For geometry optimizations and frequency calculations, the light atoms (H, C, N and F) were treated with the 6-31G(d,p) basis,[118] while the niobium atom was treated with a Stuttgart/Dresden ECP pseudopotential (SDD).[119] Calculations using PBE0 hybrid functionals were performed with the ORCA 3.0.2 program package.[120] Full optimization were carried out using the hybrid functional PBE0[121] with and without additional dispersion corrections[122] and the TZVP basis set[123], the RIJCOSX approximations and ZORA relativistic approximation.[124] The EPR g matrix and hyperfine coupling constants were obtained from single point calculations using the two hybrid functional PBE0[121] and the TZVP[123] basis set for all carbon, hydrogen atoms and niobium atom, while a IGLO-III[125] basis set has been used for hydrogen and nitrogen atoms and TZVPP for the niobium atom.[126] TD-DFT calculations were performed for 4 with the hybrid functional PBE0[121]. For all calculations, tight SFC convergence criteria were used. Differences in the geometrical parameters between structures calculated using B3LYP and PBE0 are given in Table 5.1. QTAIM analyses were performed with AIMAll Version 16.01.09.[127]

Table 5.1 Comparison of selected experimental and computed metrical parameters for **5.4**.

Bond distance (Å)	XRD	B3LYP	PBE0
Nb1-Nb2	2.717	2.753	2.686
Nb1-N1(imido)	1.974	2.021	1.970
Nb2-N1(imido)	1.974	2.021	1.999
Nb1-N2(imido)	1.991	2.006	1.953
Nb2-N2(imido)	1.991	2.006	2.011
Nb1-N(BDI)	2.095	2.147	2.093
Nb1-N(BDI)	2.113	2.148	2.109
Nb2-N(BDI)	2.095	2.147	2.107
Nb2-N(BDI)	2.113	2.148	2.116
Bond angle (˚)			
N1(imido)-Nb1-N(BDI)	119.8	119.3	125.3
N1(imido)-Nb1-N(BDI)	116.4	118.6	117.0
N2(imido)-Nb2-N(BDI)	120.2	119.3	127.8
N2(imido)-Nb2-N(BDI)	117.7	118.6	118.8

Table 5.2 Calculated and experimental g-tensors and hyperfine coupling constants for **5.4**. Magnitudes of coupling constants are given in parenthesis.

	g_1, g_2, g_3	A^{93}Nb(1) (G)	A^{93}Nb(2) (G)	ΔA^{93}Nb
PBE0	1.997 1.977 1.842	38 76 187 (100)	59 98 209 (122)	22
B3LYP	1.997 1.980 1.833	73 91 226 (130)	81 100 229 (137)	7
Exp	1.996 1.968 1.908	111 48 200 (120)	115 52 234 (134)	14

Table S3 Partial atomic charges and electron spin density on selected atoms in B3LYP-optimized structures of **5.3** and **5.4** calculated using Mulliken, NPA, Hirshfeld, and QTAIM approaches.

	Atom	Mulliken Charge	NPA Charge	Hirshfeld Charge	QTAIM Charge	Mulliken Spin	Hirshfeld Spin	QTAIM Spin
5.3	Nb	+0.85	+1.06	+0.30	+1.87			
	N(imido)	-0.60	-0.73	-0.22	-1.20			
	N(BDI)	-0.67	-0.64	-0.16	-1.32			
	μ-H	-0.24	-0.21	-0.08	-0.48			
5.4	Nb	+1.10	+1.71	+0.40	+1.89	+0.57	+0.47	+0.47
	N(imido)	-0.83	-1.17	-0.23	-1.30	-0.11	-0.05	-0.06
	N(BDI)	-0.72	-0.74	-0.14	-1.33	-0.03	-0.03	0.00

Table S4 Partial atomic charges and electron spin density on selected atoms in PBE0-optimized structure of **5.4** calculated using Mulliken and Loewdin approaches.

	Atom	Mulliken Charge	Mulliken Spin	Loewdin Spin
5.4	Nb	+1.35	+0.53	+0.49
		+1.40	+0.67	+0.62
	N(imido)	-0.76	-0.13	-0.96
		-0.77	-0.14	-1.06
	N(BDI)	-0.46	-0.40	-0.26
		-0.44	-0.39	-0.25
		-0.42	-0.27	-0.16
		-0.43	-0.29	-0.18

X-Ray Crystallographic Studies: Single crystals of **5.1**, **5.2**, **5.3**, **5.4a**, and **5.5** were coated in Paratone-N oil, mounted on a Kaptan loop, transferred to a Bruker APEX CCD area detector,[128] centered in the beam, and cooled by a nitrogen flow low-temperature apparatus that had been previously calibrated by a thermocouple placed at the same position as the crystal. Preliminary orientation matrices and cell constants were determined by collection of 36 10 s frames, followed by spot integration and least-squares refinement. An arbitrary hemisphere of data was collected, and the raw data were integrated using SAINT.[129] Cell dimensions reported were calculated from all reflections with I > 10 (Table 1). The data were corrected for Lorentz and polarization effects, but no correction for crystal decay was applied. An empirical absorption correction based on

comparison of redundant and equivalent reflections was applied using SADABS.[130] Structures were solved by direct methods with the aid of successive difference Fourier maps and were refined against all data using the SHELXTL 5.0 software package.[131] Thermal parameters for all non-hydrogen atoms were refined anisotropically. ORTEP diagrams were created using the ORTEP-3 software package[132] and Mercury.[133]

Table 5.5 Crystallographic data for compounds **5.1** – **5.3**.

Compound	**5.1 · Et_2O**	**5.2**	**5.3**
Empirical formula	$C_{36}H_{53}N_4OCl_2Nb$	$C_{29}H_{44}N_3Nb$	$C_{54}H_{78}N_6Nb_2$
Formula weight (amu)	721.63	527.58	997.1
Wavelength (Å)	0.71073	0.71073	0.71073
Space group	*P*-1	$P2_1/c$	$P2_1/n$
a (Å)	9.1510(5)	11.6055(5)	12.1729(5)
b (Å)	11.5419(7)	25.688(1)	15.8007(6)
c (Å)	17.856(1)	9.5984(4)	13.4968(5)
α (°)	87.826(1)	90	90
β (°)	77.694(1)	98.730(1)	93.481(2)
γ (°)	84.586(1)	90	90
V ($Å^3$)	1834.1(2)	2828.4(2)	2591.2(2)
Z	2	4	2
ρ_{calcd} (g/cm^3)	1.307	1.239	1.278
μ (mm^{-1})	0.506	0.445	0.482
F_{000} (e^-)	760	1120	1052
Crystal size (mm^3)	.40 x .32 x .24	.08 x .08 x .02	.06 x .04 x .04
Theta min / max (˚)	1.773 / 25.329	1.585 / 25.359	1.987 / 25.405
Reflections collected	88948	86456	25246
R_{int}	0.0408	0.0506	0.0516
T_{max} / T_{min}	0.7452 / 0.6826	0.7452 / 0.6573	0.7452 / 0.6696
Data / restr. / param.	6661 / 0 / 410	5183 / 0 / 311	4749 / 0 / 295
GoF	1.111	1.101	1.021
R_1 / wR_2 ($I>2\sigma(I)$)	0.0231 / 0.0588	0.0332 / 0.0820	0.0421 / 0.0979
R_1 / wR_2 (all data)	0.0236 / 0.0591	0.0399 / 0.0875	0.0619 / 0.1094
Res. peak / hole ($e^-/Å^3$)	0.441 / -0.446	1.183 / -0.411	1.952 / -0.379

Table 5.6 Crystallographic data for compounds **5.4** and **5.5**.

Compound	**5.4a · 1.5 Et_2O**	**5.5**
Empirical formula	$C_{83.75}H_{90.25}N_6\ O_{1.75}F_{20}BNb$	$C_{57}H_{83}N_6Nb_2$
Formula weight (amu)	1785.49	1038.11
Wavelength (Å)	0.71073	0.71073
Space group	$P2_1/c$	$P2_1/c$
a (Å)	29.313(2)	19.6714(6)
b (Å)	16.020(1)	13.6781(4)
c (Å)	27.544(1)	20.0479(6)
α (°)	90	90
β (°)	100.729(3)	92.016(2)
γ (°)	90	90
V ($Å^3$)	8094.5(9)	5390.9(3)
Z	4	4
ρ_{calcd} (g/cm^3)	1.465	1.279
μ (mm^{-1})	0.380	0.466
F_{000} (e^-)	3663	2196
Crystal size (mm^3)	.08 x .06 x .03	.04 x .02 x .02
Theta min / max (˚)	1.414 / 25.415	1.803 / 25.397
Reflections collected	116724	29828
R_{int}	0.0789	0.0718
T_{max} / T_{min}	0.7452 / 0.6997	0.7452 / 0.6327
Data / restr. / param.	14873 / 0 / 1062	9833 / 0 / 640
GoF	1.014	1.043
R_1 / wR_2 (I>2σ(I))	0.0418 / 0.0909	0.0571 / 0.1218
R_1 / wR_2 (all data)	0.0647 / 0.1004	0.0961 / 0.1363
Res. peak / hole ($e^-/Å^3$)	0.821 / -0.614	0.937 / -0.824

Table 5.7 Crystallographic data for compounds **5.6 – 5.9**.

Compound	**5.6·Et_2O**	**5.7·Et_2O**	**5.8**	**5.9**
Empirical formula	$C_{30}H_{37}Cl_6N_4NbO$	$C_{30}H_{37}Cl_6N_4TaO$	$C_{23}H_{28}Cl_4N_3Nb$	$C_{23}H_{28}Cl_4N_3Ta$
Formula weight (amu)	775.24	527.58	997.1	1785.49
Wavelength (Å)	0.71073	0.71073	0.71073	0.71073
Space group	*P*-1	*P*-1	*P*-1	*P*-1
a (Å)	10.1695(4)	10.1863(5)	11.3884(10)	11.3843(8)
b (Å)	13.0882(6)	13.0477(7)	14.1175(12)	14.1122(10)
c (Å)	14.5004(6)	14.4884(7)	17.0308(14)	16.9985(12)
α (°)	111.000(2)	110.8560(10)	93.146(4)	92.9880(10)
β (°)	103.913(2)	104.1750(10)	107.855(4)	107.7240(10)
γ (°)	95.672(2)	95.2560(10)	94.062(5)	94.3570(10)
V ($Å^3$)	1712.12(13)	1710.35(15)	2591.2(4)	2585.6(3)
Z	2	2	4	4
ρ_{calcd} (g/cm^3)	1.504	1.676	1.490	1.719
μ (mm^{-1})	0.850	3.712	0.893	4.680
F_{000} (e^-)	792	856	1184	1312
Crystal size (mm^3)	.08 x .06 x .04	.14 x .09 x .08	.25 x .20 x .13	.10 x .08 x .03
Theta min / max (˚)	1.575 / 25.538	1.576 / 25.378	1.260 / 25.478	1.262 / 25.361
Reflections collected	53743	38535	51932	42703
R_{int}	0.0780	0.0876	0.0279	0.0652
T_{max} / T_{min}	0.7452 / 0.5916	0.7452 / 0.5968	0.7452 / 0.6850	0.7452 / 0.5333
Data / restr. / param.	6333 / 0 / 386	6257 / 0 / 386	9564 / 0 / 573	9413 / 0 / 573
GoF	0.738	1.055	1.050	1.116
R_1 / wR_2 (I>2σ(I))	0.0324 / 0.0770	0.0428 / 0.0984	0.0343 / 0.0927	0.0408 / 0.0865
R_1 / wR_2 (all data)	0.0464 / 0.0890	0.0526 / 0.1029	0.0408 / 0.0966	0.0625 / 0.0944
Res. peak / hole ($e^-/Å^3$)	0.765 / -0.807	4.485 / -2.562	1.478 / -0.575	2.433 / -1.418

Notes and References

(1) Sato, F.; Urabe, H.; Okamoto, S. *Chem. Rev.* **2000**, *100* (8), 2835.
(2) Negishi, E. *Acc. Chem. Res.* **1987**, *20* (2), 65.
(3) Gell, K. I.; Schwartz, J. *J. Am. Chem. Soc.* **1981**, *103* (10), 2687.
(4) Broene, R. D.; Buchwald, S. L. *Science* **1993**, *261* (5129), 1696.
(5) Bruck, M. A.; Copenhaver, A. S.; Wigley, D. E. *J. Am. Chem. Soc.* **1987**, *109* (21), 6525.
(6) McLain, S. J.; Wood, C. D.; Schrock, R. R. *J. Am. Chem. Soc.* **1979**, *101* (16), 4558.
(7) Roskamp, E. J.; Pedersen, S. F. *J. Am. Chem. Soc.* **1987**, *109* (21), 6551.

(8) Labinger, J. A.; Schwartz, J. *J. Am. Chem. Soc.* **1975**, *97* (6), 1596.
(9) Fryzuk, M. D.; Kozak, C. M.; Bowdridge, M. R.; Patrick, B. O.; Rettig, S. J. *J. Am. Chem. Soc.* **2002**, *124* (28), 8389.
(10) LaPointe, R. E.; Wolczanski, P. T.; Mitchell, J. F. *J. Am. Chem. Soc.* **1986**, *108* (20), 6382.
(11) Neithamer, D. R.; LaPointe, R. E.; Wheeler, R. A.; Richeson, D. S.; Van Duyne, G. D.; Wolczanski, P. T. *J. Am. Chem. Soc.* **1989**, *111* (25), 9056.
(12) Figueroa, J. S.; Cummins, C. C. *Dalton Trans.* **2006**, 2161.
(13) Kilgore, U. J.; Yang, X.; Tomaszewski, J.; Huffman, J. C.; Mindiola, D. J. *Inorg. Chem.* **2006**, *45* (26), 10712.
(14) Hulley, E. B.; Wolczanski, P. T.; Lobkovsky, E. B. *Chem. Commun.* **2009**, 6412.
(15) Pool, J. A.; Lobkovsky, E.; Chirik, P. J. *J. Am. Chem. Soc.* **2003**, *125* (8), 2241.
(16) Pool, J. A.; Lobkovsky, E.; Chirik, P. J. *Nature* **2004**, *427*, 527.
(17) Bernskoetter, W. H.; Lobkovsky, E.; Chirik, P. J. *J. Am. Chem. Soc.* **2005**, *127* (40), 14051.
(18) Semproni, S. P.; Milsmann, C.; Chirik, P. J. *Organometallics* **2012**, *31* (9), 3672.
(19) Seidel, W. W.; Summerscales, O. T.; Patrick, B. O.; Fryzuk, M. D. *Angew. Chemie Int. Ed.* **2009**, *48* (1), 115.
(20) Zanotti-Gerosa, A.; Solari, E.; Giannini, L.; Floriani, C.; Chiesi-Villa, A.; Rizzoli, C. *J. Am. Chem. Soc.* **1998**, *120* (2), 437.
(21) Caselli, A.; Solari, E.; Scopelliti, R.; Floriani, C. *J. Am. Chem. Soc.* **2000**, *122* (3), 538.
(22) Wigley, D. E. *Prog. Inorg. Chem.* **1994**, *42*, 239.
(23) Parkin, G. In *Progress in Inorganic Chemistry*; Karlin, K. D., Ed.; John Wiley & Sons, Inc.: Hoboken, NJ, USA, 1997; pp 1–165.
(24) Hanna, T. E.; Keresztes, I.; Lobkovsky, E.; Bernskoetter, W. H.; Chirik, P. J. *Organometallics* **2004**, *23*, 3448.
(25) Figueroa, J. S.; Cummins, C. C. *J. Am. Chem. Soc.* **2003**, *125* (14), 4020.
(26) Veige, A. S.; Slaughter, L. M.; Wolczanski, P. T.; Matsunaga, N.; Decker, S. A.; Cundari, T. R. *J. Am. Chem. Soc.* **2001**, *123* (26), 6419.
(27) Veige, A. S.; Kleckley, T. S.; Chamberlin, R. M.; Neithamer, D. R.; Lee, C. E.; Wolczanski, P. T.; Lobkovsky, E. B.; Glassey, W. V. *J. Organomet. Chem.* **1999**, *591*, 194.
(28) Howard, W. A.; Waters, M.; Parkin, G. *J. Am. Chem. Soc.* **1993**, *115* (11), 4917.
(29) Howard, W. A.; Trnka, T. M.; Waters, M.; Parkin, G. *J. Organomet. Chem.* **1997**, *528* (1), 95.
(30) Smith, M. R.; Matsunaga, P. T.; Andersen, R. A. *J. Am. Chem. Soc.* **1993**, *115* (15), 7049.
(31) Negishi, E.; Swanson, D. R.; Cederbaum, F. E.; Takahashi, T. *Tetrahedron Lett.* **1987**, *28* (9), 917.
(32) Ozerov, O. V.; Patrick, B. O.; Ladipo, F. T. *J. Am. Chem. Soc.* **2000**, *122* (27), 6423.
(33) Kulinkovich, O. G. *Chem. Rev.* **2003**, *103* (7), 2597.
(34) Hicks, F. A.; Kablaoui, N. M.; Buchwald, S. L. *J. Am. Chem. Soc.* **1999**, *121* (25), 5881.
(35) Bruck, A.; Copenhaver, A. S.; Wigley, D. E. *J. Am. Chem. Soc.* **1987**, *109*, 6525.
(36) Gilbert, Z. W.; Hue, R. J.; Tonks, I. A. *Nat. Chem.* **2016**, *8* (1), 63.
(37) Gianetti, T. L.; La Pierre, H. S.; Arnold, J. *Eur. J. Inorg. Chem.* **2013**, *2013* (22–23), 3771.
(38) Gianetti, T. L.; Tomson, N. C.; Arnold, J.; Bergman, R. G. *J. Am. Chem. Soc.* **2011**, *133*, 14904.
(39) Gianetti, T. L.; Bergman, R. G.; Arnold, J. *Chem. Sci.* **2014**, *5* (6), 2517.
(40) Kriegel, B. M.; Bergman, R. G.; Arnold, J. *J. Am. Chem. Soc.* **2016**, *138* (1), 52.
(41) Hohloch, S.; Kriegel, B. M.; Bergman, R. G.; Arnold, J. *Dalt. Trans.* **2016**.

(42) Tomson, N. C.; Yan, A.; Arnold, J.; Bergman, R. G. *J. Am. Chem. Soc.* **2008**, *130*, 11262.
(43) Tomson, N. C.; Arnold, J.; Bergman, R. G. *Organometallics* **2010**, *29*, 2926.
(44) Tomson, N. C.; Arnold, J.; Bergman, R. G. *Dalton Trans.* **2011**, *40* (30), 7718.
(45) Gianetti, T. L.; Bergman, R. G.; Arnold, J. *J. Am. Chem. Soc.* **2013**, *135* (22), 8145.
(46) Kriegel, B. M.; Bergman, R. G.; Arnold, J. *Dalt. Trans.* **2014**, *43* (26), 10046.
(47) Camp, C.; Grant, L. N.; Bergman, R. G.; Arnold, J. *Chem. Commun.* **2016**, *52*, 5538.
(48) Nechayev, M.; Gianetti, T. L.; Bergman, R. G.; Arnold, J. *Dalton Trans.* **2015**, *44* (45), 19494.
(49) Grant, L. N.; Kriegel, B. M.; Arnold, J. *Polyhedron* **2015**.
(50) Camp, C.; Maron, L.; Bergman, R. G.; Arnold, J. *J. Am. Chem. Soc.* **2014**, *136* (50), 17652.
(51) Gianetti, T. L.; Bergman, R. G.; Arnold, J. *Polyhedron* **2014**, *84*, 19.
(52) Tomson, N. C.; Arnold, J.; Bergman, R. G. *Organometallics* **2010**, *29*, 5010.
(53) Gianetti, T. L.; Nocton, G.; Minasian, S. G.; Tomson, N. C.; Kilcoyne, A. L. D.; Kozimor, S. A.; Shuh, D. K.; Tyliszczak, T.; Bergman, R. G.; Arnold, J. *J. Am. Chem. Soc.* **2013**, *135* (8), 3224.
(54) Obenhuber, A. H.; Gianetti, T. L.; Berrebi, X.; Bergman, R. G.; Arnold, J. *J. Am. Chem. Soc.* **2014**, *136* (8), 2994.
(55) Fryzuk, M. D.; Johnson, S. A.; Rettig, S. J. *J. Am. Chem. Soc.* **1998**, *120* (42), 11024.
(56) Fryzuk, M. D.; Johnson, S. A.; Patrick, B. O.; Albinati, A.; Mason, S. A.; Koetzle, T. F. *J. Am. Chem. Soc.* **2001**, *123* (17), 3960.
(57) Fryzuk, M. D.; MacKay, B. A.; Patrick, B. O. *J. Am. Chem. Soc.* **2003**, *125* (11), 3234.
(58) Shaver, M. P.; Johnson, S. A.; Fryzuk, M. D. *Can. J. Chem.* **2005**, *83* (6–7), 652.
(59) Shaver, M. P.; Fryzuk, M. D. *J. Am. Chem. Soc.* **2005**, *127* (2), 500.
(60) Shaver, M. P.; Fryzuk, M. D. *Organometallics* **2005**, *24* (7), 1419.
(61) Ballmann, J.; Yeo, A.; MacKay, B. A.; Rijt, S. van; Patrick, B. O.; Fryzuk, M. D. *Chem. Commun.* **2010**, *46* (46), 8794.
(62) Ballmann, J.; Pick, F.; Castro, L.; Fryzuk, M. D.; Maron, L. *Organometallics* **2012**, *31* (24), 8516.
(63) Ballmann, J.; Pick, F.; Castro, L.; Fryzuk, M. D.; Maron, L. *Inorg. Chem.* **2013**, *52* (4), 1685.
(64) Kawaguchi, H.; Matsuo, T. *J. Am. Chem. Soc.* **2003**, *125* (47), 14254.
(65) Watanabe, T.; Ishida, Y.; Matsuo, T.; Kawaguchi, H. *J. Am. Chem. Soc.* **2009**, *131* (10), 3474.
(66) Kurogi, T.; Ishida, Y.; Hatanaka, T.; Kawaguchi, H. *Chem. Commun.* **2012**, *48* (54), 6809.
(67) Kawaguchi, H.; Matsuo, T. *Angew. Chemie Int. Ed.* **2002**, *41* (15), 2792.
(68) Akagi, F.; Matsuo, T.; Kawaguchi, H. *Angew. Chemie Int. Ed.* **2007**, *46* (46), 8778.
(69) Tanaka, H.; Shiota, Y.; Matsuo, T.; Kawaguchi, H.; Yoshizawa, K. *Inorg. Chem.* **2009**, *48* (8), 3875.
(70) Kurogi, T.; Ishida, Y.; Hatanaka, T.; Kawaguchi, H. *Dalton Trans.* **2013**, *42* (21), 7510.
(71) Gianetti, T. L.; Nocton, G.; Minasian, S. G.; Kaltsoyannis, N.; Kilcoyne, A. L. D.; Kozimor, S. A.; Shuh, D. K.; Tyliszczak, T.; Bergman, R. G.; Arnold, J. *Chem. Sci.* **2015**, *6* (2), 993.
(72) Fryzuk, M. D.; Johnson, S. a; Rettig, S. J. *Organometallics* **2000**, *19*, 3931.
(73) Tonzetich, Z. J.; Jiang, A. J.; Schrock, R. R.; Müller, P. *Organometallics* **2006**, *25* (20), 4725.
(74) Tonzetich, Z. J.; Jiang, A. J.; Schrock, R. R.; Müller, P. *Organometallics* **2007**, *26* (15), 3771.

(75) Addison, A. W.; Rao, T. N.; Reedijk, J.; van Rijn, J.; Verschoor, G. C. *J. Chem. Soc. Dalt. Trans.* **1984**, 1349.
(76) Berno, P.; Gambarotta, S. *Angew. Chemie Int. Ed.* **1995**, *34* (7), 822.
(77) Perevalova, E. G.; Urazowski, I. F.; Lemenovskii, D. A.; Slovokhotov, Y. L.; Struchkov, Y. T. *J. Organomet. Chem.* **1985**, *289* (2–3), 319.
(78) McLeod, N. A.; Kuzmina, L. G.; Churakov, A. V.; Mountford, P.; Nikonov, G. I. *Dalt. Trans.* **2014**, *43* (1), 188.
(79) Cotton, F. A.; Roth, W. J. *Inorg. Chem.* **1984**, *23* (7), 945.
(80) Drew, M. G. B.; Rice, D. A.; Williams, D. M. *J. Chem. Soc. Dalt. Trans.* **1983**, No. 10, 2251.
(81) Okuniewski, A.; Rosiak, D.; Chojnacki, J.; Becker, B. *Polyhedron* **2015**, *90*, 47.
(82) Yoon, M.; Lin, J.; Young, V. G.; Miller, G. J. *J. Organomet. Chem.* **1996**, *507* (1–2), 31.
(83) Lemenovskii, D. A.; Fedin, V. P.; Slovohotov, Y. L.; Struchkov, Y. T. *J. Organomet. Chem.* **1982**, *228* (2), 153.
(84) Dugan, T. R.; Bill, E.; MacLeod, K. C.; Christian, G. J.; Cowley, R. E.; Brennessel, W. W.; Ye, S.; Neese, F.; Holland, P. L. *J. Am. Chem. Soc.* **2012**, *134* (50), 20352.
(85) Robin, M. B.; Day, P. *Adv. Inorg. Chem. Radiochem.* **1968**, *10*, 247.
(86) Chisholm, M. H. *Coord. Chem. Rev.* **2013**, *257* (9), 1576.
(87) Chisholm, M. H.; Pate, B. D.; Wilson, P. J.; Zaleski, J. M. *Chem. Commun.* **2002**, No. 10, 1084.
(88) Tsai, Y.-C.; Hsu, C.-W.; Yu, J.-S. K.; Lee, G.-H.; Wang, Y.; Kuo, T.-S. *Angew. Chemie Int. Ed.* **2008**, *120* (38), 7360.
(89) Berry, J. F.; Bothe, E.; Cotton, F. A.; Ibragimov, S. A.; Murillo, C. A.; Villagrán, D.; Wang, X. *Inorg. Chem.* **2006**, *45* (11), 4396.
(90) Berry, J. F.; Bill, E.; Bothe, E.; Cotton, F. A.; Dalal, N. S.; Ibragimov, S. A.; Kaur, N.; Liu, C. Y.; Murillo, C. A.; Nellutla, S.; North, J. M.; Villagrán, D. *J. Am. Chem. Soc.* **2007**, *129* (5), 1393.
(91) Cotton, F. A.; Daniels, L. M.; Falvello, L. R.; Murillo, C. A. *Inorganica Chim. Acta* **1994**, *219*, 7.
(92) Cotton, F. A.; Daniels, L. M.; Falvello, L. R.; Matonic, J. H.; Murillo, C. A. *Inorganica Chim. Acta* **1997**, *256* (2), 269.
(93) Zall, C. M.; Clouston, L. J.; Young, V. G.; Ding, K.; Kim, H. J.; Zherebetskyy, D.; Chen, Y.-S.; Bill, E.; Gagliardi, L.; Lu, C. C. *Inorg. Chem.* **2013**, *52* (16), 9216.
(94) Camp, C.; Arnold, J. *Dalton Trans.* **2016**, *45*, 14462.
(95) Bai, G.; Wei, P.; Stephan, D. W. *Organometallics* **2006**, *25* (10), 2649.
(96) Hamaki, H.; Takeda, N.; Tokitoh, N. *Organometallics* **2006**, *25* (10), 2457.
(97) Basuli, F.; Kilgore, U. J.; Brown, D.; Huffman, J. C.; Mindiola, D. J. *Organometallics* **2004**, *23* (26), 6166.
(98) Chang, K.-C.; Lu, C.-F.; Wang, P.-Y.; Lu, D.-Y.; Chen, H.-Z.; Kuo, T.-S.; Tsai, Y.-C. *Dalton Trans.* **2011**, *40* (10), 2324.
(99) Basuli, F.; Huffman, J. C.; Mindiola, D. J. *Inorganica Chim. Acta* **2007**, *360* (1), 246.
(100) Woodul, W. D.; Richards, A. F.; Stasch, A.; Driess, M.; Jones, C. *Organometallics* **2010**, *29* (16), 3655.
(101) Li, X.; Cheng, X.; Song, H.; Cui, C. *Organometallics* **2007**, *26* (4), 1039.
(102) Wang, W.; Yao, S.; van Wüllen, C.; Driess, M. *J. Am. Chem. Soc.* **2008**, *130* (30), 9640.
(103) Choong, S. L.; Schenk, C.; Stasch, A.; Dange, D.; Jones, C. *Chem. Commun.* **2012**, *48* (19),

2504.
(104) Li, J.; Li, X.; Huang, W.; Hu, H.; Zhang, J.; Cui, C. *Chemistry* **2012**, *18* (48), 15263.
(105) Arney, D. J.; Bruck, M. A.; Huber, S. R.; Wigley, D. E. *Inorg. Chem.* **1992**, *31* (18), 3749.
(106) Gountchev, T. I.; Tilley, T. D. *Organometallics* **1999**, *18* (15), 2896.
(107) Haftbaradaran, F.; Mund, G.; Batchelor, R. J.; Britten, J. F.; Leznoff, D. B. *Dalt. Trans.* **2005**, *104* (14), 2343.
(108) Tonks, I. A.; Tofan, D.; Weintrob, E. C.; Agapie, T.; Bercaw, J. E. *Organometallics* **2012**, *31* (5), 1965.
(109) Kuprat, M.; Lehmann, M.; Schulz, A.; Villinger, A. *Organometallics* **2010**, *29* (6), 1421.
(110) Bochmann, M.; Jaggar, A. J.; Wilson, L. M.; Hursthouse, M. B.; Motevalli, M. *Polyhedron* **1989**, *8*, 1838.
(111) Araya, M. A.; Cotton, F. A.; Matonic, J. H.; Murillo, C. A. *Inorg. Chem.* **1995**, *34* (22), 5424.
(112) Budzelaar, P. H. M.; van Oort, A. B.; Orpen, A. G. *Eur. J. Inorg. Chem.* **1998**, 1485.
(113) Budzelaar, P. H. M.; Moonen, N. N. P.; Gelder, R. de; Smits, J. M. M.; Gal, A. W. *Eur. J. Inorg. Chem.* **2000**, *2000* (4), 753.
(114) Sundermeyer, J.; Putterlik, J.; Foth, M.; Field, J.; Ramesar, N. *Chem. Ber.* **1994**, *127*, 1201.
(115) Stoll, S.; Schweiger, A. *J. Magn. Reson.* **2006**, *178* (1), 42.
(116) Lee, C.; Yang, W.; Parr, R. G. *Phys. Rev. B* **1988**, *37* (2), 785.
(117) Frisch, M.; Trucks, G.; Schlegel, H.; Scuseria, G.; Robb, M.; Cheeseman, J.; Scalmani, G.; Barone, V.; Mennucci, B.; Petersson, G.; Nakatsuji, H.; Caricato, M.; Li, X.; Hratchian, H.; Izmaylov, A.; Bloino, J.; Zheng, G.; Sonnenberg, J.; Hada, M.; Ehara, M.; Toyota, K.; Fukuda, R.; Hasegawa, J.; Ishida, M.; Nakajima, T.; Honda, Y.; Kitao, O.; Nakai, H.; Vreven, T.; Montgomery, J.; Peralta, J.; Ogliaro, F.; Bearpark, M.; Heyd, J.; Brothers, E.; Kudin, K.; Staroverov, V.; Kobayashi, R.; Normand, J.; Raghavachari, K.; Rendell, A.; Burant, J.; Iyengar, S.; Tomasi, J.; Cossi, M.; Rega, N.; Millam, J.; Klene, M.; Knox, J.; Cross, J.; Bakken, V.; Adamo, C.; Jaramillo, J.; Gomperts, R.; Stratmann, R.; Yazyev, O.; Austin, A.; Cammi, R.; Pomelli, C.; Ochterski, J.; Martin, R.; Morokuma, K.; Zakrzewski, V.; Voth, G.; Salvador, P.; Dannenberg, J.; Dapprich, S.; Daniels, A.; Farkas; Foresman, J.; Ortiz, J.; Cioslowski, J.; Fox, D. *Gaussian 09, Revis. D.01, Gaussian, Inc., Wallingford CT* **2009**.
(118) Hariharan, P. C.; Pople, J. A. *Mol. Phys.* **2006**, *27* (1), 209.
(119) Fuentealba, P.; Preuss, H.; Stoll, H.; Von Szentpály, L. *Chem. Phys. Lett.* **1982**, *89* (5), 418.
(120) Neese, F. *Wiley Interdiscip. Rev. Comput. Mol. Sci.* **2012**, *2* (1), 73.
(121) Adamo, C.; Barone, V. *J. Chem. Phys.* **1999**, *110* (13), 6158.
(122) Grimme, S.; Antony, J.; Ehrlich, S.; Krieg, H. *J. Chem. Phys.* **2010**, *132* (15), 154104.
(123) Schäfer, A.; Huber, C.; Ahlrichs, R. *J. Chem. Phys.* **1994**, *100* (8), 5829.
(124) van Lenthe, E.; Ehlers, A.; Baerends, E.-J. *J. Chem. Phys.* **1999**, *110* (18), 8943.
(125) Kutzelnigg, W.; Fleischer, U.; Schindler, M. Springer Berlin Heidelberg, 1990; pp 165–262.
(126) Krishnan, R.; Binkley, J. S.; Seeger, R.; Pople, J. A. *J. Chem. Phys.* **1980**, *72* (1), 650.
(127) AIMAll (Version 16.10.31), Keith, T. A., TK Gristmill Software, Overland Park, KS, USA, 2016.
(128) SMART: Area-Detector Software Package; Bruker Analytical X-ray Systems, Inc.: Madison, WI, 2001-2003.
(129) SAINT: SAX Area-Detector Integration Program; Bruker Analytical X-ray Systems Inc.:

Madison, WI, 2003.
(130) SADABS: Bruker-Nonius Area Detector Scaling and Absorption; Bruker Analytical X-ray Systems, Inc.: Madison, WI, 2003.
(131) Sheldrick, G. M. *Acta Crystallogr. Sect. A* **2008**, *64*, 112.
(132) Farrugia, L. J. *Journal of Applied Crystallography*. International Union of Crystallography October 1, 1997, p 565.
(133) Macrae, C. F.; Bruno, I. J.; Chisholm, J. A.; Edgington, P. R.; McCabe, P.; Pidcock, E.; Rodriguez-Monge, L.; Taylor, R.; van de Streek, J.; Wood, P. A. *J. Appl. Crystallogr.* **2008**, *41* (2), 466.

Appendix A

Proposed Future Studies on Niobium Terminal Oxo-Imido, Sulfido-Imido and Related Systems

In Chapter 3 of this work, the syntheses of niobium terminal oxo-imido complexes **3.22** and **3.24** were described. While preliminary studies showed that these compounds were reactive across their terminal oxo groups (in contrast to most other group 5 oxo complexes in the literature), their utility was limited by the number of synthetic steps necessary to prepare these materials. Hence, it would be prudent to devise an alternative synthetic route to access terminal oxo complexes, as well as related terminal sulfido, selenido, phosphinidene, nitrido, and phosphido complexes. Early transition metal (group 3 to 5) complexes bearing any of these moieties in addition to a terminal imido group have not been reported, and are expected to be quite reactive due to π-loading effects.

In 2010, Tomson, Arnold, and Bergman reported the preparation of (BDI)Nb(NAr)Cl_2 (**1.4**, see Chapter 1, Scheme 1.1). In contrast to the related *tert*-butylimido systems (BDI)Nb(N^{t}Bu)Cl_2Py (**1.1**) and (BDI)Nb(N^{t}Bu)Cl_2 (**1.3**), the chemistry of **1.4** has not yet been investigated in detail. Based on the results presented in Chapter 3, the BDI-arylimido ligand scaffold provides an excellent support for monomeric complexes containing a second multiply bonded functionality. The pyridine adduct of **1.4** has not yet been reported, but is expected to be prepared in higher yield and fewer steps than **1.4**, as was observed for **1.1** and **1.3**.

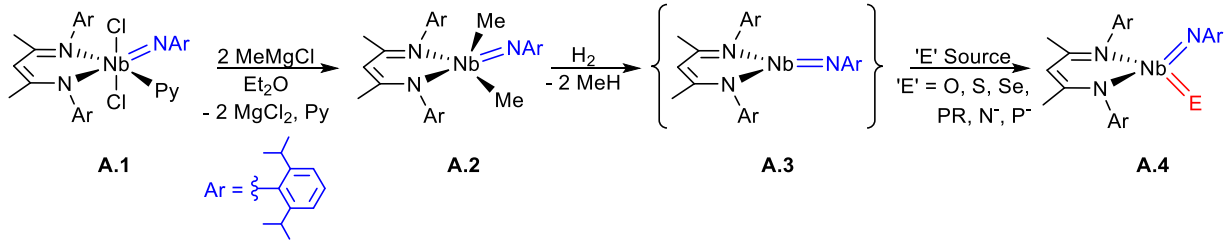

Scheme 1 Proposed route to niobium complexes with terminal multiply-bonded ligands.

Scheme A.1 shows a proposed route to terminal oxo-arylimido, sulfido-arylimido, and related complexes **A.4**. First, **A.1** can likely be prepared *via* salt-metathesis of the readily prepared ligand and metal precursors BDILi·OEt_2 and Nb(NAr)Cl_3Py_2. While this might not necessarily be the case in the arylimido system, methylation of the dichloride starting material in the *tert*-butylimido system provided the best means of accessing reactive niobium (III) species. Methylation of **A.1** will give compound **A.2**, which will likely give an isolable Nb(III) species **A.3** such as an arene adduct upon reaction with dihydrogen. It is certainly possible, however, that other routes to Nb(III) species, such as direct reduction of **A.1** with KC_8 or Na/Hg, or reactions of **A.2** with π-acids may prove more effective in this system. Once a Nb(III) source has been obtained, a wide variety of complexes **A.4** can potentially be accessed through reactions with substrates like N_2O, Ph_2SO, Ph_3P=E (E = O, S, Se), various N-oxides, S_8, Se_8, P_4, RP=C=O, $^-$P=C=O, and N_3^-. It is important to note that compounds **A.4** may require coordinating ligands such as pyridine or DMAP in order to isolate, as they are expected to be highly reactive. It is unlikely, however, that dimers with bridging 'E' ligands will be able to form due to the sterically demanding ligand framework, although the ability for the BDI ligand to coordinate in a κ^1 binding mode may allow for dimer formation, as was observed in **3.23** (see Chapter 3). The cycloaddition reactivity of complexes **A.4** with unsaturated substrates should be thoroughly investigated, as should their 1,2-addition reactivity. The chemistry of low-valent derivatives (**A.3**) may also contrast significantly with that of the *tert*-butylimido system, and may be worth investigating in detail.